



HAL
open science

Amélioration de la cinétique de dissolution nouvelle molécule antirétrovirale en utilisant la cristallisation par effet antisolvant

Suênia De Paiva Lacerda

► To cite this version:

Suênia De Paiva Lacerda. Amélioration de la cinétique de dissolution nouvelle molécule antirétrovirale en utilisant la cristallisation par effet antisolvant. Food and Nutrition. Institut National Polytechnique de Toulouse - INPT, 2013. English. NNT : 2013INPT0006 . tel-04226829

HAL Id: tel-04226829

<https://theses.hal.science/tel-04226829>

Submitted on 3 Oct 2023

HAL is a multi-disciplinary open access archive for the deposit and dissemination of scientific research documents, whether they are published or not. The documents may come from teaching and research institutions in France or abroad, or from public or private research centers.

L'archive ouverte pluridisciplinaire **HAL**, est destinée au dépôt et à la diffusion de documents scientifiques de niveau recherche, publiés ou non, émanant des établissements d'enseignement et de recherche français ou étrangers, des laboratoires publics ou privés.



THÈSE

En vue de l'obtention du

DOCTORAT DE L'UNIVERSITÉ DE TOULOUSE

Délivré par :

Institut National Polytechnique de Toulouse (INP Toulouse)

Présentée et soutenue par :

Suênia de PAIVA LACERDA

Le 01/02/2013

Titre :

Improvement of dissolution rate of a new antiretroviral drug using an anti-solvent crystallization technology.

Ecole doctorale et discipline ou spécialité :

ED MEGEP : Génie des procédés et de l'Environnement

Unité de recherche :

École des Mines d'Albi Carmaux (RAPSODEE)

Directeurs de Thèse :

M.I RÉ

F. ESPITALIER

Rapporteurs :

P. TCHORELOFF
M. DESCAMPS

Université Paris Sud
Université Lille 1

Rapporteur
Rapporteur

Autres membres du jury :

I. RICO-LATTES
M.GIULIETTI

Directrice de Recherche du CNRS
Universidade Federal de São Carlos

Examinatrice
Examineur

*“Une confrontation permanente entre théorie et expérience est une condition nécessaire
à l'expression de la créativité.”*

PIERRE JOLIOT

À mes parents et grands-parents

Remerciements

Cette thèse doit beaucoup aux nombreuses personnes qui m'ont encouragé, soutenu et conforté au long de toutes ces années. Qu'elles trouvent dans ce travail l'expression de mes plus sincères remerciements.

Je tiens à remercier très chaleureusement mes directrices de Thèse Maria Inês Ré et Fabienne Espitalier de m'avoir encadrée et accompagnée tout au long de ces trois années, pour leur aide, et compétence mais aussi pour leur patience, et leur encouragement à finir ce travail. Je vous remercie vivement pour vos qualités d'encadrement.

Je remercie les rapporteurs (Pierre Tchoreloff et Marc Descamps) et les membres du jury pour avoir accepté d'examiner et de participer à mon jury de thèse.

Je tiens ensuite à remercier les Laboratoires Cristalia et RAPSODEE, pour leur soutien et la confiance qu'ils m'ont témoignés.

Pendant ma thèse j'ai eu le plaisir de travailler avec différentes personnes constituant une formidable équipe. Grâce à leur aide, leur soutien et l'ambiance qu'elles ont fait régner j'ai pu arriver jusqu'au bout. En particulier, je souhaiterai citer Philippe Accart pour sa gentillesse et sa bonne humeur ainsi que pour ses conseils avisés, Laurent Devrient pour sa patience, son amitié et sa disponibilité, Bruno Boyer pour sa gentillesse et toute l'aide qu'il m'a donné quand j'en ai eu besoin. Je pense aussi « aux filles » Séverine Patry, Sylvie Delconfetto, Véronique Nallet et Christine Rolland, pour leur sympathie et leur implication dans leur ou mon travail.

Je n'oublie pas de remercier tous ceux avec qui j'ai passé de bons moments après avoir mangé à la salle café et tout particulièrement Rachel Calvet, Laurence Galet et Celine Boachon. Un grand merci très spécial aussi à Elsa Weiss, Marie Caria et à Manolita Boval.

J'aimerais également remercier Anne-Marie Fontes pour son aide, sa gentillesse, disponibilité, ainsi que son amabilité.

J'ai une pensée pour les doctorants et stagiaires du laboratoire avec qui j'ai partagé une tranche de vie et une tranche de vie de laboratoire et auprès de qui j'ai beaucoup appris et

partagé des bons moments. Mon grand merci à Ingrid, Nibal, Sarah, Naomi, Zhoé, Fredj, William, Anaïs, Graciela, Guillaume, Camille, Fanny, Wellington, Analice, Aline, Antoinette, Yazmine, Marie, Audrey, Claire, Claire Michel, Fabio, Michelle, Jacqueline, Paulo, Andrea, Nayane, Tassadite, Moussa, Christophe, Mohamed Raii, Sébastien, Renaud, Haroun, Marta, Rémis, Vanessa, Maxime et Ludovic.

Je tiens remercier spécialement trois personnes qui ont travaillé directement avec moi pendant cette thèse Vinciane Magan, Julia Flauder et Bruna Rêgo de Vasconcelos, sans elles je n'aurais pas pu y arriver. Avec vous trois j'ai beaucoup appris et j'ai essayé de vous passer un peu du peu que je connais.

J'exprime tous mes remerciements et mon affection à ma famille pour leur précieux soutien tout au long de ma thèse et surtout tout au long de ma vie, et plus particulièrement à mes parents. Ils ont toujours cru en moi et j'espère être toujours à la hauteur.

La thèse a parfois été un moment difficile pour mes proches. Elle a été très preneuse de temps ! Et j'avoue ne pas les avoir consacré le temps qu'ils méritaient. Raffaele D'Elia, je te remercie pour tes encouragements et ton soutien. Malgré la période difficile qu'on a traversé, tu as été toujours disponible et compréhensif.

Comme dirait le petit prince : « J'ai des amis à découvrir et beaucoup de choses à connaître » et ici en France j'ai appris à connaître chacun de vous, vous apprécier et vous admirer.

Merci à la famille Mayer pour son amitié, sa confiance et pour m'avoir reçu comme un membre de votre famille dès le début. Merci Audrey Common, la française la plus brésilienne que je connaisse, pour chaque soirée, les fous rires et tous les bons moments passés ensembles. Merci Marie Dietemann qui a été une grande amie, toujours là pour me soutenir.

Merci à ma petite famille brésilienne en France : Jacqueline, Vincius, Nayane, Bruna, Andrea et Paulo. Vous comptez beaucoup dans ma vie, et grâce à vous j'ai pu avoir une famille en France identique à ma famille au Brésil. Vous tous mes chers amis, vous avez soulagé le poids de la distance, de la solitude et vous m'avez apporté du bonheur et de la joie sans rien demander en échange.

Je vous remercie à tous. Merci de m'avoir accompagnée et aidée pendant ces années. En espérant vous croiser bientôt dans un autre Carnaval !!!

Table of Contents

INTRODUCTION.....	17
CHAPTER 1.....	21
1.1. THE BIOAVAILABILITY OF DRUGS	27
1.1.1. Absorption and bioavailability.....	27
1.1.2. Poorly-water soluble drug molecules	30
1.2. ENHANCEMENT OF SOLUBILIZATION AND BIOAVAILABILITY OF POORLY SOLUBLE DRUGS.....	31
1.2.1. Concept of dissolution.....	31
1.2.2. Dissolution testing for poorly-water soluble drugs	34
1.2.3. Strategies to increase the amount of dissolved drug at the absorption site.....	38
1.2.3.1. Alteration of pH and solvent composition	38
1.2.3.1.1. Salt formation/pH control.....	38
1.2.3.1.2. Cosolvency	39
1.2.3.2. Inclusion complexes/complexation.....	40
1.2.3.2.1. Cyclodextrin (CD)	40
1.2.3.3. Carrier System.....	42
1.2.3.3.1. Micelles.....	42
1.2.3.3.2. Micro/Nanoemulsion	43
1.2.3.4. Manipulation of solid state.....	44
1.2.3.4.1. Co-crystals	44
1.2.3.4.2. Amorphous Solid dispersion.....	45
1.2.3.5. Physical Modification	46
1.2.3.5.1. Milling	47
1.2.3.5.2. LAS Crystallization	49
1.3. CRYSTALLIZATION	51
1.3.1. Thermodynamic background.....	51
1.3.2. Nucleation.....	52
1.3.3. Crystal growth	54
1.3.4. Effect of supersaturation on nucleation and growth.....	55
1.3.5. Choice of solvent	56
1.4. LAS CRYSTALLIZATION TO IMPROVE DISSOLUTION PROPERTIES AND SOLUBILITY OF POORLY SOLUBLE DRUGS.....	57
1.4.1. Previous works.....	60

1.4.2. Control of process parameters	74
1.5. ADDITIVES IN CRYSTALLIZATION	81
1.5.1. Additives in LAS crystallization.....	82
1.6. THESIS OVERVIEW	89
CHAPTER 2.....	91
2.1. INTRODUCTION.....	95
2.1.1. The molecule: CRS 74.....	95
2.2. CHARACTERIZATION OF CRS 74.....	99
2.2.1. Methods.....	99
2.2.1.1. Particle size measurement.....	99
2.2.1.2. Density measurement.....	100
2.2.1.3. Thermal Analysis	100
2.2.1.3.1. Thermogravimetric Analysis (TGA)	100
2.2.1.3.2. Differential scanning calorimetric analysis (DSC).....	101
2.2.1.4. X-Ray Diffraction Analysis (XRD)	101
2.2.1.5. Scanning electron microscopy analysis (SEM)	102
2.2.1.6. Contact angle measurement (sessile drop method).....	102
2.2.1.7. In Vitro Dissolution Testing	103
2.2.1.7.1. Defining the operating conditions for in vitro dissolution.....	103
2.2.1.7.2. High Performance Liquid Chromatography (HPLC) to determine the content of the dissolved drug	104
2.2.1.7.3. Drug solubility in dissolution media.....	108
2.3. RESULTS AND DISCUSSION.....	109
2.3.1. Particle size, true density and morphology.....	109
2.3.2. Density	110
2.3.3. XRD analysis	110
2.3.4. TGA and DSC analysis	111
2.3.5. Determination of surface properties.....	114
2.3.6. Dissolution studies.....	116
2.3.6.1. High Performance Liquid Chromatography (HPLC) to determine the content of the dissolved drug	116
2.3.6.2. In vitro dissolution testing.....	120
2.4. CONCLUSIONS	123
CHAPTER 3.	125

3.1. INTRODUCTION.....	129
3.2. MATERIALS AND METHODS.....	130
3.2.1. <i>Materials</i>	130
3.2.2. <i>Methods for solubility measurements</i>	130
3.2.3. <i>Methods for Liquid Anti-Solvent (LAS) crystallization</i>	130
3.2.3.1. Characterization methods for particles in suspension.....	133
3.2.3.2. Characterization methods for dried powder.....	135
3.3. RESULTS AND DISCUSSION ON SOLUBILITY STUDY	136
3.3.1. <i>Measurement and correlation of solubility of CRS 74 in water-ethanol mixtures</i>	136
3.3.1.1. Experimental determination.....	136
3.3.2. <i>Correlation of solubility data by a UNIQUAC model</i>	139
3.3.3. <i>Theoretical yield of solid obtained by LAS crystallization</i>	144
3.4. RESULTS AND DISCUSSION ON CRYSTALLIZATION STUDY	145
3.4.1. <i>Characterization of particles in suspension</i>	146
3.4.1.1. Influence of the type of mixer on mixing	146
3.4.1.2. Influence of the type of mixer on particle size.....	149
3.4.1.3. Influence of flow rate in the T- mixer on particle size.....	154
3.4.1.4. Influence of addition time and steady state.....	159
3.4.2. <i>Characterization of solid particles obtained in experimental design</i>	162
3.4.3. <i>Comparative study of original CRS 74 and LAS recrystallized drug with T-mixer</i>	165
3.4.3.1. Particle size and morphology.....	165
3.4.3.2. XRD analysis	167
3.4.3.3. DSC analysis.....	167
3.4.3.4. Dissolution studies	169
3.4.3.5. Determination of surface properties.....	171
3.5. CONCLUSIONS	173
CHAPTER 4.....	175
4.1. INTRODUCTION.....	179
4.2. Materials and methods.....	182
4.2.1. <i>Materials</i>	182
4.2.2. <i>Methods</i>	184
4.2.2.1. Production of particles by LAS crystallization in presence of additives	184
4.2.2.2. Determination of solubility in presence of additive.....	186
4.2.2.3. Characterization methods.....	186
4.2.2.3.1. Measurements of particle size during the crystallization process.....	186

4.2.2.3.2. Powder physicochemical properties	187
--	-----

4.3. RESULTS AND DISCUSSION..... 188

4.3.1. CRS 74 solubility in presence of additives.....188

4.3.2. Effect of additives on yields of production of CRS 74 crystals.....190

4.3.3. Effect of presence of the additive in the aqueous phase on physical and surface properties of recrystallized powders192

4.3.1. Effect of the presence of the additive in the organic phase on physical and surface properties of recrystallized powders.....200

4.3.2. Effect of the presence of the additive in both, aqueous and organic phases205

4.3.3. Drug concentration in the organic phase.....210

4.3.4. Reorganized organic phase.....216

4.3.5. Improving process production222

4.3.6. Dissolution behaviour of recrystallized powders in presence of additives.....224

4.4. CONCLUSION..... 233

CHAPTER 5. 235

APPENDIXES 247

SYMBOLS AND ABBREVIATIONS 295

LIST OF FIGURES AND TABLES 301

REFERENCES 313

Abstract

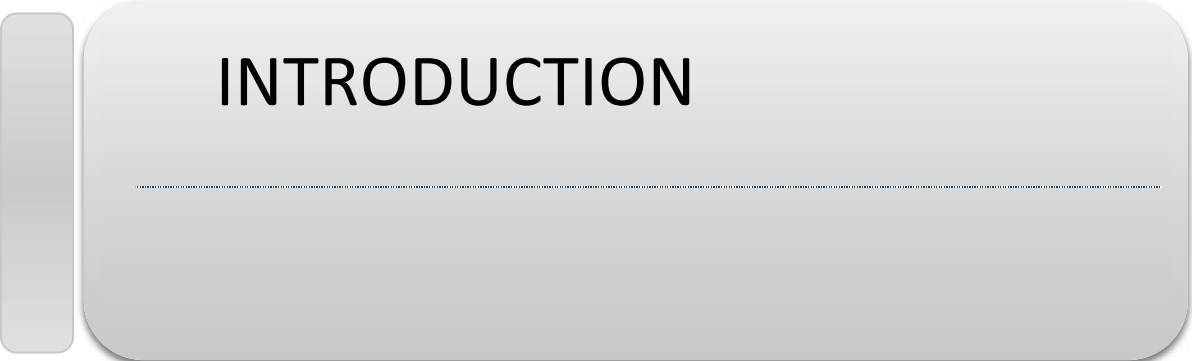
This study concerns a new antiretroviral drug named CRS 74. This molecule has a limited bioavailability because of its low aqueous solubility, poor water wettability and low dissolution rate. In an attempt to improve these properties, CRS 74 was recrystallized by using a Liquid Anti-Solvent (LAS) crystallization process. The chosen solvent is the ethanol and the anti-solvent the water. So solid-liquid equilibria in binary mixtures ethanol/water were measured at 30°C. The obtained solubility data were represented using UNIQUAC-based model. The experimental and calculated solubilities permitted to estimate the optimal ethanol/water mass ratios (25/75 % w/w) in order to maximize the theoretical yield of solid. A double-jet with premixing (T-mixer) has been used to mix the two solutions. Particles of recrystallized CRS 74 seemed more agglomerated and the dissolution profile was not modified compared to the original drug. Furthermore, the study of crystals obtained at the exit of the mixer showed that the growth and agglomeration rates of crystals are high. In an attempt to improve its dissolution properties, CRS 74 has been recrystallized using different additives to optimize process and formulation parameters. Conclusively, produced microcrystals exhibited significantly faster dissolution rates than the original CRS 74 crystals. The improved dissolution is attributable to the modification of the particle size of drug crystals and enhancement of wetting properties due to specific interactions between the drug and the additives.

Keywords: antiretroviral drug, solubility, bioavailability, dissolution rate, Liquid Anti Solvent crystallization, additive

Résumé

Cette étude concerne une nouvelle molécule antirétrovirale nommée CRS 74. Cette molécule présente une biodisponibilité limitée à cause de sa faible solubilité en phase aqueuse, sa mauvaise mouillabilité et sa faible vitesse de dissolution. Afin d'améliorer sa biodisponibilité, la molécule CRS 74 a été recristallisée par effet anti-solvant. Le solvant choisi est l'éthanol et l'anti-solvant l'eau. L'équilibre solide-liquide dans des mélanges binaires éthanol/eau a été mesuré à 30°C. Les solubilités obtenues ont été représentées en utilisant le modèle UNIQUAC pour le calcul des coefficients d'activité. Les solubilités expérimentales et calculées ont permis d'évaluer le ratio éthanol/eau optimum (25/75 % m/m) pour maximiser le rendement théorique en solide. Un mélange double jet avec pré-mélangeur type mélangeur en T a été choisi pour réaliser la cristallisation. Le solide cristallisé dans ces conditions semble plus aggloméré et son profil de dissolution comparé à celui du solide initial est inchangé. De plus, l'étude des cristaux obtenus en sortie de pré-mélangeur a montré que les vitesses de croissance et d'agglomération des cristaux sont élevées. Des additifs ont donc été utilisés en vue de modifier les propriétés de dissolution des cristaux, et d'optimiser les paramètres de formulation et de cristallisation. Les microcristaux produits en présence d'additifs présentent des profils de dissolution significativement plus rapides que les cristaux de la molécule initiale. Cette modification est attribuable à la modification de taille des cristaux et l'amélioration du mouillage en raison des interactions spécifiques entre la surface des cristaux et les additifs.

Mots clés : molécule active antirétrovirale, solubilité, vitesse de dissolution, cristallisation par effet anti-solvant, additifs, biodisponibilité



INTRODUCTION

INTRODUCTION

An increasing number of newly developed drugs are poorly soluble in aqueous media. Poorly water soluble drugs are specially challenging, as they cannot achieve dissolution and therefore they have a very difficult pass through the dissolving fluid to contact the absorbing mucosa and to be absorbed. If the dissolution process of the drug molecule is slow, due to the physicochemical properties of the drug molecules or formulation factors, then dissolution may be the rate-limiting step in absorption and will influence drug bioavailability. This is the case of a new compound, (2S, 3S, 5S)-2, -5 bis- [N-[N-[[N- methyl- N-[(2-isopropyl- 4-tiazolyl) methyl] amino] carbonyl] vanilyl] amino- 1,6- diphenyl- 3- hydroxyhexane, named **CRS 74**.

This promising candidate against HIV infections has high biological activity as disclosed in PCT documents WO 2005/111006; US 2010/7763733 (BOCKELMANN, M.A. et al, 2005; BOCKELMANN, M.A. et al, 2010) but its bioavailability is limited because of its low aqueous solubility and dissolution rate. Such properties pose difficulties not only in the design of pharmaceutical formulations but may result in biovariability. Moreover, because of their low solubility, such drugs require high doses to be administered in order to obtain their pharmacological effect, increasing the side effect incidence.

Drug dissolution is a prerequisite to drug absorption and clinical response for almost all drugs given orally. Solid forms that have been investigated for drug dissolution enhancement include salts, polymorphs and amorphous, among others. High energy polymorphs and amorphous formulations can achieve improved solubility but the system is at serious risk of crystallizing the thermodynamically stable form, even in the solid state (YU, 2011; RODRIGUEZ-SPONG et al., 2004). Such transformations can compromise the performance of the formulation.

To save time and resources in product development, relatively simple approaches should be tried first like crystallization. The Liquid Anti-Solvent (LAS) crystallization process is an attractive method. It requires mild conditions (ambient temperature and atmospheric pressure) with no requirement for expensive equipment. In LAS process, crystallization of solute is achieved by decreasing the solubility of solid in the system. This is

done by addition of a non-solvent component for solute called anti-solvent and miscible with the solvent.

This thesis presents efforts to develop and assemble tools required for improving the dissolution rate of CRS 74 by LAS crystallization process. It is divided into five chapters.

Chapter 1 is devoted to review literature themes. Many strategies to increase the dissolution rate of poorly soluble drugs and the key determinants of drug bioavailability are presented. It also focuses on topics of interest for our work, like properties of drugs influencing dissolution behavior. Emphasis was given to the LAS crystallization process.

The first elements of the understanding of the drug properties are given in **Chapter 2**. The original (as-received) molecule was characterized in terms of its physical properties (particle shape and size), crystal structure (crystalline, amorphous) and surface properties (wettability), solubility and dissolution properties in aqueous media. The methodology utilized and the results obtained are summarized in this Chapter. This characterization study was crucial to evaluate possible changes on drug properties after recrystallization by LAS process.

The solvent selection is one of the essential parameters to envisage any crystallization process. Therefore, the knowledge of the solubility of a target component in different solvents is required. The solubility of CRS 74 in ethanol and ethanol-water binary mixtures was measured in the temperature range of 5 -30°C and this study is presented in **Chapter 3**. Moreover, Chapter 3 outlines the experimental apparatus and procedures used for LAS crystallization studies. Two high jet velocity devices were tested to provide adequate mixing to incorporate the anti-solvent into the bulk solution. Recrystallized solids were compared to the original drug crystals in terms of particle size, solid state, thermal and dissolution properties.

Finally, LAS crystallization of CRS 74 in presence of additives is the subject of the **Chapter 4**. The study describes the use of different additives, which were introduced in the drug solution or in the anti-solvent or in both phases, to achieve optimum crystal properties of CRS 74. The effect of additives on the crystals particle size, dissolution kinetics and drug wettability could be investigated and are discussed in this Chapter.

Chapter 5 summarizes the main results of this research and suggests future work.

CHAPTER 1

Literature Review

Résumé Chapitre 1- Revue Bibliographique

Ce chapitre constitue une revue bibliographique sur l'amélioration de la biodisponibilité de médicaments peu solubles dans l'eau.

Un nombre croissant des nouveaux médicaments développés par l'industrie pharmaceutique sont peu solubles dans les milieux aqueux. L'industrialisation de ces médicaments devient donc un réel défi, du fait de leurs faibles vitesses de dissolution et, par conséquent, de leurs difficultés à traverser les membranes corporelles afin d'être absorbés. Si le processus de dissolution de la molécule est lent, en raison de ses propriétés physico-chimiques ou des facteurs de formulation, la dissolution peut être le facteur limitant de l'absorption et aura une influence directe sur la biodisponibilité du médicament.

Le terme médicament faiblement soluble dans l'eau fait généralement référence à un médicament dont la solubilité aqueuse est inférieure à 1mg/ml. Des exemples de médicaments couramment commercialisés qui sont peu solubles ou insolubles dans l'eau comprennent les analgésiques, les cardiovasculaires, les hormones, les antiviraux, les immunosuppresseurs et les antibiotiques (BERGESE, 2003). De plus un médicament ayant une meilleure solubilité dans l'eau peut être administré à une plus faible dose réduisant ainsi leurs effets secondaires systémiques. Ceci est crucial pour les médicaments ayant d'importants effets secondaires, tels que les antibiotiques, les antifongiques ou les antirétroviraux.

Afin d'améliorer la solubilité dans l'eau et la vitesse de dissolution de ces médicaments hydrophobes dans le *tractus gastro-intestinal* et/ou au site d'absorption, plusieurs techniques peuvent être utilisées, telles que la formation de sels, la complexation, par exemple avec des cyclodextrines, la vectorisation, des modifications chimiques ou encore des modifications physiques comme, par exemple, la réduction de taille du solide. En effet, la vitesse de dissolution est directement proportionnelle à la surface spécifique (loi de Noyes-Whitney). La dissolution peut donc être effectivement augmentée en réduisant la taille des particules. Par conséquent, de nombreux efforts ont été consacrés au développement d'opérations faciles, économiques et efficaces pour la fabrication de particules plus fines

Des micro ou nano-particules peuvent être produites par deux approches différentes. La première consiste, à partir d'un matériau massif, à le fractionner afin de réduire sa taille, c'est l'approche « *top-down* ». Par exemple, le broyage est une méthode « *top-down* » traditionnelle de réduction de la taille de matières particulaires (MENG, 2011).

La seconde au contraire, consiste en l'assemblage d'atomes ou de molécules (cristallisation), c'est l'approche « *bottom-up* ». La cristallisation par effet anti-solvant est considérée comme une opération *bottom-up*. Cette dernière est une approche efficace pour la précipitation de fines particules en solution, en présence d'un anti-solvant. L'introduction d'un anti-solvant dans une solution contenant le principe actif, génère une sursaturation élevée qui induit simultanément la nucléation, la croissance et l'agglomération des particules. Le grand défi de l'utilisation de cette opération est le contrôle des propriétés du solide cristallisé tels que la croissance des cristaux et leur agglomération.

Ces dernières années, de nombreuses méthodes de production de particules utilisant la cristallisation par effet anti-solvant ont été développées. Elles permettent un meilleur contrôle de la taille, de la cristallinité et de la morphologie des particules obtenues avec des méthodes « *bottom up* ». Le procédé de cristallisation est applicable à une large gamme de composés pharmaceutiques BCS de classes II et IV afin de produire des micro/nanoparticules. La diminution de taille des particules augmente la surface spécifique, ce qui augmente la vitesse de dissolution de médicaments peu solubles et, par conséquent, leur biodisponibilité (LIVERSIDGE et LIVERSIDGE, 2008).

Deux paramètres opératoires influençant les propriétés du solide formé ont été évalués dans ce chapitre : le mélange et l'utilisation d'additifs. Le premier est une étape essentielle pour maintenir un niveau constant et homogène de sursaturation dans le cristalliseur, induisant une nucléation uniforme et le contrôle de la formation de ces petits cristaux (DOUROUMIS et FAHR, 2006). Les additifs utilisés durant une opération de cristallisation peuvent être absorbés directement sur les particules formées permettant ainsi de produire des poudres avec des propriétés physico-chimiques optimales (ZIMMERMANN et coll., 2009). Il a été montré que la présence d'additifs dans la solution peut affecter les différents mécanismes comme la nucléation et/ou la croissance et l'agglomération et donc les propriétés du solide, comme sa solubilité, le faciès des cristaux le composant (KUBOTA et coll, 2000; GARNIER et coll, 2002; VETTER et coll., 2011), et la forme cristalline (CHONG et coll, 2002; SONG et CÖLFEN, 2011). De plus, l'adsorption des additifs sur la surface des particules peut

provoquer une inhibition de la croissance et de l'agglomération, en occupant des sites spécifiques et, par conséquence arrêter ou ralentir ces deux processus.

1.1. THE BIOAVAILABILITY OF DRUGS

1.1.1. Absorption and bioavailability

The term bioavailability is usually defined as the rate and extent of absorption of a drug from its dosage form into the systemic circulation (BLANCHARD and SAWCHUK, 1979).

By definition, when a medication is administered intravenously, its bioavailability is 100%. However, when a medication is administered via other routes (such as orally), its bioavailability (oral bioavailability) is usually less than 100%, caused by degradation or metabolism of the drug prior to absorption, incomplete absorption and first-pass metabolism not seen with intravenous administration (OSCIER et al., 2007).

The therapeutic effect of drugs depends on the drug concentration at the site of action. The absorption of the drug into the systemic circulation is a prerequisite to reach the site of action for all drugs, except those drugs that are applied at the site of action, or those that are intravenously injected.

When a drug is taken orally administration (gastrointestinal route) it passes through the mouth, esophagus, stomach, duodenum, jejunum (small intestine), colon (large intestine) (see Figure 1.1) and finally leaves the body if not absorbed. Indeed, it must withstand the effect of several physiological fluctuations like a large variation in pH along the gastrointestinal tract (Table 1.1), the presence of bile salts, food, enzymes, bacteria and the motility of the gut.

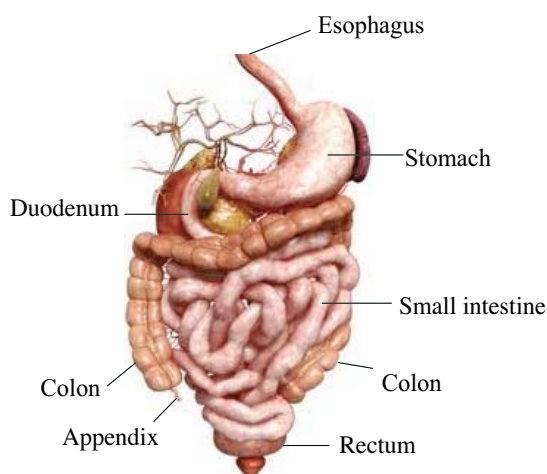


Figure 1.1. Anatomy of digestive tract (Modified from: MARTINEZ et al., 2002).

Table 1.1. Transit time and pH conditions along the GI tract (MARTINEZ et al., 2002).

GI segment	Transit time	pH
Stomach	2 h	2.0 ± 1.9
Duodenum	10 min	6.6 ± 0.5
Jejunum	2 h	7.4 ± 0.4
Ileum	1 h	7.5 ± 0.4
Colon	36-72 h	7.0 ± 0.7

Absorption of drugs after oral administration of pharmaceutical dosage forms (drug powder, tablet, capsule...) may occur at the various body sites between the mouth and rectum. After oral administration, the pharmaceutical product reaches quickly the stomach passing through esophagus. However, the small intestine has the largest surface for drug absorption in GI tract (PODCZECK et al. 2007).

After disintegration of the pharmaceutical dosage form in the gastrointestinal tract, the first requirement for absorption is that the drug dissolves. In fact, only drug that is dissolved has the ability to permeate the intestinal membrane. The oral bioavailability of a particular drug is thus determined by the magnitude of the solubility and/or permeability limitations that exist for it within the GI tract, which is an aqueous environment. These two aspects, illustrated in Figure 1.2, form the basis of the Biopharmaceutical Classification System (BCS), which is incorporated in the guidelines of the Food and Drug Administration (FDA) established by AMIDON et al. (1995) and often cited in the literature. According to the BCS, four different types of drug absorption regimes are distinguished. They are explained in Table 1.2.

According to Biopharmaceutical Classification System (BCS), *Class I* drugs dissolve rapidly in an aqueous environment and are rapidly transported over the absorbing membrane.

For *Class II* drugs, the dissolution rate in vivo is usually the rate limiting step in drug absorption. Drugs of this group are poorly water soluble.

Class III drugs dissolve readily, but cannot penetrate biomembranes of GI tract.

Class IV drugs are characterized by poor solubility and poor permeability. Oral administration is not recommended (LINDENBERG et al., 2004) and, subsequently, *Class IV* drugs are often administered parentally using formulations containing solubility/permeability enhancers.

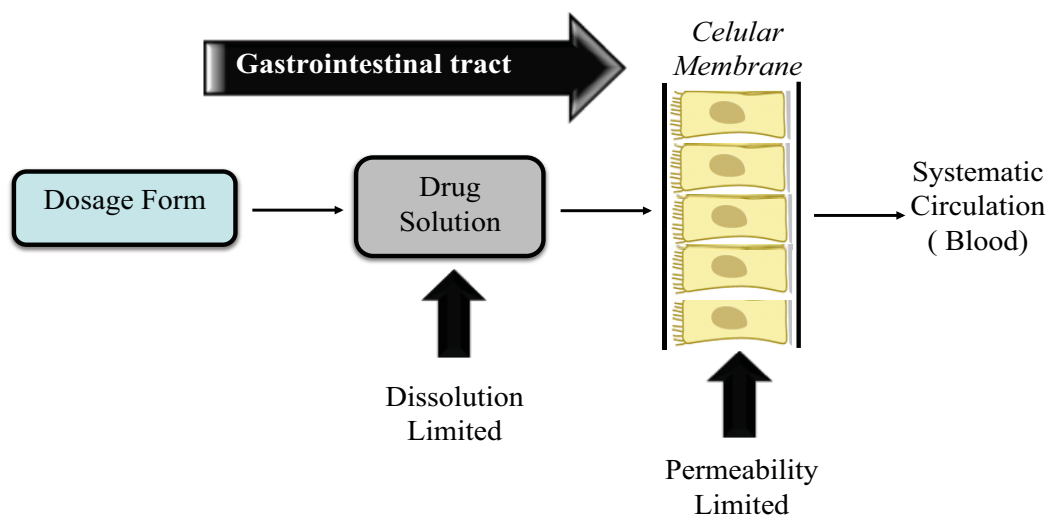


Figure 1.2. Parameters limiting absorption of drugs taken orally (Adapted from ENGMAN, 2003).

Table 1.2. Biopharmaceutical Classification System according to AMIDON (1995).

Class	Solubility in aqueous environment	Permeability over (intestinal) membrane
I	High	High
II	Low	High
III	High	Low
IV	Low	Low

It is clear that, depending on the classification of the drug, different strategies can be applied to increase or accelerate the absorption of a drug taken orally, either increasing the amount of dissolved drug or increasing the permeability of the dissolved drug through the absorbing membrane.

To sum up, *Class I* drugs do not need a formulation strategy to increase the absorption.

The rate of absorption of *Class II* drugs can be enhanced by accelerating the dissolution. This has proven to be effective in many studies (YELLELA, 2010; PATEL et al., 2011; VIÇOSA et al., 2012).

The strategy for *Class III* drugs is to increase the permeability of the absorbing membrane. Numerous studies deal with increasing membrane permeability in the gastrointestinal tract (NEELAM et al., 2012; SHAIKH et al., 2012).

For a *Class IV* drug, both dissolution as well as permeability must be increased.

Over 90% of the marketed drugs qualify under *Class II* and *Class IV* (GRIFFIN, 2012). The oral bioavailability of these drug compounds is limited due to slow drug dissolution in the gastrointestinal tract. Therefore, it is desirable to improve the solubility of these drug compounds by using various pharmaceutical technologies that will be discussed later in this Chapter.

1.1.2. Poorly-water soluble drug molecules

Poorly-water soluble drugs describe a heterogeneous group of drug compounds that exhibit poor solubility in water but are typically soluble in various organic solvents.

The degree of water solubility for drug compounds can be defined as slightly soluble (1-10mg/mL), very slightly soluble (0.1-1 mg/mL), and practically insoluble (<0.1mg/mL) (MENG, 2011)

The expression poorly-water soluble drug generally refers to a drug whose aqueous solubility falls into the range of slightly soluble and below. Examples of commonly marketed drugs that are poorly soluble or insoluble in water include analgesics, cardiovasculars, hormones, antivirals, immune suppressants and antibiotics (BERGESE, 2003). A drug with improved water solubility can be administered in a lower concentrated dose, with a reduction

of local and systemic side-effects. This is crucial for drugs with important side-effect profiles, such as antibiotics, antifungals or antiretrovirals.

The drug we deal with in this thesis belong to the category of insoluble drugs; at the best of our knowledge, it is not yet classified according to the BCS classification.

1.2. ENHANCEMENT OF SOLUBILIZATION AND BIOAVAILABILITY OF POORLY SOLUBLE DRUGS

1.2.1. Concept of dissolution

Drug must first be dissolved in the medium at the absorption site. The process that a drug particle dissolves is called dissolution.

The dissolution of a solid in a solvent is a rather complex process determined by a multiplicity of physicochemical properties of solute and solvent. However, a more intuitive approach was interestingly proposed by Berge (2003) to describe the dissolution of a solid, regardless of the mechanism by which dissolution occurs, as a consecutive process driven by energy changes (Figure 1.3).

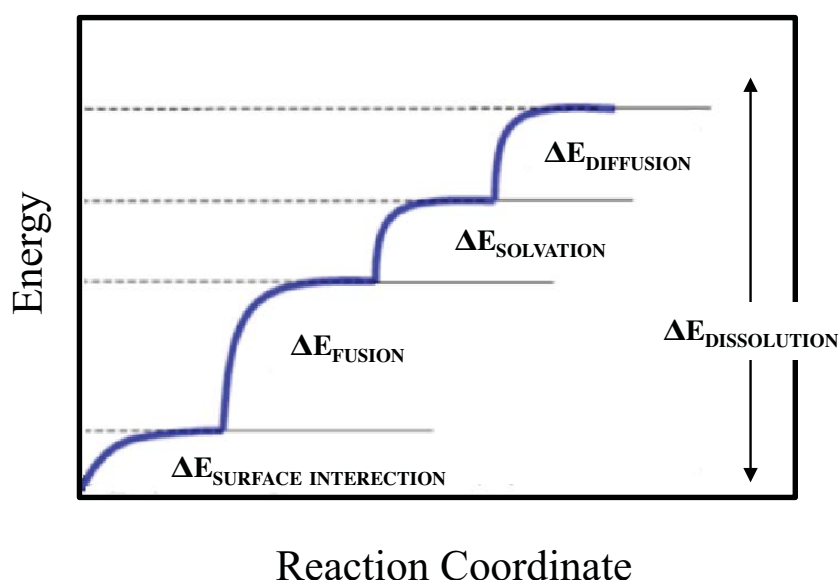


Figure 1.3. Energy diagram of the dissolution of a solid phase. Adapted from BERGESE, 2003.

The first step consists in the contact of the solvent with the solid surface (wetting), which leads to the production of a solid-liquid interface. Following the description given by Bergese (2003), the break of the molecular bonds of the solid and the molecules passage to the solid-liquid interface (solvation) are the second and third step.

The final step sees the transfer of the solvated molecules from the interfacial region into the bulk solution (diffusion). Each stage requires a certain amount of energy to be completed; the target of drug activation is to lower the overall dissolution energy.

Solvation and diffusion depend on solid and solvent chemical nature and on the system conditions (temperature, mechanical agitation...), while wetting and fusion also depend on microstructure of the solid. In the case of a given poorly water-soluble drug that dissolves into the gastrointestinal tract it is not possible to modify neither the drug molecules nor the dissolution environment (solvent and system conditions). So the efforts in enhancing drug dissolution rate are essentially spent (in trying) to tailor the drug microstructure.

To outline the properties of solids that determine their dissolution rate we start from the simplest model for the dissolution of a solid in a solvent, i.e. the Nernst's film theory (1904), considering a single particle dissolving into a large volume of solvent, under agitation (Figure 1.4).

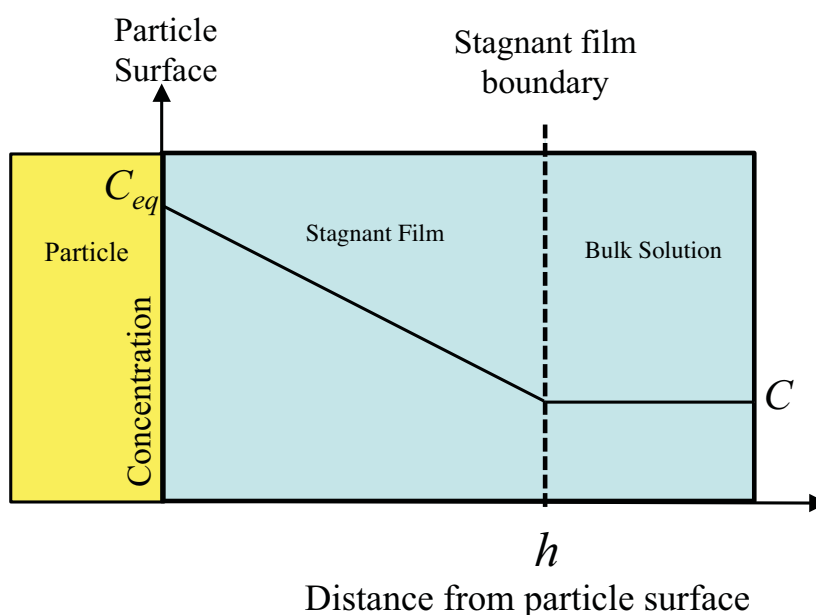


Figure 1.4. Dissolution of a single particle in a large volume of solvent (Model of Nernst). Adapted from BERGESE, 2003.

The concentration of the pure molecule at the solid surface, is assumed to be equal to the saturation concentration, C_{eq} ; the concentration in the bulk solution will be denoted with C . Despite of agitation, it can be assumed that the solid is surrounded by a stagnant film of liquid of constant thickness. Solid molecules spontaneously diffuse through this film and reach the bulk solution. If we assume steady state conditions, diffusion is described by the Fick's first law:

$$J = -D_i \frac{\partial C_i}{\partial s} \quad (1.1)$$

where J_i is the diffusion current (defined as the amount of material i passing per unit time perpendicularly through a unit surface area), C_i the molar concentration of molecule i , D_i the diffusion coefficient of molecule i , and $\partial C_i/\partial s$ the concentration gradient through the film.

In this particular case, $\partial C_i/\partial s$ is constant, since in the stagnant film laminar condition holds. To sum up, there is a linear concentration gradient from the solid surface to bulk solution that can be analytically expressed as $\partial C_i/\partial s = (C_{i,eq} - C_i)/h$. Using this expression, and denoting the volume of the solvent V and the surface area of the dissolving solid A , Equation (1.2) becomes:

$$\frac{V}{A} \frac{dC_i}{dt} = \frac{D}{h} (C_{i,eq} - C_i) \quad (1.2)$$

The more familiar form of the dissolution equation (also called Noyes-Whitney equation), which describes the increase of the mass of solute dm_i in the time dt due to dissolution, is obtained rearranging Equation (1.2):

$$\frac{dm_i}{dt} = \frac{D_i}{h} A_{particles} M_i V (C_{i,eq} - C_i) \quad (1.3)$$

where M_i is the molar weight of solid.

To eliminate the saturation effect of the solvent and increase the ability of the solid to dissolve the expected amount of drug, dissolution methods on “sink condition”, have been proposed in the literature (GIBALDI and FELDMAN, 1967; ROHRS, 2001, GOWTHAMARAJAN and SINGH, 2010). In practice, if the quantity of the medium dissolution is sufficiently large, between 3 and 10 times, of the volume needed to completely solubilize the drug, it is said that we are on sink-condition (ABDOU, 1989; ROHRS, 2001; GOWTHAMARAJAN and SINGH, 2010). When sink condition holds ($C \ll C_{eq}$), Equation simplifies to:

$$\frac{dm_i}{dt} = \frac{D_i}{h} A_{particles} M_i V C_{i,eq} \quad (1.4)$$

1.2.2. Dissolution testing for poorly-water soluble drugs

For a dosage form to produce its effect after oral administration, drug must be released and generally should be dissolved in the fluids of the gastrointestinal tract. Drug dissolution testing plays an important role as a routine quality control test and to characterize the quality of the product (FDA, 1997).

Dissolution from the dosage form involves mainly two steps: liberation of the drug from the formulation matrix (disintegration) followed by the dissolution of the drug (solubilization of the drug particles) in the liquid medium. The overall rate of dissolution depends on the slower of these two steps. In the first step of dissolution, the cohesive properties of the formulated drug play a key role.

For solid dosage forms, these properties include disintegration and erosion. If the first step of dissolution is rate-limiting, then the rate of dissolution is considered *disintegration controlled*. In the second step of dissolution (i.e., solubilization of drug particles), the physicochemical properties of the drug such as its chemical form (e.g., salt, free acid, free base) and physical form (e.g., amorphous or polymorph and primary particle size) play an important role. If this latter step is rate-limiting, then the rate of dissolution is *dissolution controlled*. This is the case for most poorly soluble compounds in immediate-release

formulations whose solubility is less than 1–2 mg/L in the pH range of 2–8 (GOWTHAMARAJAN and SINGH, 2010).

For poorly soluble compounds, dissolution study is particularly important. Different techniques have been used to improve the maximum dissolvable dose in the dissolution medium in discriminatory dissolution studies, such as addition of organic solvents to aqueous medium (DANIEL et al., 2012), increase of the dissolution medium volume, pH changes (TALARI et al., 2009), and addition of surfactants (JINNO et al., 2000; ROHRS, 2001).

Some dissolution parameters involved in the phase transformation can affect dissolution method efficiency. The dissolution of most solids is an endothermic phenomenon, thus increases in temperature tend to increase the speed, which the substance dissolves. Because of this, the United States Pharmacopeia recommends $37\pm 0.5^{\circ}\text{C}$ media temperature for dissolution tests.

The dissolution kinetics depends on the local mass transfer coefficient (which in turn is a function of suspension state and the local turbulence level). Because of this some authors have established a relationship between the intensity of agitation and dissolution rate constant ($\text{cm}\cdot\text{sec}^{-1}$). Generally, higher stirring rates result in higher dissolution rates and ideally stirring conditions must somehow simulate peristalsis physiological. The diffusion rate can decrease too, with increasing media viscosity, which implies a decrease of the dissolution rate. Another parameter that can influence the dissolution rate of a solid in a liquid is the solid wettability. For complete drug dissolution it is necessary that wetting is complete. The ability of wetting of a solid by a liquid is expressed by the contact angle.

Countless are the variables that can modify the results of dissolution tests. All should be considered, but some must be strictly monitored to obtain reliable results. Finally, construction of *in vitro-in vivo* correlation provides the most valuable data for selection of the most appropriate dissolution method and testing conditions that can be prognostic of *in-vivo* dissolution.

Micro/nanonization during crystallization (RASENACK and MÜLLER, 2002; RASENACK and MÜLLER, 2004; BADAWI et al., 2011; VIÇOSA et al., 2012), surface modification (HAN et al., 2011) and crystal structure modification (EERDENBRUGH et al., 2009) may improve the dissolution rate of poorly water-soluble APIs.

Several studies have shown that modification of the crystalline form of the drug, by the inclusion of specific additives increases the rate of dissolution of the pharmaceutical form, which can strongly affect the physicochemical properties and kinetic of absorption of the drug from the final product (SHEKUNOV and YORK, 2000).

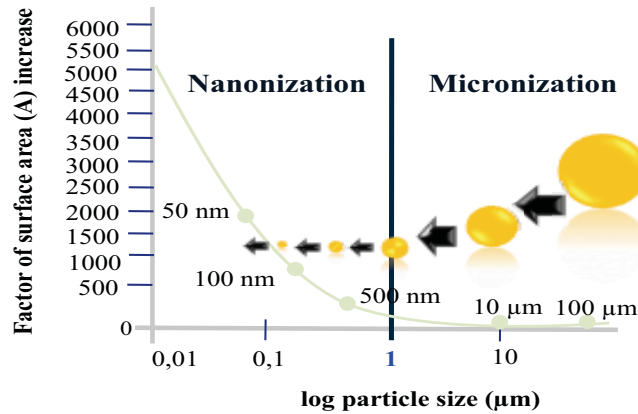
It is known that a substance in crystalline form has a lower solubility, while at the same amorphous form has higher solubility and low thermal stability. Formulations where the drug is mainly crystalline and amorphous or metastable forms, are much more soluble than the drug-containing highly crystalline. Drug amorphization can be used to promote a quicker therapeutic effect by enhancement of drug absorption rate and dissolution rate. However, formulations containing metastable amorphous forms are less stable than those prepared with the crystalline forms of the drug. Because there is generally a risk of crystallization during the production process and shelf life of the product. Such products are generally very reactive and less stable when exposed to heat and mechanical stress, and very susceptible to moisture absorption (SINGHAL and CURATOLO, 2004)

The dissolution rate can be enhanced by size reduction that can be explained by the Noyes-Whitney equation (Equation. 1.3). This is possible due to the special features of drug size reduction:

1. Increased surface area A ;
2. Increased saturation concentration and dissolution pressure ($\uparrow C_{eq}; p_x$);
3. Increased adhesiveness to surfaces/cell membranes (see Figure 1.5).

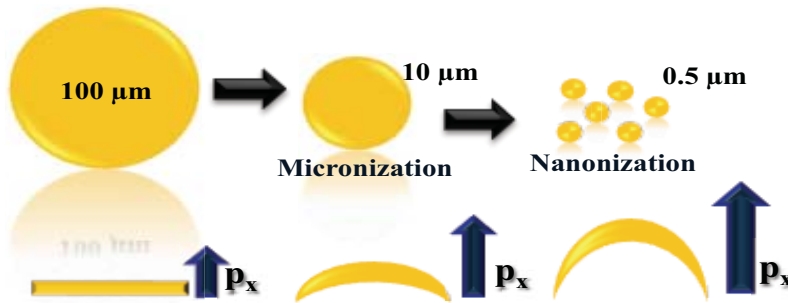
The increased area increases the dissolution rate. Moreover the transfer of particles from the macrosize range to the nanodimension changes their physico-chemical properties. This strategy also modifies the saturation concentration of the drug in solution ($C_{i,eq}$), which means an additional increase with increased speed dissolution of particles in this size range. In addition, the size reduction can increase the adhesiveness into the skin due to the increase in the saturation, leading to a larger concentration gradient and the larger gradient promotes penetration (MÜLLER et al., 2011).

1. Increase in surface area (A)



2. Saturation solubility (C_{eq})

- = f (size)
- = f (curvature)
- = f (dissolution pressure- p_x)



3. Adhesiveness

- = f (size)
- = f (contact area)

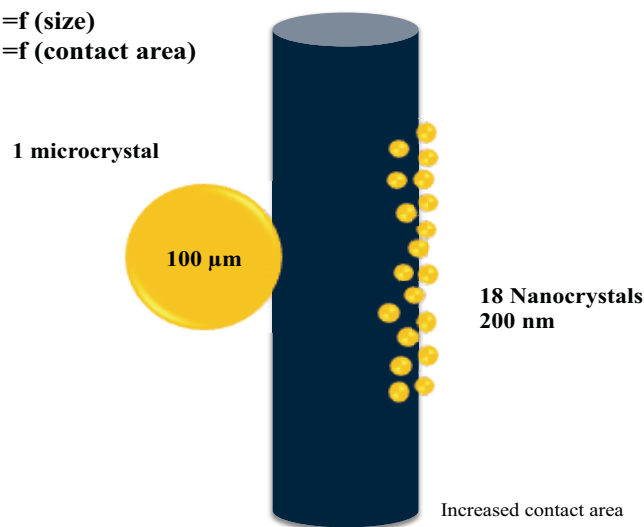


Figure 1.5. Features of size reduction: 1. Increased dissolution velocity due to increased surface area ; 2. Increased saturation solubility due to increased dissolution pressure of strongly curved small nanocrystals (upper); 3. Increased adhesiveness of reduced material due to increased contact area of small versus large particles. Modified from MÜLLER et al., 2011.

1.2.3. Strategies to increase the amount of dissolved drug at the absorption site

To enhance the aqueous solubility and the dissolution rate of hydrophobic drugs at the absorption site several strategies can be used. These methods (alteration of solvent composition, complexation, carrier system, chemical modification and physical modification) are shown in Figure 1.6. The following section is a brief review on the state of the art of this topic.

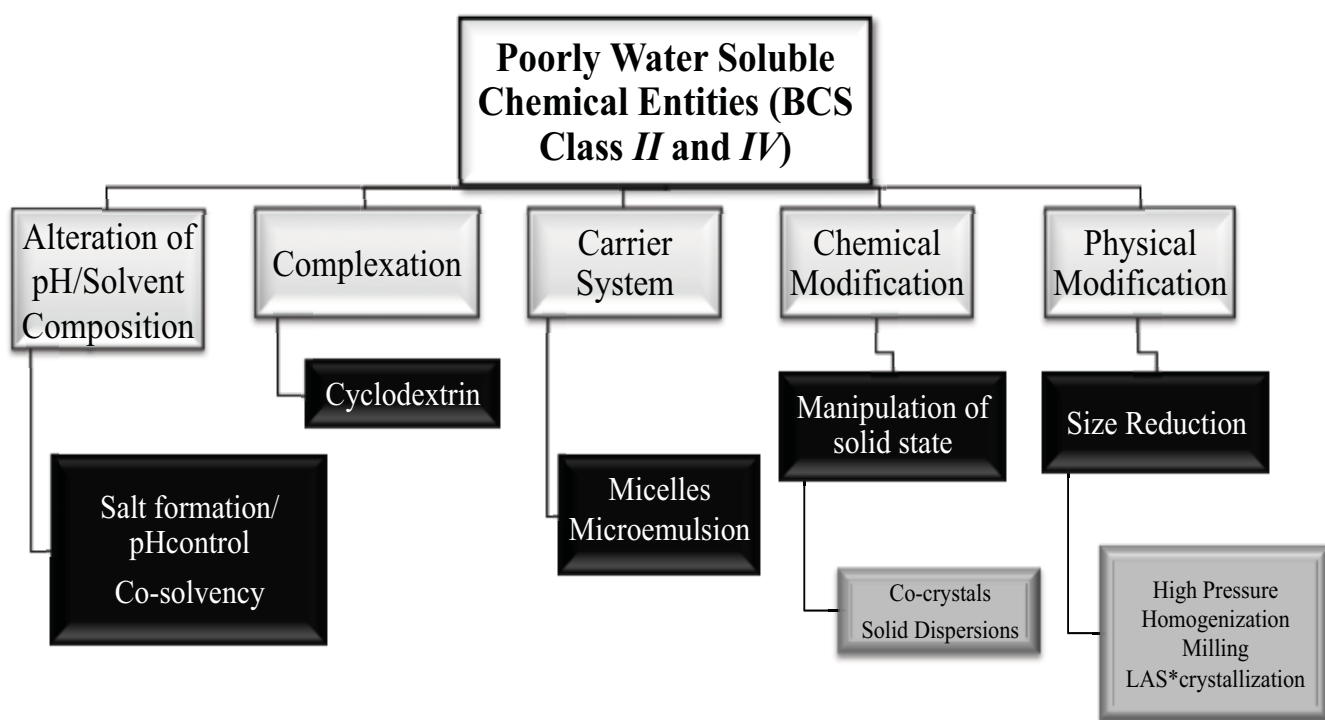


Figure 1.6. Strategies to increase the amount of dissolved drug at the absorption site (Modified from LAKSHMI et al., 2012).

1.2.3.1. Alteration of pH and solvent composition

1.2.3.1.1. Salt formation/pH control

It is well documented that the bioavailability of pharmaceuticals products is influenced by the changes in pH within the GI tract. The absorption of drug is largely dependent on

diffusion, which varies with pH of the individual regions within the GI tract, pKa of the drug, and permeability, that depends of regional pH effects upon drug ionization.

Poorly water soluble drugs can be protonated (base) or deprotonated (acid) and may potentially be dissolved in water by applying a pH change. The presence of salts can act as alkalising or acidifying agents, and may increase the solubility of weakly basic or acid drugs. After pH adjustment, ionisable compounds are stable and soluble at selected pH.

Salts of acidic and basic drug have, in general higher solubility values than their corresponding acid or basic forms (GRAHAM et al., 1986).

Generally a salt of a drug is frequently less stable chemically compared to crystalline solid. At pH extremes drug is dissolved, which can increase the chance of hydrolysis, catalyze or other degradation mechanisms (VENKATESH et al., 1996). Another disadvantage is the risk for precipitation upon dilution with aqueous media having a pH at which the compound is less soluble. Intravenously this may lead to emboli, orally it may cause variability and toxicity (local and systemic) related to the use of non physiological and extreme pH (GIACONA et al., 1982).

1.2.3.1.2. Cosolvency

Co-solvent system works by reducing the interfacial tension between the aqueous solutions and hydrophobic solute by solvent blending or cosolvency. This method is based on the mixing of solvents of different polarities to form a solvent system of optimum polarity to dissolve the solute. Co-solvent formulations of poorly soluble drugs can be administered orally and parentally (THELLY et al., 2000; BOYLAN, 1987). This type of formulation can increase the solubility of poorly soluble compounds several thousand times compared to the aqueous solubility of the drug alone. However, these modifications can cause serious side effects due to solvents use.

Yeh (2009) realized a formulation study of tenoxicam, a poorly water-soluble drug, by use of a ternary cosolvent system, DMSO/polyethoxylated castor oil/ethanol system, that had significantly enhanced the solubility. Additionally, the relative bioavailability was improved. This study provided a novel strategy for improving tenoxicam solubility, but also helps further scientific knowledge for the development of parenteral formulations.

Seedher and Bhatia (2003) investigated that the aqueous solubility of celecoxib, rofecoxib and nimesulide could be enhanced significantly by using ethanol as the second solvent and PEG-400-ethanol had highest solubilization potentiality among the mixed solvent systems.

Large quantities of organic solvent used in cosolvent formulations may result in the loss of solvent capacity of the formulation upon dilution in aqueous media *in vivo*. For drugs *Class II* and *IV*, administered orally, the use of cosolvents technique may not increase the bioavailability dramatically because the poorly soluble drug can typically uncontrollably precipitate into a crystalline or amorphous precipitate. In this case, dissolution of this precipitate is required for oral absorption. A major concern for the use of this technique is the biocompatibility, tolerability and toxicity of used solvents formulations and the loss of solvent capacity in aqueous media *in vivo*.

1.2.3.2. Inclusion complexes/complexation

1.2.3.2.1. Cyclodextrin (CD)

Another approach used to improve drug solubilization is based on the formation of inclusion complexes between molecular assemblies and drug molecules, like cyclodextrins (CD). CDs are cyclic oligosaccharides composed of glucopyranose units and adopt a truncated cone structure with hydrophobic cavity (SAENGER, 1980).

Cyclodextrins and their derivatives have been employed as complexing agents to increase water solubility, dissolution rate and bioavailability of lipophilic drugs for parenteral or oral delivery (SRIDEVI et al., 2003; MORIWAKI et al., 2008).

An inclusion complex is produced by inclusion of a non polar molecule or the nonpolar region of a molecule (known as the guest) into the nonpolar cavity of another molecule or group of molecules (known as the host), as shown in Figure 1.7. When the guest molecule enters the host molecule, they are temporarily locked or caged within the host cavity. Giving rise to beneficial modifications of guest molecules, as solubility improvement for example. Furthermore these complexes have a broad range of utilizations in different applications; they are used in the food and cosmetics industries and the pharmaceutical sector (DEL VALLE, 2004).

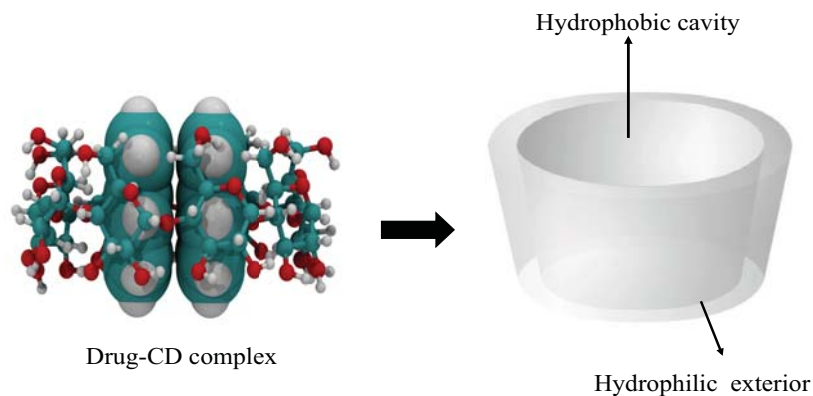


Figure 1.7. Schematic illustration of the association of free cyclodextrin (CD) and drug to form drug-CD complexes and a truncated cone structure of CD (Modified from: DEL VALLE, 2004).

The three cyclodextrins α -, β -, and γ - (CD) are composed of six, seven, and eight glucopyranose units, and are produced in industrial scales (MORIN-CRINI and CRINI, 2012). These agents have a torus structure with primary and secondary hydroxyl groups orientated outwards, as shown in Figure 1.8.

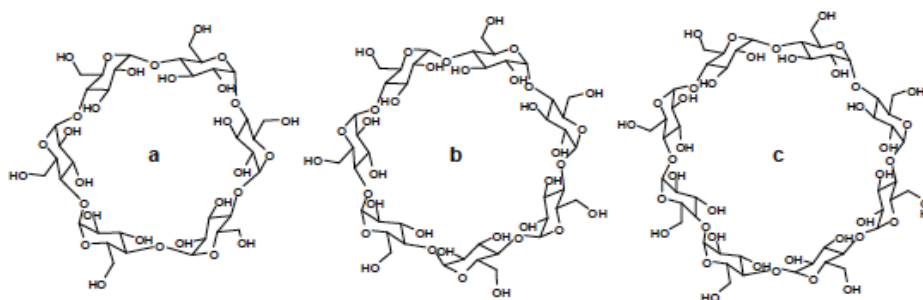


Figure 1.8. Schematic representations of Cds (a) α - CD, (b) β -CD, (c) γ -CD. Containing 6,7 and 8 glucopyranoside units, respectively (MORIN-CRINI and CRINI, 2012).

For *Class IV* drugs, the cyclodextrin complexation may not improve their oral bioavailability. However, cyclodextrins are able to improve aqueous solubility of some large lipophilic molecules leading to increase drug availability at the mucosal surface. This will frequently lead to increased oral bioavailability (LOFTSSON et al., 2005).

Even though CD seems to be ideal carriers, they possess some limitations, related to toxicological considerations, formulation and production cost. In general, the complexation

efficiency of cyclodextrins is low and thus relatively large amounts of cyclodextrins are needed to complex small amounts of drug (LOFTSSON and O'FEE, 2003).

1.2.3.3. Carrier System

1.2.3.3.1. Micelles

Micelle solution is another formulation strategy to increase drug solubility. According to IUPAC (Compendium of Chemical Terminology) (1972) micelle solubilization can be defined as colloidal association in a solvent system for solubilization of a component into or on micelles.

Of the above mentioned, for colloidal association, the use of surfactants into the media is the most popular method for micelle formation. Various synthetic surfactants can simulate the surfactants present in the gastrointestinal fluid, e.g., bile salts, lecithin, cholesterol and its esters (YALKOWSKY, 1999).

Surfactants are molecules with distinct polar and non polar regions. In water, as the concentration of surfactant increases above a critical value, its molecules self-associate into soluble structures called micelles. The concentration at which they begin to form is called the critical micelle concentration (CMC) (FLORENCE and ATTWOOD, 1981 ; MYRDAL and YALKOWSKY, 2002). These micelles are normally spherical with the nonpolar regions of surfactant molecules gathered in the center (core) and surrounded by a shell of the polar region which are in contact with the water.

Micelle is a nanoparticle structured by one hydrophilic shell and one hydrophobic core (Figure 1.9), which are capable of encapsulating drug molecules, resulting in reduction in the interfacial tension and improved solubility of the drug in the medium (SUBHASHI et al., 2009).

The stability of drug carrier micelles is the biggest challenge for the use of this technique. When in aqueous media, *in vivo* micelles become much diluted by blood (below CMC) and may be gradually disintegrated into unimers. In addition, the low drug loading efficiency and the difficulty in transporting through cell membranes, has also retarded the development of effective micellar drug (KIM et al., 2010).

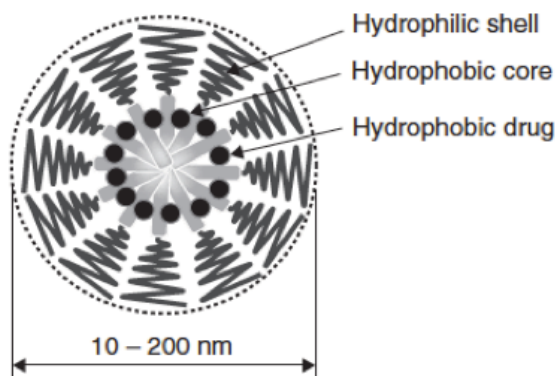


Figure 1.9. Schematic representation of a hydrophobically assembled polymer micelle. The hydrophobic core loading lipophilic drugs is protected from the environment by the hydrophilic shell (KIM et al., 2010).

1.2.3.3.2. Micro/Nanoemulsion

Microemulsion consists of dispersions of two immiscible or partially miscible liquids (water in oil or oil in water) that present droplets ranging from 5-100 nm. They are thermodynamically stable and do not require power supply for their formation (ROSSI et al., 2007). The main difference between microemulsions and nanoemulsions is that microemulsions are self-assembling nano-scale emulsions, whereas nanoemulsions are nano-scale emulsions formed under intense mechanical shear (WHITESIDE and GRZYBOWSKI, 2002).

All types of emulsions should be prepared with a certain amount of surfactant. Surfactants can promote the formation of emulsion as they reduce the interfacial tension between oil and water by attaching to the liquid-liquid interface (SHINODA, 1967). The main difference between surfactant micelles and emulsion is the liquid phase. Typically, micelles are formed by adding surfactant to a single liquid phase, either oil (reversed micelles) or water, whereas emulsions are prepared by adding surfactant to a double liquid phase (oil and water)

Microemulsions are suitable carriers for poorly water soluble drugs, because they can be dispersed easily in gastrointestinal juice in microemulsion form. Furthermore, microemulsions can enhance the drug absorption due to their small particle size. Also the drugs can be stored longer because of the stability of microemulsions (MALMSTEN, 1999).

The disadvantage of microemulsions as drug carriers is that the toxicity of the drugs tends to increase due to a large amount of the surfactant utilized in microemulsion formulation.

1.2.3.4. Manipulation of solid state

1.2.3.4.1. Co-crystals

Co-crystals are solids that are crystalline materials composed of two or more molecules in the same crystal lattice (FDA, 2011). The formation of pharmaceutical co-crystals has gained attention as attractive alternate solid forms for drug development. Their formation involves incorporation of a given API with one or more pharmaceutically acceptable molecule (Coformers) in the crystal lattice (Figure 1.10), that is a solid under ambient conditions. The co-crystals do not affect pharmacological activity of API but can improve physical properties, such as solubility, hygroscopicity, compaction behavior (RODRIGUEZ-HORNEDO et al., 2007 ; ZAWOROTKO, 2008). Of these properties, solubility is the most widely appreciated in the literature.

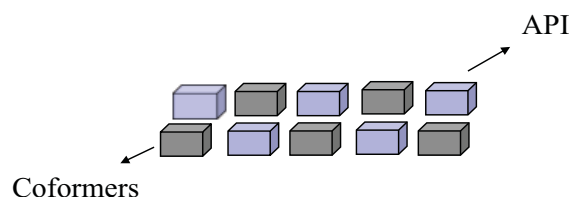


Figure 1.10. Possible solid forms of a drug cocrystal . Modified from ALHALAWEH, 2012).

Poor aqueous solubility can compromise drug performance, and co-crystals are an emerging strategy to design materials with desirable properties. Co-crystal solution phase behavior was first investigated by Higuchi and Connors (HIGUCHI and CONNORS, 1965).

Co-crystals are usually prepared by evaporation from a solution containing stoichiometric amounts of components (co-crystal formers). However sublimation, blending of powders, sonication, growth from melt, slurries and grinding of the components together are suitable methodologies (KRISHNAIAH, 2010).

The major disadvantage of co-crystals technique is the notoriously difficult situation of these systems related to their preparation— it has been known to take 6 months to prepare a single co-crystal of suitable quality for single X-ray diffraction analysis (PORTALONE and

COLAPIETRO, 2004). In addition, for solution co-crystallization, the two components must have similar solubility; otherwise the least soluble component will precipitate out exclusively. On the other hand, similar solubility of two components alone will not promise success. It has been recommended that it possibly useful to consider polymorphic compounds which exist in more than one crystalline form as co-crystallising components (BLAGDEN, 2007).

1.2.3.4.2. Amorphous Solid dispersion

In amorphous solid dispersion, drug molecules are dispersed molecularly but irregularly within amorphous excipient (biologically inert matrix) (Figure 1.11). Chiou and Riegelman (1971) defined the term solid dispersion as “a dispersion of one or more active ingredient in an inert carrier or matrix at solid state prepared by the melting (fusion), solvent or melting-solvent method”. This method, involves the formation of eutectic mixtures of drugs with water-soluble carriers by the melting of their physical mixtures.

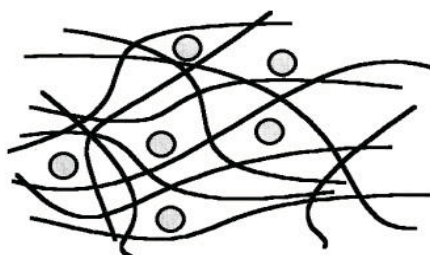


Figure 1.11. Amorphous solid dispersion (From GHASTE et al., 2009).

There are various reasons for the improvement of solubility of poorly water-soluble drug using solid dispersion technology. The reasons for solid dispersion or advantages of solid dispersions are as follows: particle size reduction, improved wettability, higher degree of porosity, drugs in amorphous state (KUMAR et al., 2011).

The major disadvantages of solid dispersions are related to their instability. During processing (mechanical stress) or storage (temperature and humidity stress) the amorphous state may undergo crystallization and dissolution rate decrease with ageing. The effect of moisture on the storage stability of amorphous pharmaceuticals is also a significant concern. By absorbing moisture, phase separation, crystal growth or a change from metastable crystalline form to stable form can take place which leads to the reduction of drug solubility, dissolution rate, and consequently a bad *in vivo* drug performance (WANG et al., 2005).

1.2.3.5. Physical Modification

It has been proven, as expressed by Noyes-Whitney (equation 1.3, section 1.2.1), that the dissolution rate is directly proportional to the specific surface area, which can be effectively increased by reducing the particle size. Therefore, considerable efforts have gone into developing reliable and efficient methods for the manufacture of fine particles.

Micro- or nano-particles can be produced by two different technology approaches as illustrated in Figure 1.12, called “top-down” and “bottom-up” technologies. Top-down technologies start with coarse materials and apply forces to break down into micro or nano-particles, while bottom-up technologies start with the molecules in solution and the molecules are aggregated to form the solid particles (RABINOW, 2004).

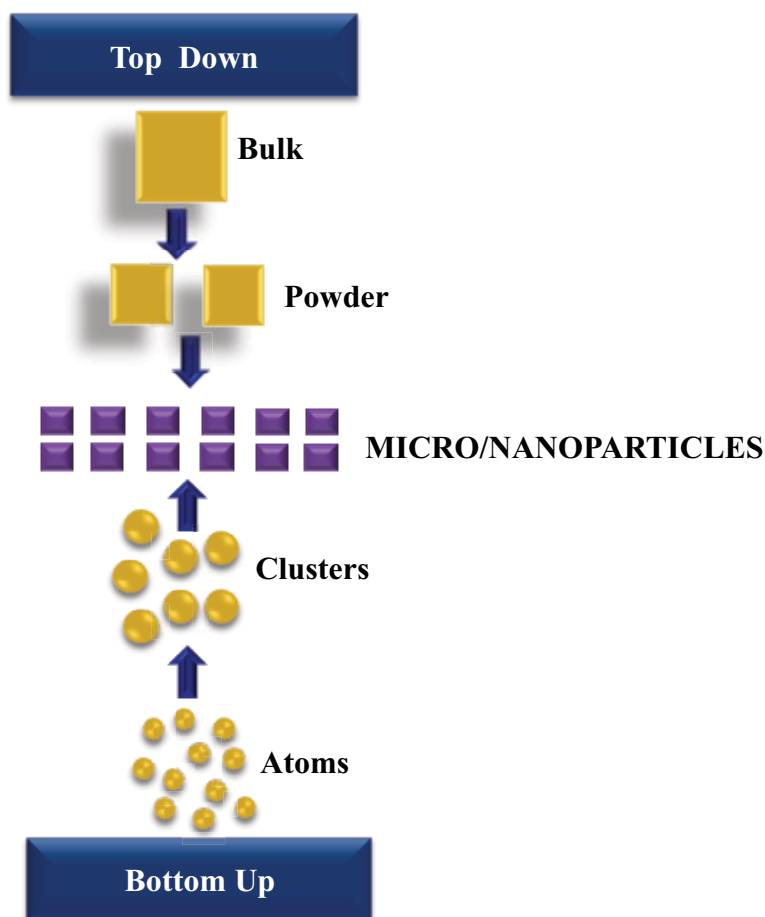


Figure 1.12 Schematic representation of ‘bottom up’ and top down’ technology approaches for ultra-fine particles production (micro- or nanometric scale of particle size). Modified from FLORENCE and KONSTANTIN, 2010.

1.2.3.5.1. Milling

Milling and homogenization are the traditional top-down methods for size reduction of large quantities of particulate materials (MENG, 2011). In the milling operation, the applied stress is applied on the material, which causes the breakage of the particle.

Drug particles can be broken between moving pearls by shear forces and forces of impaction generated by a movement of the milling media (MÜLLER and AKKAR, 2004), as schematized in Figure 1.13.

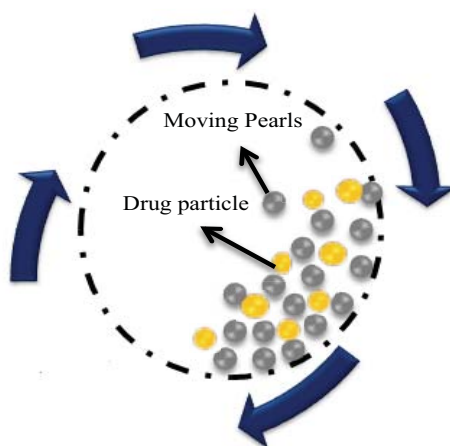


Figure 1.13. Particle size reduction by milling of drug particles between moving pearls schema.

This process can reduce drug particle size, depending on the drug hardness and drug quantities to be milled. Milling period and speed had critical impact on particle size distribution (CHE et al., 2012). However, this method has limited opportunity to control the final particle size, shape, morphology, surface properties and electrostatic charge and it is difficult to reduce the particle size below 1 μm because of the cohesiveness of the particle (BHAKAY et al., 2011).

There are different milling materials available, traditionally steel, glass, and zircon oxide and more recently, special polymers (hard polystyrene) are used. A problem associated with the pearl milling technology is the erosion from the milling material during the milling process. In general, very few data have been published on contamination of pharmaceutical drug suspensions by erosion from the milling material. Of course it should be noted that the extent of erosion depends on the solid concentration of the macrosuspension to be processed,

the hardness of the drug, and based on this, the required milling time and milling material. Apart from the milling material, the erosion from the container also needs to be considered.

Moreover, disadvantages that have also been reported are potential growth of germs in the water phase when milling for a long time, and time and costs associated with the separation procedure of the milling material from the drug suspensions (CHE et al., 2012).

High-pressure homogenization (HPH) has been utilized for many years for production of emulsion and suspensions (TIPPETTS and MARTINI, 2009; LOVELYN and ATTAMA, 2011 ; LACERDA et al., 2011). Piston-gap principle and jet-stream technology are the two basic technologies for most homogenizers, illustrated in Figure 1.14. For instance, in the piston-gap homogenizer, particles to be milled suspended in a liquid medium coming from the sample container are forced to pass through a tiny gap (e.g., 10 mm), and the particle diminution is affected by shear force, cavitation and impaction. In jet-stream homogenizers, the collision of two high-velocity streams leads to particle diminution mainly by impact forces.

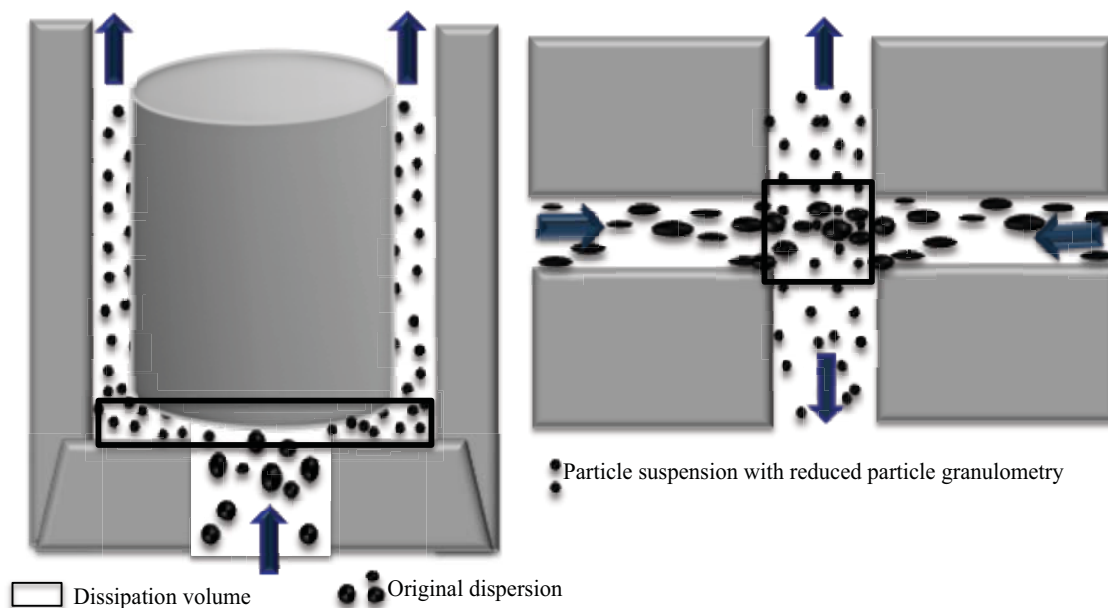


Figure 1.14. Basic homogenization principles: piston-gap (left) and jet-stream arrangement (right). Adapted from SIVASANKAR and KUMAR, 2010.

High pressure-homogenization (HPH) has been used to generate nanosuspensions of many poorly water soluble drugs such as azithromycin, quercetin and nitrendipine (ZHANG et al., 2007; KAKRAN etl., 2012; QUAN et al., 2012).

Generally, high-energy input resulting in enormous impact forces produced effective size reduction of a suspension (median diameters less than 500 nm have been reported by Muller and co-workers (MÜLLER et al., 2001; MÜLLER et al., 2004). However, only fragile drug candidates can be broken up into nanoparticulates using this technique (RADZUAN, 2010).

In general, the particle size decreases with an increasing number of cycles and increasing homogenization pressure and they are mainly influenced by the hardness of the drug, the finesse of the starting material (GRAU et al., 2000; SALAZAR et al., 2011). The optimum number of homogenization cycles is determined by considering the particulate size and polydispersity index of the drug after each cycle.

During milling, additives such as surfactants and stabilizers have been used for the physical stability of the produced drug with reduced particle size (BHAKAY et al., 2011).

1.2.3.5.2. LAS Crystallization

Particle size reduction technologies such as milling or high-pressure homogenization have been used over the years. However, controlling of size distribution, morphology, and surface properties can be challenging. As many hydrophobic drugs are soluble in various water miscible organic solvents, an effective approach is the precipitation of fine particles from solution phase while mixing with an anti-solvent.

LAS crystallization is considered as a bottom-up process, which means that one starts from the molecular level, and goes via molecular association to the formation of a solid particle (GASSMANN et al., 1994; RASENACK and MÜLLER, 2003).

The basic advantage of anti-solvent technique is the use of simple and low cost equipment, compared with milling and high-pressure homogenization technique. Typically, the drug is first dissolved in an organic solvent and the drug solution is mixed with an anti-solvent (Figure 1.15). The solvent and the anti-solvent must be miscible at the operating conditions. One of the advantages of the method is to avoid the use of high energy like in disintegration technique as used for milling, which prevents denaturation of drug due to high energy input (ZHONG et al., 2005).

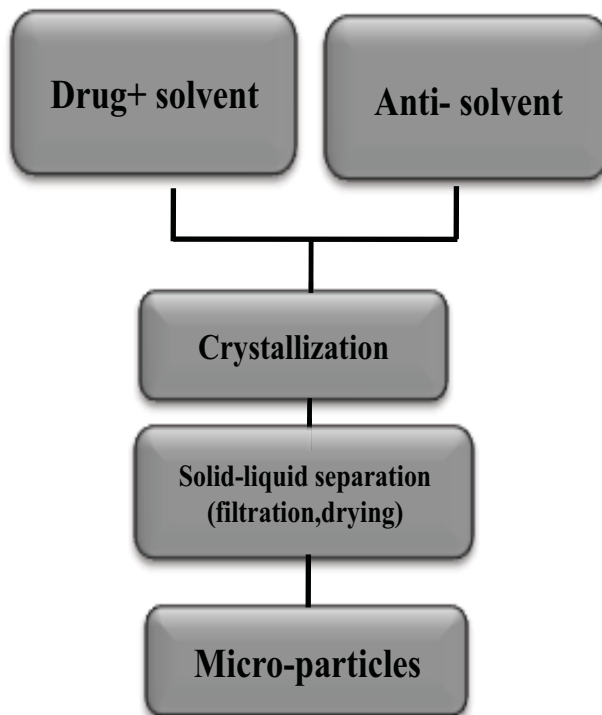


Figure 1.15. Approach for drug particle formation by LAS crystallization.

The introduction of the drug solution to the anti-solvent generates high supersaturation that subsequently induces nucleation and simultaneous growth by condensation and coagulation. The whole process is schematized in Figure 1.16. One formidable challenge remains to control the properties of the crystallized solid such as crystal growth and agglomeration to ensure good further dispersion for dissolution.

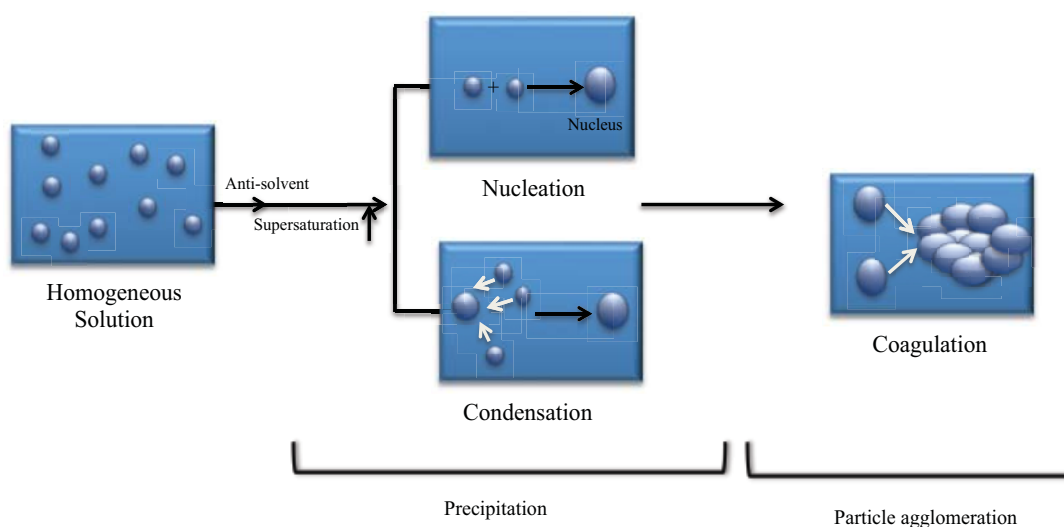


Figure 1.16. Schematic representation of the different steps involved in drug particle formation by an LAS crystallization process. Adapted from MENG, 2011.

The next section reviews in more details some concepts in the crystal engineering field, with emphasis on the driving force for crystallization, control of the two key steps (nucleation and growth) and of solid properties.

1.3. CRYSTALLIZATION

Crystallization is a key process in the manufacturing of most pharmaceutical compounds. Over 90% of all pharmaceutical products, such as tablets, aerosols, capsules, suspensions and suppositories contain drug in particulate, generally crystalline, form (VALDER and MERRIFIELD, 1996). The most common type of crystallization is crystallization from solution, in which a material that is a crystalline solid at a temperature of interest is dissolved in a solvent while crystallization is induced by changing the state of the system in some way that reduces the solubility of the solute. That results in the formation of a crystalline or amorphous solid (MYERSON, 1999).

Crystallization process is considered a two-stage process. Nucleation is the first step in which the “birth” of nuclei (a new solid phase) from the supersaturated solution occurs. The stable crystal grows in size, going from dissolved drug in solution to solid in suspension.

The crystallization process is governed mainly by the kinetics of nucleation and crystal growth, and these processes depend on the driving force called supersaturation (i.e. the concentration of the solute exceeds its equilibrium concentration). This can be achieved in several ways – for example by cooling a solution, or by solvent evaporation, or by the addition of an anti-solvent, or by changing the solution pH.

1.3.1. Thermodynamic background

For crystallization to occur, the system must be brought into a non-equilibrium state where the concentration of the solute exceeds its equilibrium concentration (i.e. the solution is supersaturated). This phenomenon is better represented in the phase diagram (Figure 1.17), represented by a curve of the equilibrium concentration of solute as a function of temperature (solid line). At concentrations below solid line, the solid will dissolve until equilibrium is reached. At solid concentrations between the dashed and solid lines, crystals will grow by seeding but fresh crystals will not nucleate. This is the "metastable zone", which defines the compositions at which spontaneous crystallization occurs and the region bounded by the

solubility curve and the metastable limit. Above the dashed line, the solution produces crystals spontaneously; in this region the supersaturation is achieved.

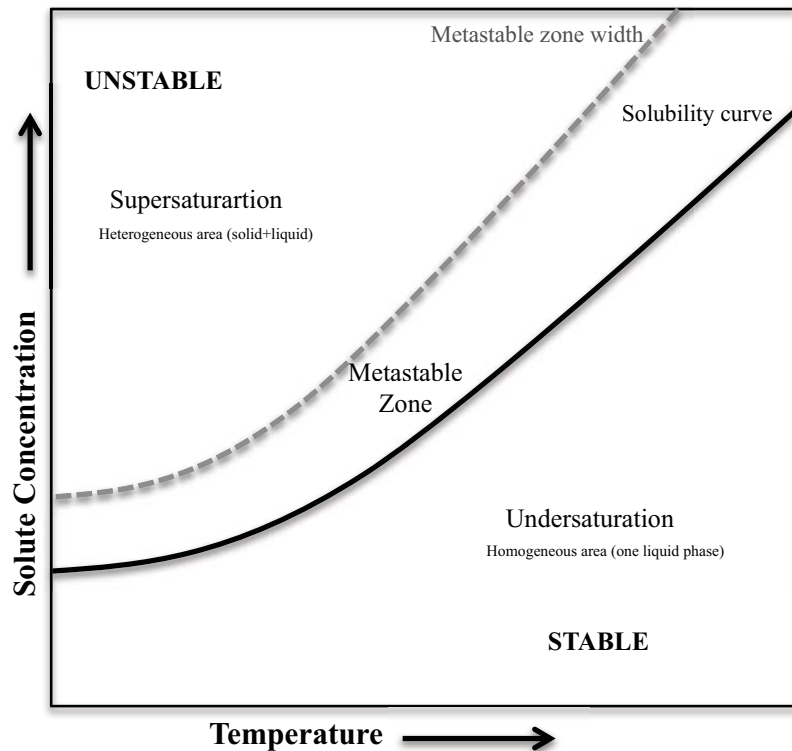


Figure 1.17. The solubility / supersolubility phase diagram. Modified from DAVEY and GARSIDE, 2000.

1.3.2. Nucleation

The nucleation is the stage of solid formation from a supersaturated mother phase (DAVEY and GARSIDE, 2000). Supersaturation generated leads to nucleation and precipitation. According to equation 1.5, nucleation rate J depends to the supersaturation ratio. It is defined as:

$$J = A \exp\left(-\frac{B}{\ln^2 S T^3}\right) \quad (1.5)$$

where $S = \frac{C}{C_{eq}}$ is the supersaturation ratio, T the temperature, C the actual concentration of API in the solution (mol/L) and C_{eq} the solubility (mol/L) of API in a mixture of organic solvent and water. The ratio of activity coefficient $\frac{\gamma}{\gamma_{eq}}$ is assumed to tend towards 1.

Unfortunately, the mechanisms of nucleation are very poorly understood which leads to significant problems in the design, operation and control of crystallization processes. Nucleation is therefore an important issue. Crystal nucleation denotes the formation and physical characteristics (i.e. size distribution, habit morphology) of new crystalline solid. It involves the aggregation of dissolved molecules in solution, leading to the formation of a nucleus.

In general, nucleation mechanisms can be divided into three main categories: homogeneous, heterogeneous, and secondary nucleation (Figure 1.18).

If a solution contains neither solid foreign particles nor crystals of its own type, nucleus can be formed only by homogeneous nucleation. This type of nucleation rarely occurs in volumes larger than 100 μ l, since “real” solutions tend to contain random impurities which may induce nucleation (PEREPEZKO, 1997). If foreign particles are present, nucleation is facilitated and the process is known by heterogeneous nucleation.

On the other hand, secondary nucleation can only happen when crystals of the solute are already present or are deliberately added to the solution, as seeds. This nucleation mechanism generally occurs at much lower supersaturations than homogeneous or heterogeneous nucleation, and it is caused mostly by collisions of crystals with crystallizer and mixer.

Nucleation processes are of practical importance in production of pharmaceutical compounds, for example: A great interest in pharmaceutical research are the concepts of heterogeneous nucleation to be applied in the directed nucleation of specific polymorphs (WEISSBUCH et al., 1987). These studies provide us with the attractive possibility that “a library” of organic seeds can be used to control polymorphism, or to search for unknown polymorphs (WARD, 1997).

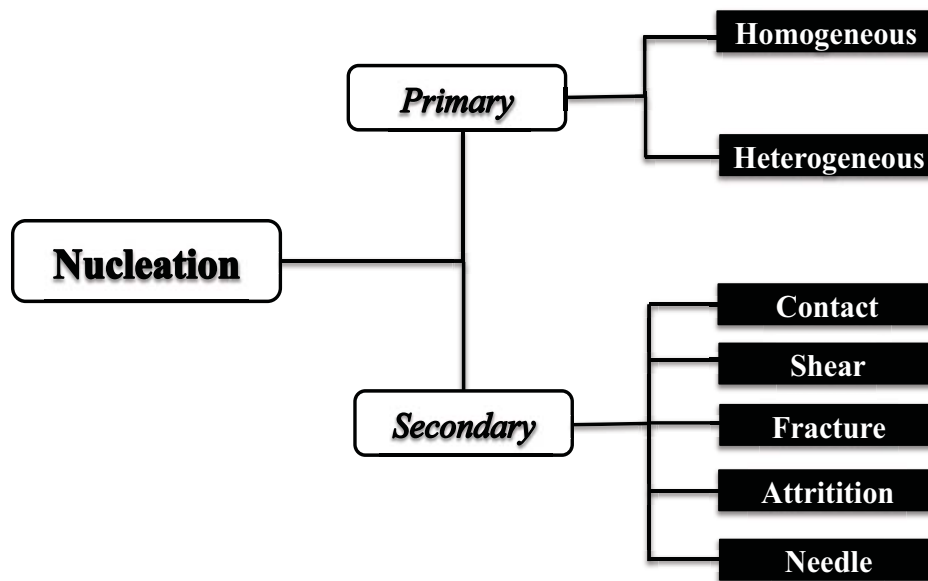


Figure 1.18. Various kinds of nucleation. Modified from MARSMANN et al., 2001.

1.3.3. Crystal growth

Once formed, nucleus begins to grow larger through the addition of solute molecules to the crystal lattice, and this stage of crystallization process is known as crystal growth. The nucleation and growth processes compete for solute molecules in function of their dependence on supersaturation, and their relative rates will determine the crystal size distribution (RODRIGUEZ-HORNEDO and MURPHY, 1999). The sites to capture arriving growth units can be differentiated in kink, ledge and flat faces (Figure 1.19). Growth process occurs by diffusion of solute molecules (atoms, molecules, ions) from the bulk solution to the interface by diffusion and convection and then integration of the solute molecules into the crystal lattice, under supersaturation conditions. The first step is the diffusion of growth units from the growth medium to an impingement site (step I) of the crystal to adsorb on the surface. In most cases (except rough growth), the growth can migrate to the surface of crystal to a step or a growth site (step II). Finally, either the growth unit back in the solution (phase II*), either it becomes part of the growth site and incorporate into the crystal lattice. Desolvation of the growth unit may take place anywhere in step II or the solvent may be adsorbed with the growth unit. The relative importance of each step depends on the surface structure of the crystals and the properties of the solution (MEENAN et al., 2002).

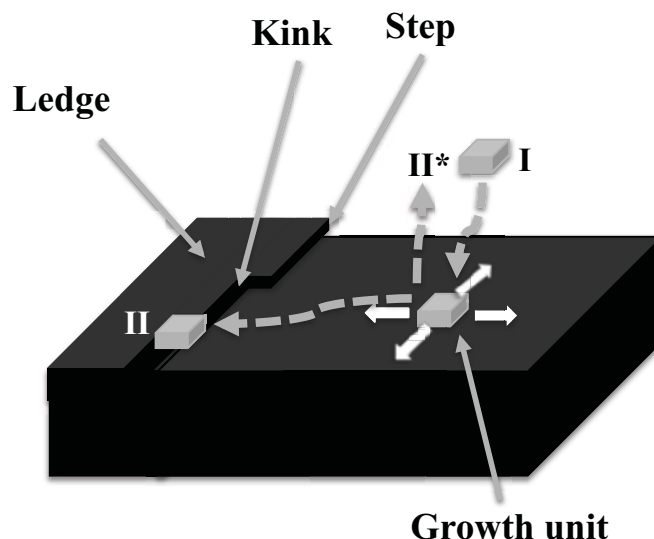


Figure 1.19. A three-dimensional crystal surface showing three type of growth sites and different steps (I, II and II*) involved in the process of growth to unit cubic. Modified from MERSMANN, 2001.

In pharmaceutical field, particles of uniform size in a product are desirable for the convenience of selection of filter, washing, uniform time of dissolution and good appearance of product. Besides this, caking tendency of crystals during pharmaceutical form storage period can be prevented since number of points of contact between crystalline particles is significantly less in uniform crystals size.

1.3.4. Effect of supersaturation on nucleation and growth

Supersaturation (see section 1.3.2) is defined as a measure of the deviation of a dissolved molecule from its equilibrium value (MYERSON, 1993).

Supersaturation can have a profound effect on crystal growth, resulting in morphological changes in the crystallizing compound over a range of supersaturations (YOSHIZAKI et al., 2001; RISTIC, 2002). The variation of the ratio C/C_{eq} (section 1.2.3) enables control of particle size. In general, the number of crystals produced increases with the supersaturation, while the size of crystals decreases (GARNIER and COQUEREL, 2002). For a very high supersaturated solution, crystals nuclei are formed rapidly and may produce a vast quantity of small, elongated crystals over a very short timescale. In the extreme case, when the material is completely and fastly precipitated (larger number of nuclei produced per unit of time) in the form of primary particles, lacking time sufficient for crystal growth, so that

smaller crystals are obtained. If the degree of supersaturation is low, relatively few nuclei are formed and the growth rate is low due to the dissolution of the material. In these conditions, a few crystals are formed, but perfect. In this case is likely to produce larger, granular-shaped crystals over a longer period (HALEBLIAN, 1975). The size and habit of many crystalline products are particularly sensitive to degree of supersaturation (RISTIC et al., 2001).

1.3.5. Choice of solvent

The manufacture of pharmaceuticals often involves crystallization from organic solvents or mixtures of solvents. Generally, solvents are selected based on the resulting solubility, the mode of crystallization and the type of crystals, but the role of solvents in different parts of pharmaceutical processes and some of the limitations and difficulties are related to their toxicity.

Solvent can strongly affects the nucleation rate and habit of crystalline materials in enhancing or inhibiting crystal growth of each crystal face by its properties in solution (e.g. density, viscosity, diffusivity), solubility of the crystallizing species and surface-solvent interactions. For example, changing the solvent polarity during crystallization of ibuprofen provided crystals with a polyhedral crystal habit for ethanol and methanol and needlelike for hexane. Furthermore the results showed that crystal habit modification had a great influence on the mechanical properties (compressibility, flow rate, and bulk density) (GAREKANI et al., 2001).

The solvent composition may also influence the aggregation properties, as well as the solvent incorporation of the crystals (KLUG, 1993).

To date, although the role played by the solvent at the molecular level is still not completely understood (WEISSBUCH et al., 1995), two theories have been proposed regarding the influence of the solvent on nucleation and growth.

In one theory, favourable interactions between solute and solvent on specific faces may lead to a reduction in solid-liquid interface energy. Hence, the activation energy for nucleation on the crystal is reduced and the crystal becomes rougher, leading to enhanced faster surface growth. In the second one, it has been proposed for solvent molecule interaction that can be strongly bound to the crystallizing compound; the preferential adsorption of solvent molecules at specific faces may inhibit their growth as removal of bound solvent

poses an additional barrier for continued growth. In the latter case, solute–solvent interactions at the crystal interfaces could be similar to stereospecific interaction of tailor-made impurities (LAHAV and LEISEROWITZ, 2001).

1.4. LAS CRYSTALLIZATION TO IMPROVE DISSOLUTION PROPERTIES AND SOLUBILITY OF POORLY SOLUBLE DRUGS

Considerable research efforts have been made to optimize crystals properties for pharmaceutical products. The complexity and variety of crystallization pharmaceutical processes can provoke significant changes in the crystal properties, such as their granulometry.

Particle size is one of the physicochemical properties influencing the performance of the drug product and its manufacturability. In addition, a very strict control is needed to achieve particle size requirements, which is defined depending on the pharmaceutical dosage form prepared with the drug crystals and of its administration route (see Table 1.3).

Table 1.3. Particle size distribution of pharmaceuticals with respect to dosage form and route of administration (SHEKUNOV et al., 2007).

Dosage form or route of administration	Particle size (µm)	
	<i>Min</i>	<i>Max</i>
Oral granules	200	1000
Oral depot	50	200
Intraperitoneal	10	50
Nasal	5	20
Aerosols	1	5
Ocular	0.1	2.5
Intravenous/intramuscular	0.2	2
Gene delivery	0.2	0.9
Transdermal	0.06	0.6
Long-circulating (brain, tumor)	0.06	0.2
Lymphatic	0.01	0.06

In practice, crystal morphology is usually described in terms of length, width and thickness. The classifications of crystal shapes adopted by either British Standard (BS 2955:1993) or the US Pharmacopoeia (monograph 776) (Table 1.4) are commonly used for routine microscopically examination of solid pharmaceutical materials.

Table 1.4. Classification of common crystal morphologies for pharmaceutical solids accepted by the US Pharmacopoeia

Morphology	Description	Diagram
Equant	Crystal with similar length, width, and thickness	<p>The diagram shows six 3D representations of crystal shapes. At the top left is a 'Plate (tabular)', a flat rectangular prism. To its right is a 'Columnar (prismatic)', a tall rectangular prism. Below the plate is a 'Flake', a very thin rectangular prism. To the right of the flake is a 'Needle (acicular)', a long, thin rectangular prism. Below the needle is a 'Lath (blade)', a rectangular prism with a larger width than height. At the bottom left is an 'Equant', a cube-like rectangular prism with similar dimensions on all sides.</p>
Flakes	Thin, flat crystals of similar width and length	
Plates	Flat, tabular crystals with similar width and length but thicker than flakes	
Laths	Elongated, thin and blade-like crystals	
Needles	Acicular, thin and highly elongated crystals having similar width and breadth	
Columnar	Elongated, prismatic crystals with greater width and thickness than needles	

Particle size control during crystallization is a challenging area, mainly for the synthesis of nano/microparticles (CHOW et al., 2007). As already said, the growth rates of the different crystal faces are determined by intermolecular interactions between molecules in the crystal as well as by a number of external parameters such as solvent, supersaturation, temperature, and impurities (MYERSON, 1999). Changes in any of these parameters may lead to significant modifications in crystal morphology. This gives rise to crystal habit diversity of a chemical entity grown under various crystallization conditions and provides the basis for morphological crystal engineering.

Besides particle size, other crystal properties can be strongly modified by crystallization as summarized in Table 1.5.

Table 1.5. The most important solid-state characteristics, which are affected by crystallization, and the influence of these properties on the stability and downstream processing of pharmaceutical materials. Modified from SHEKUNOV and YORK, 2000.

Crystal properties	Effect on drug substance and/or drug product
Structural	•
<i>Crystallinity (existence of amorphous and semi-crystalline forms)</i>	• Physical and chemical stability
Polymorphism	• Solubility profile and dissolution rate
<i>Polymorphs</i>	• All aspects of processing
<i>Solvates (hydrates)</i>	
<i>Salts</i>	
<i>Crystal defects</i>	
Dimensional	• Processing behavior: bulk density, agglomeration, flow, compaction
<i>Particle size distribution</i>	• Particle permeability (i.e. particle adsorption)
<i>Particle surface structure</i>	• Bioavailability (drug absorption)
	• Consistency and uniformity of the dosage form
Chemical	
<i>Presence of impurities, residual solvent, and decomposition products</i>	• Toxicity
<i>Chiral forms and chiral separation</i>	• Chemical, physical, and enantiomeric stability
Mechanical	
<i>Brittle/ductile transitions, fracture stress, indentation hardness, stress/strain relaxation, Young's modulus</i>	• Milling and tableting behavior
Electrical	• Agglomeration and flow properties
<i>Electrostatic charge distribution</i>	

The next sections introduce LAS crystallization in the context of process design and what role additives currently play in LAS crystallization research.

1.4.1. Previous works

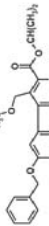
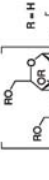
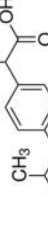
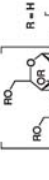
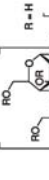
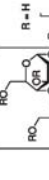
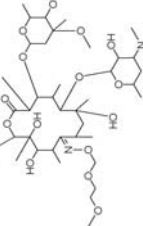
In recent years, many methods of particle production using LAS crystallization have been developed, as shown in Table 1.6. They allow a better control of the size, crystallinity, and morphology of particles that not achieved with top-down methods. The crystallization method is applicable for a wide range of pharmaceutical drugs BCS *Class II* and *IV* to prepare micro/nanoparticles. Decrease in particle size increases the surface area, which increases the solubility and dissolution rate of poorly water soluble drugs and hence bioavailability (LIVERSIDGE and LIVERSIDGE, 2008), as discussed before in the section 1.2.2.

Table 1.6 reveals that several poorly soluble drugs are crystallized by LAS crystallization using different apparatus in laboratory scale like batch reactors, magnetic stirring, injection method and sonoreactors. The drug powders obtained in these studies presented particle size in a range between 0.010- 20 μm .

It could be noted from this literature review, that the major crystallization assays were realized in presence of additives like surfactants (ionic or non ionic) and polymers or both. Since the molecules have a different orientation at the different crystal faces, the additives will have different effect on the growth rate of different faces. Each additive can act like a stabilization agent through a different mechanism; these mechanisms are a relatively less explored area but are important for morphologic, polymorphic and technologic screening of a compound during its developmental stage. Any relationship between the chemical structure of the stabilization agent and the chemical structure of the drug to be stabilized against growth is related in the literature. However the attempt of the use of stabilizers agents is actually turned on the changes of drug compound characteristics.

The majority of the recrystallized drugs investigated is asymmetric drugs and do not possess a very large molecular structure, which facilitated the achievement of crystals with a reduced size, generally in presence of additives. The different aspects to controlled LAS crystallization will be discussed in more detail in the following sections.

Table 1.6. Obtention of drug crystals by LAS precipitation method.

Apparatus	Stabilizer	Stabilization mechanism	Solvent	Anti-solvent	Drug	Particle Size (µm)	Author
Magnetic/Mechanic stirring	X 	X	Isopropyl acetate	Hexane	 Abecarnil	20	BECKMANN, 1999
Batch reactor	 HPMC	Steric and removal of solvent	Isopropyl alcohol	Water	 Ibuprofen	2	RASENACK and MÜLLER, 2002
Batch reactor	 HPMC	Steric and removal of solvent	Acetone	Water	 Itraconazole	0.600	RASENACK and MÜLLER, 2002
Batch reactor	 HPMC	Steric and removal of solvent	Acetone	Water	 Ketoconazole	1.200	RASENACK and MÜLLER, 2002
Magnetic/Mechanic stirring - Injection method	 HPMC	Steric	NaOH solution	HCl solution	5-(3-ethoxy-4-pentyloxyphenyl)-2,4-thiazolidinedione	10-15	TERAYAMA et al., 2004
Sonoreactor	X	X	Acetone	Water	 Roxithromycin	X	GUO et al., 2005

CHAPTER 1

Table 1.6. Continued

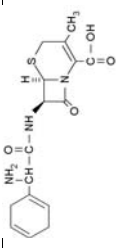
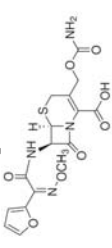
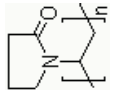
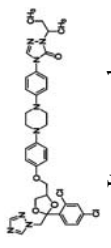
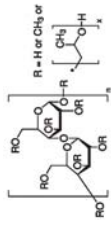
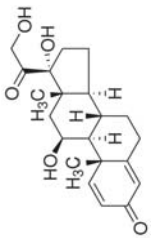
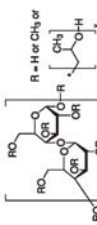
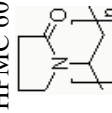
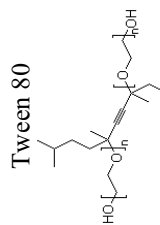
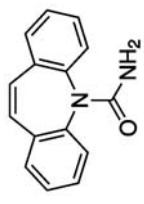
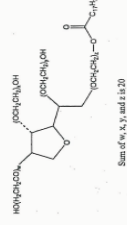
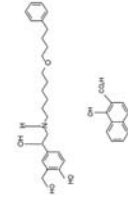
Apparatus	Stabilizer	Stabilization mechanism	Solvent	Anti-solvent	Drug	Particle Size (µm)	Author
Rotating packed bed	X 	X	HCl solution	Acetone and Triethylamine	 Cephadrine	0.200-0.400	ZHONG et al. 2005
Magnetic/Mechanic stirring	X	X	Acetone	Isopropyl ether	 Cefuroxime axetil	0.300	ZHANG et al, 2006
Magnetic/Mechanic Stirring-Injection method	 PVP $\text{CH}_3(\text{CH}_2)_{10}\text{CH}_2\text{O}-\text{S}(\text{O})_2-\text{ONa}$ SDS and Miglyol®	Steric Electrostatic, steric and inhibition of Ostwald ripening	Tetrahydrofuran	Water	 Itraconazole	0.300	MATTEUCCI et al, 2006
Sonoreactor	 HPMC	Steric	N,N-dimethylacetamide	Water	AZ68	0.145-0.162	SIGFRIDSSON et al., 2007
Magnetic/Mechanic stirring		Steric	N-Methyl-2-pyrrolidinone	Water	 Prednisolone	1.460	LI et al., 2007

Table 1.6. (continued)

Apparatus	Stabilizer	Stabilization mechanism	Solvent	Anti-solvent	Drug	Particle Size (µm)	Author
Magnetic/Mechanic stirring	 <p>HPMC 606</p>  <p>PVP PF17</p>  <p>Tween 80</p>  <p>PEG-400</p>	Steric	PEG-300	Water	 <p>Carbamezepine</p>	0.010-0.020	DOUROMIS and FAHR, 2007
Magnetic/Mechanic stirring		Steric	DMSO	Water	2-2-devinyl pyropheophorbide-a	0.100-0.200	BABA et al., 2007
Magnetic/Mechanic stirring	 <p>Salmeterol xinafoate</p>	Steric	PEG-400	Water		2.540	MURNANE et al., 2008

CHAPTER 1

Table 1.6. (continued)

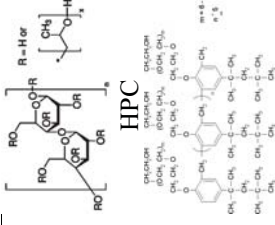
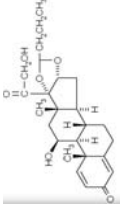
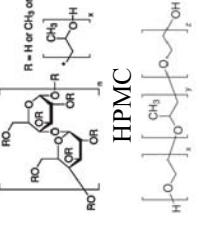
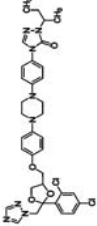
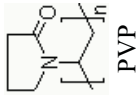
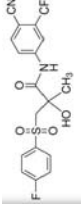
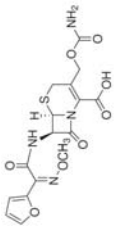
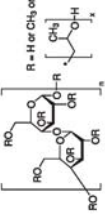
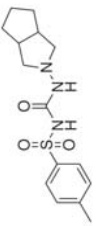
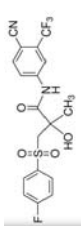
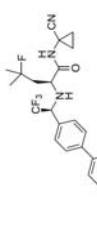
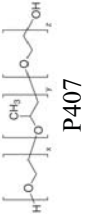
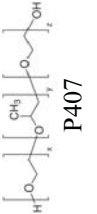
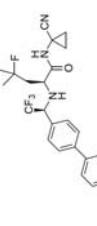
Apparatus	Stabilizer	Stabilization mechanism	Solvent	Anti-solvent	Drug	Particle Size (μm)	Author
Magnetic/Mechanic stirring	 <p>HPC Tyloxapol</p>	Steric	Acetone and MeOH	Water	 <p>Budesonide</p>	5	HU et al.,2008
Batch reactor	 <p>HPMC P407</p>	Steric	Tetrahydrofuran	Water	 <p>Itraconazole</p>	0.300	MATTEUCCI et al., 2008
Magnetic/Mechanic stirring	 <p>PVP</p>	Steric	N,N-dimethylacetamide	Water	 <p>Bicalutamide</p>	0.115	LINDFORS et al. 2008
Sonoreactor	X	X	Acetone	Isopropyl ether	 <p>Cefuroxime axetil</p>	0.800	DHUMAL et al., 2008

Table 1.6. (continued)

Apparatus	Stabilizer	Stabilization mechanism	Solvent	Anti-solvent	Drug	Particle Size (μm)	Author
Magnetic/Mechanic stirring	 HPMC	Steric	Acetone	Water	 Glioclazide	6.200	VARSHOSAZ et al., 2008
Magnetic/Mechanic stirring	X	X	EtOH and DMSO	Water	 Bicalutamide	0.450	Y.LE et al., 2009
Sonoreactor	PS _{1k-b} -PEO _{3k}	Steric	Tetrahydrofuran	Water	 Itraconazole	0.145	KUMAR et al., 2009
Sonoreactor	PS _{1k-b} -PEO _{3k}	Steric	Tetrahydrofuran	Water	 Itraconazole	0.352	KUMAR et al, 2009
Sonoreactor	 P407	Steric	Tetrahydrofuran	Water	 Odanacatib	0.158	KUMAR et al., 2009
Sonoreactor	 P407	Steric	Tetrahydrofuran	Water	 Odanacatib	0.350	KUMAR et al, 2009

CHAPTER 1

Table 1.6. (continued)

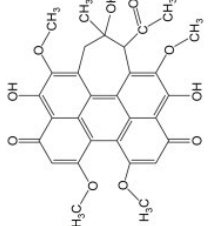
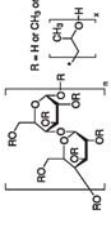
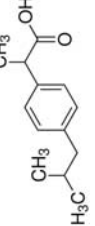
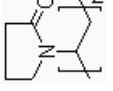
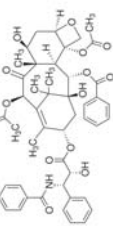
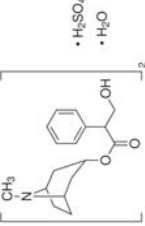
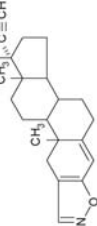
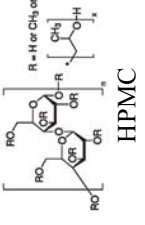
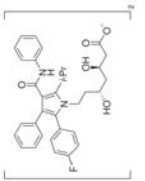
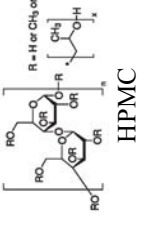
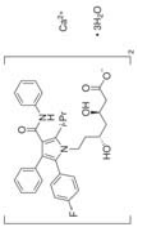
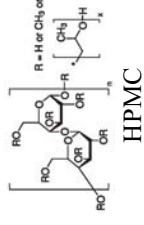
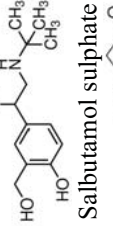
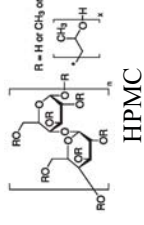
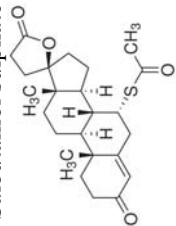
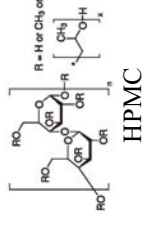
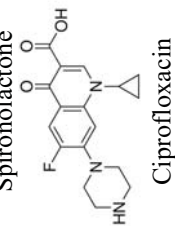
Apparatus	Stabilizer	Stabilization mechanism	Solvent	Anti-solvent	Drug	Particle Size (μm)	Author
Magnetic/Mechanic stirring	X	X	DMSO	Buffer pH 7.4	 Hypocrellin A	0.350-0.800	L. ZHOU et al., 2009
Sonoreactor	 HPMC K3	Steric	Acetone	Water	 Ibuprofen	0.702	VERMA et al., 2009
Sonoreactor	 PVP K90	Steric	Acetone	Water	 Paclitaxel	0.299-0.359	EL-GENDY and CBERKLAND, 2009
Magnetic/Mechanic stirring	X	X	X	Water	 Atropine sulfate	0.100-0.600	ALJ et al., 2009
Rotating packed bed	X	X	EtOH	Water	 Danazol	0.190	ZHAO et al., 2009

Table 1.6. (continued)

Apparatus	Stabilizer	Stabilization mechanism	Solvent	Anti-solvent	Drug	Particle Size (μm)	Author
Magnetic/Mechanic stirring	X  HPMC	Removal of solvent	Water	MeOH	Insulin 	2	KLINGLER et al., 2009
Magnetic/Mechanic stirring	X  HPMC	Steric and removal of solvent	MeOH	Water	Atorvastatin calcium 	0.240-0.410	ZHANG et al., 2009
Magnetic/Mechanic stirring	X  HPMC	Removal of solvent	Acetonitrile	Water	Salbutamol sulphate 	0.060	BHAVNA et al., 2009
Magnetic/Mechanic stirring	X  HPMC	Steric	1-Methyl-2-pyrrolidone	Water	Spirolactone 	0.300	DONG et al., 2009
Multi-stage liquid impingers	X  HPMC	X	HCl sol. and NaOH sol.	Isopropyl alcohol	Ciprofloxacin 	1-2	ZHOA et al., 2009

CHAPTER 1

Table 1.6.(continued)

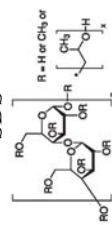
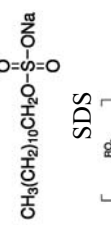
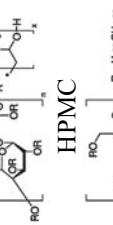
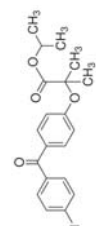
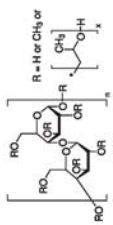
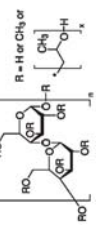
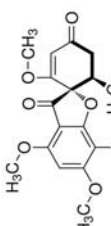
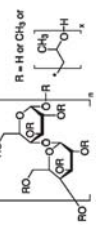
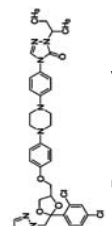
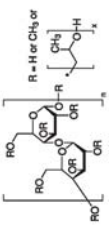
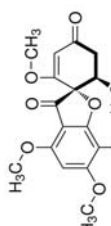
Apparatus	Stabilizer	Stabilization mechanism	Solvent	Anti-solvent	Drug	Particle Size (μm)	Author
Sonoreactor	$\text{CH}_3(\text{CH}_2)_{10}\text{CH}_2\text{O}-\text{S}(=\text{O})_2\text{ONa}$ SDS  HPMC $\text{CH}_3(\text{CH}_2)_{10}\text{CH}_2\text{O}-\text{S}(=\text{O})_2\text{ONa}$ SDS  HPMC 	Electrostatic and steric	Acetone	Water	 Fenofibrate	3.400	MENG et al., 2009
Sonoreactor	SDS  HPMC 	Electrostatic and steric	Acetone	Water	 Griseofulvin	1.900	MENG et al., 2009
Sonoreactor	HPMC 	Steric	Tetrahydrofuran	Water	 Itraconazole	0.830	DALVI and DAVE, 2010
Sonoreactor	HPMC 	Steric	Acetone	Water	 Griseofulvin	2.400	DALVI and DAVE, 2010

Table 1.6. (continued)

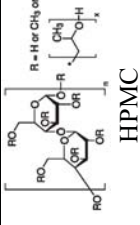
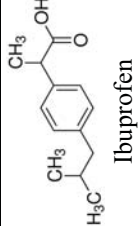
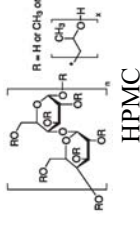
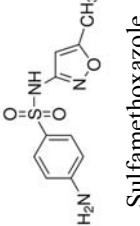
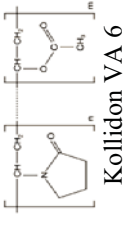
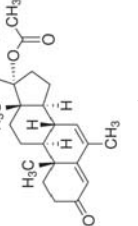
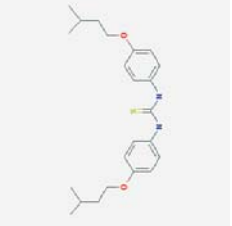
Apparatus	Stabilizer	Stabilization mechanism	Solvent	Anti-solvent	Drug	Particle Size (μm)	Author
Sonoreactor	 <p>HPMC</p>	Steric	Acetone	Water	 <p>Ibuprofen</p>	8.400	DALVI and DAVE, 2010
Sonoreactor	 <p>HPMC</p>	Steric	Acetone	Water	 <p>Sulfamethoxazole</p>	30	DALVI and DAVE, 2010
Magnetic/Mechanic stirring	 <p>Kollidon VA 6</p>	Steric	Acetone	Water	 <p>Megestrol acetate</p>	1.654	CHO et al., 2010
Magnetic/Mechanic stirring - Injection method	X	X	EtOH	Water	 <p>Isoxyl</p>	0.220	WANG and HICKEY, 2010

Table 1.6. (continued)

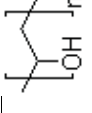
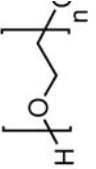
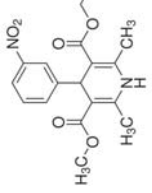
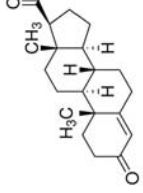
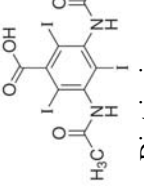
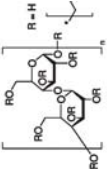
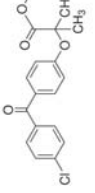
Apparatus	Stabilizer	Stabilization mechanism	Solvent	Anti-solvent	Drug	Particle Size (μm)	Author
Sonoreactor	 PVA  PEG 200	Steric	PEG 200 and Acetone	Water	 Nitrendipine	0.209	XIA et al., 2010
Injection method under sonication	 Stearic acid	Steric	EtOH	Water	 Progesterone	0.267	SALEM, 2010
Sonoreactor	X	X	EtOH	Water	 Diatrizoic acid	2.400	EL-GENDY et al., 2010
Batch reactor	 SDS  HPMC	Electrostatic, steric and removal of solvent	EtOH	Water	 Fenofibrate	0.318	HU et al., 2011

Table 1.6. (continued)

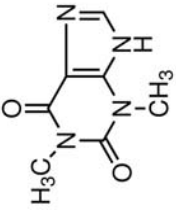
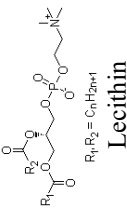
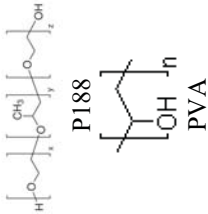
Apparatus	Stabilizer	Stabilization mechanism	Solvent	Anti-solvent	Drug	Particle Size (μm)	Author
Injection method under sonication	 <p>Stearic acid</p>	Steric	Dimethylformamide and EtOH	Water	 <p>Theophylline</p>	0.290	SALEM et al., 2011
Magnetic/Mechanic stirring	 <p>Lecithin</p>	Vesicles and freeze drying	Tert-butyl alcohol	Water	Lysozyme	0.200	TAN et al., 2011
Magnetic/Mechanic stirring	 <p>P188 PVA</p>	Steric and removal of solvent	Water	Acetonitrile	 <p>Alpha ketoglutarate</p>	0.110	SULTANA et al., 2011
Sonoreactor	X	X	DMSO	Water pH4	Camptothecin	0.234	ZHANG et al., 2011

Table 1.6. (continued)

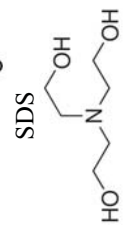
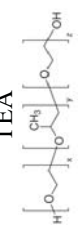
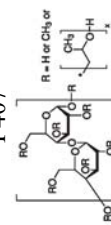
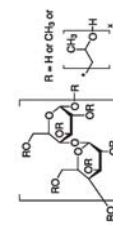
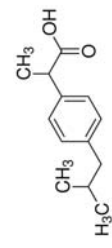
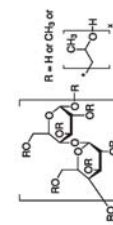
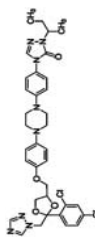
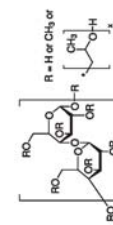
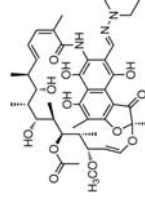
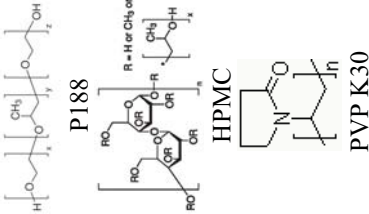
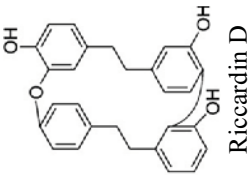
Apparatus	Stabilizer	Stabilization mechanism	Solvent	Anti-solvent	Drug	Particle Size (µm)	Author
Magnetic/Mechanic stirring	$\text{CH}_3(\text{CH}_2)_{10}\text{CH}_2\text{O}-\text{S}(=\text{O})_2\text{ONa}$ SDS  TEA  P407  HPMC Inutec SP1® Tween 80  HPMC	Electrostatic and steric	Isopropyl alcohol	Water	 Ibuprofen	0.300-0.400	MANSOURI et al., 2011
Sonoreactor	HPMC Inutec SP1® Tween 80  HPMC	Steric	Methylene chloride	Ethyl alcohol	 Itraconazole	0.170-0.380	BADAWI et al., 2011
Magnetic/Mechanic stirring	HPMC Inutec SP1® Tween 80  HPMC	Steric	1-Ethyl 3-Methylimidazolium methylphosphonate	Phosphate Buffer pH6,8	 Rifampicin	0.283-0.353	VIÇOSA et al., 2012

Table 1.6. (continued)

Apparatus	Stabilizer	Stabilization mechanism	Solvent	Anti-solvent	Drug	Particle Size (μm)	Author
Magnetic/Mechanic stirring	 <p>P188 HPMC PVP K30</p>	Steric and freeze drying	EtOH	Water	 <p>Riccardin D</p>	0.184	LIU et al., 2012

Legend: **SDS**- Sodium *dodecyl sulfate* / **HPC**-Hydroxypropyl Cellulose / **HPMC**- hydroxypropyl methyl *cellulose* / **PS** _{1K-3K} - **PEO**_{3K} - **1,000 M_w polystyrene-block-3,000 M_w polyethylene oxide** / **PVP**- Polyvinylpyrrolidone / **MeOH**- Methanol / **EtOH**- Ethanol / **PEG**- Polyethylene glycol / **DMSO**- Dimethylsulfoxide/ **P407**-Poloxamer 407 / **P188**- Ploxamer 188 / **TEA**- Triethanolamine/ **Tween 80** - Polysorbate 80/ **PVA**- Polyvinyl alcohol// **NaOH**- Sodium Hydroxide / **HCl**- Hydrochloric acid.

1.4.2. Control of process parameters

Mixing devices

Mixing between drug solution and anti-solvent is a critical step to maintain a constant level of supersaturation throughout the crystallizer, uniform nucleation and control of small embryo particles formed in the process (DOUROUMIS and FAHR, 2006).

The initial contacting between the drug solution and the anti-solvent is an important parameter, which will influence the nucleation rate. Two different manners to bring them into contact are illustrated in Figure 1.20.

Single-jet configuration is the simplest manner by which one solution is pumped into the stirred vessel containing the other liquid (Fig. 1.20a). Alternatively, two solutions can be premixed before entering the tank as a single jet (Fig. 1.20b). The two feeding configurations have different temporal and spatial supersaturation profiles.

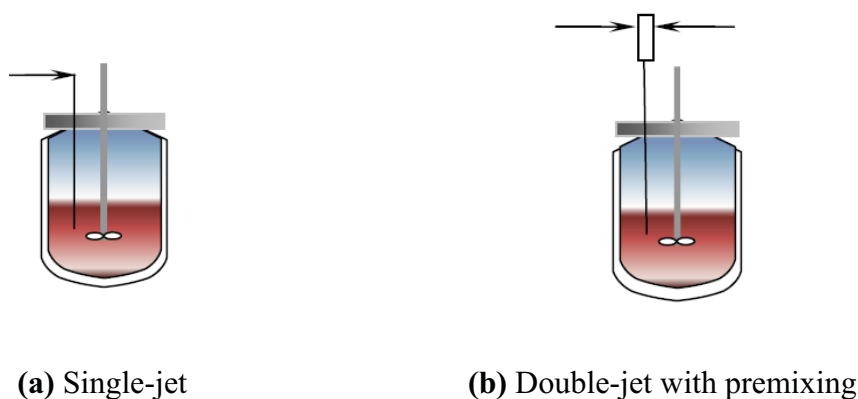


Figure 1.20. Feeding configuration for anti-solvent crystallization
(a) single-jet, (b) double-jet with premixing.

Typically, mixing is divided into three main groups: macromixing, mesomixing and micromixing. Macromixing is the mixing occurring on a crystallizer scale, which represents the uniformity of the local average of the concentrations of all the species within the entire crystallizer. Mesomixing is the mass transfer of a solution, also known as turbulent mixing and micromixing comprises the molecular diffusion and engulfment of different solvent composition region, which represents molecular scale mixing (BALDYGA and BOURNE, 1989).

Actually, to achieve the rapid mixing the high jet velocity mixing devices have been described in the literature. These mixing devices are reported in the literature as static mixer, high gravity jet, confined impinging jet, multi-inlet vortex mixer (MIVM), Y-shaped microchannel reactor, Y and T-mixer, Roughton mixer, as illustrate in Figure 1.21. They show advantages when compared to the traditional CSTR (Continuous Stirring Tank Reactor), such as small space requirement, low equipment cost, no power required except pumps, short residence times and good mixing at low shear rates (THAKUR et al., 2003). Because of this they have been extensively related in the literature for LAS crystallization of drugs. The details of such mixing devices are reported in Table 1.7.

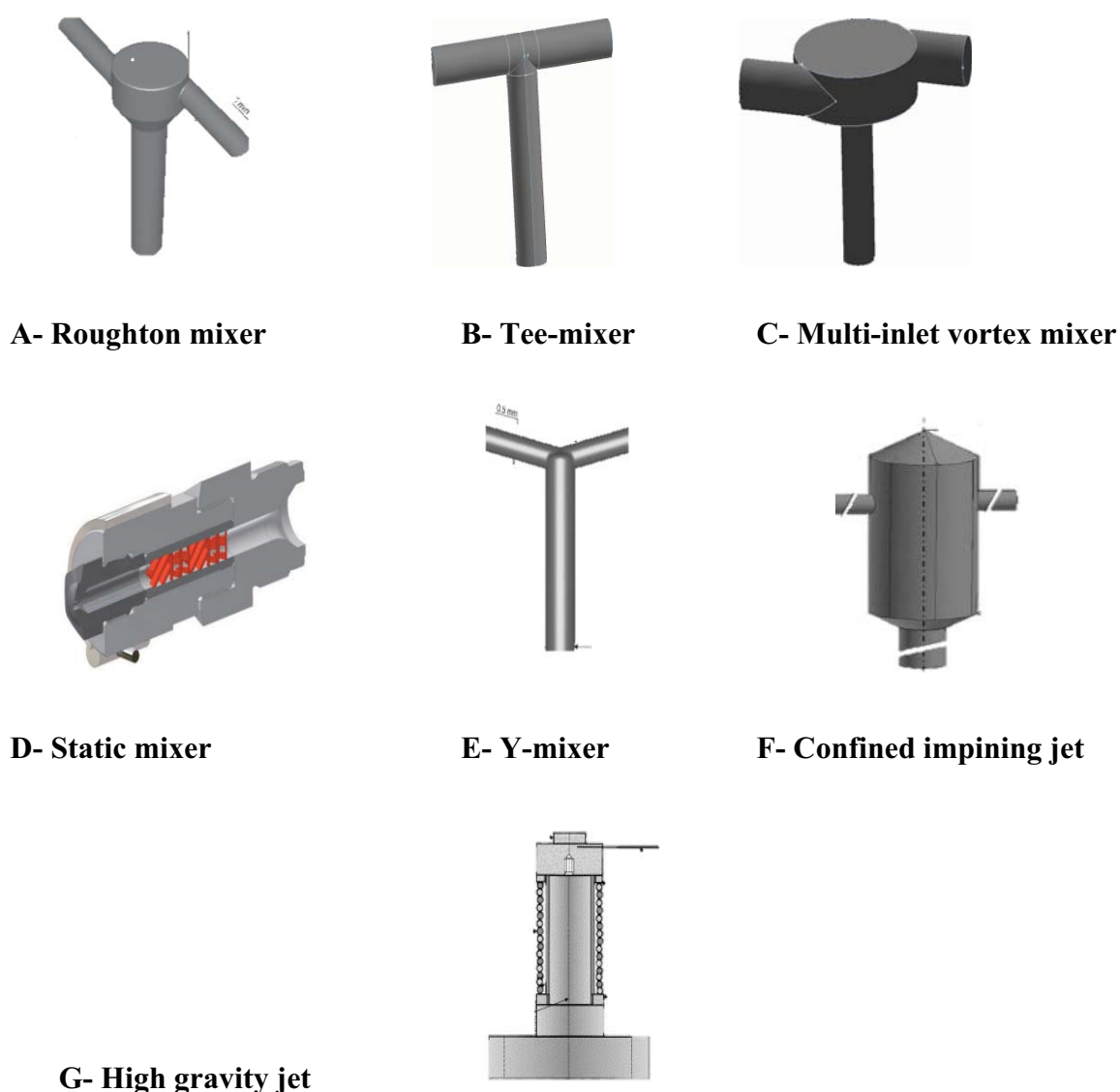


Figure 1.21. Schematics of mixing devices used in chemical and pharmaceutical field. Modified from THORAT and DALVI, 2012.

CHAPTER 1

Table 1.7. Summary of mixing intensification reports using mixing devices for LAS drug crystallization. Modified from THORAT and DALVI, 2012

Mixing device	Dimensions of mixing device	Flow rates/velocity	Mixing time and energy dissipation	Drug	Particle size (μm)	Author
Static mixer	SMX DN3 static mixer	Solvent flow rate: 12.5 mL/min Antisolvent flow rate: 400 mL/min	x	Progesterone	1.45 ± 0.17	DOUROMIS and FAHR, 2006.
	Mixing elements Diameter: 3.2 mm, length: 3.2 mm. welded together with offset of 90° with each other in stainless steel tube of inner diameter: 3.3 mm 6-element of a size 25 mm welded together with offset of 90° with each other in glass tube-SMV DN25 static mixer	Solvent flow rate: 18.75 mL/min Antisolvent flow rate: 300 mL/min	x	β -metahsone valerate- 17	0.25 ± 0.03	
		Solvent flow rate: 83.33 mL/min	x	Carbamazepine	4.09 ± 0.47	
		Antisolvent flow rate: 500 mL/min Solvent flow rate: 150 mL/min	x	Oxcarbazepine	0.97 ± 0.11	
		Antisolvent flow rate: 450 mL/min Solvent flow rate: 0.1-0.3 L/min, antisolvent flow rate: 0.9-2.7 L/min	x	Spiroinolactone	0.5	
		Solvent flow rate: 50 mL/min, antisolvent flow rate: 500 mL/min	x	Fenofibrate	0.328 ± 0.0022	
High-gravity reactive precipitation (HGRP)	x	Continuous addition of solvent and antisolvent	x	Cephadrine	0.3	ZHONG et al., 2005.

Table 1.7. (continued)

Mixing device	Dimensions of mixing device	Flow rates/velocity	Mixing time and energy dissipation	Drug	Particle size (μm)	Author
High-gravity reaction anti-solvent precipitation (HGAP)	Rotating packed bed (RPB) Inner diameters : 50mm Outer diameters: 150 mm, Axial width of rotating bed: 50 mm, Distributor: two pipes (10 mm in outer diameter and 1.5 mm in wall thickness), each having a slot (1 mm in width and 48 mm in length)	Solvent: 10 L/h Antisolvent: 200 L/h	Micromixing time: 100 μs	Cefuroxime axetil	0.305	CHEN et al., 2006.
	Rotor Inner diameter: 25 mm Outer diameter: 90.Axial height: 28 mm mm Packing: Material: wire mesh. Voidage: 95% Production capacity: 116.1 g/h	Solvent flow rate: 70ml/min Antisolvent flow rate: 1500 mL/min	Micromixing time: 100 μs	Danazol	0.19	ZHAO et al., 2009.
Confined liquid impinging jets (CLIJ)	Jet inlet diameter 0.50 mm, outlet diameter 1 mm, chamber diameter: 2.38 mm	Solvent and antisolvent flow rate: 72 mL/min At the maximum flow of 120mL/min	x	β -Carotene	0.1	ZHU et al., 2007
			Mixing time~16.7ms	Cyclosporine A	0.18-0.7	CHIOU et al., 2008

CHAPTER 1

Table 1.7. (continued)

Mixing device	Dimensions of mixing device	Flow rates/velocity	Mixing time and energy dissipation	Drug	Particle size (μm)	Author
Two-impinging-jets (TIJ)	Jet nozzle diameter: 0.5, 1 and 2mm. Mixing chamber diameter: 2.54 cm	Inlet fluid velocity ~40m/s	(2) CIJR-d2(~0.05-0.1 s) Micromixing time: 65 and 145ms	Lovastatin	2-10	MAHAJAN and KIRWAN, 1996
Impinging device	Solvent inlet diameter: 0.5, 1, 1.5mm, antisolvent inlet diameter 1.5, 3, 4.5mm, outlet diameter 0.5mm	Solvent flow rate : 25-100 mL/min, antisolvent flow rate: 22-900 mL/min, rate ratio of solvent to antisolvent (1:9)	x	Spiroinolactone	0.302-0.360	DONG et al., 2011.
Multi-inlet vortex mixer	x	In let velocity from 0.12 to 0.37 m/s. Antisolvent flow rate: 120 mL/min, solvent flow rate: 13.3 mL/min.	x	β -Carotene	0.14	D'ADDIO et al., 2010.
Microfluidic reaction technology (MRT)	Channels depth: 50-150 μm , channels width: 50-150 μm , scalable to tens of L/min	Inlet fluid velocity 500m/s	Micromixing time: 4ms, mesomixing time : 20s, energy dissipation rates $\sim 10^7$ W/kg	β -Carotene	0.1	ZHU et al., 2011
Microfluidic reaction technology (MRT)	Channels depth: 50-150 μm , channels width: 50-150 μm , scalable to tens of L/min	Inlet fluid velocity 500m/s	Micromixing time: 4ms, mesomixing time : 20s, energy dissipation rates $\sim 10^7$ W/kg	Norfloxacin	0.17	PANAGIOTOU et al., 2009.

Table 1.7. (continued)

Mixing device	Dimensions of mixing device	Flow rates/velocity	Mixing time and energy dissipation	Drug	Particle size (μm)	Author
Y-shaped microfluidic reactor (YMCR)	Inlet diameter: 300 μm , inner length: 300 μm , outlet diameter: 300 μm , outlet length: 600 μm	Antisolvent flow rate: 80 mL/min, solvent flow rate: 4 mL/min	Micromixing time : 0.25-0.35ms, energy dissipation rates : 2000-4000 W/kg	Danazol	0.364	ZHAO et al., 2007.
	Channel diameters: 0.1, 0.5 and 1mm, inlet angles 25 and 50.	Antisolvent flow rate: 2.5 mL/min, solvent flow rate: 1 mL/min	x	Hydrocortisone	0.08-0.45 and 0.295 \pm 0.0032	ALI et al., 2009 ; ALI et al., 2011
	Mixing chamber: 60 (width) \times 10 (depth) \times 105 (length) mm	Antisolvent flow rate: 30 mL/min, solvent flow rate: 3 mL/min	0.04-0.4ms	Atorvastatin calcium	0.48	ZHANG et al., 2010
	Unlet channels: 400 \times 500 \times (width \times depth m) \times 20 (length mm), cross section of the mixing channel: 800 \times 500 (width \times depth) μm , \times 40 (length, mm)	Antisolvent flow rate: 50-60 mL/min, solvent flow rate: 2 mL/min, overall flow rate : 63 mL/min	0.04-0.4ms	Cefuroxime axetil	0.35	WANG et al., 2010.

CHAPTER 1

Table 1.7. (continued)

Mixing device	Dimensions of mixing device	Flow rates/velocity	Mixing time and energy dissipation	Drug	Particle size (μm)	Author
Microporous tube-in-tube microchannel reactor	Micropore size: 5 μm length of micropore zone: 1 mm porosity: 46%, outer tube diameter: 15.5 mm, inner tube diameter: 15 mm	Total volumetric flow rate :6L/min	Micromixing time: 2ms	Cefuroxime axetil	0.4-1.4	ZHU et al., 2010.
T-shaped micro-channel	Inlet and outlet: 250 μm (depth \times width of channel)	Antisolvent flow rate: 1.2 mL/min, solvent flow rate: 1.2 mL/min	Mixing time: 0.18	Curcumin	0.19	LIU et al., 2010.
Micromixer	Inlet diameter: 1 mm, outlet diameter: 1 mm, cross-section: width 200 μm \times height 200 μm	Antisolvent flow rate: 10 $\mu\text{L}/\text{min}$, solvent flow rate: 10 $\mu\text{L}/\text{min}$	x	Curcumin	0.03-0.05	HE et al., 2010 ; HE et al., 2011.

1.5. ADDITIVES IN CRYSTALLIZATION

Additives in crystallization processes have gained attention in recent years, because they can be adsorbed directly onto drug particles to produce powders with optimized physicochemical properties (ZIMMERMANN et al., 2009).

It has been shown that the presence of additives in solution can affect all parameters of crystallization, either the solubility, the nucleation or growth, and hence the resulting morphology (KUBOTA et al., 2000; GARNIER et al., 2002; VETTER et al., 2011) and polymorphic form (CHONG et al., 2002; SONG and CÖLFEN, 2011)

Some theories are presented in literature to describe the mechanisms of additive influence on crystallization process, which comprises:

- Inhibition of nucleation by formation of hydrogen bonds between the additive and the molecule. This interaction inhibits or retards the formation of nucleus by collision and therefore the induction time period is different from that of pure systems (TAYLOR and ZOGRAFI, 1997);
- Adsorbed additives on crystal surface form a mechanical barrier that prevents the diffusion of solute molecules from the bulk solution to the crystal surface (ZILLER and RUPPRECHT, 1988);
- Additives do not inhibit nucleation, but just reduce supersaturation of the solution by modifying the saturation of solute. Consequently the width of the metastable zone is also influenced (RODRIGUEZ-HORNEDO and MURPHY, 1999; MERSMANN, 2001);
- Non-adsorbed additive are rejected by the crystal surface and accumulate in the boundary region. This creates a greater resistance to drug molecules limiting their diffusion through the barrier and leads to growth inhibition, as shown in Figure 1.22 (RAGHAVAN et al., 2001).

The adsorption of additives at different sites can cause growth inhibitions, even block the growing surface and in consequence stop the growth process. However, the adsorbed impurities may simultaneously lead to a reduction in the edge free energy,

which results in an increase in crystal growth rate (RAK et al., 2005). For pharmaceutical technology, understanding of these mechanisms may help to control the quality and purity of raw crystalline substances and, consequently, to improve the manufacture and performance of the final dosage forms.

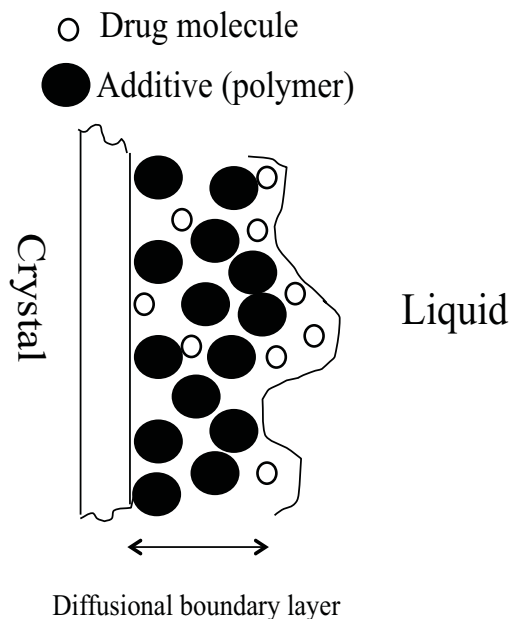


Figure 1.22. Schematic diagram showing the mechanism of growth inhibition and habit modification of crystals by polymers. Modified from RAGHAVAN et al., 2001.

1.5.1. Additives in LAS crystallization

The stabilization and controlled crystal growth mechanism during LAS crystallization depend on the strength of adsorption of stabilizer molecules on the drug surface. Two main mechanisms have been investigated in additive screening studies on drug LAS recrystallization: steric stabilization and electrostatic repulsion (WU et al., 2011; THORAT and DALVI, 2012), as illustrated in Figure 1.23.

Each mechanism has its benefits for particulate systems. The stabilization mechanisms used in LAS crystallization, described in the literature, are summarized in Table 1.6.

In the case of *steric stabilization*, non ionic surfactants, polymers and amphiphilic block copolymers are usually used (MATTEUCCI et al., 2008; KUMAR et al., 2009;).

Block copolymers are particularly well suited for steric stabilization, as they can provide a high degree of coverage with strong adsorption while still having extended tails which interact favorably with the medium (BUDIJONO et al., 2010).

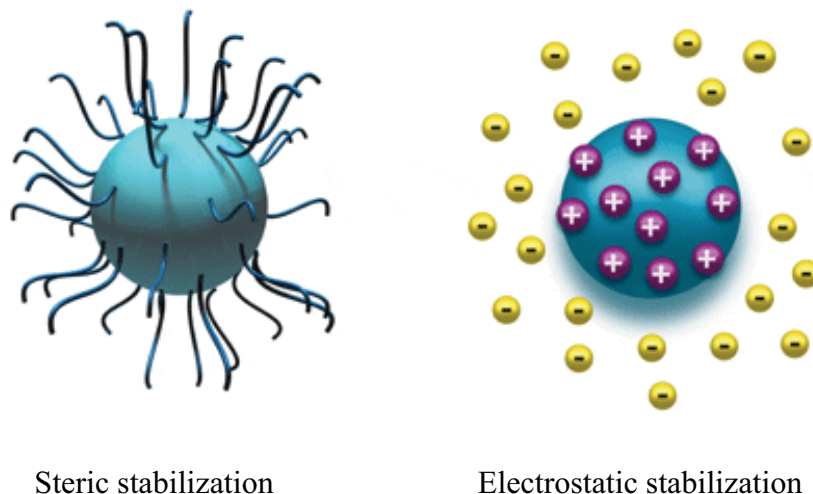


Figure 1.23. Types of colloidal stabilization. Modified from WU et al., 2011.

Stabilization by steric mechanism is achieved by attaching of hydrophobic group of the drug and polymer. The resulting polymer layer masks the attractive force and also provides a repulsive force. There are several mechanisms proposed in the literature for steric stabilization as discussed below:

- *Drug-polymer interaction:* The interaction between polymers and particle surface has been extensively studied for decades due to its wide application. The adsorption properties of stabilizers can be affected by the nature of stabilizer and drug surface, for example molecular weight is an important factor for polymeric stabilizers. The chain length should be high enough, so that polymers chain have an optimum length to overcome the Van der Waals forces of attraction (PELTONEN and HIRVONEN, 2010). Furthermore, another important factor is the size of the polymer. The polymer's chain was divided into three sub-types: trains, loops and tails. (as shown in Figure 1.24). Trains are all contacted (adsorbed) with the particle surface. Loops are

not in contact with the particle surface, but connect with two trains. Tails are non-adsorbing chain ends. The portion of polymer chain in solution provides the steric protection depending on molecular weight of polymer (NAPPER, 1983).

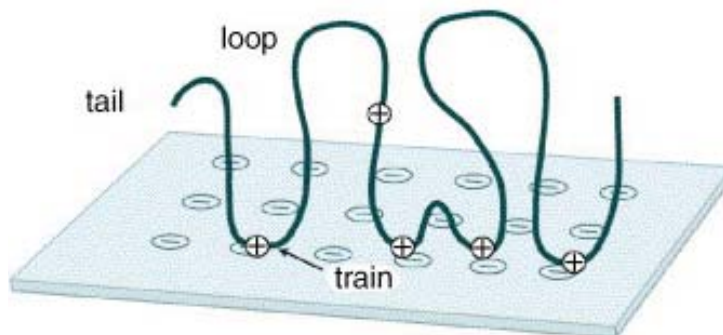


Figure 1.24. Schematic illustration of adsorbed polymer layer. From NYLANDE et al., 2006.

Apart the size and the molecular weight the effect of polymer concentration is an important aspect to be considered. For polymer concentration, there is a maximum value full coverage of surface, or saturated adsorption (SCHOTT,1980; OTSUBO,2003) concentration with free polymer in the dispersion medium, above a critical volume fraction of polymer in solution. This phenomenon is called depletion flocculation. This one occurs when the distance separating two colloidal particles is too small to admit the presence of polymer coils in solution. They are forced out of the space in between, resulting in an osmotic pressure difference between the area in between the particles and the rest of the bulk solution. As a result, an attractive force is generated which pushes the particles together, leading to agglomeration. (OTSUBO, 2003).

Another such mechanism is the formation of hydrogen bond between the stabilizer molecule and the particle surface. Some functional groups in polymers, such as carboxyl, hydroxyl, amine, and ester group play an important role in the steric stabilization. These functional groups can interact with the particle surface and act as good anchors (SHI, 2002)

The adsorption of polymer on crystal surface can occur as a result of forces as those arising from hydrophobic interactions. It has been observed that these

hydrophobic interactions can enhance the stability by occupying the adsorption sites and inhibiting the incorporation of drug molecules in solution in crystal lattice (RAGHAVAN et al., 2001).

Actually in the literature there are a lot of reports that describe the use of block co-polymers for stabilization of crystals obtained by LAS crystallization. Hydrophobic part of block copolymers gets anchored on the hydrophobic drug surface and hydrophilic chains extend in solution. Depending on the solvent quality, affinity of the chain monomers to the surface and crowding conditions on the surface, the conformation of polymer chains on a surface can be rather different. Chain exists as isolated free coils in solution, also called the “mushroom” regime (Figure 1.25 A). In this case, chain will lay almost flat on the surface. When more block copolymer is attached the chains will extend perpendicularly to the hydrophobic surface, called “semi brush”(Figure 1.25B). When the surface gets more crowded, the chains will start to mutually interact, eventually resulting in a stretching of the individual chains away from the surface leading to a so-called “brush” formation (Figure 1.25C). This state is the result of a balance, where at full equilibrium the free energy of the stretched chain balances the interfacial energy of the solvent–particle surface (S.J. BUDIJONO et al.,2010).

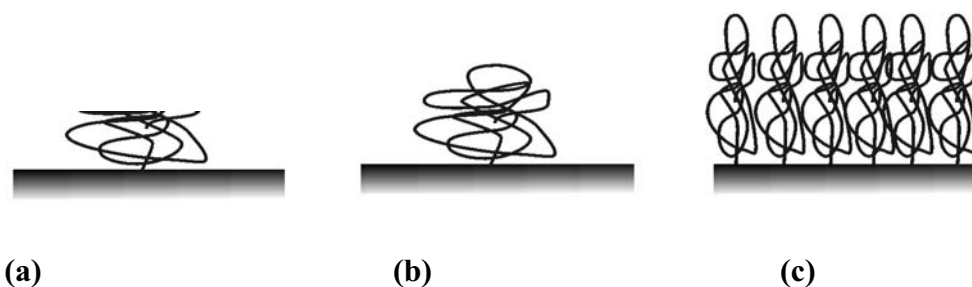


Figure 1.25. Different conformations of polymers at surfaces: (a) mushrooms conformation of a single adsorbed, where chains are non-interacting on the surface and achieve a size given by the polymer (b) semi-brush where crowding among chains causes extension of the chain from the surface, and (c) brush conformation for high grafting densities, leading to extension of the chains away from the surface. Modified from J. BUDIJONO et al., 2010.

The use of block co-polymers play a key role in both halting particle growth and stabilizing particle suspensions during rapid LAS crystallization. Its use as stabilization agent has been reported for LAS crystallization of Itraconazole, Odanacatib (KUMAR et al., 2009), β -carotene (JOHNSON and PRUD'HOMME, 2003 ; J. BUDIJONO et al., 2010 ; SHEN et al., 2011 ; CAPRETTO et al., 2012). According to these reports, with a rapid change in solvent conditions, the drug and polymer precipitate, the polymer assembling around the drug. The particle size is controlled by the polymer concentration and the mixing time.

- *Solvent-polymer interactions*: Solvent-polymer affinity is a very important factor in steric stabilization. Choi et al. (2002) have shown that solvent-polymer interaction is very important for the effective formation of nanoparticles. Choi et al. (2002) obtained PLGA using different solvents (ethyl acetate, methyl ethyl ketone, propylene carbonate, and benzyl alcohol). Ethyl acetate solvent formed the smallest nanospheres (approx. 120 nm in size). In this case, the authors suggest that solvents with low exchange ratio between diffusion from solvent to water and vice versa, form small nanoparticles due to small supersaturation region produced.
- *Drug-polymer-solvent interaction*: The polarity of the solvent can affect the relative diffusion rates of polymer and drug molecules towards the solid-liquid interface. It has been also reported that slower diffusion of API molecules and relatively quick adsorption of stabilizer molecules on particle surface leads to inhibition of growth and hence, smaller particle size (THORAT and DALVI, 2012).

In *electrostatic stabilization* ionic surfactants and polymers are usually used to prevent aggregation and have stable crystalline particles. The ions in solution adsorb onto the surface of a particle and the substances acquire surface electrical charges when brought in contact with a polar medium. The surface charge influences the spatial distribution of ions or molecules in the surrounding solution, attracting ions of opposite charge but repelling ions of similar charge from the surface.

The electrostatic stabilization depends on DLVO theory (DERJAGUIN and LANDAU, 1941 ; VERWEY and OVERBEEK in 1948) i.e. repulsive electrostatic forces and attractive Van der Waals forces. Therefore, electrostatic stabilization of dispersion occurs when the electrostatic repulsive force overcomes the attractive Van

der Waals forces between the particles (WU et al., 2011). Due to the charge on particle surface, there exists a double layer surrounding the particle surface. This double layer is referred as electric double layer (GRAHAME, 1947). There exists a potential difference between bulk of solution and the outer layer of double layer which is called zeta potential. The magnitude of the zeta potential gives an indication of the potential stability of the colloidal system. The zeta potential is a measure of the stabilization provided by electrostatic stabilization. If all the particles in suspension have a large negative or positive zeta potential ($>\pm 30$ mV) then they will tend to repel each other, i.e. good suspension stability.

Surfactants can provide stabilization at concentrations below critical micelle concentration (CMC). When concentration is increased above the CMC, the number of micelles increases leaving the particles unprotected (WU et al., 2011 ; THORAT and DALVI, 2012). In the order hand, some literature reports have focused on beneficial effects of additives, which have the capacity to form micelles, above the CMC. For example, Santander-Ortega et al., (2006) observed a variety of stabilization mechanisms for the Pluronic-coated PLGA nanoparticles. These complexes were completely stable by adding poloxamer at concentrations above the CMC, The explanation was the formation of surface aggregates that gives a highly enriched polymer layer concentration.

The *synergistic effects* of a neutral polymer and an ionic surfactant together can enhance the stabilization effect. This synergistic behavior is typically brought about by the interaction between different types of stabilizing molecules, which provides a driving force for the mixtures to form mixed aggregates or structures. However, the ability of synergistically stabilizing depends on the pair of stabilizers used. Hu et al. (2011) observed the synergistic effect of Sodium dodecyl sulfate (SDS) and hydroxylpropyl methyl cellulose (HPMC) E3, such as an effective system to retain the particles of fenofibrate within the nanosized range by minimizing particle aggregation.

Actually both steric and electrostatic stabilizing agent (polyelectrolytes) have been studied in the literature (ZHU et al., 2010 ; PATTEKARI et al., 2011 . They form a

strong double layer around hydrophobic drug particle and, adsorbs loosely, the extending polymer loops provide the steric stabilization, if the polyelectrolyte adsorbs on particle surface. Chitosan can be cited as an example. The chitosan is a cationic polyelectrolyte of natural origin. Furthermore, chitosan is physiologically safe. It can be biodegraded by several human enzymes. It is inexpensive and approved as a safe dietary. The properties of chitosan include the ability to adhere to mucosal layers, due to the electrostatic interaction with negatively charged mucus. This makes chitosan especially useful for poorly water soluble drug delivery and targeting (ZHU et al., 2010).

Finally, it has been shown that additives can increase their dissolution rate by increasing aqueous wettability of LAS recrystallized drugs of (SRITAPUNYA et al., 2012). This ability of additives will permit the gastrointestinal fluids to wet more effectively and to come into more intimate contact with the solid dosage forms, which will tend to increase the dissolution and absorption rates of the drugs (BUCH et al., 2011 ; SAHARAN and CHOUDHURY, 2012).

It has been reported in the literature, that poloxamer 407 (P-407) has improved significantly the dissolution of poorly water soluble drugs (DUMORTIER et al., 2006 ; VIKRANT et al., 2009 ; CHOWDARY and ANNAMMA, 2012). P-407 is characterized by its highest hydrophilicity and surfactant property, that results in greater wetting and increases the surface available to dissolution by reducing interfacial tension between the hydrophobic drug and dissolution medium (VIKRANT et al., 2009).

1.6. THESIS OVERVIEW

This Chapter reviewed the literature about the improvement of bioavailability of poorly water soluble drugs. It focuses on topics of interest for our work, like properties of drugs influencing dissolution behaviour, technologies to enhance dissolution rate and solubility of this category of drugs. Emphasis was given to the LAS crystallization process.

An overview of the literature on LAS crystallization summarized the main results of previous works. The main points to be highlighted are:

- Till now, several poorly water soluble drugs have been micronized by various particle formation processes for particle size and morphology but the main challenges are the control of particle size distribution and particle growth.
- The continuous production of recrystallized drug particles can be achieved by using rapid mixing devices such as impinging jets and static mixers, among others. Moreover, polymers and surfactants are used in most cases for prevent crystal growth and/or agglomeration. However, the selection of correct stabilizers for the LAS crystallization of a given drug is of crucial importance.

This chapter concludes with a statement of research objectives:

LAS crystallization is used for particle formation of a new antiretroviral drug named CRS 74. The objective is to enhance dissolution properties by reducing particle size of an original (as-received) sample from industry.

To generate high mixing rates and help in generating rapid and uniform supersaturation, rapid mixers are used (T-mixer, Roughton mixer).

The best conditions for LAS crystallization of this new molecule are defined through solubility studies, dissolution method development and screening of LAS

CHAPTER 1

crystallization process parameters such as ratio between drug solution and anti-solvent and additive screening study.

CHAPTER 2

Characterization of CRS 74

Résumé Chapitre 2- Caractérisation du CRS 74

Cette étude porte sur un nouveau composé, l'acide (2S, 3S, 5S) -2, -5 bis-[N-[N-[[N-méthyl-N-[(2-isopropyl-4 - tiazolyl) méthyl] amino] carbonyl] vanilyl] amino-1,6 - diphényl-3 - hydroxyhexane, nommée par la suite CRS 74. Ce principe actif possède une activité de l'inhibition du VIH (virus de l'immunodéficience humaine) protéase, une enzyme essentielle impliquée dans le processus de réplication du VIH.

Dans la première partie de notre étude, cette molécule a été caractérisée sous forme solide en terme de faciès et de taille de particules, de structure cristalline, de mouillabilité, de solubilité en milieu aqueux à 37 ° C. Un test de dissolution a été développé en milieu aqueux à 37 °C afin de déterminer les profils de libération de la poudre initiale et des poudres synthétisées, car ce test n'existait pas dans la littérature.

Cette molécule sous forme solide a une solubilité aqueuse limitée ($<0.5\mu\text{g/mL}$), qui peut être expliqué par sa cristallinité, son point de fusion et son enthalpie de fusion élevés (188,6 °C et 86,6 J/g). Elle présente aussi un faible taux de dissolution dans l'eau pouvant être liée à sa large distribution granulométrique, sa faible solubilité et sa mouillabilité très faible ($\theta = 136,4 \pm 0,8^\circ$).

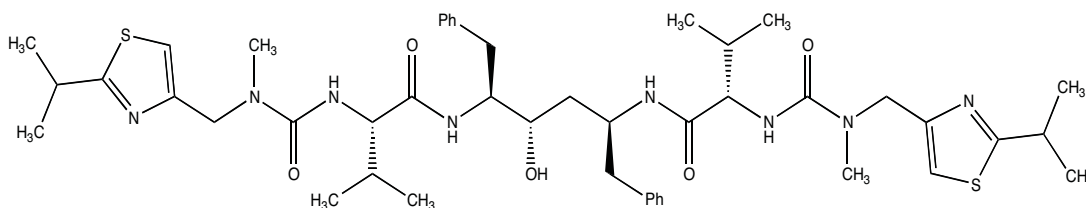
Afin d'améliorer son taux de dissolution une opération de cristallisation par effet anti-solvant a été proposée afin d'augmenter sa surface spécifique et améliorer sa mouillabilité.

2.1. INTRODUCTION

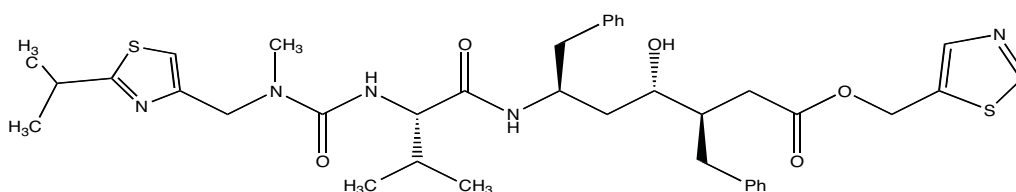
In the first part of our study, the selected molecule (as-received) was characterized in terms of their physical properties (particle shape and size), crystal structure, surface properties (wettability), solubility and dissolution properties in aqueous media at 37°C. The methodology used and the results obtained are summarized in this Chapter.

2.1.1. The molecule: CRS 74

This study concerns a new compound, (2*S*, 3*S*, 5*S*)-2, -5 bis- [N-[N-[N- methyl- N-[(2-isopropyl- 4- thiazolyl) methyl] amino] carbonyl] vanilyl] amino- 1,6- diphenyl- 3- hydroxyhexane, named CRS 74. Its chemical formula is C₄₆H₆₆N₈O₅S₂ and its molecular weight 875.2 g/mol. Its molecular structure is shown in Figure 2.1. It is obtained as courtesy from Cristália Ltda (Itapira, SP, Brazil). The drug samples have a purity of 99 %.



(a) CRS 74 - (2*S*, 3*S*, 5*S*)-2, -5 bis- [N-[N-[N- methyl- N-[(2-isopropyl- 4- thiazolyl) methyl] amino] carbonyl] vanilyl] amino- 1,6- diphenyl- 3- hydroxyhexane, is disclosed at PCT document number WO 20005/111006; US 2010/7763733 (BOCKELMANN et al., 2005; BOCKELMANN et al., 2010).



(b) RITONAVIR - (2*S*, 3*S*, 5*S*)-5-[N-[N-[N- methyl- N-[(2- isopropyl-4-thiazolyl) methyl] amino] carbonyl] vanilyl] amino- 2- [N [(5-thiazolyl) methoxycarbonyl] amino]-1,6- diphenyl-3-hydroxyhexane, is disclosed at PCT document number WO 94/14436 (KEMPF et al., 1994).

Figure 2.1. Chemical structures of (a) CRS 74 and (b) Ritonavir.

This compound can be prepared by methods disclosed in PCT document WO 111006 and US 7763733 (BOCKELMANN et al., 2005; BOCKELMANN et al., 2010) following the scheme shown on Figure 2.2. In a general way, the compound (4) can be obtained by coupling the compound (1) and (2), wherein Y can be OH or an activate ester group and P is a N-protective group, to the formation of (3) following the N-deprotection. Finally the compound (4) is coupled to the compound (5) wherein Z can be OH or an activate ester group to provide the analogous compound (6).

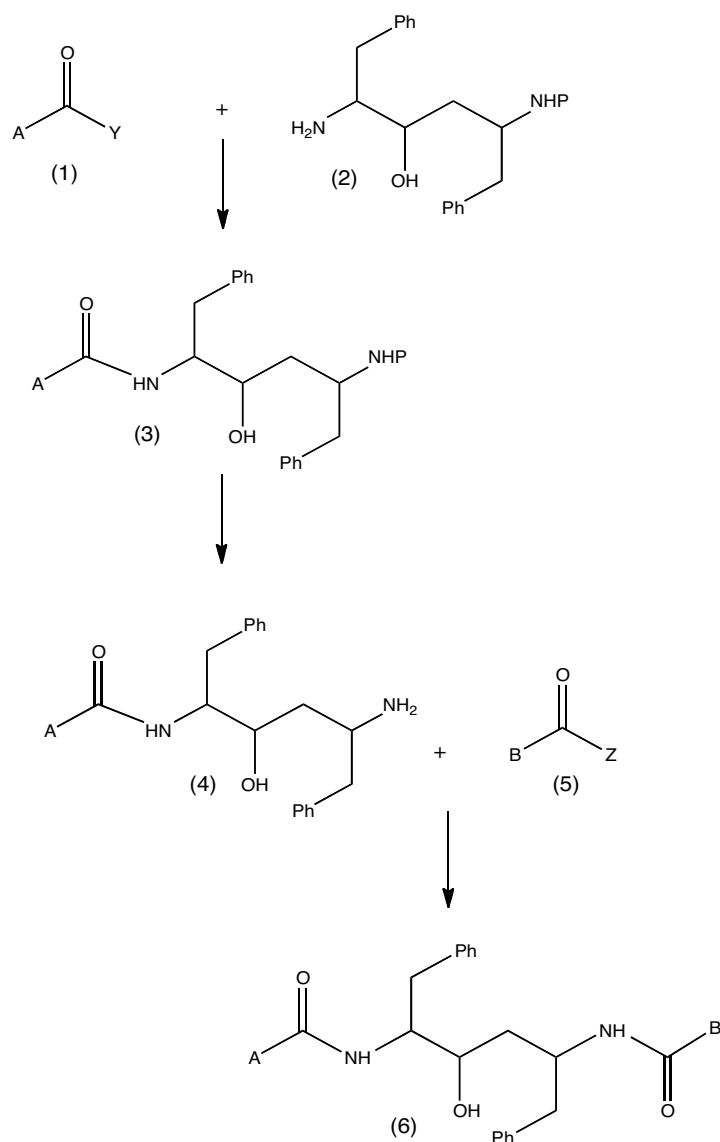


Figure 2.2. Schematic synthesis of CRS 74 (BOCKELMANN et al., 2005; BOCKELMANN et al., 2010).

CRS 74 has activity for inhibiting HIV (Human immunodeficiency virus) protease, an essential enzyme involved in HIV replication process (see Appendix I). Consequently, this new compound can be used for the treatment of HIV infections, itself or in combination with other anti-HIV medicines.

CRS 74 is an analogous compound of Ritonavir, an important antiretroviral drug developed and patented by Abbot Laboratories (WO 94/14436; KEMPF et al., 1994.). The chemical structure of Ritonavir can be compared to that of CRS 74 in Figure 2.1 and their physicochemical properties in Table 2.1.

Table 2.1. Physicochemical properties of Ritonavir and its analogous compound CRS 74 .

Drug identification		
Name of the drug	Ritonavir	CRS 74
Molecular formula	$C_{37}H_{48}N_6O_5S_2^1$	$C_{46}H_{66}N_8O_5S_2^3$
Molecular weight (g/mol)	721 ¹	875.2 ³
Innovator	Abbot Laboratories (USA)	Cristalia Laboratories (BR)
Therapeutic category	HIV protease inhibitor	HIV protease inhibitor
Physicochemical properties		
Melting point (°C)	122-124 ²	180-185 ³
Polymorphism	Form I and II ⁴	*
Description	white or almost white powder ¹	white powder ³
Solubility	Soluble in ethanol, methanol, sparingly soluble in acetone R and very slightly soluble in acetonitrile and insoluble in water ¹	*

*Data not determined

¹-The International Pharmacopoeia. Fourth edition, 2011.

²-ALENCAR et al., 2006.

³- Patent WO 2005/111006 and US 7763733 (BOCKELMANN et al, 2005 ; BOCKELMANN et al., 2010)

⁴-BAUER et al., 2001

To date, there are some ambiguities regarding the BCS of Ritonavir. This molecule has been classified as a molecule belonging to *Class II* (WU and BENET, 2005; SINHA et al., 2010) or *Class IV* (HERMAN et al., 1989; WILLIAMS and SINKO, 1999; LINDENBERG et al., 2004; GOYAL and VAVIA, 2012) of the Biopharmaceutical Classification System (AMIDON et al., 1995).

Published data have shown that Ritonavir presents crystalline polymorphism (BAUER et al., 2001). Crystalline polymorphism, or the ability of a compound to exist in multiple solid-state structures, has significant impact on the physical properties, performance, and safety of an active pharmaceutical ingredient (API) and its formulated product(s). From the discovery of Ritonavir until the new drug application (NDA) filing, only one crystalline form was known to exist (Form I). Attempts to identify other possible crystal forms were unsuccessful. Ritonavir is marketed as Norvir. Two years after the launch of Norvir to the market, some lots of Norvir capsules failed a dissolution specification. Investigation of this phenomenon revealed the existence of a crystal form of Ritonavir other than the one already known (Form I). This new crystal form was designated as Form II. The two crystal forms are polymorphs and differ substantially in their physical properties such as solubility, as given in Table 2.2.

Table 2.2. Solubility of Ritonavir polymorphs at 5°C in hydroalcoholic solvent systems (CHEMBURKAR et al., 2000).

Ethanol/water (w/w)	100/0	75/25
Form I (mg/mL)	90	170
Form II (mg/mL)	19	30

The key challenge of this antiviral drug present on the Market is still drug reformulation to modify its bioavailability and pharmacokinetics. Improving bioavailability of Ritonavir (in most case, solubility) is a subject of current interest as confirmed by numerous research works in the last decade, among them:

- Nanonization by wet milling, homogenization or sonication (BALKUNDI et al,

2011);

- Prodrug synthesis (HAMADA et al., 2002). A prodrug is a drug that is administered in an inactive (or significantly less active) form. Once administered, the prodrug is metabolised *in vivo* into an active metabolite;
- Inclusion complexes with cyclodextrins and surfactants (GOYAL and VAVIA, 2012; CHOWDARY et al., 2012);
- Solid Dispersions (LAW et al., 2004 ; SINHA et al., 2010; MUSLE, 2012);
- Micro/nano-encapsulation in polymeric micelles (BORGSMANN et al., 2011);
- Self-emulsifying drug delivery systems (SEEDS) (LEI et al., 2010).

One of the requirements for a drug to be considered suitable for a therapeutic usage is its therapeutic efficacy, so, to achieve such requirement, the drug should present adequate characteristics of bio-absorption and bioavailability. CRS 74 has high biological activity as disclosed at PCT document WO 111006 and US 7763733 (BOCKELMANN et al, 2005; BOCKELMANN et al., 2010, respectively) but its bioavailability is limited because of its low aqueous solubility and dissolution rate. Such properties pose difficulties not only in the design of pharmaceutical formulations but may result in bio-variability.

2.2. CHARACTERIZATION OF CRS 74

2.2.1. Methods

Samples of CRS 74 were characterized as received by using different instrument and measurement techniques that will be described in the following.

2.2.1.1. Particle size measurement

Mean particle size and particle-size distribution are the most important parameters in designing a novel formulation and are routinely the first to be measured. Particle size distribution of the powder samples was determined by laser diffractometry. The technique of laser diffraction is based on the principle that particles passing through a laser beam will scatter light at an angle that is directly related to their size: large

particles scatter at low angles, whereas small particles scatter at high angles. The laser diffraction is accurately described by the Fraunhofer approximation and the Mie theory, with the assumption of spherical particle morphology.

The equipment used for the measurements was a MasterSizer 3000 laser granulometer (Malvern Instruments, United Kingdom), which has a reading range of 0.1-3500 μm . All the dry samples were firstly mixed with Tween 20 and then dispersed in water until achieve the good obscuration. The laser diffraction data obtained were evaluated using the volume distribution diameters $dv_{10\%}$, $dv_{50\%}$ and $dv_{90\%}$. The diameter values 10% to 90% indicate the percentage of particles possessing a diameter equal or lower than the given size value.

2.2.1.2. Density measurement

In this work, the true densities of CRS 74 powder sample (0.9282 g) was determined using a helium pycnometer (Accupyc 1330, Micromeritics, UK) that was operated according to the manufacturer's recommended procedures. Calibration was performed using standard stainless steel spheres of known mass and volume. The sample was used as they were received from the supplier. Mean values and standard deviations were determined from 25 successive measurements.

2.2.1.3. Thermal Analysis

Thermal analysis of the CRS 74 powder was performed to characterize the properties of this material as they change with temperature. Two different thermal techniques were employed here distinguished by the property which is measured: mass loss by thermogravimetric analysis (TGA) and enthalpy of transition (melting, crystallization) by differential scanning calorimetry (DSC).

2.2.1.3.1. Thermogravimetric Analysis (TGA)

Thermogravimetric Analysis (TGA) measures the amount and rate of change in the weight of a material as a function of temperature or time in a controlled atmosphere. The technique can characterize materials that exhibit weight loss or gain due to decomposition, oxidation, or desolvation (dehydration). Measurements were conducted here to predict the thermal stability of CRS 74 at temperatures up to 300°C.

Thermogravimetric analysis (TGA) of original CRS 74 crystals was performed by a thermogravimetric analyser TG-DSC 111 (SETARAM, France). The dynamic thermogravimetric curve was recorded with a mass of sample of around 5 mg packed in aluminium cell under a dynamic nitrogen atmosphere ($50 \text{ mL}\cdot\text{min}^{-1}$). The experiments were run from 20 to 300°C at a heating rate of $10^\circ\text{C}/\text{min}$.

2.2.1.3.2. Differential scanning calorimetric analysis (DSC)

Differential scanning calorimetric (DSC) is based upon the detection of changes in the heat content (enthalpy) or the specific heat of a sample at a certain temperature. As thermal energy is supplied to the sample, its enthalpy increases and its temperature rises by an amount determined for a given energy input by the specific heat of the sample. The specific heat of a material changes slowly with temperature in a particular physical state, but alters discontinuously at a change of state. As well as increasing the sample temperature, the supply of thermal energy may induce physical or chemical processes in the sample, e.g. melting or decomposition, accompanied by a change in enthalpy, the latent heat of fusion, heat of reaction etc. Such enthalpy changes may be detected by thermal analysis and related to the processes occurring in the sample (GILL, 1984).

DSC measurements were carried out using a DSC-Q200 thermal analyzer (TA Instruments, France) in a temperature range of 20 to 210°C at a heating rate of $10^\circ\text{C}/\text{min}$ under nitrogen atmosphere ($50 \text{ mL}\cdot\text{min}^{-1}$). The samples (about 3 mg) were placed in a hermetically closed aluminium pan. The transition temperature and the enthalpy of fusion (ΔH_f) were calculated using the DSC software.

2.2.1.4. X-Ray Diffraction Analysis (XRD)

X-ray diffraction is based on constructive interference of monochromatic X-rays and a crystalline sample. These X-rays are generated by a cathode ray tube, filtered to produce monochromatic radiation, collimated to concentrate, and directed toward the sample. The interaction of the incident rays with the sample produces constructive interference (and a diffracted ray) when conditions satisfy Bragg's Law ($n\lambda=2d \sin \theta$).

These diffracted X-rays are then detected, processed and counted. Conversion of the diffraction peaks to d-spacing allows identification of the material.

X-rays diffraction patterns (diffractograms) can be used to confirm the crystalline nature of a sample. Therefore, this information is used to verify whether the substances are amorphous, partially amorphous crystalline or fully crystalline (MAULUDIN, 2008) as well as the polymorphic form being present. A powder X-ray diffractometer (XPERT, Philips) was used here for diffraction studies. X-ray diffraction analysis was conducted with $\text{CuK}\alpha$ radiation at a scanning rate of $1.228^\circ/\text{min}$ from 5 to 30° , applying 40 kV at 30 mA.

2.2.1.5. Scanning electron microscopy analysis (SEM)

The surface morphology of powder samples was viewed under a scanning electron microscope (ESEM, FEG, Philips) operated at an excitation voltage of 20 kV. The powder samples were fixed on an SEM stub using double-sided adhesive tape and sputter coated with platinum at 50 mA for 6 min using an ion sputter (SC7640, Polaron), before analysis.

The principle of this technique consists in the emission of primary electrons. Once they reach the sample surface, they interact with the atoms of the material, giving rise to secondary electrons, backscattered electrons and photons. The number of electrons emitted varies according to the geometry and other properties of the sample. These electrons are collected by a detector, producing image.

2.2.1.6. Contact angle measurement (sessile drop method)

Contact angles (θ) of water on drug substrates were measured by the sessile drop method using a Contact Angle Measuring Instrument DSA30E (Kruss Instruments, France). This method of contact angle measurement uses optics to measure the angle of a drop sitting level on a surface. The drop shape is recorded with a high speed framing camera, images are then processed by a computer and stored. The camera determines a baseline, forms a line around the drop, and calculates the contact angle. The powder sample was placed on the sample holder. A 5 μL droplet of the liquid probe (deionized water) was placed on the sample surface and the image of the drop was captured by a

CCD digital video camera. All measurements were performed in air under ambient conditions and the reported values are an average of at least three measurements for each experiment.

2.2.1.7. In Vitro Dissolution Testing

2.2.1.7.1. Defining the operating conditions for in vitro dissolution

To date, there is no published dissolution test for the evaluation of in vitro release profiles of CRS 74 from immediate-release solid oral dosage forms (powders for example). To study the dissolution properties of the CRS 74 powder sample, this part of the work was planned with the following objectives:

1. To develop and validate a dissolution methodology for this newer antiretroviral drug;
2. To estimate antiretroviral drugs by HPLC method.

A dissolution tester DT 60 (ERWEKA, Germany) was used in this study. A schematic diagram of the type II dissolution apparatus is shown in Figure 2.3, where paddle was used as the source of agitation (the paddle method).

Three different dissolution media (pH 6.8 phosphate buffer, 0.1 M hydrochloric acid and deionized water) without additives were tested to find the best conditions to evaluate the drug dissolution rate. From preliminary experiments whose results will be shown in the section 2.3.6, the selected medium was 0.1 M HCl.

Three different rotation speeds were tested before setting a rotation speed of 75 rpm for the CRS 74 dissolution study (no enough powder dispersion in the medium at 50 rpm; no additional effect on powder dispersion at 100 rpm). In the following, experiments were carried out using 30 mg of the reference product (as received CRS 74) in 900 g of 0.1 M HCl at 75 rpm and $37.0 \pm 0.5^\circ\text{C}$. Two milliliters samples were withdrawn at specific intervals. The samples were filtered through a 0.22 μm filter before the injection (20 μL) into the HPLC system (Agilent 1100 Series) for evaluate

the amount of CRS 74 dissolved. The sample volume taken was not replaced by fresh dissolution medium to prevent any possible interference with the chemical equilibrium.

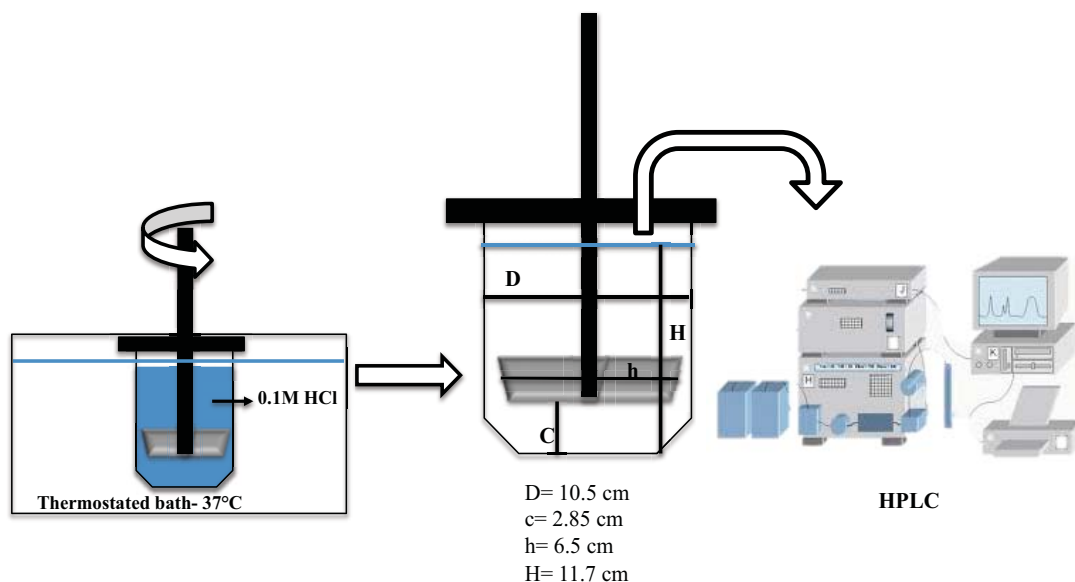


Figure 2.3. Schematic diagram of Apparatus II (Paddle Apparatus): **D**: vessel diameter; **h**: paddle width, **c**: distance between the paddle and the vessel bottom, **H**: liquid height into the vessel.

2.2.1.7.2. High Performance Liquid Chromatography (HPLC) to determine the content of the dissolved drug

Dissolved drug in dissolution media was determined by high performance liquid chromatography (HPLC). This technique utilizes different types of stationary phases contained in columns, a pump that moves the mobile phase and sample components through the column and a detector capable of providing characteristic retention times for the sample components and area counts reflecting the amount of each analyte passing through a detector (Figure 2.4).

The HPLC system consists of an Agilent chromatograph (Model 1100 series) equipped with a UV-vis detector. There are several parameters that quantitatively measure how well a HPLC column separates the components of interest. These

parameters will vary based on the dimension of the column, type of column, type of mobile phase or stationary phase used, and HPLC instrument. The different HPLC conditions tested during our method development were shown in Table 2.3. The mobile phase was chosen after several trials with acetonitrile, methanol and phosphate buffer pH 4.0 in different volume proportions. Finally, a mobile phase consisting of acetonitrile/water (50:50) in an isocratic mode was selected to achieve maximum separation.

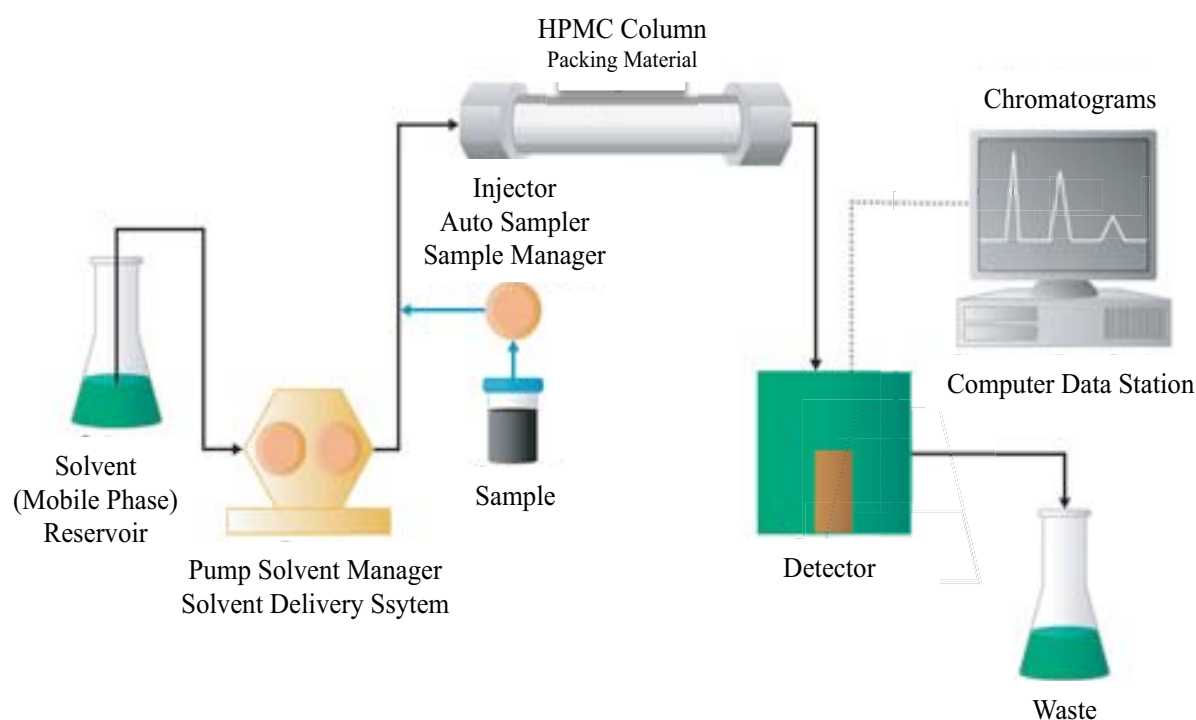


Figure 2.4. Schematic representation of a High Performance Liquid Chromatography system.

Flow rates were arranged between 0.8 and 1.3 mL/min (Table 2.3). A flow rate of 1.0 mL/min gave an optimum signal/noise ratio with a reasonable separation time (10 min) between the analyte peak and dissolution media peak. After comparison between the different columns shown in Table 2.3 such as C₈ Prontosil 100 mm x 4.6 mm, 5 μ m, C₈ Prontosil 250 mm x 4.6 mm, 5 μ m and C₁₈ Prontosil 250 mm x 4.6 mm, 5 μ m, the

best separation efficiency was obtained using ProntoSIL 120-5 C8 SH, 150 x 4.0 mm column.

The retention time, i.e., the time taken for CRS 74 molecule to reach the detector once it has been injected into the system, was observed to be 12 min. UV spectrum – of CRS 74 showed maximum absorption at 210 nm; therefore, the compounds were monitored at this wavelength. In summary the best conditions were set to the HPLC analyses: the elution was done using a mobile phase consisting of acetonitrile/water in the ratio of 50:50 on HPLC column ProntoSIL 120-5 C8 SH, 150 x 4.0 mm ID, at a flow rate of 1.0 mLmin⁻¹ with UV detection at 210 nm. Each experiment was carried out in quadruplicate.

There is no monograph of this drug in any pharmacopoeia. After setting the HPLC parameters for analysis, the HPLC quantification method was developed for the quantification of CRS 74 concentrations and two validation parameters were tested through specificity and linearity.

Specificity of the method was determined by analyzing the dissolution media with and without the standard substance to verify the interference of the eluent in the CRS 74 concentration measurements. To assess the linearity of the method, seven calibration standard solutions of CRS 74 dissolved in 0.1 M HCl were prepared over the concentration range of 13- 289 µg/g_{solution}. The calculation of regression line was carried out by plotting the peak area against standard concentration.

Table 2.3. Different HPLC parameters tested during the HPLC method development.

Column	Mobile phase (volume %)	Flow rate (mL/min)	Volume injection (μL)
C8 PRONTOSIL 100mmx4.6mm, 5μm	ACN: 50% ; PB : 40% ; MeOH : 10%	1.3	10
C8 PRONTOSIL 250mmx4.6mm, 5μm	ACN : 50% ; PB : 40% ; MeOH : 10%	1.0	10
		0.8	
	ACN : 50% ; PB : 50%	1.0	20
		0.8	
	ACN : 30% ; PB: 70%	0.8	20
	ACN: 50%; PB: 40% ; MeOH: 10%	1.0	10
C18 PRONTOSIL 250mmx4.6mm, 5μm	ACN : 50% ; PB: 30% ; MeOH : 20%	1.0	10
	ACN : 60% ; PB: 30% ; MeOH : 10%	1.3	10
		1.0	
Prontosil 300-5- ODSH, 5μm	ACN : 70 % ; Pure water : 30%	1.0	20
ProntoSIL 120-5 C8 SH, 150 x 4.0 mm, 5μm	ACN : 50 % ; Pure water : 50%	1.0	20

ACN: Acetonitrile; PB: Phosphate buffer ; MeOH: Methanol.

The obtained results in HPLC analysis were used to calculate the percentage dissolved at each time of dissolution profile. The cumulative percentage of dissolved drug was plotted against time, in order to obtain the dissolution profile and to calculate the in vitro dissolution data, using the equation (2.1).

$$Dissolved\ Drug\ (\%) = \frac{Abs_{sample}}{Abs_{std}} StdPurity(\%) \quad (2.1)$$

where Abs_{std} is the absorbance of the standard solution containing the original CRS 74 100% dissolved, Abs_{sample} the absorbance of the sample during the dissolution essay as a function of time and $StdPurity$ (%) the purity of the raw material, provided by the supplier.

2.2.1.7.3. Drug solubility in dissolution media

The solubility of CRS 74 was determined by equilibrating an excess of CRS 74 in 5g of 0.1 M HCl at $37^{\circ}C \pm 0.5^{\circ}C$ in a temperature-controlled bath for 24 h (Figure 2.5).

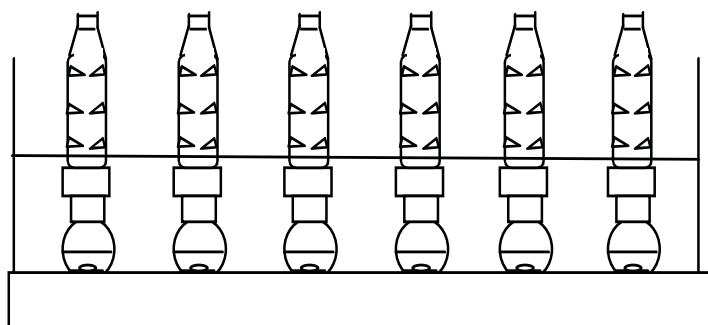


Figure 2.5. Experimental setup for solubility measurements.

The flasks were sealed for the duration of the tests and the concentration was determined by removing the solid phase by filtration (0.22 μ m pore size) and injection of the filtered solution into the HPLC system to be analyzed at wavelength of 210 nm. The HPLC parameters were already presented in the methodology.

2.3. RESULTS AND DISCUSSION

2.3.1. Particle size, true density and morphology

The particle size distribution is shown in Figure 2.6. Laser diffractometry yields the volume-weighted diameters. Particle size analysis values of $dv_{90\%}$, $dv_{50\%}$ and $dv_{10\%}$ were 515 μm , 101 μm and 4.3 μm , respectively. The broad particle size distribution exhibited by the original drug powder is confirmed by the SEM micrographs (Figure 2.7).

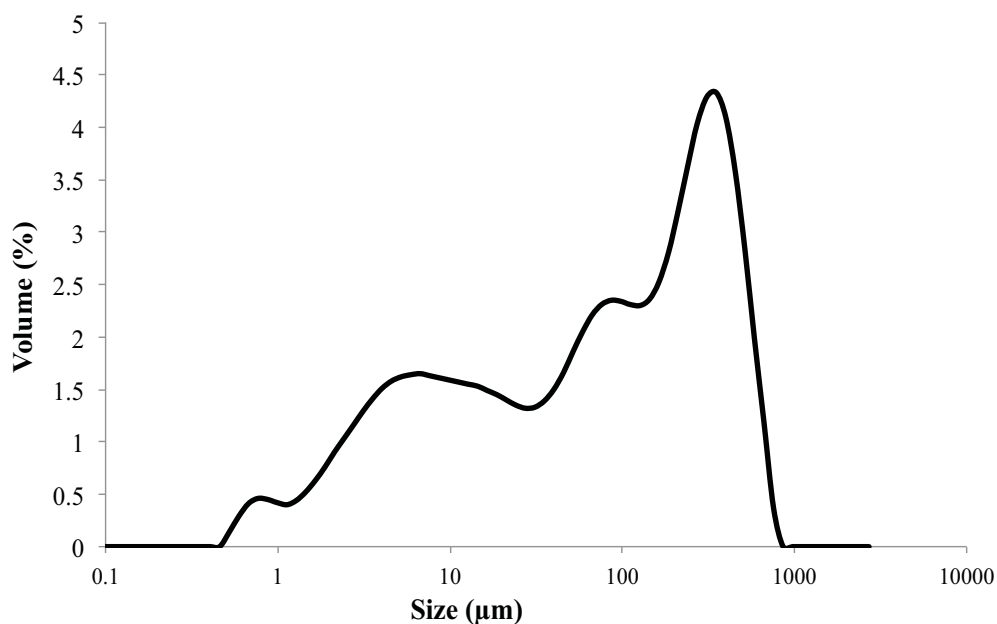


Figure 2.6. Particle size distribution for as-received CRS 74 powder sample.

In addition, the SEM images at a higher magnification showed that the original CRS 74 sample consisted of columnar crystals that were several micrometers long (Figure 2.7 (b)). SEM images show the presence of agglomerates of small columnar crystals (Fig 2.7 (a))

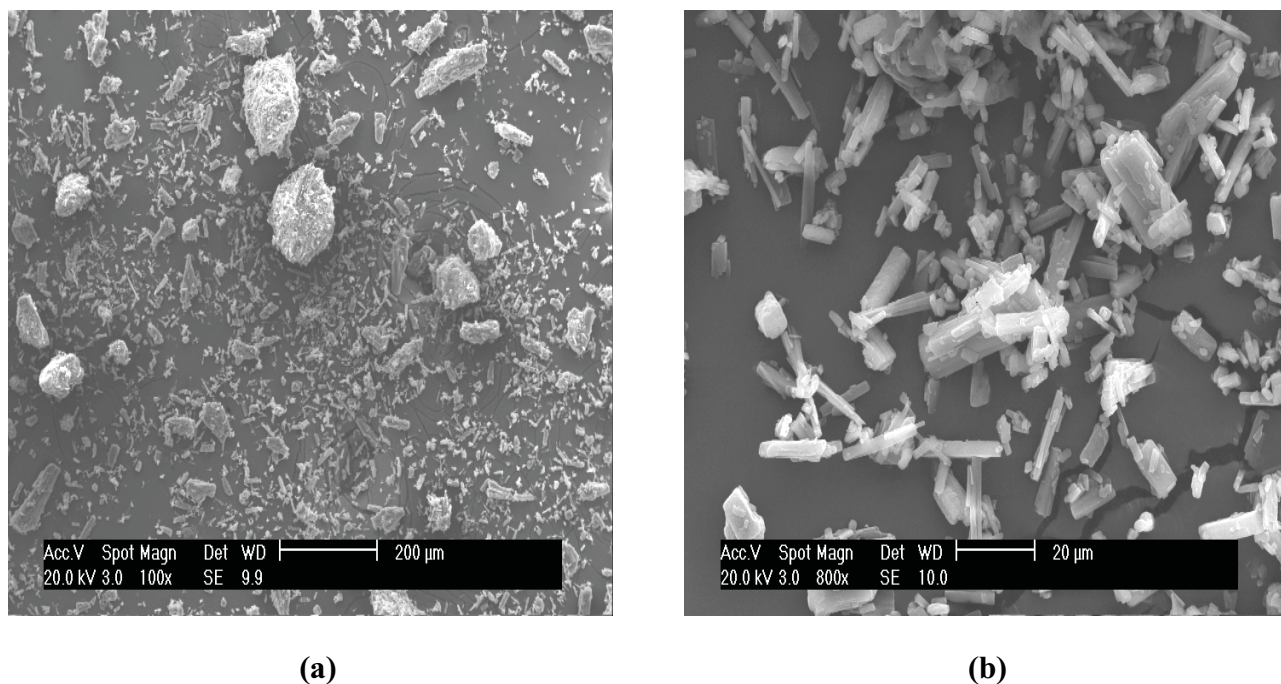


Figure 2.7. SEM micrographs of the original CRS 74.

2.3.2. Density

The powder had a true density of $1.2295 \pm 0.0205 \text{ g/cm}^3$ when analyzed using helium pycnometry.

2.3.3. XRD analysis

XRD analysis was performed to detect the changes in the physical state and crystalline phases of the drug, before and after LAS crystallization. Figure 2.8 shows the XRD patterns for the as-received powder sample. CRS 74 shows peaks at approximately 8.5 , 14 , 16.9 , 18.7 , 19.4 and 21.3° , indicating that the drug was a crystalline powder.

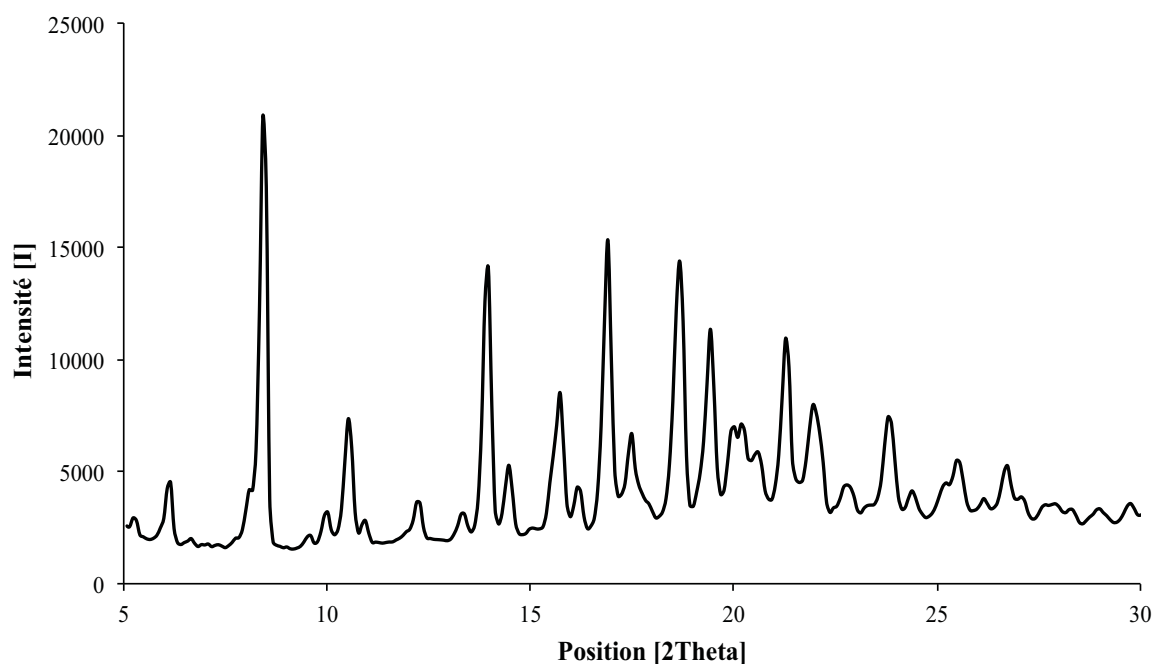


Figure 2.8. X-Ray diffractograms of the as-received CRS 74 sample.

2.3.4. TGA and DSC analysis

Thermogravimetric analysis (TGA) was used in this study to determine the thermal stability of CRS 74 by monitoring the weight change that occurred as the sample was heated. From TGA data (Figure 2.9) it was observed that the drug becomes thermally unstable from 215°C. Mass loss and a large peak were observed respectively on the mass loss and on the heat flow at 242°C. This endothermic peak was observed in an only one step. It probably characterizes the degradation of the drug. For this reason, in the following, DSC analyses were carried out between 20 and 210°C to avoid the drug thermal degradation.

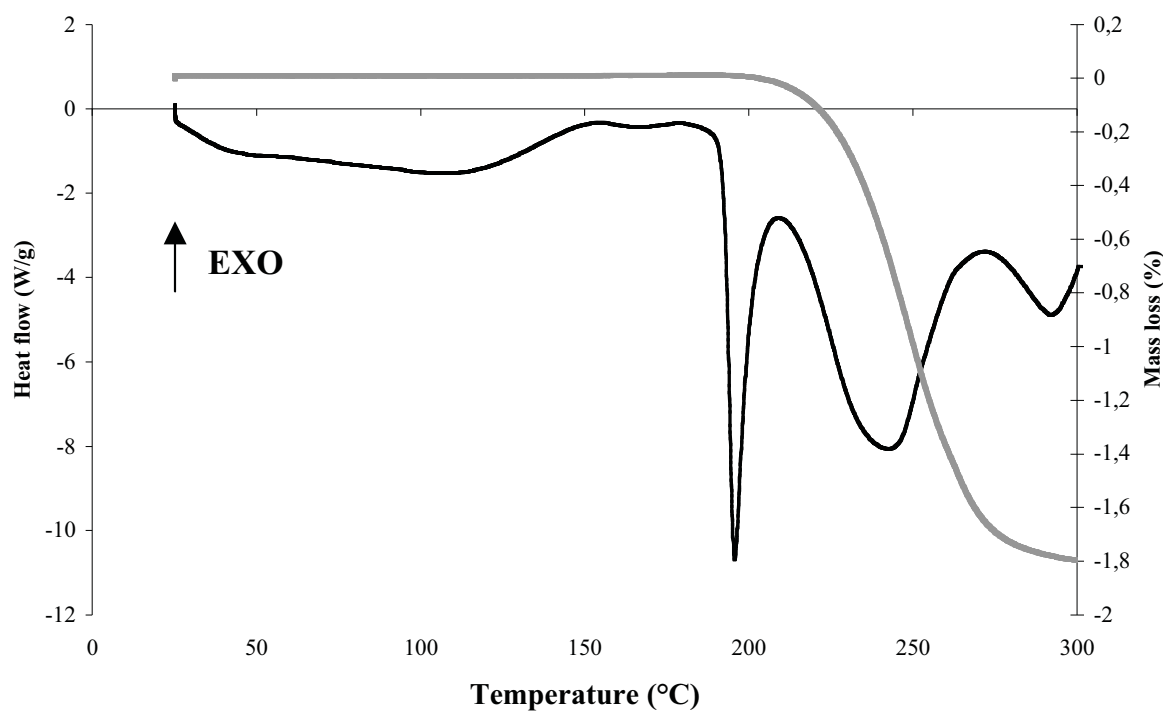


Figure 2.9. TGA-DSC curve of CRS 74 run in a nitrogen atmosphere and heating rate of 10°C/min.

The DSC thermograms of CRS 74 powder, is presented in Figure 2.10. During the heating-cooling cycle it was observed a broad endotherm peak at 188.6°C, which may correspond to the melting of crystalline product.

Crystal energy is known to correlate with $T_{m(\text{Onset})}$ (onset melting point) and ΔH_m (enthalpy of melting), which refers to the energy a compound must overcome to dissolve the drug (VIPAGUNTA et al., 2007). The onset melting point and fusion enthalpy obtained from the DSC study are summarized in Table 2.4. The molecule was then characterized by a high melting point (188.6°C) and a high enthalpy of fusion (86.6 J/g).

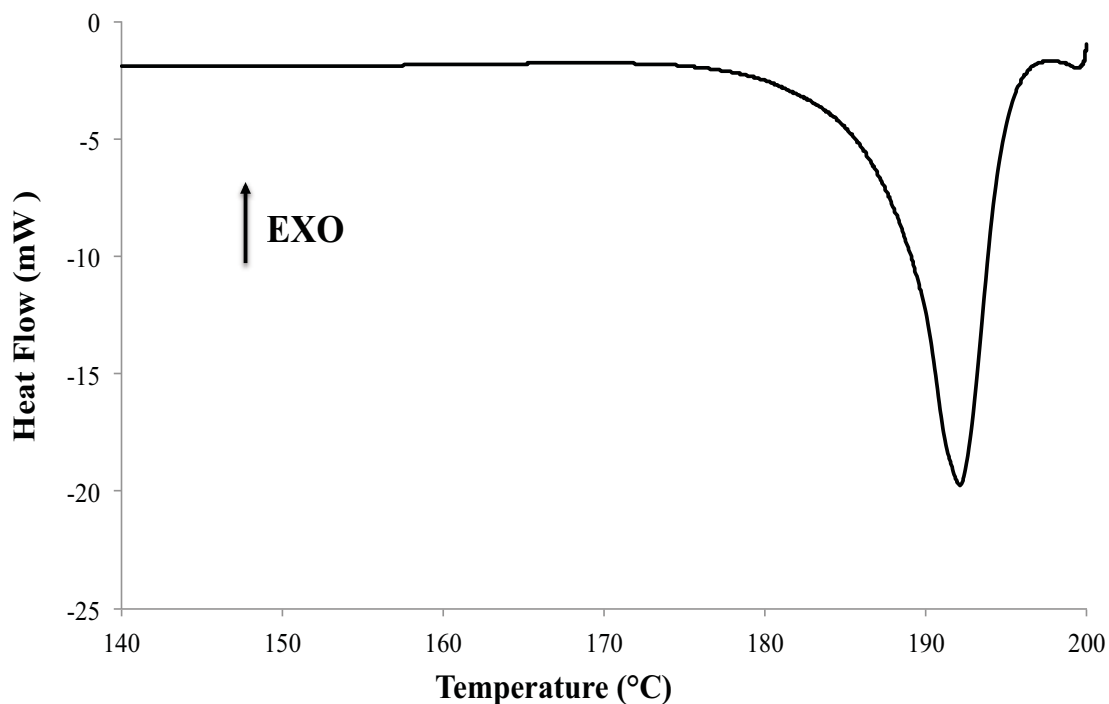


Figure 2.10. DSC thermograms of as-received CRS 74 sample (*first heating*), which consists of a melting endotherm (peak onset temperature) $T_{m(\text{Onset})} = 188.6^{\circ}\text{C}$.

Table 2.4. Melting Temperature ($T_{m(\text{Onset})}$), Enthalpy of fusion (ΔH_m) for as-received CRS74 sample.

Thermal parameters	Cycle 1 (heating-cooling)
$T_{m(\text{Onset})}(\text{°C})$	188.6
ΔH_m (J/g)	86.6

2.3.5. Determination of surface properties

The surface properties of drug samples were investigated to find a possible relation between surface properties and dissolution. Sessile drop contact is most commonly measured on compacted powder disc surface. However, compaction of the material can alter the particle morphology and surface energy (BUCKTON, 1955). Alternatively, some of the authors (AHFAT et al, 2000; HE et al, 2008) have reported the use of powder layer adhered to an inert support. The powder layer was adopted for the present work as it allows the study of “as is” powder properties. This method gave reproducible values. It has been seen that contact angle measurements can vary with experimental methodology, however the technique was used for evaluation of the surface properties of original drug powder.

The contact angle of drop deposited on powder surface was plotted as a function of time from 0 to 10 s, beyond which there was no significant change in the contact angle. With water as the wetting liquid, original drug crystals exhibited a contact angle almost unchanged with time from $136.4 \pm 0.8^\circ$ (0 s) to $136.6 \pm 0.6^\circ$ (10 s), as shown in Figure 2.11.

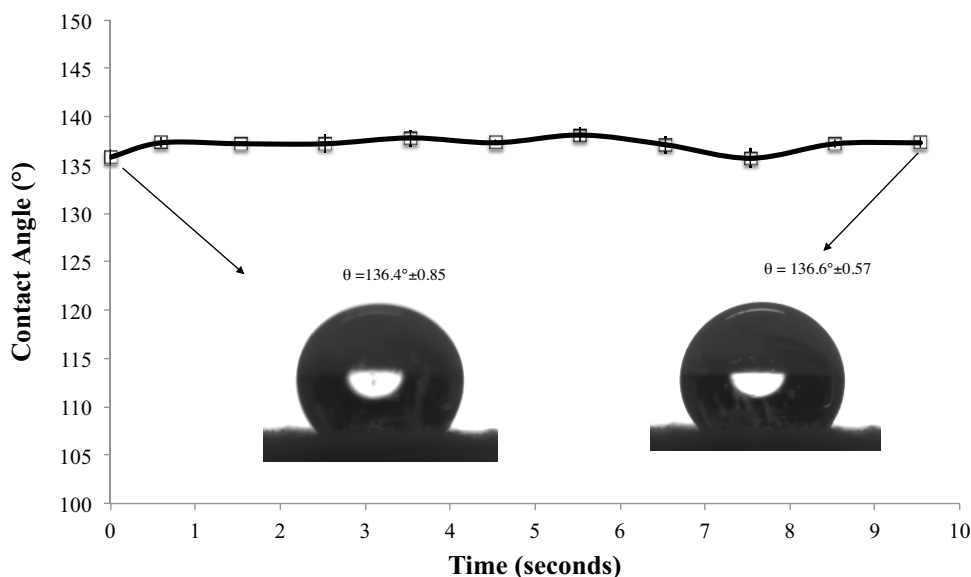


Figure 2.11. Contact angle ($^\circ$) of water as a function of time for original CRS 74.

The wetting process with water was quantified for the work of adhesion (W_A), calculated using a combination of the Young and Dupré Equations (SCHRADER, 1995), cohesion (W_{CL}) and the spreading coefficient (λ_{LS}), are calculated by the following equations, derived from the Young's equation (IVESON et al., 2001):

$$W_{CL} = 2\gamma_{LV} \quad (2.2)$$

$$W_A = \gamma_{SL} - (\gamma_{SV} + \gamma_{LV}) = \gamma_{LV} (\cos\theta + 1) \quad (2.3)$$

$$\lambda_{LS} = W_A - W_{CL} \quad (2.4)$$

where, γ is the surface free energy and L, S and V refer to the state as being liquid, solid and vapor respectively. Equation 2.3 is only valid for θ higher than 0, which is a common case for hydrophobic powders. The contact angle made at 0 s was considered as the initial contact angle and the surface tension of water was taken from the literature (72.8 mN/m; PURI et al., 2010). These values were used to determine W_A , W_{CL} and λ_{LS} from equations (2.1), (2.2) and (2.3) for the drug powder (Table 2.5).

Table 2.5. Work of adhesion (W_A), work of cohesion (W_{CL}) and spreading coefficient (λ_{LS}) for CRS 74.

Sample	W_A (mN/m)	W_{CL} (mN/m)	λ_{LS} (mN/m)
CRS 74	20.08	145.6	-125.6

The thermodynamic driving force for each process is indicated by the work value, where a negative value denotes the spontaneity of the process (YOUNG and BUCKTON, 1990). The positive W_A and W_{CL} obtained for this new antiretroviral drug

indicated that the adhesion and the cohesion processes are not spontaneous over the original powder sample. Further, a negative spreading coefficient ($\lambda_{LS} < 0$) means that this powder displayed an unfavorable spreading of water (NGUYEN and HAPGOOD et al., 2010).

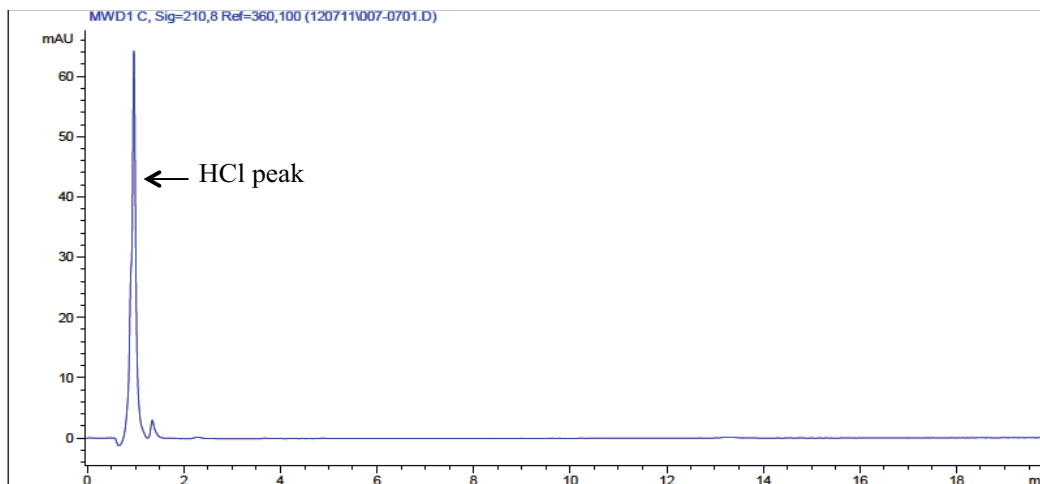
2.3.6. Dissolution studies

2.3.6.1. High Performance Liquid Chromatography (HPLC) to determine the content of the dissolved drug

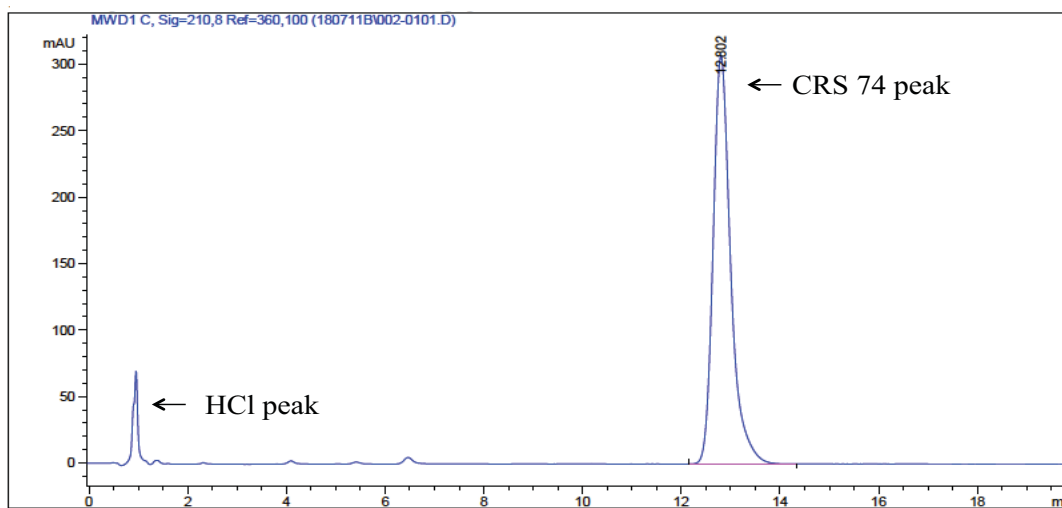
Specificity of the HPLC method

The specificity of a method gives us the guarantee that the result of the method only comes from the analyte. Specificity of our method was determined by analysing the dissolution media with and without the reference product to verify the interference of the eluent in the CRS 74 concentration measurements.

The specificity of the HPLC quantification method was demonstrated in Figure 2.12. No interferences from the dissolution medium with the peak of interest were observed in the HPLC chromatograms, confirming the selectivity of the method.



(a)



(b)

Figure 2.12. Specific test for CRS 74 in dissolution medium (0.1M HCl); (a) HPLC chromatograms of placebo (dissolution medium); (b) HPLC chromatograms of the component of interest dissolved in the dissolution medium. Flow rate of 1.0 mL/min; mobile phase consisted of acetonitrile:water (50:50).

Linearity of the HPLC method

A linear analytical method indicates that it has the ability to demonstrate experimentally that the results obtained are directly proportional to the concentration of analyte in the sample within a specified range (FDA, 1997). To assess the linearity of the method, seven solutions of CRS 74 dissolved in 0.1M HCl were prepared: 13 $\mu\text{g}/\text{g}_{\text{solution}}$, 26 $\mu\text{g}/\text{g}_{\text{solution}}$, 34 $\mu\text{g}/\text{g}_{\text{solution}}$, 51 $\mu\text{g}/\text{g}_{\text{solution}}$, 99 $\mu\text{g}/\text{g}_{\text{solution}}$, 213 $\mu\text{g}/\text{g}_{\text{solution}}$ and 289 $\mu\text{g}/\text{g}_{\text{solution}}$.

The standard curve (Figure 2.13) showed an excellent correlation in the concentration range of 13- 289 $\mu\text{g}/\text{g}_{\text{solution}}$ ($y = 36.2x$, $r^2 = 0.99917$, exceeding 0.99, which is the minimum recommended by the regulating agencies ICH, 1996 and FDA, 1997). The limit of quantification (LOQ) of the assay was 0.5 $\mu\text{g}/\text{mL}$. The calculation method used is based on the standard deviation (SD) of the y-intercepts of regression lines and the slope of the calibration curve (S), according to the formula: $\text{LOQ} = 10(\text{SD}/\text{S})$ (ICH, 1996).

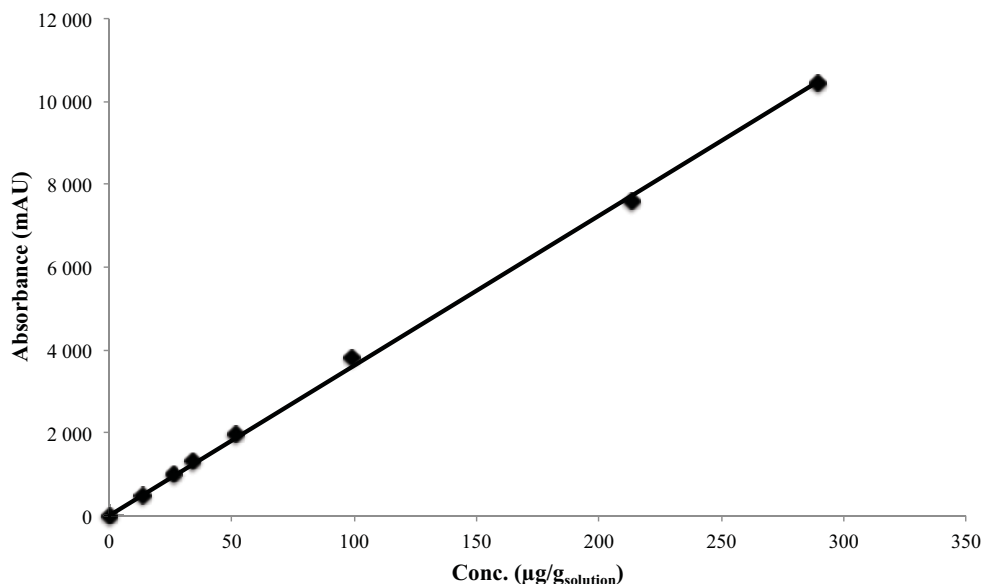


Figure 2.13. Standard curve used for the determination of CRS 74 in samples produced during dissolution experiments.

CRS 74 solubility in dissolution medium and sink conditions

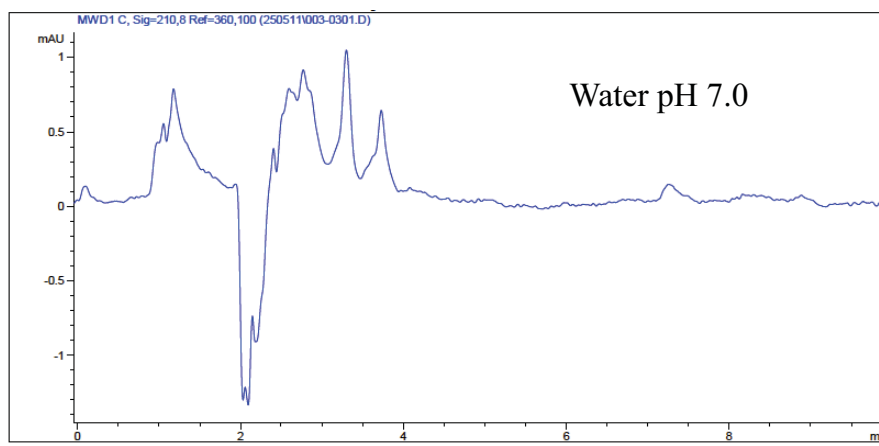
Sink conditions describe a dissolution system that is sufficiently diluted so that dissolution process is not impeded by approach of saturation of compound of interest (ROHRS, 2001). The amount of reference product (30 mg) set for our experiments assured the presence of *sink* conditions in the dissolution medium because it corresponds to a maximum drug concentration in the acidic medium $33 \mu\text{g}/\text{g}_{\text{solution}}$, three times less the equilibrium concentration of the drug in this medium, also determined experimentally, $102 \pm 8 \mu\text{g}/\text{g}_{\text{solution}}$ at 37°C .

Any optimal separations and symmetrical chromatographic peaks were observed in HPLC chromatograms for CRS 74 in water or phosphate buffer 6.8 (Figures 2.14-a and 2.14-b, respectively), reason for which the dissolution method were tested only in acidic medium.

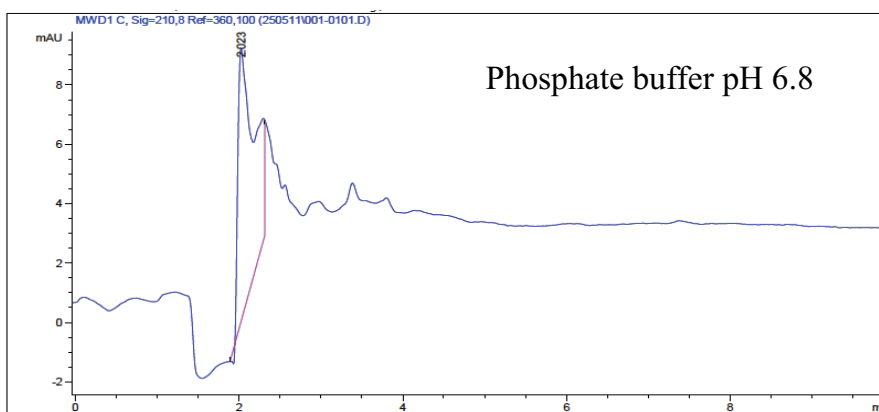
Most drugs are weak acids or weak bases that are present in solution as both the ionized and unionized species. The solubility of a weak acid or a weak base is related to pH. Acids ionize in alkaline medium, while bases ionize in acidic medium. The pKa is the pH at which concentrations of ionized and un-ionized forms are equal (NEAU, 2008).

CRS 74 is a new ritonavir analogous compound (BOCKELMANN et al., 2005; BOCKELMANN et al., 2010). Ritonavir is a weak base with two ionisable sites that dissociate below pH 3 (BERTZ et al, 2004). The pK_a of 2.8 for ritonavir refers to loss of a hydrogen from a protonated thiazole group because thiazole itself is a weak base (pK_{BH+}, 2.4) (LIDE, 1988). Analogous to Ritonavir, CRS 74 is probably a weak base with a pKa close to 3 with similar pH-dependent solubility behaviour.

According to the literature, Ritonavir is poorly water soluble with a solubility of $400 \mu\text{g}/\text{mL}$ in 0.1M HCl at 37°C , which is reduced to $1 \mu\text{g}/\text{mL}$ at phosphate buffer pH 6.8 (LAW et al, 2001). In comparison, the solubility of CRS 74 experimentally measured in this work was $102 \mu\text{g}/\text{mL}$ in 0.1M HCl and not detected ($<0.5 \mu\text{g}/\text{mL}$) by HPLC in phosphate buffer pH 6.8 or water at the same temperature.



(a)



(b)

Figure 2.14. HPLC chromatograms of the component of interest dissolved in (a) water and (b) phosphate buffer pH 6.8.

2.3.6.2. *In vitro* dissolution testing

Figure 2.15 shows the dissolution profiles of original CRS 74 drug in 0.1 M HCl (pH 1.2). It can be seen that the as-received drug did not even reach 20% dissolution within 3h, confirming its poor tendency to dissolve in aqueous media. The poor dissolution rate measured in this study can be related to the poor surface properties of the powder presented in section 2.3.5, such as unfavourable spreading of water ($\lambda_{LS} < 0$)

and not spontaneous adhesion and the cohesion processes (positives values of W_a and W_{CL}).

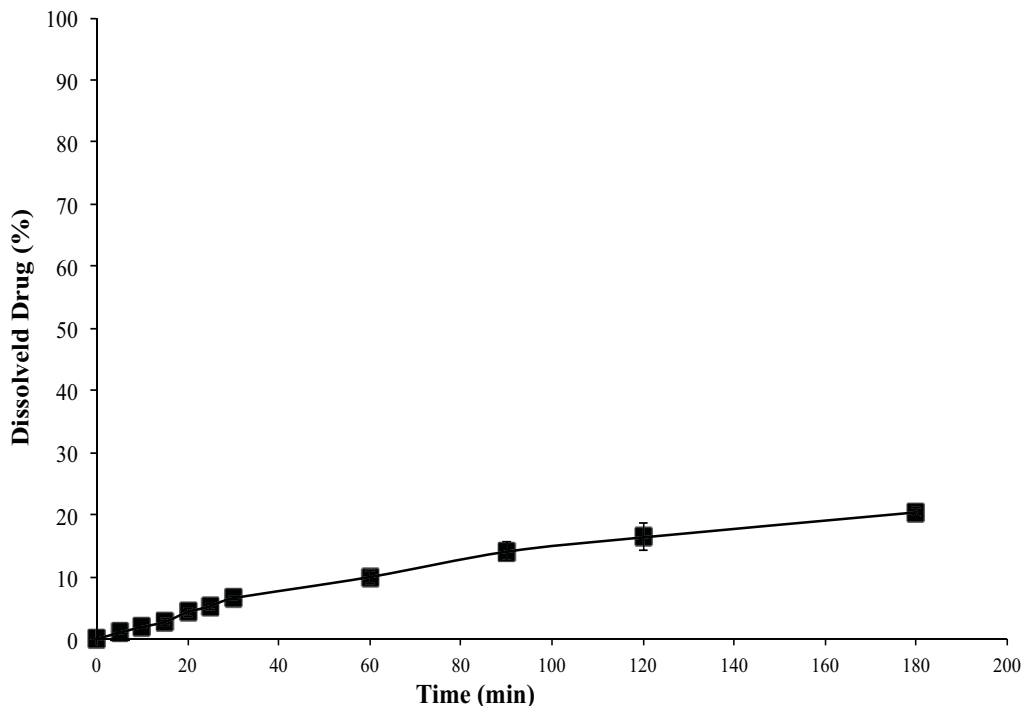


Figure 2.15. Dissolution profile of CRS 74 in 0.1 M HCl at 37°C (n=4; SD =±2).

The dissolution step seems to be the limiting step of this process of CRS 74 release in the aqueous medium. The model of Hixson–Crowell (HIXSON and CROWELL, 1931) describes the release from dosage forms, which show dissolution rate limitation and which do not dramatically change during the release process. The equation of Hixson–Crowell cube-root kinetic model is given by Equation 2.5.

$$1 - \left(1 - \frac{M_t}{M_0}\right)^{1/3} = kt \tag{2.5}$$

where k is the kinetic constant (min^{-1}), M_t is the mass of the drug dissolved in time t and M_0 is the initial drug mass in the dissolution medium.

Our dissolution data were then plotted in accordance with Hixson–Crowell cube root law (Figure 2.16) (correlation coefficient $r^2 = 0.984$) to determine the dissolution rate constant k , as given in Table 2.6.

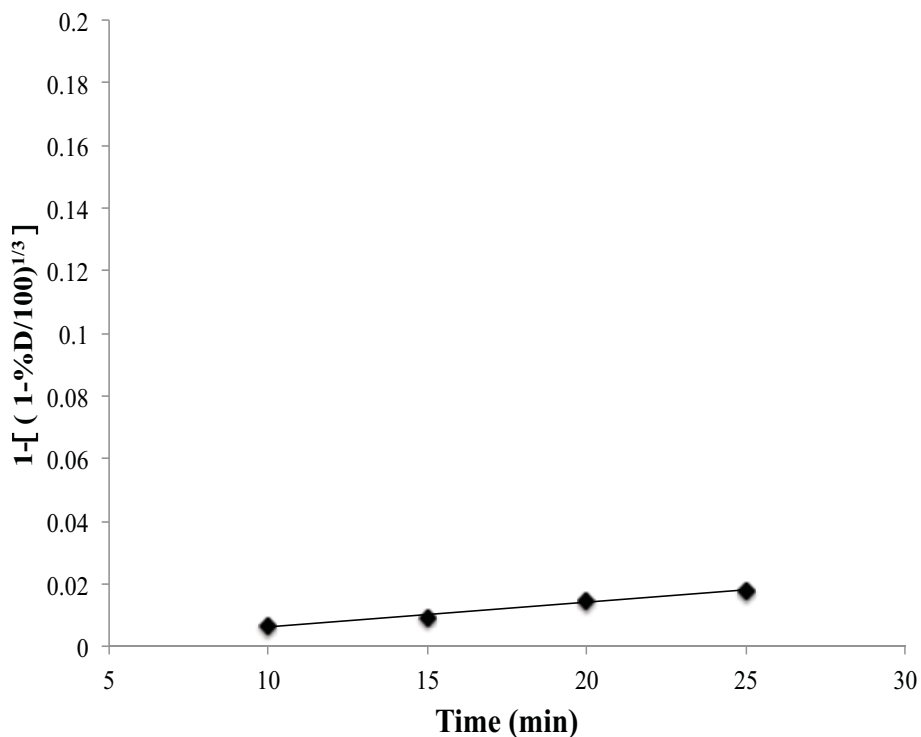


Figure 2.16. Application of Hixson-Crowell mathematical model on CRS 74 release profile.

Table 2.6. Values of k and regression equations for the mathematical models of Hixson-Crowell applied to the CRS 74 dissolution data.

Sample	Hixson-Crowell	
	k (min ⁻¹)	Linear equation
CRS 74	0.0008	$y = 0.0008 x - 0.0017^{**}$

k = dissolution rate constant.

** $x = t$ (min) and $y = 1 - [(1 - \%Dissolved/100)^{1/3}]$

2.4.CONCLUSIONS

As-received CRS 74 was characterized by laser diffractometry, powder X-ray diffraction (XRD), thermal gravimetric analysis (TG), differential scanning calorimetry (DSC), scan electronic microscopy (SEM), surface properties and dissolution testing. The results were presented and discussed in this chapter.

The saturation concentration of this molecule in water and phosphate buffer 6.8 was not detected by HPLC analysis. The molecule is slightly soluble in acid medium (0.1M HCl pH 1.2) : $102 \pm 8 \mu\text{g}/\text{g}_{\text{solution}}$. Its low aqueous solubility can be explained by its high crystallinity, its high melting point (188.6°C) and high enthalpy of fusion (86.6 J/g).

The dissolution *in vitro* test is an important tool in quality control of drugs and it becomes more important for drugs with low aqueous solubility such as CRS 74. Some characteristics of this drug are not well defined, for instance, its classification in the biopharmaceutical classification system. The aim of the dissolution study carried out here was to contribute to define CRS 74 dissolution conditions, what can be the focus for further studies. To date, there is no published dissolution test for the evaluation of *in vitro* release profiles of CRS 74 from immediate-release solid oral dosage forms. Therefore, we developed a dissolution method for CRS 74 to determine its release profiles from powder samples. The low dissolution rate presented by this molecule can be related to its large particle size (micrometric range, with a broad particle size dispersion) and very poor water wettability ($\theta = 136.4 \pm 0.8^\circ$).

Physical factors important to drug dissolution include particle size, molecular size, hydrophobicity, and crystalline structure. Physical modifications often aim to increase the surface area, solubility, and wettability of the powder particles and, therefore, typically focus on particle size reduction or generation of amorphous states. This work planned to improve the dissolution rate of as-received CRS 74 molecule using a Liquid Anti-Solvent crystallization process to increase the surface area and improve its wettability.

CHAPTER 3

*CRS 74 solubility studies in hydroethanolic solutions
and design of experimental apparatus for crystallization*

Résumé Chapitre 3- Étude de la solubilité et développement du protocole expérimental

Le choix du solvant est un des paramètres essentiels pour pouvoir envisager une opération de cristallisation. La connaissance de la solubilité d'un composant dans différents solvants est requise. L'éthanol et l'eau ont été retenus respectivement comme solvant et anti-solvant.

Dans ce chapitre, la solubilité du CRS 74 en mélanges binaires éthanol et éthanol-eau a été mesurée dans la plage de température de 5 – 30 °C, afin de déterminer le cadre expérimental pour permettre la cristallisation par effet anti-solvant.

Dans un premier temps, les équilibres solide-liquide dans l'éthanol pur et dans des mélanges binaires (éthanol/eau) ont été étudiés pour une gamme de température comprise entre 5 et 30 °C. Le solide étudié est très soluble dans l'éthanol à 30 °C : 92,6 mg/g de solution. A 30°C, la solubilité de la molécule diminue quand la quantité d'eau dans le mélange augmente. Les solubilités obtenues ont été représentées en utilisant le modèle UNIQUAC pour le calcul des coefficients d'activité. Les solubilités expérimentales et calculées présentent un bon accord. La solubilité calculée dans des mélanges eau-éthanol présente un maximum de 130,20 mg/g de solution pour un ratio massique éthanol/eau de 0,83/0,17 (w/w). Les résultats de la modélisation indiquent que ce modèle est l'outil approprié pour représenter le comportement de solubilité de CRS 74 dans des mélanges de solvants (éthanol-eau). Les solubilités expérimentales et calculées ont permis d'évaluer le ratio éthanol/eau optimum (25/75 % m/m) pour maximiser le rendement théorique en solide.

Dans un second temps, un mélange double jet avec pré-mélangeur type mélangeur en T ou mélangeur Roughton a été choisi pour réaliser la cristallisation. Dans les deux cas, des nanoparticules sont créées en sortie du pré-mélangeur. Des expériences préliminaires ont montré que le solide présente des vitesses de croissance et d'agglomération élevées. Les particules obtenues avec le mélangeur en T semblent moins agglomérées.

Ce type de mélangeur a donc été retenu pour la suite de l'étude. Deux principaux résultats ont été obtenus.

Le solide cristallisé est toujours aggloméré. Son profil de dissolution dans une solution acide (0,1M HCl) reste inchangé. À partir de ces résultats, il a été conclu que les débits d'entrée des solutions (paramètre opératoire) n'ont pas d'influence sur les particules recristallisées. Après avoir défini, les paramètres du processus de cristallisation, le produit synthétisé ne présente pas de changements de cristallinité ni de changements liés aux propriétés de surface (mouillabilité). Toutefois, une diminution de la taille des particules a été observée. Aucun réel impact sur la vitesse de dissolution de la poudre synthétisée par effet anti-solvant n'a été observé.

Le mélangeur se colmate après quelques minutes d'utilisation. Il peut s'agir d'un problème d'affinité du solide avec la paroi inox du pré-mélangeur et/ou d'un phénomène d'agglomération très rapide. Afin d'améliorer la cinétique de dissolution de la poudre recristallisée, il est nécessaire de rendre leur surface plus hydrophile en utilisant par exemple des additifs différents afin d'optimiser les paramètres du procédé et de formulation.

3.1. INTRODUCTION

Chapter 2 summarizes the crystal properties, which are experimentally determined in this work. The poor water solubility, bad wettability and the low dissolution rate in acidic medium could be confirmed. In order to modify these properties, this work proposed a recrystallization using an Anti-Solvent-Liquid process.

The solvent selection is one of the essential parameters to envisage any crystallization process. Therefore, the knowledge of the solubility of a target component in different solvents is required. In this work, the solubility of CRS 74 in ethanol and ethanol-water binary mixtures was measured in the temperature range of 5 -30°C.

Although experimental data on solubility are essential to provide information about a system and help to understand its behavior, correlations and prediction models are also required for the correct design of crystallization processes. Solid-liquid equilibria of ternary mixtures containing ethanol (solvent), water (anti-solvent) and the new antiretroviral drug were studied. The solubility data were estimated using UNIQUAC-based model.

After determining the solubility of the active ingredient in ethanol (solvent)-water (anti-solvent), an experimental system was developed to study CRS 74 recrystallization. As mentioned in Chapter 1, crystal properties are influenced by a number of operating variables in anti-solvent crystallization, some of which are more influential than others.

The present Chapter is composed of two sections. The first one concerns the solubility study and the second one the crystallization process design. The methodology and the results obtained are presented.

3.2. MATERIALS AND METHODS

3.2.1. Materials

The active pharmaceutical ingredient (CRS 74) with 99% purity was provided as courtesy from Cristalia Ltda (Itapira, SP, Brazil), ethanol (EtOH) from Fluka Analytical (Sigma–Aldrich, France) and acetonitrile (ACN) high performance liquid chromatography (HPLC) grade from Scharlau Chemie (Barcelona, Spain). Ethanol and Acetonitrile had purity higher than 99%. All products were used as supplied.

3.2.2. Methods for solubility measurements

The solubility of CRS 74 was determined by equilibrating an excess of CRS 74 in 5 g of water, ethanol and different ethanol/water combinations at $30 \pm 0.5^\circ\text{C}$ in a temperature-controlled bath for 72 h (Figure 2.5). The flasks were sealed for the duration of the tests and the concentration was determined by removing the solid phase by filtration (0.22 μm pore size) and injection of the filtered solution into the HPLC system to be analyzed at wavelength of 210 nm. The HPLC system consisted of an Agilent Chromatograph (Model 1100 series) equipped with a UV-vis detector, and of an HPLC column ProntoSIL 300-5-ODSH 5 μm , 250x4 mm ID. The flow rate of mobile phase (acetonitrile/water in the ratio of 70:30) is 1.0 mLmin⁻¹.

3.2.3. Methods for Liquid Anti-Solvent (LAS) crystallization

After drug solubility characterization and definition of the best crystallization conditions, some process parameters were evaluated. In this part of the study, different essays at different operational conditions were realized in order to evaluate the influence of the process parameters on the final size and agglomeration state of particles at the end of the crystallization process.

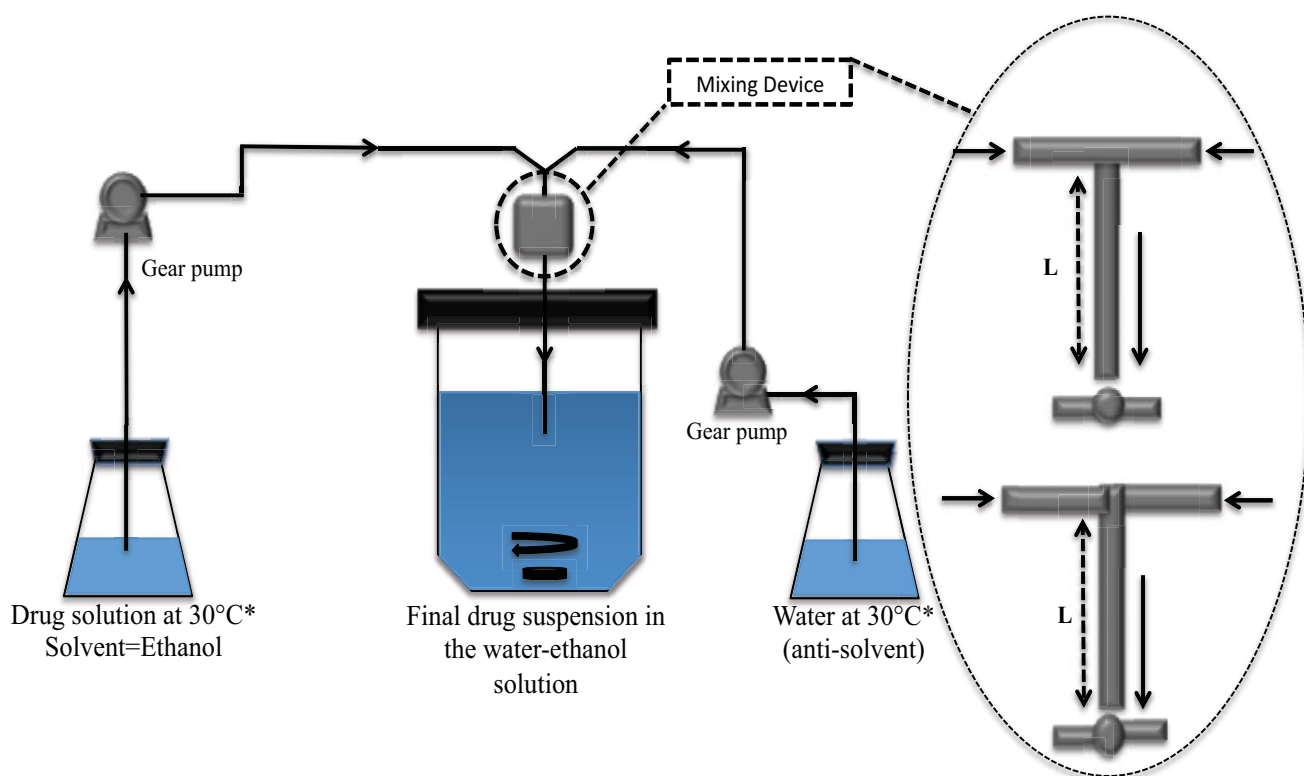
The original CRS 74 crystals were recrystallized by a LAS crystallization method. As already discussed in Chapter 1, this method is based on saturation changes, when the drug is dissolved into a solvent and then this solution is mixed with an anti-solvent of solute.

Anti-solvent and saturated solutions can be brought into contact in several manners: single-jet, double-jet or double-jet with premixing (Chapter 1).

In the crystallization proceeding for CRS 74 (expensive pharmaceutical drug) the use of single jet was not viable due to use of a large amount of drug for each experiment. So, a double-jet with premixing has been used. So rapid mixers combined with a stirred vessel were used as process configuration. Briefly, the drug was recrystallized via the concurrent introduction of the CRS 74 ethanol solution and an anti-solvent stream of water in stainless steel mixers specially manufactured for this study, on the basis of previous works published in the literature (LINDENBERG et al., 2008; LINDENBERG, 2009). The experimental setup is shown in Figure 3.1, in which the mixing device can be easily changed to test different mixers, which are presented in more details hereafter.

Briefly, a certain amount of original CRS 74 samples was completely dissolved in ethanol at $30 \pm 0.5^\circ\text{C}$ at definite concentration ($90 \text{ mg}_{\text{CRS 74}}/\text{g}_{\text{solution}}$). The solution was filtrated through $0.22 \mu\text{m}$ pore size membranes to remove the possible particulate impurities. To each experiment the solutions were fed into the mixing device by gear pumps (mzr-7255-hs-f S, mzr-7205-hs-f S; HNP Mycosysteme). The freshly formed crystals were collected in a vessel under magnetic stirring and then they were filtered and dried under vacuum at $50 \pm 1^\circ\text{C}$ for 24h. The dried samples produced by this LAS crystallization process were characterized by laser diffractometry, differential scanning calorimetric analysis, X-ray diffraction analysis, scanning electron microscopy analysis, wetting properties and dissolution testing.

The flow rates of CRS 74 ethanol solution and water were fixed at flow rates of 11.29 g/min and 33.22 g/min respectively, such after mixing a definite supersaturation ratio (S) was calculated from the conditions at the entries of the T-mixer ($S = C/C_{\text{eq}} = 894$). Gear pumps and a digital mass flow meter/controller (M1X, Bronkhorst) were used in the experimental process to ensure minimal flow rate fluctuations and good mixing. In order to validate the flow of gear pumps the pumps were previously calibrated (data shown in Appendix II).



* Temperature-controlled bath

Figure 3.1. Schematic of the experimental apparatus used for the LAS crystallization experiments.

Mixers

Two different types of mixers were tested: a T-mixer with two radial entries and a two jets vortex mixer also called Roughon mixer. The T-mixer had two radial entries with a diameter of 1 mm and its outlet tube had a diameter of 2 mm and a length of 17.5 mm. The Roughon mixer has a mixing chamber diameter of 3 mm and its outlet tube has a diameter of 1.75 mm and a length of 15 mm. A schematic of both mixers is showed in Figures 3.2a and 3.2b.

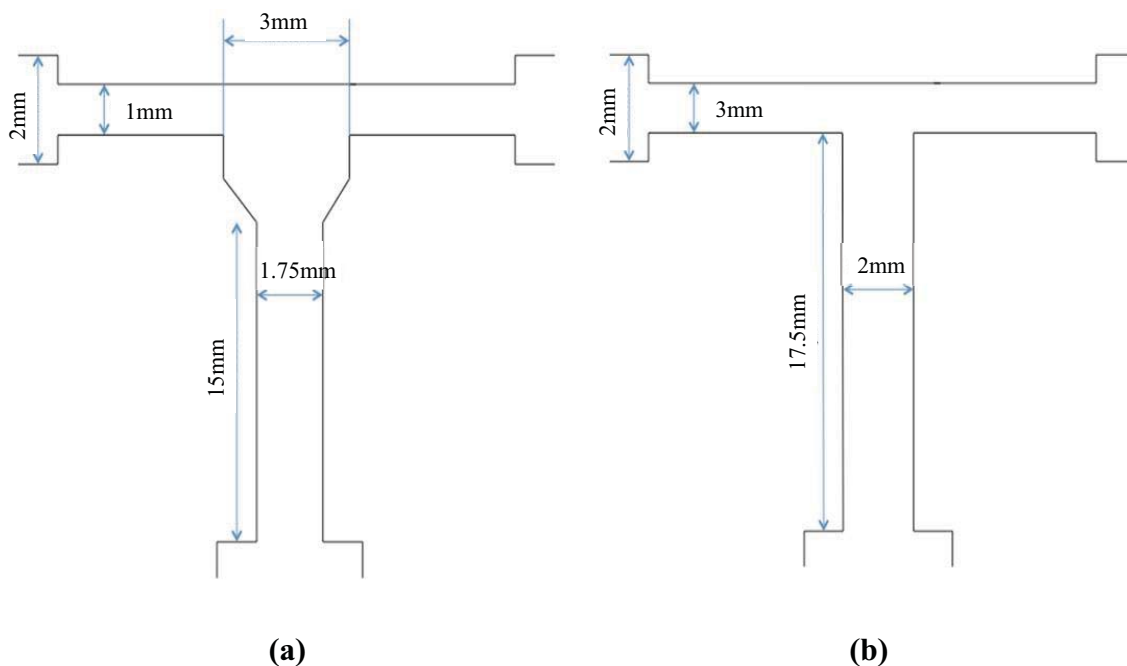


Figure 3.2. Sketch of the mixers used: (a) Roughton mixer, (b) T-mixer.

3.2.3.1. Characterization methods for particles in suspension

Particle size analysis

The mean size and particle size distribution of the drug particles generated by LAS recrystallization were analysed in different phases of the process.

Firstly, freshly particles were analysed by Photon correlation spectroscopy (PCS) using a Zetasizer Nano Zs (Malvern Instruments, United Kingdom) to measure the mean size at the exit of the mixer right after the mixing proceeding (from the outlet of the mixer), as shown in Figure 3.3. Two measurements are made at 0 and 150 seconds (measure time). Before analysis, the suspension was diluted 5 times using a saturated at 30°C. This saturated solution was composed by water, ethanol and drug, to achieve appropriate measurement concentration. It was filtrated through 0.22 μm pore size membranes to remove the possible particles. The new supersaturation of solution S' can be calculated by this expression:

$$S' = 5/6 + S/6 \tag{3.1}$$

In a second time the drug suspension was analysed by laser granulometry, using a MasterSizer 3000 (Malvern Instruments, United Kingdom). The samples were taken from the outlet of the mixer (right after the mixing) and immediately diluted with the same saturated solution in order to monitor the evolution of crystal size as a function of the time in the cell of the granulometer, as shown in Figure 3.3.

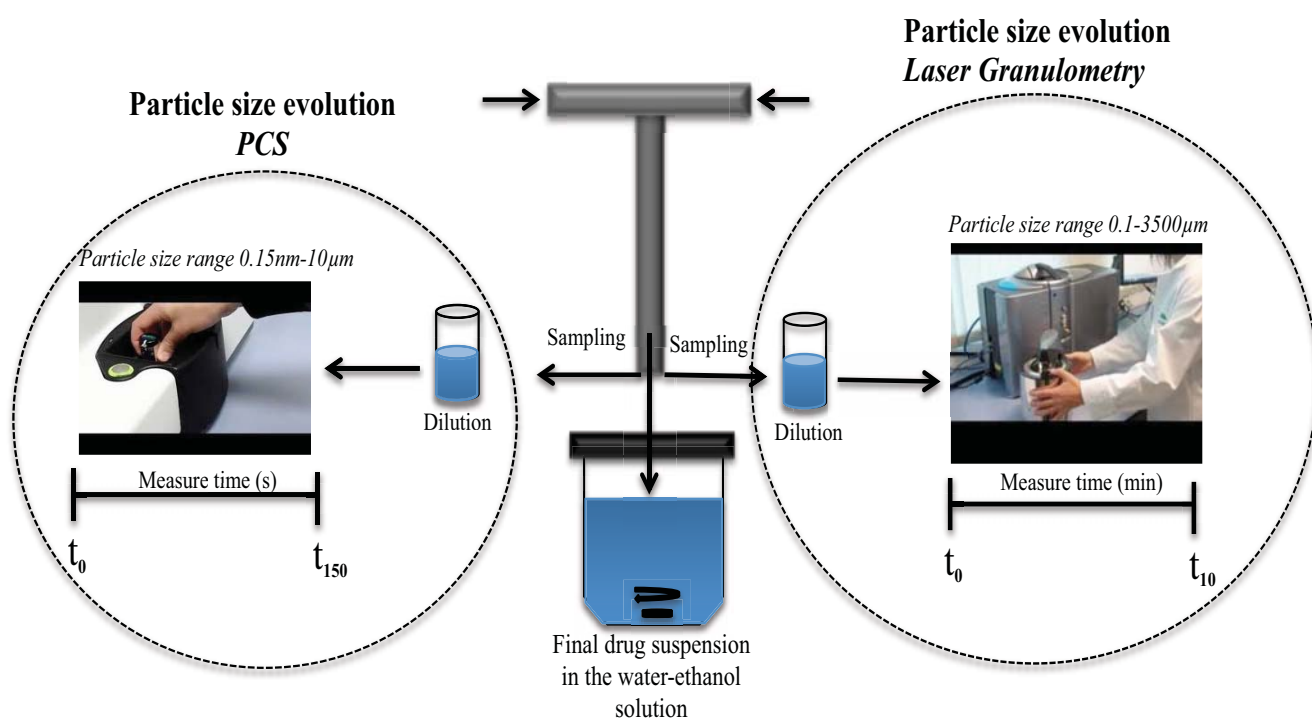


Figure 3.3. Sketch of particle size analysis for particles in suspension by PCS and laser granulometry.

Optical microscopy analysis

Samples were taken from the final suspension into the vessel and immediately analysed by optical microscopy.

3.2.3.2. *Characterization methods for dried powder*

The dried samples were analysed by laser diffractometry, powder X-ray diffraction (XRD), thermal gravimetric analysis (TG), differential scanning calorimetry (DSC), scan electronic microscopy (SEM), contact angle measurement and dissolution testing, using the same procedure already described in Chapter 2. Furthermore, purity and solvent content were determined too.

Purity

In order to evaluate the purity of drug solid, approximately 1.5 mg of CRS 74 was solubilized in approximately 40 g of ethanol. This solution was then assayed by HPLC analysis at wavelength of 210 nm to evaluate the amounts of dissolved drug. The HPLC system consisted of an Agilent Chromatograph (Model 1100 series), equipped with a UV-vis detector, column Prontosil 300-5-ODSH 5 μ m (5 μ m, 250x4 mm). The flow rate of mobile phase (acetonitrile/water in the ratio of 70:30) is 1.0 mL min⁻¹. All experiments were carried out in triplicate. The purity is the ratio between the measured concentration of the synthesized powder and the initial concentration of the raw material. The purity of the synthesized powders was calculated as shown below.

$$Purity(\%) = \frac{Abs_{sample}}{Abs_{CRS74}} \times Purity_{CRS74} (\%) \quad (3.2)$$

where Abs_{CRS74} is the absorbance of the standard solution containing the raw material 100% dissolved, Abs_{sample} is the absorbance of the sample containing the synthesized material 100% dissolved. And $Purity_{CRS74}$ is the purity of the raw material, provided by supplier. For all purity results, the standard deviation was not shown, because it was not significant.

Residual solvent content

The residual solvent (water+ethanol) content was determined using Infrared balance (LJ16, Mettler) at 100°C until constant weight was achieved.

3.3. RESULTS AND DISCUSSION ON SOLUBILITY STUDY

3.3.1. Measurement and correlation of solubility of CRS 74 in water-ethanol mixtures

3.3.1.1. Experimental determination

Solubility data were experimentally measured in the temperature range of 5 to 30°C for pure ethanol and for a mixed solvent system containing 95%(w/w) water and 5% (w/w) ethanol. For analytical purposes, the solubility in pure water could not be measured. Indeed, the low concentration of a solid in solution, that should lead to analytical results unreliable, that can be not quantified due to sensitivity of the quantification method.

Concentration measurements have made as function of time and are shown in Tables 3.1 and 3.2.

The standard deviation obtained ($\pm 5\%$), is mainly due to evaporation losses of solvent after sampling, but also closely related to systematic error (analytical method), like dilution and calibration curve.

For the two mass ratios, the concentrations measured at 24, 48, 72 h are identical (Tables 3.1 and 3.2). Subsequently we have considered, for all solutions, the liquid-solid system has reached equilibrium after 24 h of stirring at a controlled temperature $\pm 0.5^\circ\text{C}$. Thereafter, all the experimental results are the average of the three concentrations measured respectively at 24, 48 and 72 h (Table 3.1 and Table 3.2).

As shown in Table 3.1, the solubility of CRS 74 in pure ethanol was enhanced by temperature rise above 15°C, whereas the solubility in the mixed aqueous system containing 95% (w/w) water - 5% (w/w) ethanol was not affected by the temperature in all studied temperature range. With this last ratio, the solubility of CRS 74 is equal to 0.0040 ± 0.0001 mg/g solution.

The solubility of CRS 74 in different water-ethanol mixtures at 30°C was listed in Table 3.3.

Table 3.1. Solubility of CRS 74 in ethanol as function of sample time in temperature range (5-30°C).

T (°C)	C (mg/g)	C (mg/g)	C (mg/g)	\bar{C} (mg/g)	SD (mg/g)
	24h	48h	72h		
5	68.1	65.3	73.4	68.9	4.1
10	67.5	67.8	68.9	68.1	0.8
15	66.4	69.7	61.4	65.8	4.1
20	72.0	74.8	77.7	74.8	2.8
25	78.3	82.7	81.6	80.9	2.3
30	90.6	93.0	94.3	92.6	1.9

Table 3.2. Solubility of CRS 74 in 95% (w/w) water - 5% (w/w) ethanol mixture as function of sample time in temperature range (5-30°C).

T (°C)	C (mg/g)	C (mg/g)	C (mg/g)	\bar{C}	SD
	24h	48h	72h	(mg/g)	(mg/g)
5	0.0042	0.0048	0.0036	0.0042	0.0006
10	0.0042	0.0041	0.0038	0.0040	0.0002
15	0.0042	0.0041	0.0038	0.0040	0.0002
20	0.0036	0.0036	0.0036	0.0036	0.0000
25	0.0039	0.0041	0.0039	0.0040	0.0001
30	0.0041	0.0041	0.0040	0.0041	0.0001

The results revealed that this molecule exhibited a very poor solubility in water (not detected by HPLC analysis) and a solubility of 92.6 mg/g_{solution} in pure ethanol. On the one hand, Table 3.3 shows that the addition of ethanol to water at 30°C changed the solubility of CRS 74 and that ethanol could be used as an organic co-solvent to change its solubility in aqueous media. It is well-known that the addition of an organic co-solvent to water can dramatically change the solubility of drugs (YALKOWSKY and ROSEMAN, 1981) as observed here for more than 40%(w/w) ethanol. It is reported that a solvent is sufficient for pharmaceutical processing when the solubility exceeds 1 mg/mL (LEE et al., 2006; SMITH et al., 2011). On the other hand, combinations containing more than 60% (w/w) water as an anti-solvent are favourable for further crystallization studies.

Table 3.3. Solubility of CRS 74 in Ethanol/water mixtures at 30 °C.

Solvent	Mean Solubility (mg/g _{solution}) ± SD
Water	not detected by HPLC analysis
95%(w/w) water - 5%(w/w) ethanol	0.004±0.0001
85%(w/w) water - 15%(w/w) ethanol	0.010±0.0004
80%(w/w) water - 20%(w/w) ethanol	0.020±0.0020
75%(w/w) water - 25%(w/w) ethanol	0.030±0.0020
70%(w/w) water - 30%(w/w) ethanol	0.070±0.0030
60%(w/w) water - 40%(w/w) ethanol	2.290±0.0900
50%(w/w) water - 50%(w/w) ethanol	12.300±1.4100
40%(w/w) water - 60%(w/w) ethanol	60.960±5.2400
30%(w/w) water - 70%(w/w) ethanol	87.890±4.0000
Ethanol	92.600±1.9000

3.3.2. Correlation of solubility data by a UNIQUAC model

At the liquid-solid equilibrium, the chemical potential of the constituent CRS 74 in solid phase is equal to the chemical potential of the constituent CRS 74 in liquid-phase at constant temperature and pressure. From this equality of chemical potential, we can show that the activity of the solute CRS 74 in liquid-phase ($a_{CRS\ 74\ solute} = \gamma_{CRS\ 74\ solute} X_{CRS\ 74\ solute}$) is a function of melting enthalpy of CRS 74, ΔH_m , melting temperature T_m and solution temperature T (WALAS, 1985):

$$\ln \gamma_{CRS\ 74\ solute} X_{CRS\ 74\ solute} = - \frac{\Delta h_m}{R} \left(\frac{1}{T} - \frac{1}{T_m} \right) \tag{3.3}$$

$x_{\text{CRS 74 solute}}$ being the molar fraction of the solute at saturation, $\gamma_{\text{CRS 74 solute}}$ the activity coefficient of solute.

The model UNIQUAC (UNIversal QUASI Chemical) is chosen to calculate the activity coefficient of solute.

For a ternary system, twelve parameters are necessary: six parameters concerning the geometry of molecules and six binary interaction parameters. The first parameters, R_k and Q_k , are estimated from the molecular formula of component. The second parameters, binary interaction parameter water/CRS 74 and ethanol/CRS 74, will be identified from solubilities measurement. Binary interaction parameters water/ethanol are available in DIPPR table.

The volume and surface area parameters R_k and Q_k of three components are given in Table 3.4.

Table 3.4. Parameter R_k and Q_k .

Molecule	Water (DIPPR)	Ethanol (DIPPR)	CRS 74
R_k (cm ³ /mol)	0.9200	2.1055	37.4015
Q_k (cm ³ /mol)	1.4000	1.9720	29.4640

The binary interaction parameters of the UNIQUAC model have been identified in two steps. Initially, solubility data on the binary ethanol/CRS 74 as function of temperature were considered to estimate the two binary interaction parameters ethanol/CRS 74 from the activity coefficient of the solute calculated by the equation (3.3) (Table 3.5).

In a second stage, the binary interaction parameters of water/CRS 74 were calculated from experimental data over the ternary water/ethanol/CRS 74 with a mass ratio ethanol/(ethanol-water) of 5% and variable temperature (Table 3.5). A ternary mixture has been chosen because the solubility data in water as a function of temperature are not available.

In both cases, the minimized function f_{\min} used for parameter estimation is calculated the following relation:

$$f_{\min} = (\gamma_{CRS\ 74\ solute}^{exp} - \gamma_{CRS\ 74\ solute}^{calc}) \quad (3.4)$$

Table 3.5. Binary interaction parameters.

Binary Systems	i-j	u_{ij} (cal/mol)
Water-CRS 74	1-3	-400.55
	3-1	22 132.13
Ethanol-CRS 74	2-3	-381.47
	3-2	23 701.66
Water-Ethanol	1-2	$-96.4730 + 0.6843 * T(K)$
(database Simulis)	2-1	$31.6290 + 0.4759 * T(K)$

The experimental and calculated activity coefficients ($\gamma_{CRS\ 74\ solute}^{exp}$ and $\gamma_{CRS\ 74\ solute}^{calc}$) for the two systems are reported in Table 3.6. The means of standard deviation (equation 3.5) for the binary system ethanol/CRS 74 and for the ternary system water/ethanol/CRS 74 are respectively 0.123 and 0.196 on the ternary system.

$$STD = \frac{2}{npt} \sqrt{\frac{(\gamma_{Molecule\ A}^{exp} - \gamma_{Molecule\ A}^{calc})^2}{(\gamma_{Molecule\ A}^{exp} + \gamma_{Molecule\ A}^{calc})^2}} \quad (3.5)$$

Table 3.7 gives the solubilities calculated in pure ethanol as a function of temperature. The calculated concentrations are in good agreement with experimental values for temperatures above 15°C. Below this temperature, the calculated concentrations are significantly underestimated.

Figure 3.4 shows the calculated solubility at 30°C as a function of the ethanol mass proportion in the mixture ethanol-water with the identified parameters. The calculated data showed good agreement with experimental results and revealed a maximum solubility of CRS 74 of 130.20 mg/g_{solution} for a mass ratio of 17%(w/w) water - 83%(w/w) ethanol. The maximum solubility for a solute in a mixed solvent system has been observed experimentally for other systems (water/acetone/ketoprofen-ESPITALIER et al., 1995; water /ethanol /paracetamol and water/dioxane/phenacetin-RUCKENSTEIN and SHULGIN, 2003; water/ethanol /hydrocortisone- ALI et al., 2009 and n-heptane/ethanol/eflucimide - TEYCHENE and BISCANS, 2011). Different studies on Hidelbrand solubility approach have shown that the location and the height of the peaks could be linked with the polarity of the solute (JOUYBAN-GHARAMALEKI et al., 2000, PEÑA et al. 2006). Hydroxyl and amine groups of solute give a polar character to this molecule that could explain the maximum of solubility calculated for a high ratio of ethanol in the mixture.

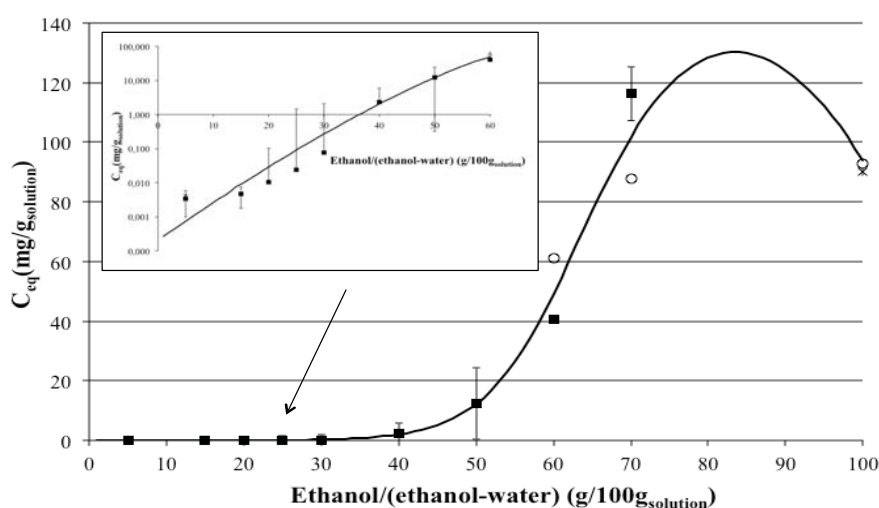


Figure 3.4. Experimental (characters) and calculated CRS 74 solubilities (—) in different ethanol-water mixtures at $30 \pm 0.5^\circ\text{C}$.

Table 3.6. Experimental and calculated activity coefficients for ethanol/CRS 74 and ethanol/water/CRS 74.

	System ethanol/CRS 74 SD = 0.123		System water/ethanol/CRS 74 Ethanol/(Ethanol+water) = 0.05 SD = 0.196	
T (°C)	$\gamma_{CRS\ 74\ solute}^{exp}$	$\gamma_{CRS\ 74\ solute}^{calc}$	$\gamma_{CRS\ 74\ solute}^{exp}$	$\gamma_{CRS\ 74\ solute}^{calc}$
			10^{-4}	10^{-4}
5	0.0957	0.1842	0.4165	1.0533
10	0.1765	0.2562	0.7947	1.5338
15	0.3261	0.3475	1.4161	2.2045
20	0.4965	0.5200	2.7487	3.1296
25	0.7829	0.7449	4.2884	4.3908
30	1.1373	1.1081	6.9886	6.0919

Table 3.7. Solubility of CRS 74 in pure ethanol at different temperatures.

T (°C)	\bar{C} (mg/g)	SD (mg/g)	C^{calc} (mg/g)
5	68.9	4.1	46.4
10	68.1	0.8	54.6
15	65.8	4.1	63.4
20	74.8	2.8	72.9
25	80.9	2.3	83.1
30	92.6	1.9	93.9

3.3.3. Theoretical yield of solid obtained by LAS crystallization

Measurements and correlation of solubility of CRS 74 in different ethanol/water mixtures provided useful data for a better understanding of the solubility phenomenon in these media and to estimate the theoretical efficiency of the LAS recrystallization process as a function of ethanol/water mass ratios. Theoretical solid efficiency is the theoretical solid yield of crystallization based on the drug solubility in the liquid media, calculated from the ratio of weight particles obtained by assuming solid-liquid equilibrium attained and the initial weight of solute. Figure 3.5 depicts the theoretical solid efficiency of the LAS crystallization for the drug. It can also be seen that an ethanol concentration up to 50%(w/w) in ethanol/water mixtures is still favorable for the crystallization process, resulting in recovery of 82.6% (50 %Ethanol) of CRS 74 based on the drug solubility in the liquid media.

In an attempt to improve its dissolution properties, CRS 74 can be recrystallized by using a Liquid Anti-solvent (LAS) crystallization process and the data generated here can represent a useful tool to define the mass proportion between solvent (ethanol) and anti-solvent (water) for LAS crystallization studies.

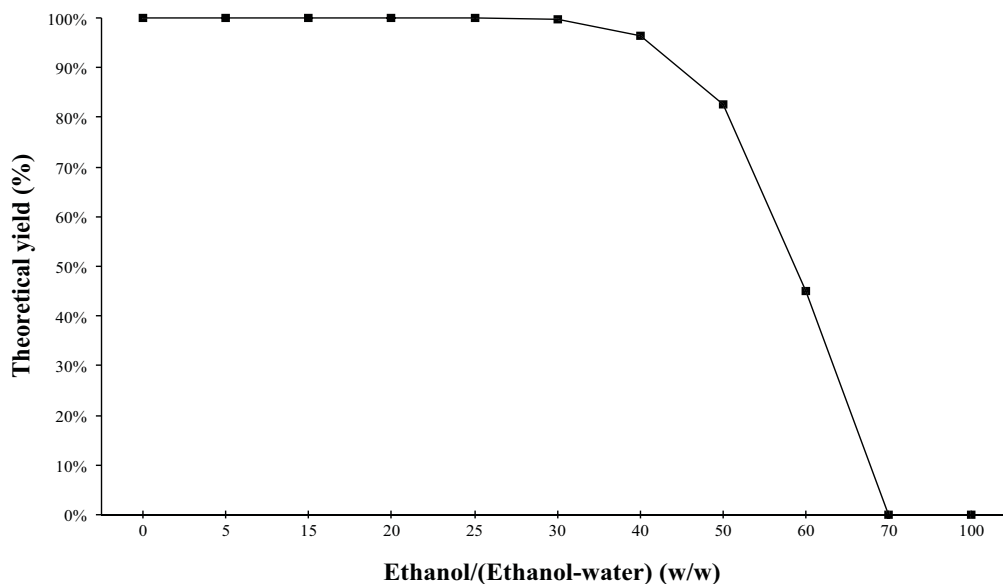


Figure 3.5. Theoretical yield of CRS 74 in different ethanol/(ethanol-water) mass ratios.

3.4. RESULTS AND DISCUSSION ON CRYSTALLIZATION STUDY

After determining the solubility of the active ingredient in ethanol (solvent)-water (anti-solvent), it was developed an experimental system to study CRS 74 recrystallization solvent. The crystals of CRS 74 were prepared by LAS crystallization from an ethanolic saturated solution at 30 °C (90 mg/g_{solution}) and water, used like anti-solvent. The crystals suspension obtained after the crystallization process had a milky aspect that changed into a clear solution, after some seconds under magnetic stirring. This phenomenon can indicate the growth and the subsequent agglomeration of the crystals in solution. That can be observed in the form of long and big macroscopically visible agglomerates.

Two different rapid mixing devices for controlling the properties of CRS 74 particles produced by LAS crystallization were used. Two process parameters were tested: type of mixer and flow rate, which will be discussed here. For all essays at least two replicates were realized to evaluate the repeatability of the process and particle size measure method. The process conditions are given in the Table 3.8.

The solid has been characterized after crystallization (still in suspension) and after crystallization, filtration and drying. The characterization step concerns the particle size measurement at the outlet tube of the mixer and the characterization of dried powder by particle size measurement, morphology, crystalline structure and dissolution properties.

Table 3.8 Experimental LAS crystallization process conditions

Experiment	Solvent flow rate (g/min)	Antisolvent flow rate (g/min)	Total flow (g/min)	Type of mixer
1	11.29	33.22	44.51	Roughton
2	11.29	33.22	44.51	T
3	6.77	20.32	27.09	T
4	17.46	52.1	69.56	T

3.4.1. Characterization of particles in suspension

3.4.1.1. Influence of the type of mixer on mixing

In order to compare the efficiency of both mixers parameters such as residence time (τ), Reynolds number (Re) and energy dissipation rate (E_D) were calculated for each mixer and for each flow rate tested.

The residence time τ in the mixer is calculated from V the volume of the mixer (mL) and Q the volume flow rate (mL/s):

$$t = V/Q \quad (3.6)$$

In our system, the Reynolds number can be calculated as follows (FOX et al., 2004).

$$Re = \frac{\rho u D}{\mu} = \frac{\rho \dot{Q} D}{\mu A} \quad (3.7)$$

with Re = Reynolds number, ρ = density of the mixture (kg/m^3), u = velocity of the mixture (m/s), \dot{Q} = flow rate of the mixture (m^3/s), D = diameter of the outlet tube (m), μ = viscosity of the mixture (N.s/m^2), A = cross sectional area of the outlet tube (m^2).

It has been described that for Reynolds number above 1600, the mixing process is completed in the main mixing chamber. On the other hand, for low Reynolds number, this process continues at the outlet tube. Therefore, the larger the Reynolds number, the faster the mixing process and, consequently, a uniform composition in the mixer will be faster achieved.

The energy dissipation is a factor that strongly influences the quality of mixing. The purpose of the mechanical energy dissipated by the moving fluid is to homogenize fields of concentrations by displacement of fluid portions. The perfect mixing at the molecular level is sometimes achieved so late that the solute molecules are already chemically transformed or in phase change. The energy dissipated can be calculated as follow.

$$E_D = \frac{f \cdot V^3}{2 \cdot D} \tag{3.8}$$

where E_D = energy dissipated (W/kg), f = friction factor, V = velocity of the fluid at the outlet tube (m/s), D = diameter of the outlet tube (m).

By generating homogenized fields of concentration in the solution, the energy dissipation influences the mean velocity convection, the turbulent diffusion and the viscous-convective deformation (LINDENBERG and al, 2008). The improvement of these factors means an improved mixing.

Properties of solvent mixture used, like density (ρ) and viscosity (μ) were calculated as shown in Table 3.9. These values were determined for the solvents mixture composed by ethanol (25%, w/w) and water (75%, w/w) at 30°C, without taking into account the influence of the solid (KHATTAB et al., 2012).

Table 3.9 Density (ρ) and viscosity (μ) of ethanol/water mixtures at 30°C (KHATTAB et al., 2012).

$\rho_{\text{mixture}} \text{ (kg/m}^3\text{)}$	$\mu_{\text{mixture}} \text{ (N.s/m}^2\text{)}$
955.4	0.0017

According to Table 3.10, Reynolds numbers were lower than 1600, so the mixing process continues at the outlet tube. Moreover, Roughton mixer shows better mixing efficiency when compared to the T-mixer. For the same flow rate, the Roughton mixer presents lower mixing time, which is required in order to have a uniform concentration distribution in the mixer, wide causes particle size distribution (ZHAO et al., 2011). It also shows higher Reynolds numbers and energy dissipation rates. It means a greater turbulence in the system that favours a closer contact between the fluid for total flow rate higher than 7 g/min and, consequently, results in improved mixing.

Table 3.10. Calculated mixers parameters for: Roughton mixer (a) and T-mixer (b).

$Q_{\text{EtOH}} \text{ (g/min)}$	$Q_{\text{H}_2\text{O}} \text{ (g/min)}$	$Q_{\text{total}} \text{ (g/min)}$	$\tau \text{ (s)}$	Re	$E_D \text{ (W/Kg)}$
6.77	20.32	27.09	0.08	195	0.7
11.29	33.22	44.51	0.05	321	2
17.46	52.1	69.56	0.03	503	4.9

(a)

$Q_{\text{EtOH}} \text{ (g/min)}$	$Q_{\text{H}_2\text{O}} \text{ (g/min)}$	$Q_{\text{total}} \text{ (g/min)}$	$\tau \text{ (s)}$	Re	$E_D \text{ (W/Kg)}$
6.77	20.32	27.09	0.11	171	0.3
11.29	33.22	44.51	0.07	281	0.9
17.46	52.1	9.56	0.04	440	2.2

(b)

3.4.1.2. Influence of the type of mixer on particle size

For CRS 74 LAS crystallization the proportion ethanol:water equal to 25%:75% (w/w) and total flow rate of 44.51 g/min, were used, as given in Table 3.8. Results obtained by PCS and laser granulometry are presented.

PCS results

In a first time the influence of the type of mixer on particle size (PSD) by PCS was evaluated. Different essays using Roughton and T mixers at the same process conditions were realized. In order to follow the evolution of particle size and understand the influence of each mixer on the size of the final product.

It was clear observed, that the particle size at 0 s for both mixers is small (nanoscale), but they evolved very fast inside the equipment during the measurement time (150 s), as shown in Table 3.11. This fast evolution of size could be explained by two phenomena: growth or aggregation/agglomeration. A certain variation of size value for the same essay was noticed as well. This difference of the measures values can be acceptable due to the high growth or agglomeration rates of the particles produced, which complicates the measurement accuracy. This variation among the measures was noted at 0 and 150 s for both mixers.

It was noted, that the mean size of particle obtained with Roughton mixer seems to be smaller than that obtained with T-mixer at $t_0 = 0$ s. After $t_f = 150$ s, none difference is observed. This behaviour can be explained by the fact that it provokes a better mixing when compared to the T-mixer, as showed before in Table 3.10 of this chapter.

Table 3.11. Evolution of crystallized particle size by PCS in different mixers, Roughton mixer (a) and T-mixer (b) at total flow rate of 44.51 g/min and ethanol-water ratio of 25-75 % (w/w).

Experiment	Size (nm) at $t_0 = 0$ s		Size (nm) at $t_f = 150$ s
1A	224	→	778
1B	153	→	926
1C	120	→	655
Average	166± 54	→	787± 136
(a)			
Experiment	Size (nm) at $t_0 = 0$ s		Size (nm) at $t_f = 150$ s
2A	269	→	845
2B	393	→	815
Average	331± 88	→	830± 21
(b)			

Laser granulometry results

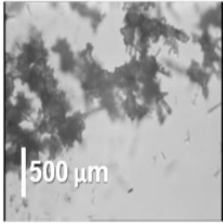
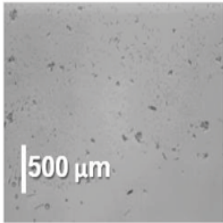
The evolution of the particle size was still followed by laser granulometry, from the outlet of the mixer, until size stabilization of crystals during 10 minutes, in which each measure lasts around one minute. The first and the last measure of this period of 10 minutes were shown in Figures 3.6 and 3.7.

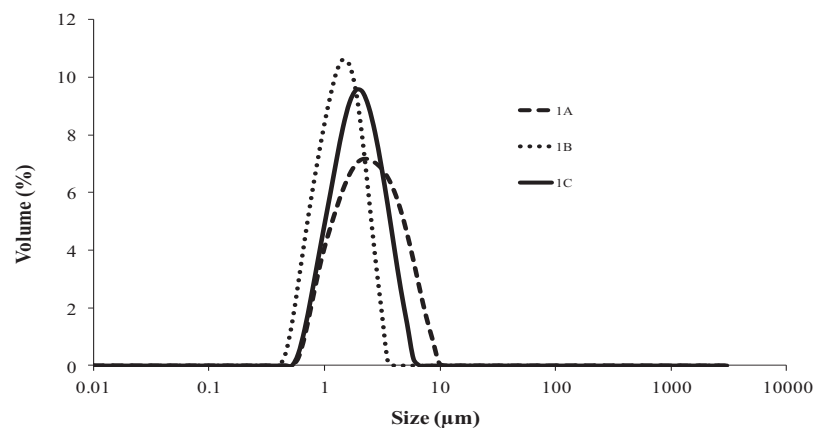
Analysing the results for each mixer separately, it was noted the fast crystal growth or agglomeration. During the 10 minutes analysis the particle size increased 30 times of its initial size of 2 μm , i.e. almost a mean growth rate of 7 $\mu\text{m}/\text{min}$. This behaviour is due to tendency of the molecule to grow quickly and/or to form larger agglomerates.

In figure 3.7 it was noted that T-mixer presents particles with smaller sizes at the end of the measure (10 min) when compared with the size particle distribution of the particles crystallized in the Roughton mixer (see Figure 3.6).

Optical microscopy photos can confirm the agglomeration phenomenon in the cell of laser granulometer. However, as shown in Table 3.12, the particles obtained using the Roughton mixer presented an agglomeration state of particles more significant, when compared to the particles obtained using the T-mixer. The presence of these agglomerates was observed too in Figure 3.6, where a family of particles was noticed at 500 μm .

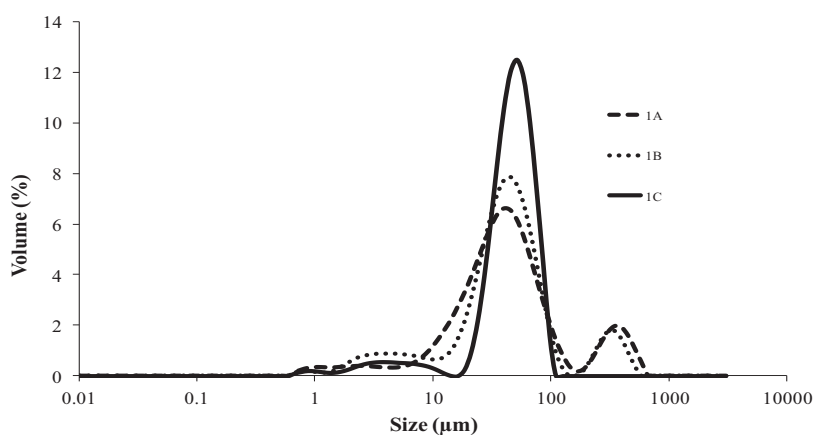
Table 3.12. Crystals at $t_f=10$ min in suspension observed by optical microscopy

Experiment	Type of mixer	Total Flow rate	 500 μm
1A	Roughton	44.51 g/min	
2A	T	44.51 g/min	



Experiment	D[4;3] (μm)	Span
1A	3	1.8
1B	1	1.2
1C	2	1.4
Average	2±1.0	1.5±0.3

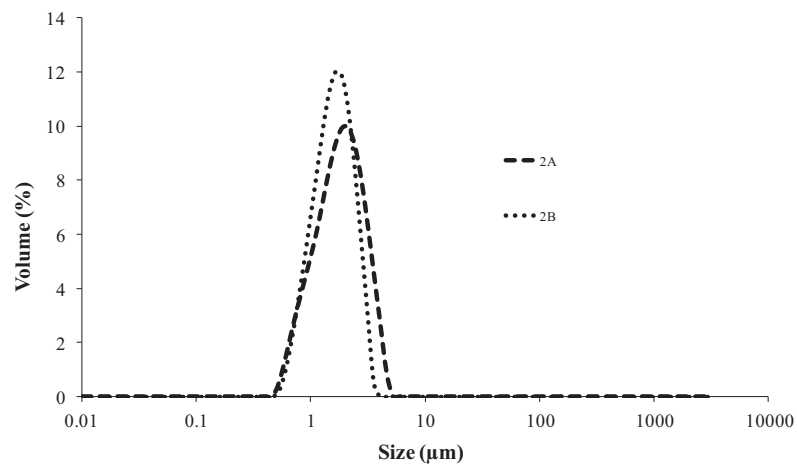
$t_0 = 0$ min



Experiment	D[4;3] (μm)	Span
1A	85	6.3
1B	72	2.6
1C	51	1.1
Average	69±17.0	3.3±2.7

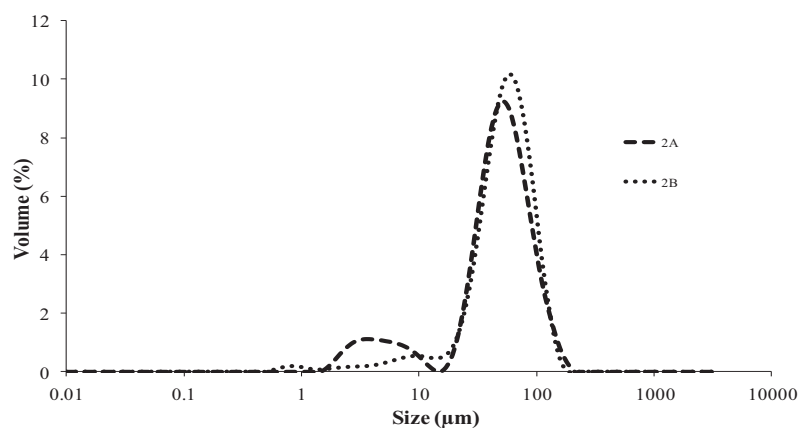
$t_f = 10$ min

Figure 3.6. Particle size distributions by laser granulometry for Roughton mixer at $t_0 = 0$ min and $t_f = 10$ min at total flow rate of 44.51 g/min and ethanol-water ratio of 25-75 % (w/w).



Experiment	D[4;3] (µm)	Span
2A	2	1.3
2B	2	2.6
Average	2±0.0	1.9±0.9

$t_0 = 0$ s



Experiment	D[4;3] (µm)	Span
2A	56	1.8
2B	62	1.4
Average	59±4.0	1.6±0.3

$t_f = 10$ min

Figure 3.7. Particle size distribution by laser granulometry for T-mixer at $t_0 = 0$ min and $t_f = 10$ min at total flow rate of 44.51 g/min and ethanol-water ratio of 25-75 % (w/w).

3.4.1.3. Influence of flow rate in the T- mixer on particle size

In this section the influence of the flow rate on particle size was analyzed using the T-mixer. Three different experiments varying the flow rate were performed (Table 3.8) and the particle size was measured with the same experimental procedure.

PCS results

Analyzing the results for initial size and final size in different flow rates by PCS in Table 3.13. It was noted that there is no a great influence of flow rate on the particle size.

Laser granulometry results

The evolution of the particle size was still followed by laser granulometry during 10 minutes. Like it was made in previous section.

For all experiments the quickly grow or agglomeration rates of crystals was observed as illustrate in Figures 3.8, 3.9 and 3.10. During the 10 minutes analysis the particle size increased between 20 and 30 times of its initial size of 2 and 4 μm , i.e. almost a mean growth rate between 9 and 7 $\mu\text{m}/\text{min}$.

According these results, the particles still continue to grow fast and/or to form larger agglomerates, which means that the flow rate does not influence the growth of the particle size after the mixing. The average flow (44.51 g/min) was chosen in the following essays.

Table 3.13. Evolution of crystallized particle growth by PCS in different total flow rate: a) 27.09 g/min; b) 44.51 g/min; c) 69.56 g/min and ethanol-water ratio of 25-75 % (w/w).

Experiment	Total flow (g/min)	Size (nm) at $t_0 = 0$ s	Size (nm) at $t_f = 150$ s
3A	27.09	354	→ 942
3B	27.09	350	→ 1195
Average		352 ± 3	→ 1068 ± 179

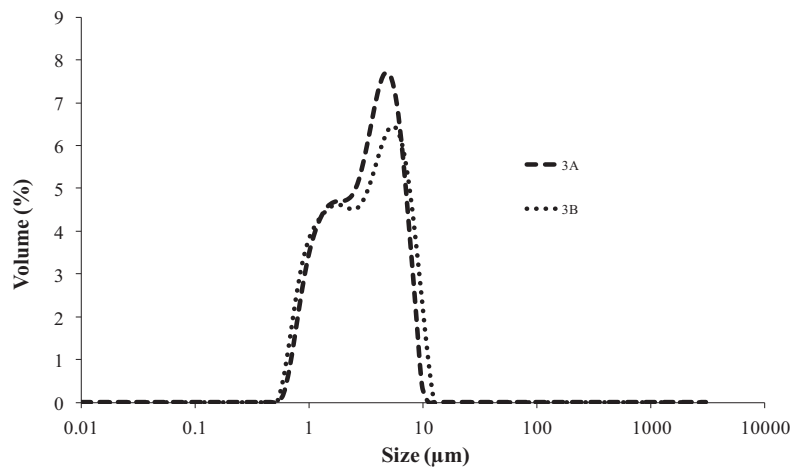
(a)

Experiment	Total flow (g/min)	Size (nm) at $t_0=0s$	Size (nm) at $t_f=150s$
2A	44.51	269	→ 845
2B	44.51	393	→ 815
Average		331 ± 88	→ 830 ± 22

(b)

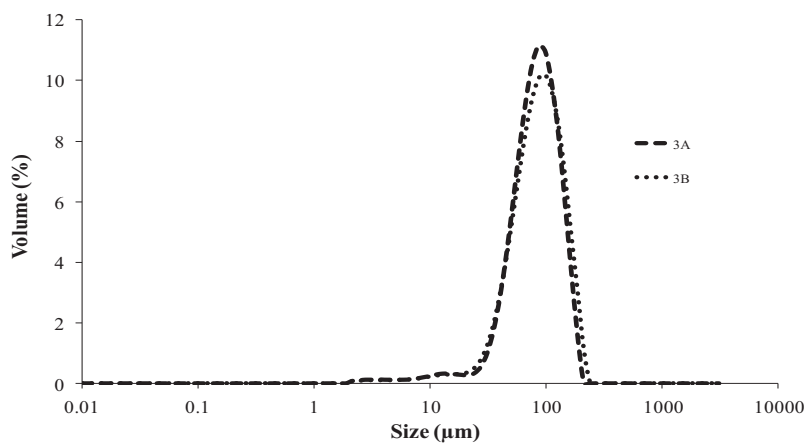
Experiment	Total flow (g/min)	Size (nm) at $t_0 = 0$ s	Size (nm) at $t_f = 150$ s
4A	69.56	385	→ 1241
4B	69.56	257	→ 963
Average		321 ± 63	→ 1102 ± 197

(c)



Experiment	D[4;3] (µm)	Span
3A	4	1.7
3B	4	2.1
Average	4±0.0	1.9±0.3

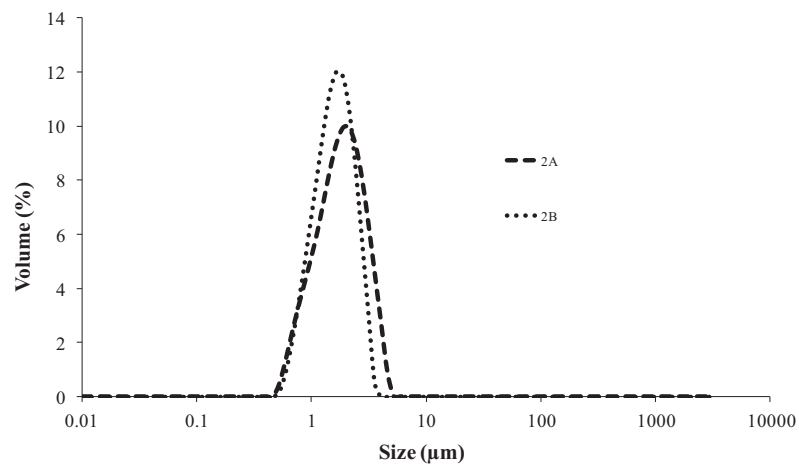
$t_0=0s$



Experiment	D[4;3] (µm)	Span
3A	92	1.2
3B	97	1.3
Average	94±3.0	1.2±0.1

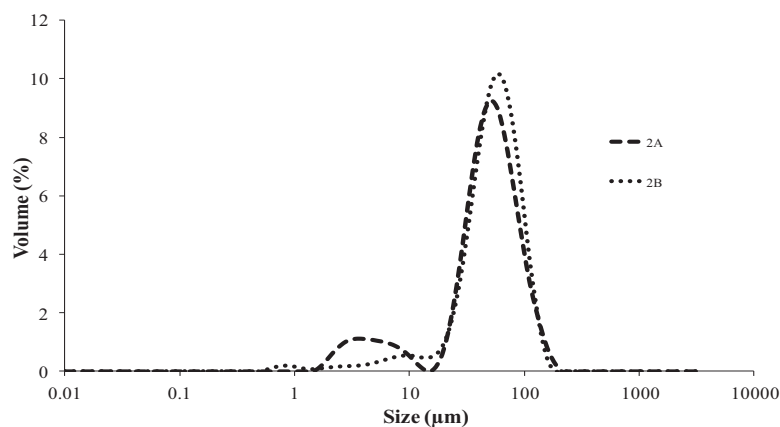
$t_f=10min$

Figure 3.8. Particle size distribution by laser granulometry for T-mixer at total flow rate of 27.09 g/min and ethanol-water ratio of 25-75 % (w/w)., at $t_0 = 0$ min and $t_f = 10$ min.



Experiment	D[4;3] (μm)	Span
2A	2	1.3
2B	2	2.6
Average	2±0	1.9±0

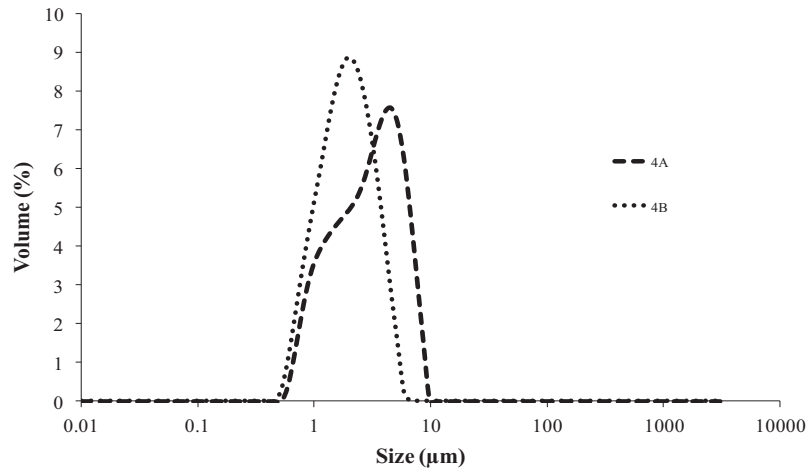
$t_0 = 0$ s



Experiment	D[4;3] (μm)	Span
2A	56	1.8
2B	62	1.4
Average	59±4	1.6±0

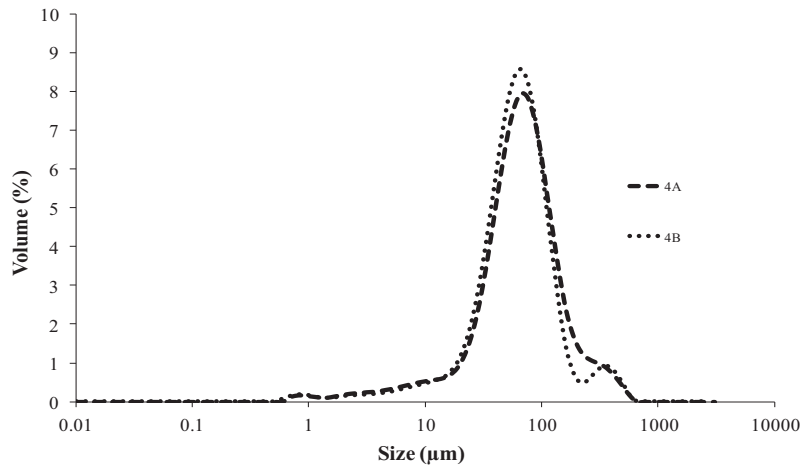
$t_f = 10$ min

Figure 3.9. Particle size distribution by laser granulometry for T-mixer at total flow rate of 44.51 g/min and ethanol-water ratio of 25-75 % (w/w), at $t_0 = 0$ min and $t_f = 10$ min.



Experiment	D[4;3] (μm)	Span
4A	4	1.7
4B	2	1.5
Average	3±1.0	1.6±0.1

$t_0 = 0$ s



Experiment	D[4;3] (μm)	Span
4A	93	2.1
4B	85	1.8
Average	89±6.0	1.9±0.2

$t_f = 10$ min

Figure 3.10. Particle size distribution by laser granulometry for T-mixer at total flow rate of 69.56 g/min and ethanol-water ratio of 25-75 % (w/w), at $t_0 = 0$ min and $t_f = 10$ min.

3.4.1.4. Influence of addition time and steady state

From the previous section, for all experiments the particle size average (PCS) presented a nanometric range right after crystallization. But the crystals size has evolved quickly until stabilization, i.e. micrometric range.

In the case of uncontrolled crystallization, the size evolution of crystals can be due to growth or agglomeration mechanism. To know which crystallization phenomenon control the increase of size crystal, the population balance was proposed. For this simple calculation the steady state must be achieved, i.e. particle of size constant.

An experiment over the time under the best crystallization condition was realized. The ethanol-water ratio equal to 25-75 % (w/w) and total flow rate of 44.51 g/min, were chosen, based on previous results.

The experiment does not last very long, only 6 min. This is due to problems of blockage, caused by affixation of solid on the surface of the mixer, as shown in Figure 3.11. This problem can be caused by the affinity of the molecule with the material, which constitutes the surface of the mixer. It precludes the system from reaching the steady state and consequently, it prevents to calculate the growth and nucleation rates from population balance.

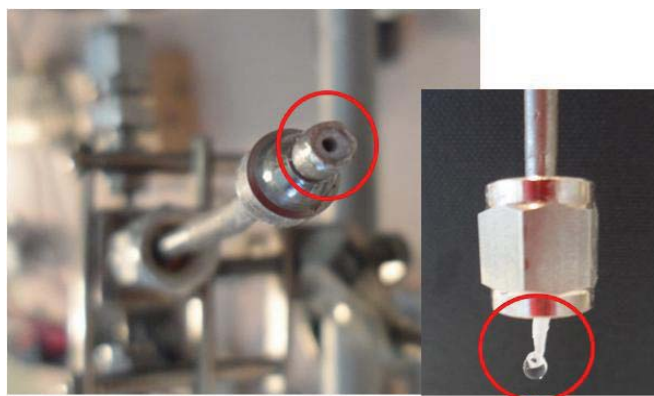


Figure 3.11. Blockage and affixation of CRS 74 crystals on surface of the T-mixer.

The blockage problem can be related to high saturation (S) of the alcoholic solution. In order to prevent the blockage problem, a second experiment with a low flow rate and a low supersaturation was performed, as shown in Table 3.14. In this experiment, different samplings from the outlet of the mixer as a function of time were realized.

Table 3.14. Experimental LAS crystallization process conditions

Experiment	Total flow (g/min)	ethanol-water ratio (w/w)	S^*
5	44.51	25-75 %	894.0
6	27.09	25-75 %	15.4

* $S = C / C_{eq}$, C is concentration after dilution with anti-solvent by assuming no crystallization (mg/g) and C_{eq} is the equilibrium concentration of the pharmaceutical active in the solution water+ethanol (mg/g)

Comparing the results of both supersaturations at the same time, it was perceived that there is no big difference between the size particles values, as a function of time, as given in Table 3.15. It means that the supersaturation does not have a great influence on the particle size. It can be noted too, that the particle size for both experiments increases as a function of time. It means that, the steady state was not achieved for population balance calculus.

Table 3.15. Particle size distribution by PCS: $S = 894.04$ and $S = 15.4$.

	$S= 894.0$	$S= 15.4$
t (min)	Size (nm) at $t_0 = 0s$	Size (nm) at $t_0 = 0s$
0	438	421
2	455	491
4	503	579
6	688	x

For both experiments, the particle size measurement as a function of time does not last very long ($t < 6$ min) due to problems of blockage.

The essay with the lower supersaturation and flow rate lasted less than the other one, only 4 minutes. In this process condition the residence time of the crystals is bigger, as shown in Table 3.10 (0.11 s for 27.09 g/min and 0.07 for 44.51 g/min). It means, that the crystals have more time to be in contact with the surface of mixer, causing problems of blockage. Furthermore, the particles in nanometric range have a high-energy surface; this property can potentiate the high affinity of CRS 74 on the surface material.

Because of this drug behaviour, which precluded the realization of essays over time, it was not possible to simply calculate the nucleation and agglomeration rates. In addition this drug behaviour prevent the use of this crystallization proceeding in industrial applications.

3.4.2. Characterization of solid particles obtained in experimental design

By comparing the SEM photos of raw material and the synthesized powders, a decrease of the crystal size (elementary particles and agglomerates) and no shape changes can be observed in Table 3.16. This size reduction can indicate an influence of the crystallization process on the size particle. On the other hand, the presence of powder compact agglomerates was noted. This agglomeration phenomenon may be due to the crystallization process (particle surface state) and to the powder recuperation process (filtration and drying).

The powder obtained were characterized by purity ranging from $97.00\% \pm 2.76\%$. This value can prove that the experimental proceeding does not induce the product contamination by germs in tubing elements of pump or in mixer device.

Table 3.16. Identification and characterization of dried powder regarding solid state properties.

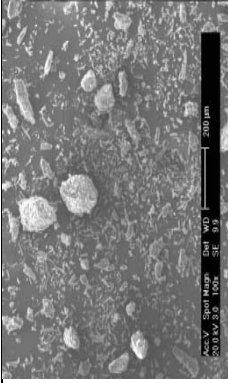
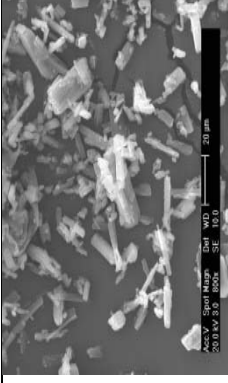
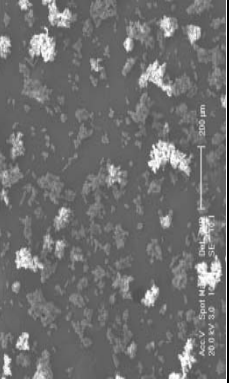
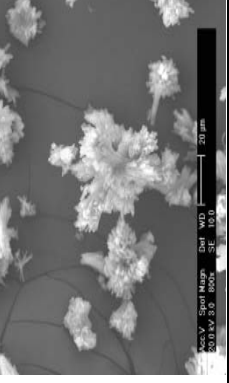
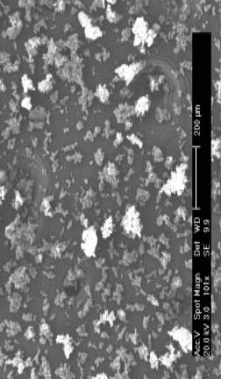
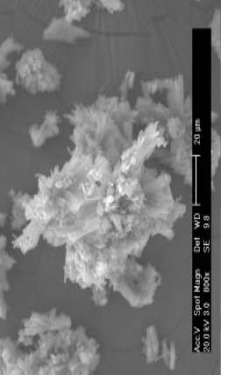
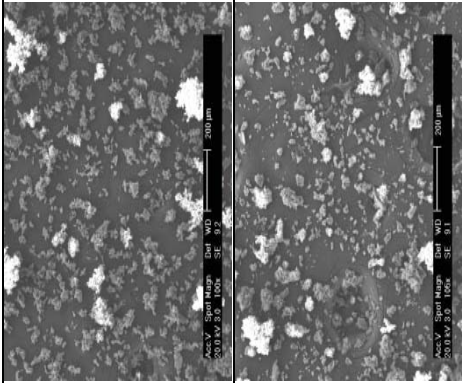
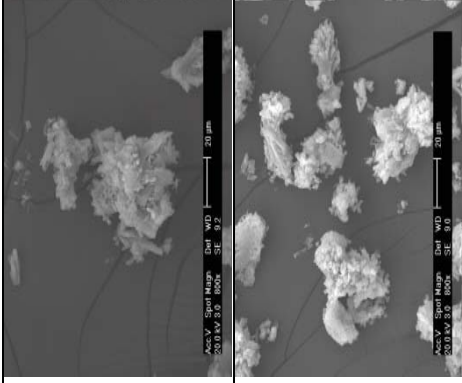
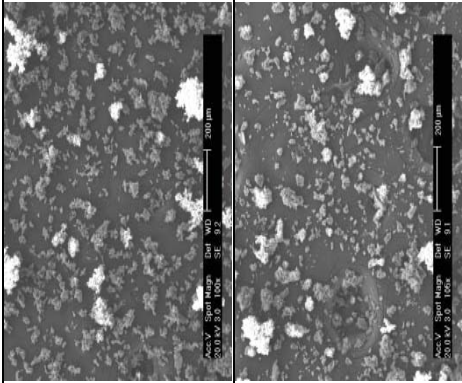
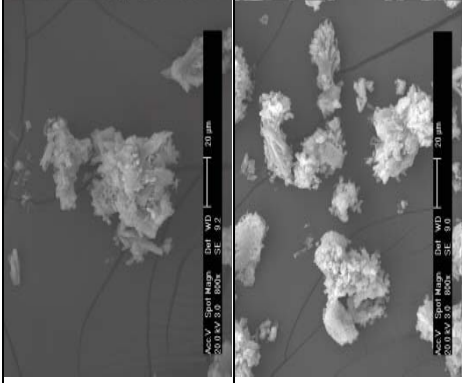
Exp.	Type of Mixer	Total flow rate (g/min)	Ethanol-water ratio (w/w)	SEM Image 200 µm	SEM Image 20 µm	Residual solvent Content (%)
Original CRS	X	X	X			0.37
1A	Roughton	44.51	25-75 %			1.00
2A	T	44.51	25-75 %			0.56

Table 3.16. Continued

Exp.	Type of Mixer	Total flow rate (g/min)	Ethanol-water ratio (w/w)	SEM Image 200 μm	SEM Image 20 μm	Residual solvent Content (%)
3A	T	27.09	25-75 %			0.56
4A	T	69.56	25-75 %			0.54

3.4.3. Comparative study of original CRS 74 and LAS recrystallized drug with T-mixer

According to experimental result (see section 3.4.1.2) the T-mixer was chosen for the following steps. The original CRS 74 (raw material) and recrystallized powder using T-mixer using the best experimental conditions was characterized in order to verify physicochemical changes, among the products after recrystallization process.

3.4.3.1. Particle size and morphology

Laser diffractometry yields the volume-weighted diameters. The $dv_{10\%}$, $dv_{50\%}$ and $dv_{90\%}$ represent the sizes in which 10%, 50% and 90% of the particles are below the given sizes, respectively. From Figure 3.12, it can be seen that the particle size distribution changed as follows: the original CRS 74 with 90%, 50% and 10% of the particles smaller than 515 μm , 101 μm and 4.3 μm were reduced respectively to 138 μm ($dv_{90\%}$), 34 μm ($dv_{50\%}$) and 4.4 μm ($dv_{10\%}$) after LAS recrystallization.

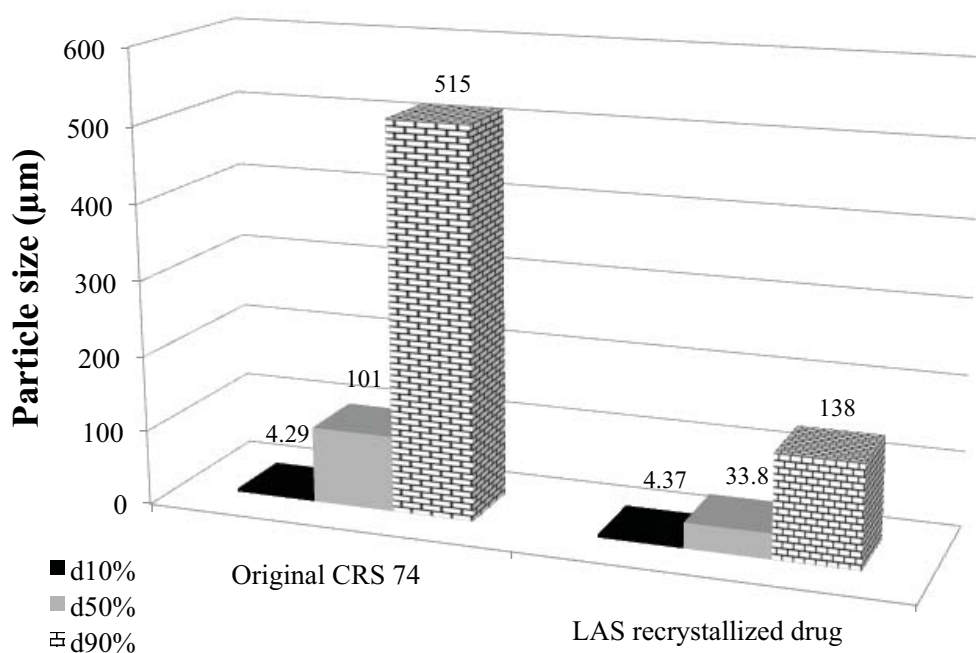
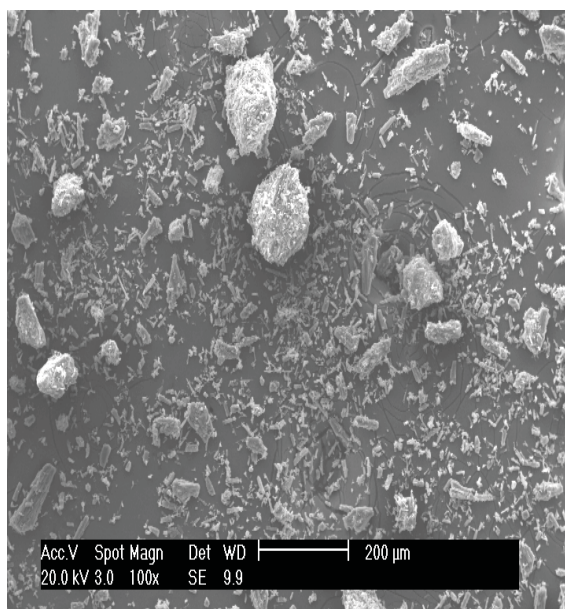
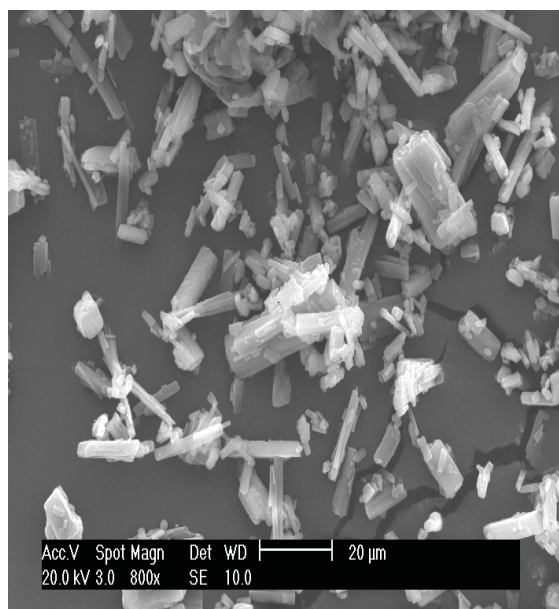


Figure 3.12. Particle size (laser diffraction data) of CRS 74, before and after the LAS recrystallization process.

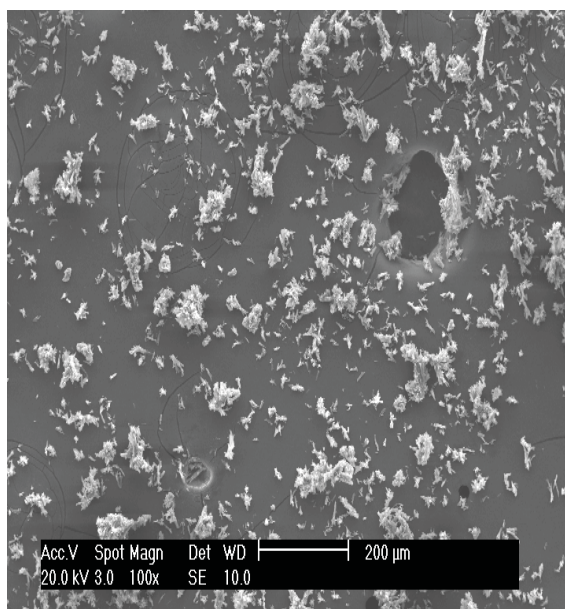
These results are supported by the powder morphology observed by SEM (Figure 3.13). The particles of the original powder were found to be larger and exhibiting a broad particle size distribution compared to the LAS recrystallized drug.



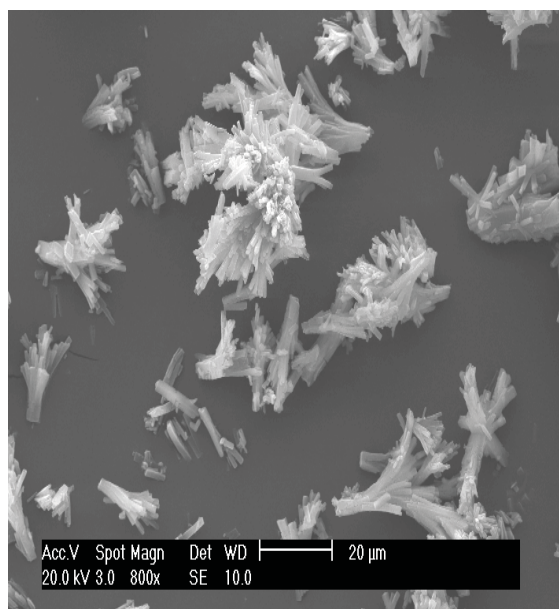
(a)



(b)



(c)



(d)

Figure 3.13. SEM micrographs of the original (a, b) and LAS recrystallized CRS 74 (c, d).

3.4.3.2. XRD analysis

XRD analysis was performed to detect the changes in the physical state and crystalline phases of the drug, before and after LAS recrystallization. Figure 3.14 shows the XRD patterns for the two studied samples. CRS 74 shows peaks at approximately 8.5, 14, 16.9, 18.7, 19.4 and 21.3°, indicating that the drug was a crystalline powder. Comparing the DRX diffractograms of LAS recrystallized drug to the original CRS 74 it can be seen that the crystalline phases were preserved.

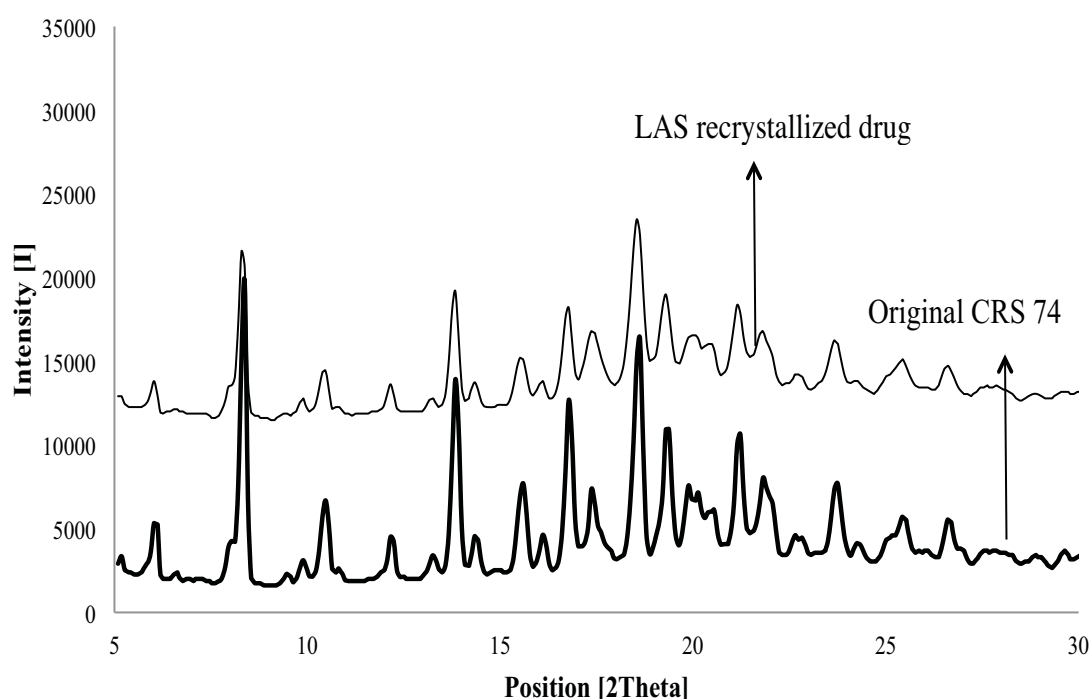
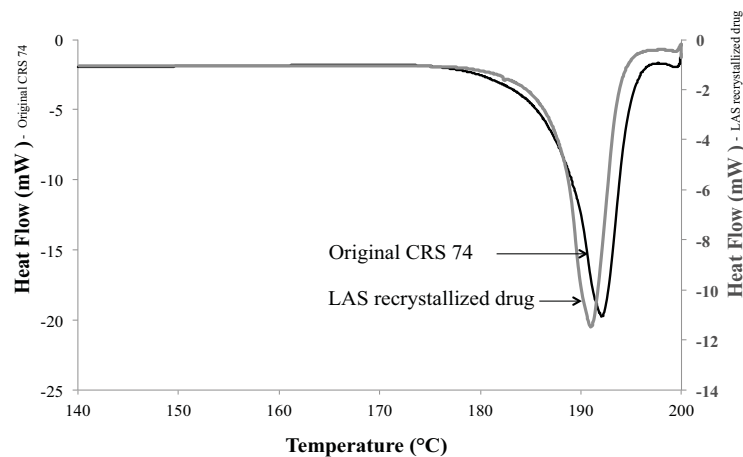


Figure 3.14. X-Ray diffractograms of the original and LAS recrystallized drug powders.

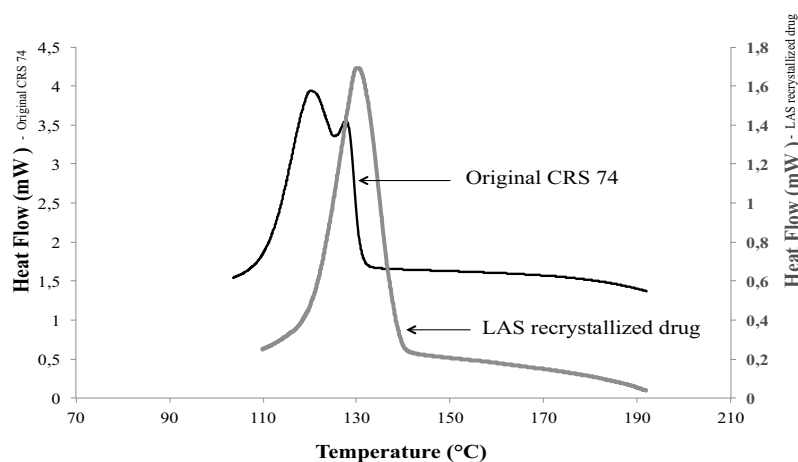
3.4.3.3. DSC analysis

The DSC thermograms of original and LAS recrystallized drug are presented in Figure 3.15. The onset melting point and fusion enthalpy obtained from the DSC study are summarized in Table 3.17. Relative enthalpy is calculated by taking the fusion enthalpy of original CRS 74 powder as 100%.

From DSC data, it was concluded that LAS recrystallization changed marginally the thermal properties of the drug.



(a)



(b)

Figure 3.15. a) DSC thermograms of original CRS 74 (*first heating*), which consists of a melting endotherm (peak onset temperature $T_{m(\text{Onset})} = 188.64^{\circ}\text{C}$) and LAS recrystallized drug, which consists of a melting endotherm (peak onset temperature $T_{m(\text{Onset})} = 187.79^{\circ}\text{C}$); b) DSC thermograms of original CRS 74 (*cooling after first heating*), which consists of a crystallization exotherm (peak onset temperature $T_{c(\text{Onset})} = 132.12^{\circ}\text{C}$) and LAS recrystallized drug, which consists of a crystallization exotherm (peak onset temperature $T_{c(\text{Onset})} = 138.43^{\circ}\text{C}$).

The observed reduction of the fusion enthalpy (Table 3.17) may be caused by the higher surface/volume ratio exhibited by the LAS recrystallized powder, needing lower energy for melting. Crystal energy is known to correlate with $T_{m(\text{Onset})}$ (onset melting point) and Δh_f (enthalpy of fusion), which refers to the energy a compound must overcome to dissolve (VIPAGUNTA et al., 2007).

Table 3.17. Melting Temperature ($T_{m(\text{Onset})}$), Heat of Fusion (Δh_m) for the original and LAS recrystallized drug.

Thermal and dissolution parameters	Original CRS 74	LAS recrystallized CRS 74
$T_{m(\text{Onset})}(\text{°C})$	188.6	187.8
Δh_m (J/g)	86.6	79.2
Relative enthalpy(%)	100	91.5

3.4.3.4. Dissolution studies

Figure 3.16 shows the dissolution profiles of original and LAS recrystallized CRS 74 in 0.1 M HCl (pH 1.2). It can be seen from Figure 3.13 that both drug samples did not even reach 50% dissolution within 3 h.

The dissolution profiles were compared through the model-independent simple method. The model-independent simple method includes the difference factor ($f1$) and the similarity factor ($f2$), calculated by using the following equations (3.7) and (3.8) (MOORE and FLANNER, 1996; COSTA and LOBO, 2001).

$$f1 = 100 \left\{ \frac{\sum_{t=1}^n |R_t - T_t|}{\sum_{t=1}^n R_t} \right\} \quad (3.9)$$

$$f2 = 50 \log \left[100 \left\{ 1 + \frac{1}{n} \sum_{t=1}^n (R_t - T_t)^2 \right\}^{-0.5} \right] \quad (3.10)$$

where R_t and T_t are the percentage of drug dissolved at each time point for the reference and test products, respectively; n is the number of dissolution sample times and t is the time points for collecting dissolution samples.

The f_1 factor measures the percentage of the error between two curves over all time points. This percentage is zero when the test and drug reference profiles are identical and increases proportionally with the dissimilarity between the two dissolution profiles. The f_2 factor is a logarithmic transformation of the sum-squared error of differences between the test and the reference products over all time points. When the two profiles are identical, $f_2=100$. An average difference of 10% at all measured time point results in a f_2 value of 50. FDA has set a public standard of f_2 value in the range 50-100 to indicate similarity between two dissolution profiles.

Since original CRS 74 is the reference, the factors f_1 and f_2 are calculated between this product and the LAS recrystallized powder. The results of f_1 and f_2 , 24.8 and 98.8, respectively, showed that the profiles of original CRS 74 and LAS recrystallized drug are almost similar.

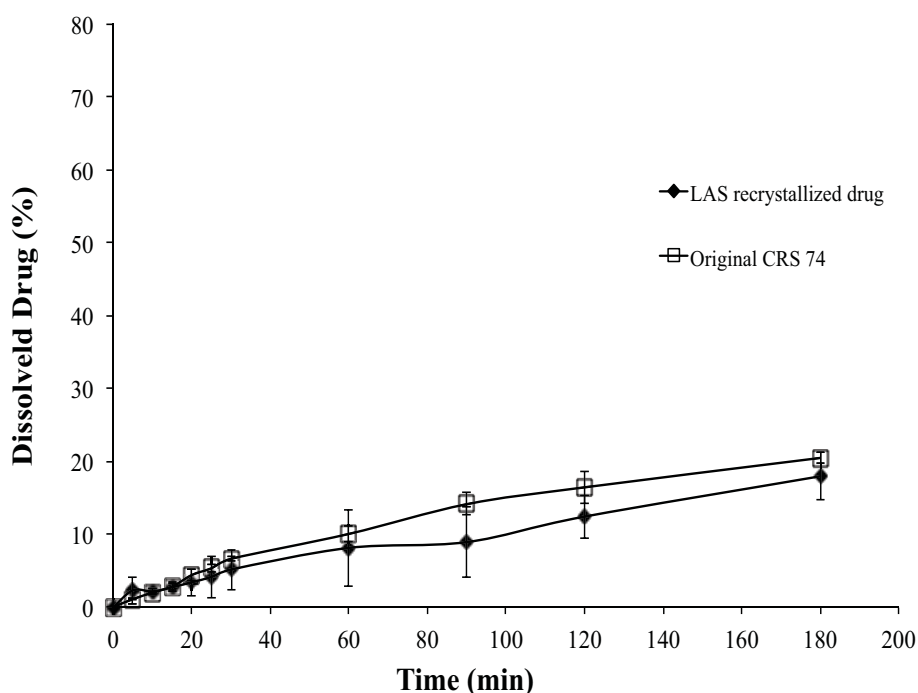


Figure 3.16. Dissolution profiles of CRS 74, before and after LAS recrystallization (in 0.1 M HCl at 37 °C, $n = 4$).

3.4.3.5. Determination of surface properties

The surface properties of drug samples were investigated to find a possible relation between surface properties and dissolution. Sessile drop contact is most commonly measured on compacted powder disc surface. However, compaction of the material can alter the particle morphology and surface energy (BUCKTON, 1955). Alternatively, some of the authors (AHFAT et al, 2000; HE et al, 2008) have reported the use of powder layer adhered to an inert support. The powder layer was adopted for the present work as it allows the study of “as is” powder properties. This method gave reproducible values. It has been seen that contact angle measurements can vary with experimental methodology, however the technique was used for comparative evaluation between LAS recrystallized samples and the original drug powder.

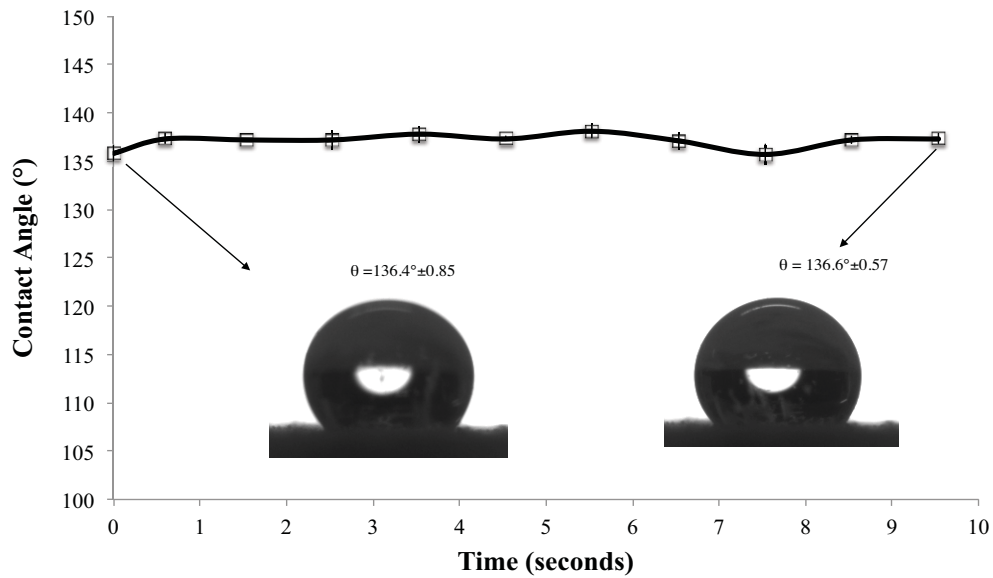
The contact angle of drop deposited on powder surface was plotted as a function of time from 0 to 10 s, beyond which there was no significant change in the contact angle. With water as the wetting liquid, original drug crystals exhibited a contact angle almost unchanged with time from $136.4 \pm 0.8^\circ$ (0 s) to $136.6 \pm 0.6^\circ$ (10 s), as shown in Figure 3.17. In turn, LAS recrystallized drug exhibited an initial contact angle of $133.5 \pm 1.8^\circ$ which changed marginally to $132.9 \pm 1.7^\circ$ over the 10 s period.

The wetting process with water was quantified for the work of adhesion (W_a), cohesion (W_{CL}) and the spreading coefficient (λ_{LS}), as already calculated in Chapter 2, section 2.3.5.

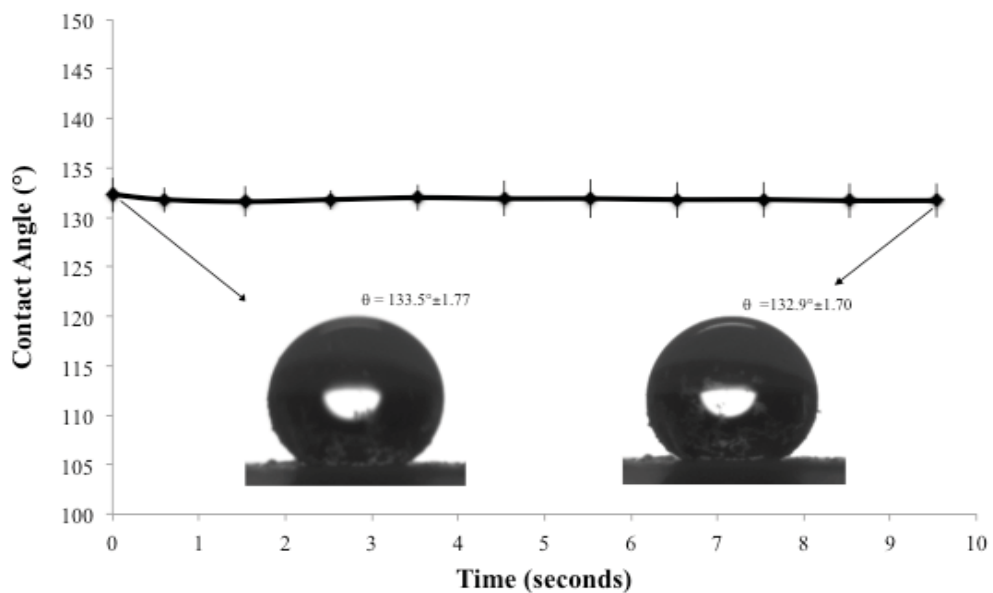
The contact angle made at 0 s was considered as the initial contact angle and the surface tension of water was taken from the literature (72.8 mN/m; PURI et al., 2010). These values were used to determine W_a , W_{CL} and λ_{LS} from equations (2.2), (2.3) and (2.4) for the drug powders (Table 3.18).

The thermodynamic driving force for each process is indicated by the work value, where a negative value denotes the spontaneity of the process (Young and Buckton, 1990). The positive W_a and W_{CL} obtained for both drug powders indicated that the adhesion and the cohesion processes are not spontaneous in both cases. Further, a negative spreading coefficient ($\lambda_{LS} < 0$) means that the original CRS 74 displayed an unfavorable spreading of

water (NGUYEN and HAPGOOD et al., 2010), characteristic which remained unchangeable after LAS recrystallization of the drug. This poor wettability can be related to the poor dissolution rates measured.



(a)



(b)

Figure 3.17. Contact angle (°) of water as a function of time for: a) original CRS 74; b) LAS recrystallized drug.

Table 3.18. Work of adhesion (W_A), cohesion (W_{CL}) and spreading coefficient (λ_{LS}) for CRS 74.

Sample	W_A (mN/m)	W_{CL} (mN/m)	λ_{LS} (mN/m)
CRS 74	20.08	145.6	-125.6
LAS recrystallized powder	22.69	145.6	-122.9

3.5. CONCLUSIONS

The present chapter had the purpose to determine the solubility of CRS 74 in binary solvent mixture (ethanol-water) and to study the influence of operational parameters on the synthesis of a pharmaceutical drug.

The CRS 74 is soluble in ethanol (92.6 mg/g_{solution}) and seems to present a maximum in solubility in ethanol-water mixtures as determined in this study using UNIQUAC-based model at 30°C. To the best of our knowledge, there are no published data of the solubility of such given solute in ethanol-water mixtures to compare with.

The synthesis process should result in a powder with small crystal size with the view to improve the bioavailability of the drug.

According to two main parameters tested, type of mixer and flow rate, uncontrolled crystal growth and no change on the final product was observed, i.e. the operational parameters do not have influence on recrystallized particles. These experiments proved to be quite laborious due to the rapid growth and agglomeration of the produced particles and problems of blockage of the mixer. Because of this drug behaviour, which precluded the realization of essays over time, it was not possible to simply calculate the nucleation and agglomeration rates. In addition this drug behaviour prevent the use of this crystallization proceeding in industrial applications.

After setting process conditions, a solid crystallized by LAS crystallization (operating conditions) was compared (or has been compared) to the raw material. After crystallization process the synthesized product do not present any crystallinity changes. However, a decrease of particle size was observed and consequently a considerable agglomeration of crystals. Furthermore, in the case of CRS 74 LAS crystallization does not have a real impact on the dissolution rate of synthesized powder.

In an attempt to improve its dissolution properties, CRS 74 can be recrystallized by using a Liquid Anti-solvent (LAS) crystallization process and the data generated here can represent a useful tool to define the mass proportion between solvent (ethanol) and anti-solvent (water) for LAS crystallization studies. However, to improve its dissolution kinetics, smaller particles with a more hydrophilic surface need to be produced. This research is going on and our specific aims are to consider the feasibility of the LAS crystallization using different excipients to optimize process and formulation parameters.

CHAPTER 4

Effect of additives in LAS crystallization

Résumé Chapitre 4- Etude de la recristallisation par effet anti-solvant en présence d'additifs

En vue d'améliorer sa dissolution en milieux aqueux, le CRS 74 a été recristallisé en utilisant une opération de cristallisation par effet anti-solvant en présence d'additifs.

Des additifs ont donc été utilisés en vue de modifier les propriétés de dissolution des cristaux, et les vitesses de cristallisation (nucléation, agglomération, croissance).

L'effet des additifs sur la taille des cristaux, la cinétique de dissolution et la mouillabilité du solide synthétisé a été étudié.

Les additifs ont été choisis en accord avec des applications pharmaceutiques futures de cette molécule. Ils sont de quatre types

- des tensio-actifs non ioniques : Tween 20 (ester de sorbitan polyoxyéthylénique) et HPMC (Hydroxypropylméthylcellulose) pour une stabilisation stérique,

- un copolymère à bloc, le poloxamer 407 (P-407) pour une stabilisation stérique,

- un tensio-actif anionique, le dodécylsulfate de sodium (SDS) pour une répulsion électrostatique,

- un copolymère composé de D-glucosamine et de N-acétyl-D-glucosamine (chitosane) pour un effet combiné de stabilisation stérique et répulsion électrostatique.

Ils ont été introduits dans le solvant (éthanol) ou dans l'anti-solvant (eau), ou dans les deux phases.

Par rapport aux additifs testés, des changements des propriétés de surface ont été constatés. Une diminution remarquable de l'angle de contact a été observée pour deux formulations, une avec le copolymère à bloc P-407 (concentration de 0,02 %, > CMC dans la phase organique) et l'autre avec ce dernier combiné avec du chitosane (P-407 concentration de 0.02 %, > CMC dans la phase organique et le chitosane avec une concentration de 0,5 % dans la phase aqueuse). De plus, la dissolution a été améliorée de façon très notable : à 20 min de dissolution, le pourcentage dissous du principe actif est de 4% avec la poudre initiale et de l'ordre 40% pour la poudre recristallisée avec ces deux formulations.

Dans l'ensemble, les résultats ont montré de façon concluante que la technique de cristallisation par effet anti-solvant en présence d'additifs a permis de produire des microcristaux présentant des profils de dissolution nettement plus rapide que la poudre originale. L'amélioration de la dissolution peut-être due à la réduction de la taille des particules des cristaux du principe actif mais aussi à l'amélioration des propriétés de mouillage due aux interactions spécifiques entre le principe actif, les additifs et le milieu aqueux de dissolution. Il est important de noter qu'aucun colmatage n'a été observé avec la formulation combinant les additifs P-407 et chitosane.

4.1.INTRODUCTION

Up to now, we could demonstrate that LAS recrystallization process reduced the mean particle size and particle size distribution of the CRS 74 crystals. However, this particle size reduction did not change the dissolution rate as it could be expected with the increased surface area of the powder. In fact, the powder is characterized by a very high hydrophobicity as confirmed experimentally, and the particles once formed in a nanometric size range grew up very fast and finally agglomerated, reducing the powder surface area in contact with the dissolution medium. In addition, a very strong attraction between the drug particles and the metallic surface of the rapid mixers used in the process led to a retention of the solid inside the mixers and to the interruption of the continuous process.

In this last part of the work, we investigated the effect of organic additives in the CRS 74 recrystallization using the LAS process. Changes in drug-crystal properties were evaluated for particle size and shape, crystal structure, surface characteristics such as wettability and dissolution rate. The methodology and the results obtained are presented in this Chapter.

Considerations for selection of stabilizers

In LAS crystallization, the mixing process and the control of supersaturation are crucial factors to control the production of uniform and small solid drug particles. However, as already discussed in Chapter 1, the addition of stabilizers in the process in order to inhibit excess crystal growth or particle aggregation has been related by a great number of scientific publications (ALI et al., 2011, GHOSH et al., 2011, SU et al., 2011).

Stabilizers can be added either in solvent or anti-solvent, acting as surface modifiers. Polymers are often used for steric stabilization, while surfactants are often used for electrostatic stabilization. The suitable stabilization depends on properties of the substance that should crystallize. Charge and hydrophilicity are some important properties to consider. The stabilizer must of course have sufficient affinity for the particles surface, and it must also have a rather high diffusion rate in order to rapidly cover the generated surface. Unfortunately, there exists no systematic technique to determine the effectiveness of additives a priori. Stabilizing agents are chosen from the list of pharmaceutically acceptable substances, with surface active properties capable to provide steric and/or ionic stabilization against

growth and agglomeration of drug particles, during LAS crystallization. In this study, stabilizers were screened and introduced in the solvent, or in the anti-solvent, or in both phases.

Two main mechanisms of stabilization were tested: steric stabilization and electrostatic repulsion.

For *steric stabilization*, we used non ionic polymers and amphiphilic block copolymers:

- **Polyoxyethylene sorbitan monooleate (Tween 20)**, a nonionic surfactant.

If this additive is adsorbed on the surface of a hydrophobic drug like CRS 74, we could expect that a mechanical barrier would be formed against crystal growth and agglomeration. The additive would occupy the adsorption sites on the surface of freshly formed CRS 74 crystals during LAS crystallization, and inhibits subsequent growth by inhibiting the incorporation of drug molecules from solution into crystal lattices, as already observed for other drugs such as Fenofibrate and Acid Folic (WU et al. 2011; PARDEIKE et al., 2011); In addition, Tween 20 was selected because it is also very well tolerated in pharmaceutical formulations, being accepted even for intravenous injection (FDA, 2007).

- **Hydroxypropylmethylcellulose (HPMC)**, a neutral polymer.

It could be expected that this polymer adsorbs on the hydrophobic CRS 74 surface and the portions of polymer chain extending in solution provides steric protection. HPMC is a stabilizer frequently used in LAS crystallization studies due to its characteristic of good solubility in water and not being toxic (DONG et al., 2009).

- **Poloxamer 407 (P-407) copolymer** (ethylene oxide and propylene oxide blocks), a hydrophilic non-ionic surfactant of the more general class of copolymers known as poloxamers.

Poloxamer-407 can induce the steric stabilization and its use in pharmaceutical formulations is approved (oral solutions, ophthalmic solutions, periodontal gels and topical emulsions (REHMAN, 2011).

For *electrostatic repulsion*, the anionic surfactant **Sodium dodecyl sulfate (SDS)** was chosen. This surfactant has been used as an electrostatic stabilizer with high affinity to adsorb onto particle surfaces leading to high zeta potentials. It is a regulatory accepted stabilizer for oral dosage forms (e.g. tablets and capsules), and is therefore suitable to be used in nanosuspensions (HU et al., 2011).

For a *combined effect of steric stabilization and electrostatic repulsion*, we tested **Chitosan**, a copolymer of glucosamine and N-acetyl glucosamine, a polycationic, biocompatible and biodegradable *polymer*.

Chitosan is a compound which combines the electrostatic stabilization due to its positive charge in acidic medium, and the steric stabilization because of its polymeric nature. Theoretically, that means that if the polyelectrolyte adsorbs onto the surface of small embryo drug particles surface, it should be the ideal stabilizer because it combines electrostatic and steric stabilization, it forms a strong double layer around hydrophobic drug particle. In addition, the chitosan can increase the drug bioavailability due to mucoadhesion, that is able to increase cellular permeability (BOWMAN and LEONG, 2006).

Concerning surfactants, in aqueous solution, dilute concentrations of surfactant act much as normal electrolytes, but at higher concentrations a very different behavior is observed. This behavior is explained in terms of formation of organized aggregates of large numbers of molecules called micelles, in which the lipophilic parts of the surfactants associate in the interior of the aggregate leaving hydrophilic parts to face the aqueous medium.

The physico-chemical properties of surfactants vary markedly above and below the CMC value. As an example, below the CMC value, the physico-chemical properties of ionic surfactants like sodium dodecylsulfate, SDS, (e.g., conductivities, electromotive force measurements) resemble those of a strong electrolyte. Above the CMC value, these properties change dramatically, indicating a highly cooperative association process is taking place, This is illustrated in Figure 4.1. (LAURIER et al., 2003).

Based on this discussion, the CMC values can be important in our additives study, and the additive concentration for the surfactants Tween 20, SDS and Poloxamer 407 were varied from below to above their CMC. The CMC is also of interest because at concentrations above

this value, the adsorption of surfactant at interfaces usually increases very little. This means that the CMC frequently represents the solution concentration of surfactant from which nearly maximum adsorption occurs (LAURIER et al., 2003).

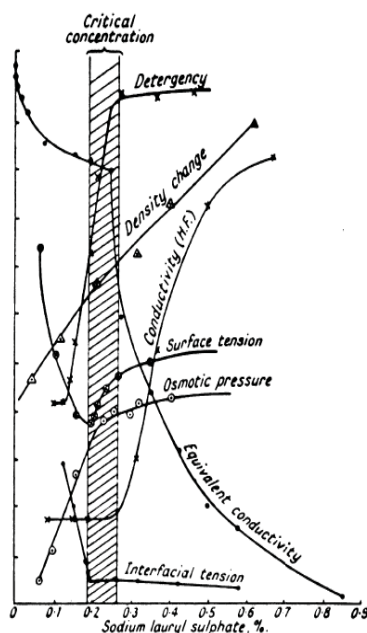


Figure 4.1. Variation in physical properties of sodium lauryl sulfate (or SDS) surfactant solutions below and above the CMC value (from Laurier et al, 2003).

To sum up, Tween 20, SDS, Poloxamer 407, HPMC and Chitosan are the chosen additives expected to improve particle size control during the LAS crystallization process of CRS 74, and they were introduced in the solvent (Poloxamer 407) or in the anti-solvent (all the other ones) in our CRS 74-ethanol-water system.

4.2. Materials and methods

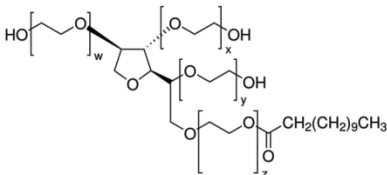
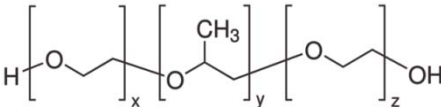
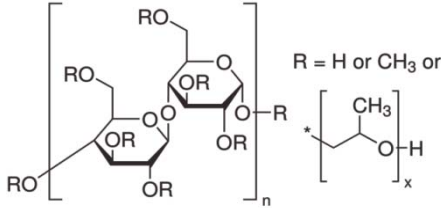
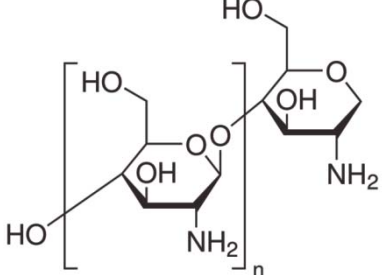
4.2.1. Materials

The additives used are shown in Table 4.1.

CMCs of Tween 20, SDS and Poloxamer 407 are given in Table 4.2. The CMC values for Tween 20 and SDS were found in the literature (Silva and Volpato, 2002). The CMC for P-

407 was measured in the laboratory, using a tensiometer 3S ILMS (GBX Instruments, France).

Table 4.1. Different additives used in LAS crystallization of CRS 74.

Additives	Chemical structure	Supplier
Sodium dodecyl sulfate (SDS) <i>M.W.</i> : 288 g/mol		Fluka, France.
Polyoxyethylene sorbitan monolaurate (Tween 20) <i>M.W.</i> : 1228 g/mol		Sigma-Aldrich, France.
Poloxamer 407 or Pluronic F127 <i>M.W.</i> : 8400 g/mol		Basf, France.
Hydroxypropylmethylcellulose (HPMC) <i>M.W.</i> : 22000 g/mol		Sigma-Aldrich, France.
Chitosan Low molecular weight <i>M.W.</i> : 227000 g/mol		Sigma-Aldrich, France.

M.W.: Molecular weight

A maximum concentration was fixed for all additives to give a mass ratio of 1:4 (additive:drug). This corresponds to 0.5%w/w for HPMC, Chitosan, Tween 20 and SDS in water and 0.02% (w/w) for P-407 in ethanol.

Table 4.2. Critical micelle concentration of additives used in LAS crystallization at 25°C.

Additive	CMC value (w/w)	Reference
Tween 20	0.05 %	SILVA and VOLPATO, 2002
SDS	0.1 %	SILVA and VOLPATO, 2002
Poloxamer P-407	0.0008 %	Measured experimentally

4.2.2. Methods

4.2.2.1. Production of particles by LAS crystallization in presence of additives

The original CRS 74 crystals were recrystallized by the LAS crystallization method already described in Chapter 3, using the same experimental set-up. Briefly, a certain amount of original CRS 74 samples was completely dissolved in ethanol at $30 \pm 0.5^\circ\text{C}$ at definite concentration ($90 \text{ mg}_{\text{CRS 74}}/\text{g}_{\text{solution}}$). The solution was filtrated through $0.22 \mu\text{m}$ pore size membranes to remove the possible particulate impurities. The drug was then recrystallized via the concurrent introduction of the CRS 74 ethanol solution and an anti-solvent stream of water in the T-mixer. The freshly formed crystals were collected in a vessel under magnetic stirring and then filtered and dried under vacuum at $50 \pm 1^\circ\text{C}$ for 24 h. The dried samples produced in the process were characterized by laser diffractometry, differential scanning calorimetric analysis, X-ray diffraction analysis, scanning electron microscopy analysis, sessile drop method and dissolution testing.

The experimental conditions are summarized in Table 4.3. The studied parameters were:

1. Phase for incorporation of the additive (organic solution, aqueous solution or both solutions);
2. Additive concentration (above and below CMC);
3. Drug concentration in the organic phase;
4. Re-structured organic phase containing P-407: Poloxamer 407 was introduced in a dilute ethanol solution (concentration below its CMC), before the drug. The resulting solution was then heated under controlled conditions (rotoevaporator) to promote a partial evaporation of the solvent and concentrate the solution to a surfactant concentration above its CMC.

Table 4.3. Experimental conditions for LAS crystallization in presence of additives.

Experiment	Additive _{Organic phase}	Ratio _{addit.org.:drug}	Additive _{Aqueous phase}	Ratio _{addit.aqu.:drug}	S ($S=C/C_{eq}$)
1	X	X	X	X	894.04
<i>Additive in the aqueous phase</i>					
2	X	X	HPMC 0.5% w/w SDS < CMC	1:6	445.63
3	X	X	(0.008% w/w)	1:4000	391.85
4	X	X	SDS 0.5% w/w Tween 20 < CMC	1:6	150.51
5	X	X	(0.008% w/w)	1:4000	541.13
6	X	X	Tween 20 0.5% w/w	1:6	398.72
7	X	X	Chitosan 0.5% w/w	1:6	*
<i>Additive in the organic phase</i>					
8	P-407 < CMC (0.0003%w/w)	1:8000	X	X	901.97
9	P-407 > CMC (0.02% w/w)	1:4	X	X	673.40
<i>Additive in both, organic and aqueous phases</i>					
10	P-407 < CMC (0.0003%w/w)	1 :10000	SDS 0.5% w/w	1:6	217.11
11	P-407 > CMC (0.02% w/w)	1:4	SDS 0.5% w/w	1:6	194.93
12	P-407 < CMC (0.0003% w/w)	1 :10000	Chitosan 0.5% w/w	1:6	*
13	P-407 > CMC (0.02% w/w)	1:4	Chitosan 0.5% w/w	1:6	*
<i>Drug concentration in the organic phase</i>					
14	P-407 > CMC (0.02% w/w)	1:4	X	X	374.51
15	P-407 > CMC (0.02% w/w)	1:4	X	X	156.41
16	P-407 > CMC (0.02% w/w)	1:4	SDS 0.5% w/w	1:3	104.50
17	P-407 > CMC (0.02% w/w)	1:4	SDS 0.5% w/w	1:1.5	43.25
18	P-407 > CMC (0.02% w/w)	1:4	Chitosan 0.5% w/w	1:3	*
19	P-407 > CMC (0.02% w/w)	1:4	Chitosan 0.5% w/w	1:1.5	*
<i>Reorganized organic phase containing P-407</i>					
20	P-407 < CMC (0.0003% w/w)	1:4	X	X	77.59
21	P-407 < CMC (0.0003% w/w)	1:4	Chitosan 0.5% w/w	X	*

*Data not determined

4.2.2.2. Determination of solubility in presence of additive

The equilibrium concentration (C_{eq}) for the CRS 74-ethanol-water system was previously measured and presented in Chapter 3. The presence of additives can modify the drug saturation concentration in this system. The solubility of CRS 74 was then determined in presence of additives, for a mass proportion of 1 (25% solvent) to 3 (75% anti-solvent) using the same procedure as described previously. The new solubility data were used to estimate the theoretical efficiency of the process as a function of the additive used.

4.2.2.3. Characterization methods

4.2.2.3.1. Measurements of particle size during the crystallization process

Particle size was measured during the crystallization process and at the end of the process, after product drying.

In a first step, at the exit of the T-mixer, the mixed phases were poured into a vessel under agitation and a sample was immediately submitted to a particle size analysis in a Zetasizer Nano Zs (Malvern Instruments, United Kingdom) to follow the growth of small embryo particles in the crystallization medium during 150 seconds. To achieve appropriate measurement concentration for analysis, the sample was diluted 5 times using a saturated solution composed of water, ethanol, drug and the additive.

At the end of the process (2 min), the final suspension was filtered and the solids were dried under vacuum at $50 \pm 1^\circ\text{C}$ for 24h. The dry powder was then analyzed by laser granulometry, using a MasterSizer 3000 (Malvern Instruments, United Kingdom). All samples were firstly mixed with Tween 20 to increase the powder dispersion in dispersive media, and then dispersed in water until achievement of the good obscuration. The sampling procedure is schematized in Figure 4.2.

Zeta potential

The zeta potential was also determined in the Zetasizer Nano Zs (Malvern Instruments, United Kingdom) by measuring the electrophoretic mobility of the particles. The

measurements were performed on the same sample taken at the exit of the T-mixer immediately diluted with the saturated solution.

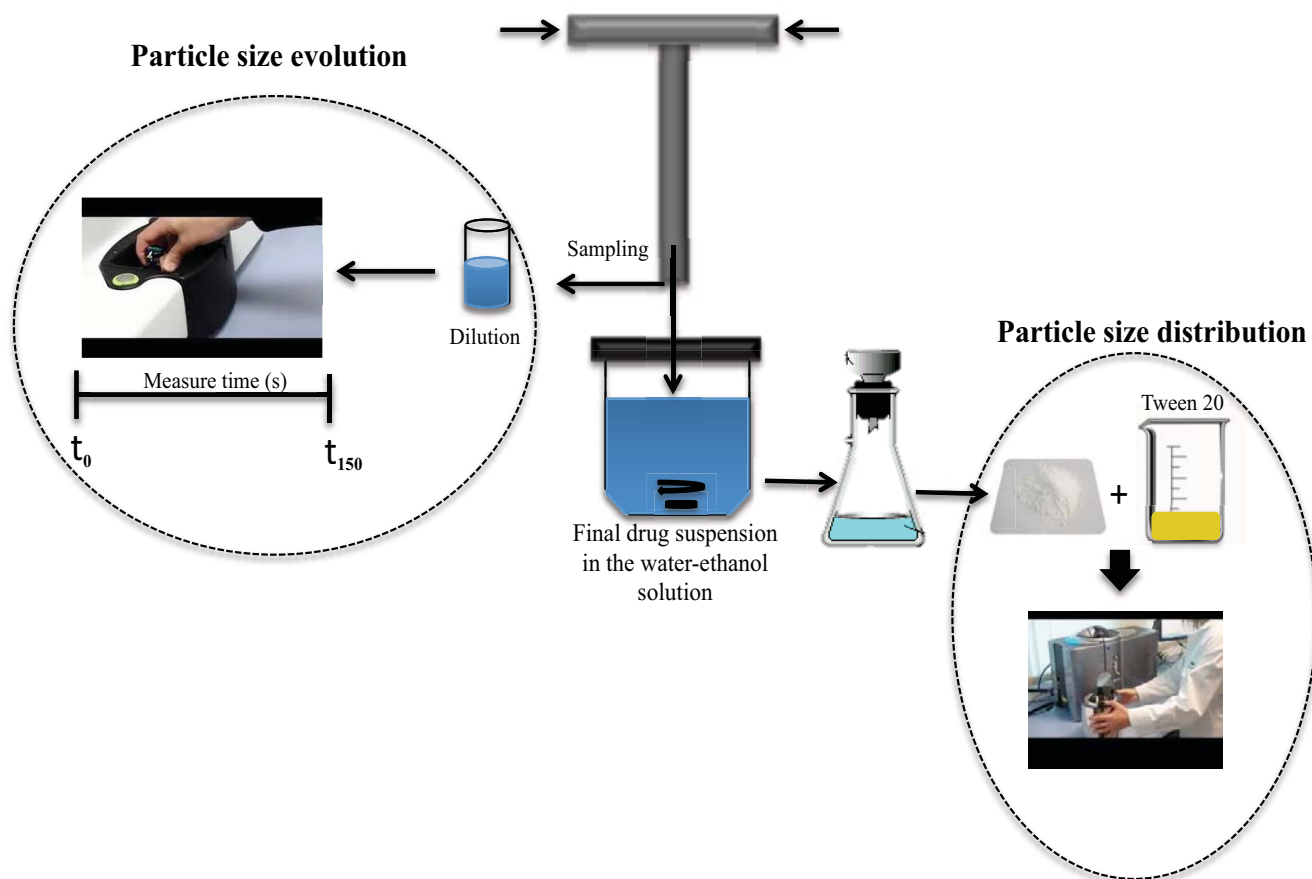


Figure 4.2. Particle size analysis using Zetasizer Nano Zs (particles in suspension) and MasterSizer 3000 (dried powders).

4.2.2.3.2. Powder physicochemical properties

Size distribution, surface properties, morphology, drug purity and dissolution kinetics of recrystallized powders were determined as previously described in Chapter 3.

4.3. RESULTS AND DISCUSSION

4.3.1. CRS 74 solubility in presence of additives

The results obtained for the solubility of CRS 74 in presence of additives are presented in Table 4.4. Figure 4.3 displays the same data graphically. It can be seen that the effect of additives on the drug solubility in the ethanol-water mixture depended on the type and the concentration of the additive used.

Surfactants in solution below their critical micelle concentration (CMC) improve drug solubility by providing regions for hydrophobic drug interactions in solution (NARANG et al, 2007). It can be seen that the presence of the three additives used here in a concentration below their CMC (Tween 20, SDS and P-407) improved only modestly the drug solubility in the ethanol-water mixture (0.025-0.05 mg/g_{solution}).

Above the CMC, surfactants self-aggregate in defined orientation to form micelles with a hydrophobic core and a hydrophilic surface. The hydrophobic core enhances the entrapment of drug, thus increasing its solubility (RANGEL-YAGUI et al., 2005), which probably happened to CRS 74 but the effect is still marginal with Tween 20 and P-407 (0.025-0.057 mg/g_{solution}).

The extent of CRS 74 solubility in the micelle cores formed with the different additives is probably dependent on the compatibility between the drug and the micelle core. In contrast, SDS in concentration above its CMC increased the C_{eq} from 0.025 to 0.151 mg/g_{solution}. The highest solubilization capacity of SDS can be attributed in part to its anionic charge. According to the literature, the solubilizing powers of the surfactants is in the order of anionic < cationic < nonionic (TOKIWA, 1968).

Finally, the presence of HPMC did not have a significant influence on the C_{eq} .

The solubility of CRS 74 in presence of chitosan could not be measured because any drug peak was detected by HPLC analysis.

Table 4.4. CRS 74 solubility in ethanol-water mixture with a ratio of 25-75 % (ww) at 30°C.

Additive	Solubility (mg/g _{solution}) ±SD
No additive (original CRS 74)	0.025±0.000
No additive (recrystallized CRS 74)	0.025±0.000
P407< CMC (0.0003%w/w)	0.025±0.000
P407> CMC (0.02%w/w)	0.033±0.002
HPMC 0.5%w/w	0.051±0.002
Tween 20 < CMC (0.008%w/w)	0.042±0.000
Tween 20 0.5%w/w	0.057±0.001
SDS<CMC (0.008%w/w)	0.058±0.003
SDS 0.5%w/w	0.151±0.003
SDS 0.5% +P407< CMC (0.0003%w/w)	0.106±0.001
SDS 05%+P407> CMC (0.02%w/w)	0.114±0.003

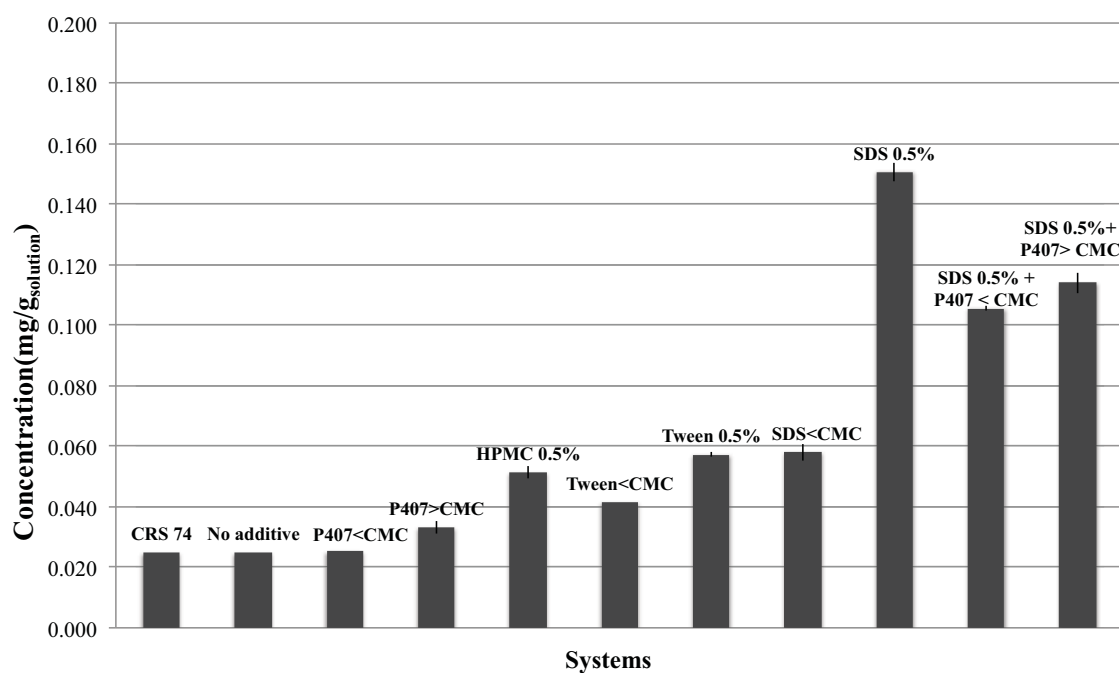


Figure 4.3. CRS 74 solubility in ethanol-water mixture with a ratio of 25-75 % (w/w) at 30°C, in presence of different additives.

4.3.2. Effect of additives on yields of production of CRS 74 crystals

The crystals suspension obtained immediately after the crystallization process, in absence of additives, had a milky aspect, which changed into a clear solution after several minutes. In contrast, for the particles crystallized in presence of additives, this phenomenon was not observed. The crystal suspension maintained a milky appearance until the filtration step, which could represent a first indication on the additive effect for covering the CRS drug crystal surfaces and inducing steric or electrostatic hindrance to prevent crystal growth or/and agglomeration.

Theoretical yield is the maximum amount of recrystallized dry crystals that can be created by the given amount of initial mass of raw crystals. The yields of production were calculated as the weight percentage of the crystal powder after drying with respect to the initial total amount of drug used for recrystallization. Table 4.5 shows that the percent yield of production that was obtained from the LAS crystallization ranged from approximate 50 to 87%. Tween 20 0.5% was proven to be the most effective stabilizer to improve the percent yield of crystals.

There are some unavoidable errors that prevented the experiments from achieving 100% yield. Probably the most common error was mass losses in all experiments due to operation of solid and liquid transfer. The filtration process may allow some of the product to pass through. Also during recovery there was some product lost. For instance, some of the product was stuck inside the T-mixer and could not be completely removed.

The next sections will present and discuss experimental data related to the solid properties when additives were placed respectively in the aqueous phase, in the organic phase and in both phases.

Table 4.5. Theoretical and Practical Yield (%) of CRS 74 crystals obtained by LAS crystallization process.

Experiment	Additive	Theoretical Yield (%)	Yield of production (%)
1	X	99.67	79.44
<i>Additive in aqueous phase</i>			
2	HPMC 0.5% w/w	99.84	50.23
3	SDS<CMC (0.008%w/w)	99.86	76.61
4	SDS 0.5% w/w	99.95	75.56
5	Tween 20<CMC (0.008%w/w)	99.80	47.15
6	Tween 20 0.5% w/w	99.86	86.77
7	Chitosan 0.5% w/w	*	64.78
<i>Additive in organic phase</i>			
8	P-407<CMC (0.0003%w/w)	99.67	65.63
9	P-407>CMC (0.02%w/w)	99.75	70.96
<i>Additive in both, organic and aqueous phase</i>			
10	P-407<CMC (0.0003%w/w)+ SDS 0.5% w/w	99.92	72.74
11	P-407>CMC(0.02%w/w)+ SDS 0.5% w/w	99.91	87.83
12	P-407<CMC(0.0003%w/w)+Chitosan 0.5% w/w	*	76.43
13	P-407>CMC(0.02%w/w)+Chitosan 0.5% w/w	*	83.74
<i>Drug concentration in the organic phase</i>			
14	P-407>CMC (0.0003%w/w)	99.75	52.81
15	P-407>CMC(0.02%w/w)	99.75	74.55
16	P-407>CMC(0.02%w/w)+ SDS 0.5% w/w	99.91	72.48
17	P-407>CMC(0.02%w/w)+ SDS 0.5% w/w	99.91	65.43
18	P-407>CMC(0.02%w/w)+Chitosan 0.5% w/w	*	65.00
19	P-407>CMC(0.02%w/w)+Chitosan 0.5% w/w	*	60.19
<i>Reorganized organic phase</i>			
20	P-407<CMC(0.0003%w/w)	99.75	57.56
21	P-407<CMC(0.0003%w/w)+Chitosan 0.5% w/w	*	57.92

*Data not determined

4.3.3. Effect of presence of the additive in the aqueous phase on physical and surface properties of recrystallized powders

Table 4.6 summarizes the results related to the particle size evolution of the small embryo particles formed at the exit of the T-mixer, when the additive was added in the aqueous phase (HPMC, SDS, Tween 20 and Chitosan). As it can be seen, in all studied systems, the drug particles presented almost the same size (140 - 240 nm), regardless of the type of additive used. However, these particles grew fast reaching in 150 s (t_{150}) almost 2 times their initial particle size (t_0).

Table 4.6. Initial average particle size (APS) and characteristics of CRS 74 crystals in suspension in presence of different additives in the aqueous phase

Experiment	Additive	Time (s)	APS(nm)	Zeta potential (mV)	pH suspension
1	X	t_0	248	*	*
		t_{150}	417	-2.11± 0.28	3.28
2	HPMC 0.5% w/w	t_0	245	*	*
		t_{150}	459	-2.44±0.27	4.88
3	SDS<CMC(0.008%w/w)	t_0	174	*	*
		t_{150}	325	-18.57±0.31	4.48
4	SDS 0.5% w/w	t_0	161	*	*
		t_{150}	358	-38.90±2.12	4.44
5	Tween 20<CMC (0.008%w/w)	t_0	138	*	*
		t_{150}	411	-8.67±1.27	4.53
6	Tween 20 0.5% w/w	t_0	154	*	*
		t_{150}	308	-6.77±1.12	4.45
7	Chitosan 0.5% w/w	t_0	204	*	*
		t_{150}	653	+35.20±1.40	4.44

The particle charge was quantified as the so-called zeta potential, which was measured via the electrophoretic mobility of the particles in an electrical field. The zeta potential theory is described in very detail in the literature (HUNTER, 1981), here only a brief explanation is

given. In general, particles possess a surface charge which occurs due to the dissociation of surface functional groups, the so-called Nernst potential. Of course, the degree of dissociation of the functional groups depends on the pH of the suspension; therefore the zeta potential is pH dependent.

Table 4.6 shows the changes on the zeta potential of the particles in presence of additives. When the crystals were synthesized without additives, they possessed a low negative surface charge (-2.1mV). The zeta potential remained almost unchanged when nonionic stabilizers, i.e. HPMC (-2.4mV) and Tween 20 (-8.7/-6.8mV) were used. However, charged additives like SDS (negatively charged) and Chitosan (positively charged) adsorbed with the charged parts of the respective molecules onto the drug particle surface. The surface coverage increased with the increase in SDS concentration, leading subsequently to an increase of the zeta potential (-18.6/-38.9mV). The higher particles are equally charged, the higher is the electrostatic repulsion between particles.

As a rule of thumb, suspensions with zeta potential above $|30|$ mV are physically stable. Suspensions with a potential above $|60|$ mV show excellent stability. Suspensions below $|20|$ mV are of limited stability; below $|5|$ mV they undergo pronounced aggregation (LEE et al., 2008; PATEL and AGRAWAL, 2011). Chitosan and SDS 0.5% were proven to be the best additives to ensure an electrostatic repulsion between freshly CRS 74 crystal formed in the LAS process.

Table 4.7 summarizes some properties of the dried powder obtained at the end of the LAS crystallization process e.g., particle size, SEM images, contact angle and composition (drug content and residual solvent). For easier comparison, the $dv_{10\%}$, $dv_{50\%}$ and $dv_{90\%}$ for the dried powders produced in presence of all additives tested in this study are gathered in Figure 4.4. The corresponding particle size distributions are graphically presented in Appendix III.

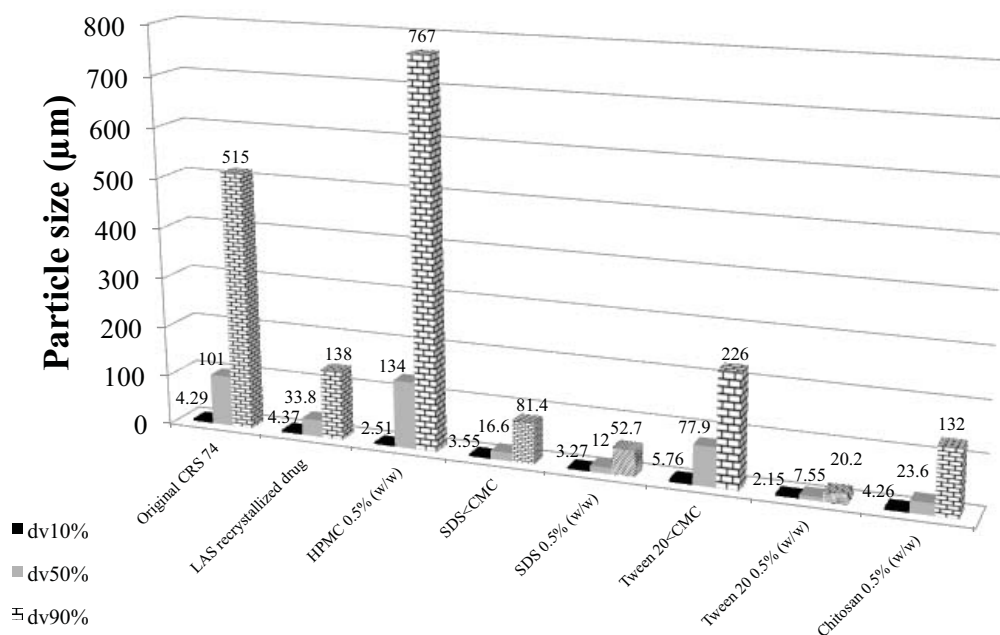


Figure 4.4. Particle size of the drug powders synthesized in presence of additives in the aqueous phase (laser diffraction data).

The primary role of stabilizers is to inhibit excessive crystal growth. In a general way, Figure 4.4 shows that most CRS 74 crystals produced in presence of additives had a smaller particle size compared to original or recrystallized powder without additives. Additives such as HPMC and Tween 20 (concentration below CMC) were less effective to inhibit agglomeration, while a higher concentration of Tween 20 (above CMC) had a very positive effect on particle size control.

Concerning particle morphology (see Table 4.7), the SEM images revealed that in the case of SDS, Tween 20 and Chitosan there was not particle shape changes on the columnar crystals or very little; Contrarily, clusters of thinner (predominantly needle-shaped) primary particles forming agglomerates or aggregates were obtained in presence of HPMC. This effect can be also confirmed by light microscopy (Appendix V) revealing agglomerates or particle assemblies composed of a large number of individual needle-shaped crystals). In this case, a possible explanation could be an inappropriate diffusion (too slow) of the solvent toward the anti-solvent caused by a high viscosity of the anti-solvent containing 0.5%w/w HPMC. A high viscosity could prevent diffusion between solution and anti-solvent and resulted in nonuniform supersaturation and agglomeration.

XRD analysis was performed to detect the changes in the physical state and crystalline phases of the drug due to the presence of additives in the aqueous phase. Figure 4.5 shows the XRD patterns for all powder samples. Comparing the DRX diffractograms of recrystallized drug in presence of HPMC, Tween 20 (below and above CMC), SDS (below and above CMC) and Chitosan, it can be seen that the crystalline phases were preserved (the peaks at 8.5, 14, 16.9, 18.7, 19.4 and 21.3° detected for the original drug remained unchanged after recrystallization in presence of these additives).

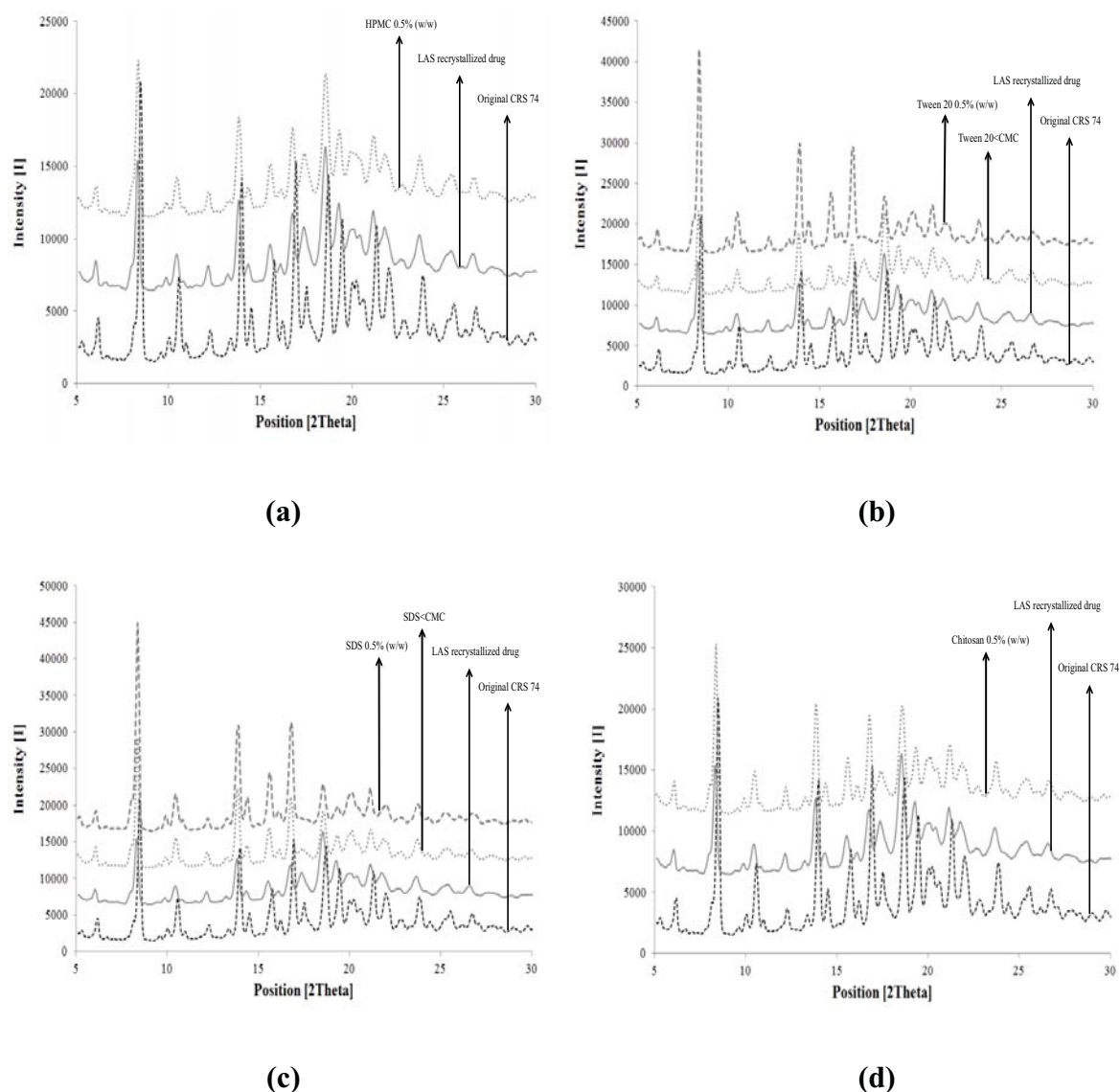


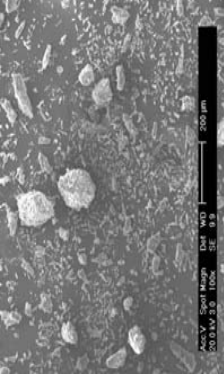
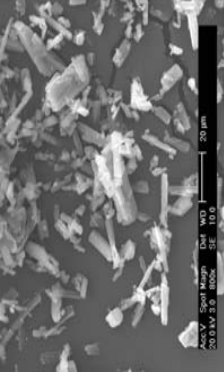
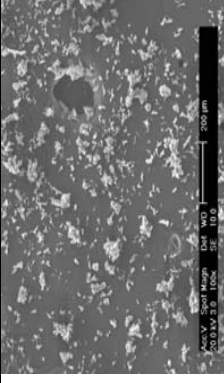
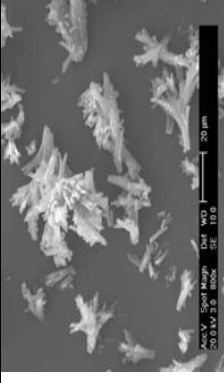
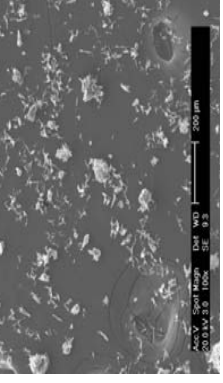
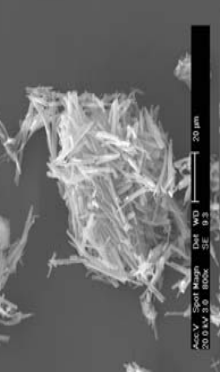
Figure 4.5. X-Ray diffractograms of the drug powders synthesized with additives in the aqueous phase: a) HPMC 0.5% (w/w); b) Tween 20 <CMC and 0.5% (w/w); c) SDS<CMC and 0.5% (w/w); d) Chitosan 0.5% (w/w).

The contact angle measurements were employed to describe the effect of the presence of additives in the aqueous phase on the wettability of the recrystallized powders compared to original CRS 74. The contact angle of drop deposited on all powders surface was plotted as a function of time from 0 to 10 s, and the results are given in Appendix IV. Table 4.6 presents the initial contact angle made at 0 s for all powders. The original powder and the powder recrystallized without additives were strongly hydrophobic ($\theta > 132^\circ$) as already discussed in Chapter 3. This surface characteristic remains practically unchanged after recrystallization in presence of most of additives tested up to here. It can be observed that the powder produced in presence of Chitosan possessed a contact angle higher than the contact angle for the original drug ($\theta = 140.9^\circ \pm 0.4$). In fact, the measure is not totally effective as it became difficult to measure experimentally liquid contact angles on high charged surfaces. To sum up, the unique additive that was able to reduce consistently the contact angle of this drug with water to approximately 100° was Tween 20 0.5 % (w/w).

Finally, Table 4.7 also gives the powder composition in terms of drug content and residual solvent. The drug contents of the CRS 74 microcrystals were above 98% for all CRS 74 recrystallized samples. These results show that almost all of the additives were removed by washing.

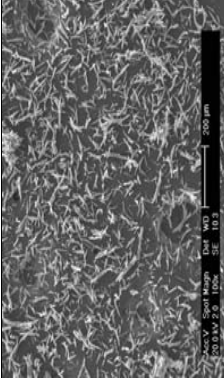
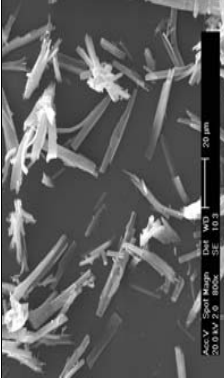
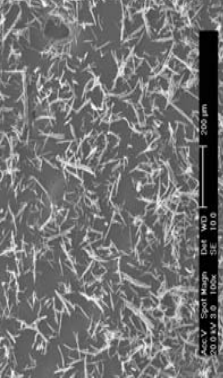
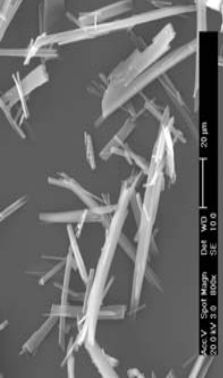
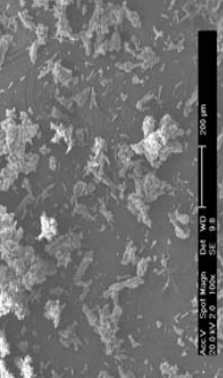
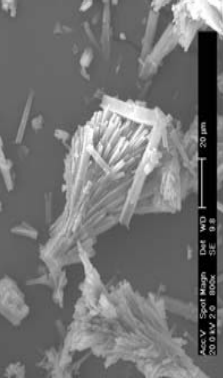
Effect of Additives in LAS crystallization

Table 4. 7. Summarizes some properties of the dried powder obtained at the end of the LAS crystallization process e.g., particle size, SEM images and contact angle.

Exp.	Additive	Contact Angle (°)	Size distribution (µm)	SEM images 200µm	SEM images 20µm	Purity (%w/w)	Residual solvent (%)
Original CRS 74	X	136.4±0.85	D[10] : 4.29 D[50] : 101 D[90] : 515 D[4.3] : 191 Span : 5.06			98.90	0.37
1	X	133.5±1.77	D[10] : 4.37 D[50] : 33.8 D[90] : 138 D[4.3] : 77.7 Span : 3.94			97.00	0.60
2	HPMC 0.5% w/w	124.5±0.14	D[10] : 2.51 D[50] : 134 D[90] : 767 D[4.3] : 287 Span : 5.68			98.64	0.89

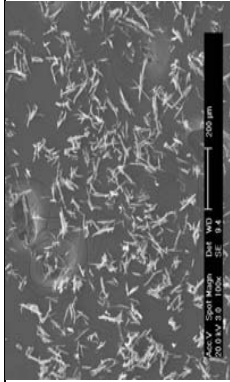
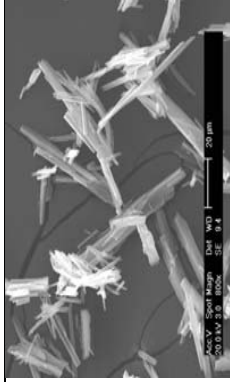
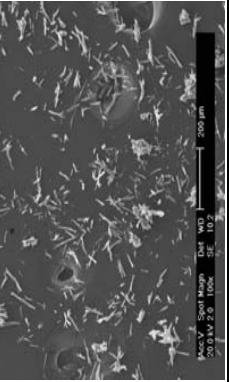
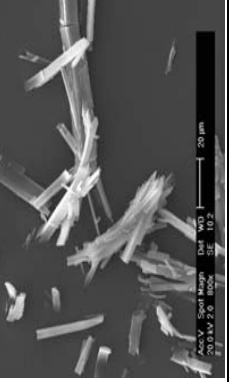
CHAPTER 4

Table 4.7. Continued

Exp.	Additive	Contact Angle (°)	Size distribution (µm)	SEM images 200µm	SEM images 20µm	Purity (%w/w)	Residual solvent (%)
3	SDS<CMC (0.008%w/w)	135.7±0.78	D[10] : 3.55 D[50] : 16.6 D[90] : 81.4 D[4.3] : 32.8 Span : 4.67			99.14	0.59
4	SDS 0.5% w/w	136.2±1.77	D[10] : 3.27 D[50] : 12.0 D[90] : 52.7 D[4.3] : 21.0 Span : 4.11			100.45	0.74
5	Tween 20<CMC (0.008%w/w)	136.8±2.33	D[10] : 5.76 D[50] : 77.9 D[90] : 226 D[4.3] : 103 Span : 2.82			101.50	0.57

Effect of Additives in LAS crystallization

Table 4.7 Continued

Exp.	Additive	Contact Angle (°)	Size distribution (µm)	SEM images 200µm	SEM images 20µm	Purity (%w/w)	Residual solvent (%)
6	Tween 20 0.5% w/w	100.5±0.21	D[10] : 2.15 D[50] : 7.55 D[90] : 20.2 D[4.3] : 9.56 Span : 2.39			98.16	0.59
7	Chitosan 0.5% w/w	140.9±0.42	D[10] : 4.26 D[50] : 23.6 D[90] : 132 D[4.3] : 58.2 Span : 5.40			100.17	0.56

4.3.1. Effect of the presence of the additive in the organic phase on physical and surface properties of recrystallized powders

In the second part of the additive screening study, P-407 was incorporated in the organic phase (ethanol + drug + P-407).

Block co-polymeric surfactants such as P-407, consist of ethyleneglycol and propylene glycol, and are very efficient non-ionic stabilizers owing to multiple attachments of hydrophobic domains at the drug particle surface (KIPP, 2004; CHO et al, 2010). Because P-407 has hydrophobic moieties that adsorb onto hydrophobic drug particle surface and two hydrophilic blocks, the adsorption of P-407 onto CRS 74 drug particle surface could provide an effective steric barrier against crystal growth. From the polymer screening, P-407 was selected as an additive for this part of the work. The effect of the polymer concentration was investigated by incorporating the additive in ethanol in two different concentrations (Table 4.4): 0.0003%w/w (<CMC) and 0.02%w/w (> CMC), before the incorporation of the drug.

Following the same experimental procedure already described, Table 4.8 shows the particle size evolution of the small embryo particles formed in presence of P-407 when the mixed phases exiting the T-mixer were poured into a vessel and immediately sampling for analysis. From the results, it can be observed that nanometric particles were obtained, which continued to grow to reach an approximate particle size average of 350 nm at the end of the measure time (150 s), independently of the additive concentration. These particles were slightly more negative charged (-5.4/-7.5 mV) compared to those of drug suspension without additives (-2.1 mV).

Table 4.8. Initial particle size average (APS) and characteristics of CRS 74 crystals in suspension in presence of P-407 in the organic phase

Experiment	Additive	Time (s)	APS (nm)	Zeta potential (mV)	pH suspension
1	X	t ₀	248	*	*
		t ₁₅₀	417	-2.11±0.28	3.28
8	P-407<CMC(0.0003%w/w)	t ₀	199	*	*
		t ₁₅₀	351	-5.43±0.51	4.41
9	P-407>CMC(0.02%w/w)	t ₀	133	*	*
		t ₁₅₀	341	-7.52±0.37	5.68

Particle size, SEM micrographs, contact angle, drug content and residual solvent of recrystallized particles are given in Table 4.9. $Dv_{10\%}$, $dv_{50\%}$ and $dv_{90\%}$ for the dried powders produced are also presented in Figure 4.6. The corresponding particle size distributions are graphically presented in Appendix III. When compared to the original or the recrystallized powder without additives (Figure 4.6), a remarkable effect of reduction of particle size ($dv_{50\%}$ and $dv_{90\%}$) was observed with P-407 at the higher concentration (> CMC). SEM images confirmed that the CRS 74 microcrystals crystals were clearly homogeneously distributed. Hardly any agglomerated or aggregated particles were found. This result confirmed that the microcrystals, which normally aggregate in order to lower the surface energy, could be stabilized sterically against crystal growth by a layer of protective polymer.

The higher concentration of P-407 also modified the surface properties of the recrystallized powder (see Table 4.9). Contact angle of the powder with water was reduced from $133.5 \pm 1.8^\circ$ (without additive) to $85.3 \pm 0.8^\circ$ (P-407 0.5 %w/w).

Table 4.9 also shows a drug content of 96 % for the recrystallized sample with the higher concentration of P-407. This results shows that all additive was probably not removed by washing. The remarkable effect on the contact angle can confirm this finding the additive probably remained attached to the hydrophobic drug particle surface lowering the interfacial tension.

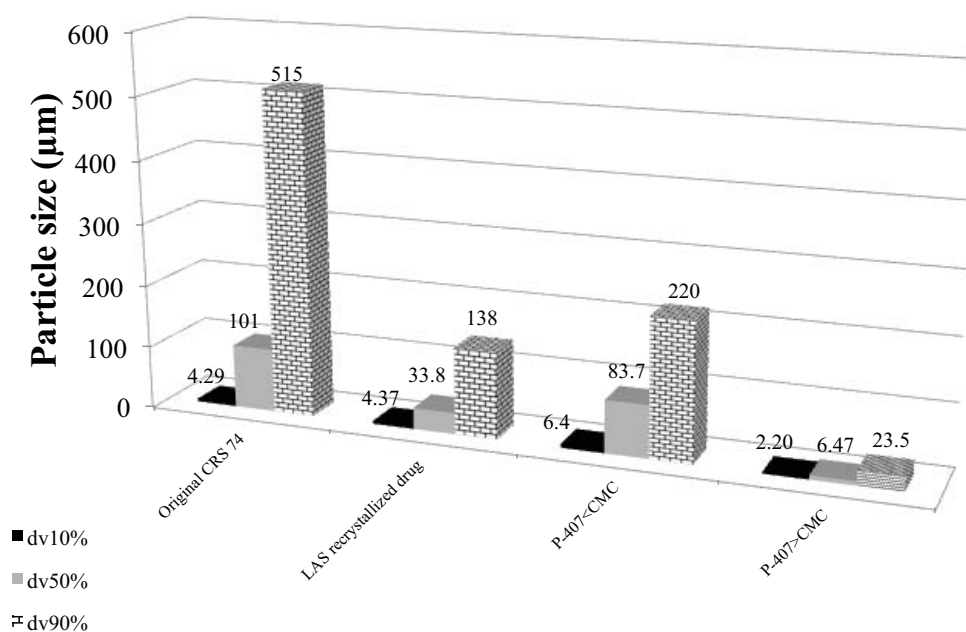


Figure 4.6. Particle size of the drug powders synthesized in presence of P-407 in the organic phase.

Figure 4.7 shows the XRD patterns for the powder samples obtained in presence of P-407. It can be noted that the crystalline phases were preserved after recrystallization in presence of this additive.

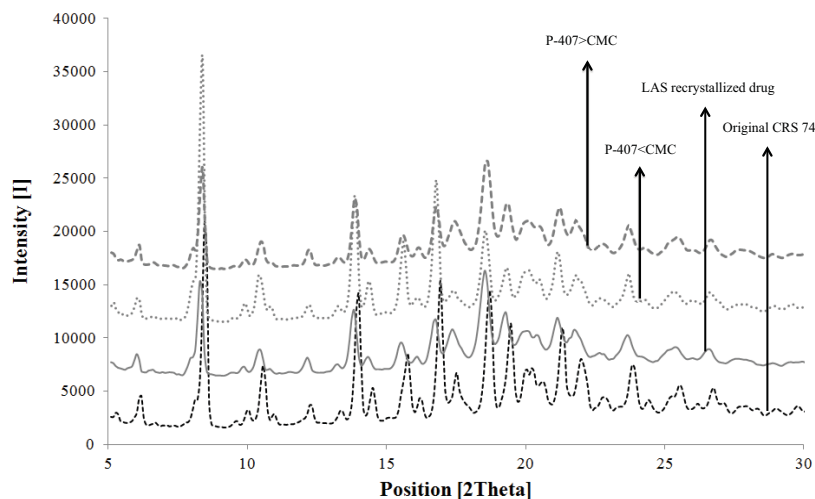


Figure 4.7. X-Ray diffractograms of the drug powders synthesized in presence of P-407 in the organic phase.

Effect of Additives in LAS crystallization

Table 4.9. Identification and characterization of dried powder regarding solid state properties

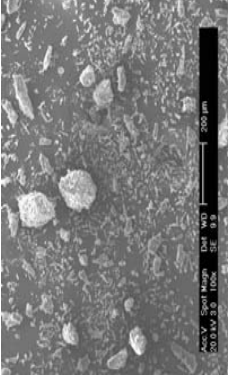
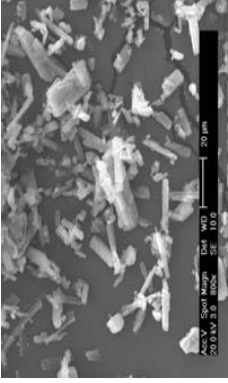
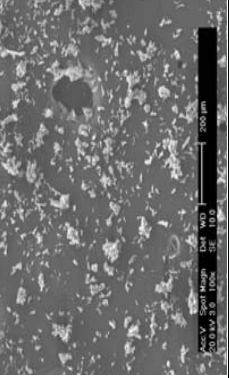
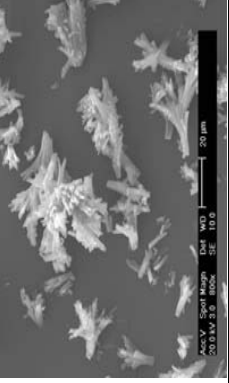
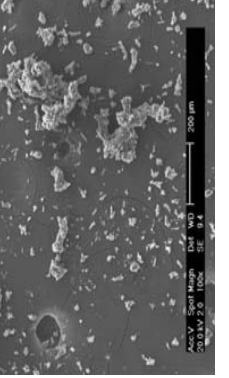
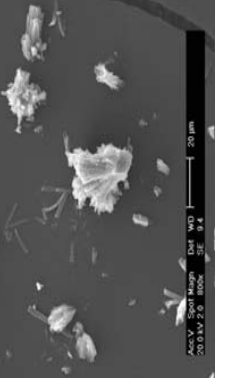
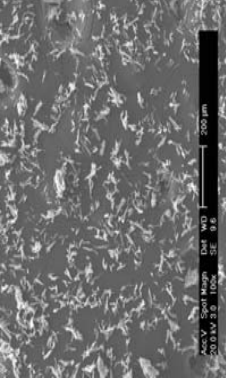
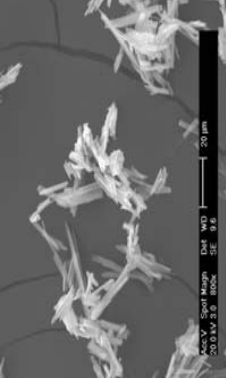
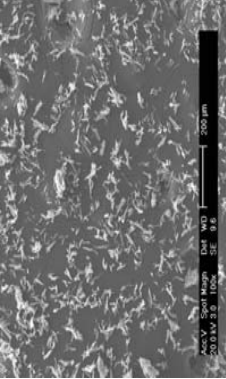
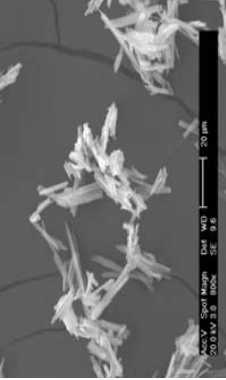
Exp.	Additive	Contact Angle (°)	Size distribution (µm)	SEM images 200µm	SEM images 20µm	Purity (%w/w)	Residual solvent (%)
Original CRS 74	X	136.4±0.85	D[10] : 4.29 D[50] : 101 D[90] : 515 D[4.3] : 191 Span : 5.06			98.90	0.37
1	X	133.5±1.77	D[10] : 4.37 D[50] : 33.8 D[90] : 138 D[4.3] : 77.7 Span : 3.94			97.00	0.60
8	P-407<CMC (0.0003% w/w)	133.1±3.04	D[10] : 6.40 D[50] : 83.7 D[90] : 220 D[4.3] : 101 Span : 2.55			100.45	0.75

Table 4.9. Continued

Exp.	Additive	Contact Angle (°)	Size distribution (μm)	SEM images  200 μm	SEM images  20 μm	Purity (%w/w)	Residual solvent (%)
9	P-407>CMC (0.02% w/w)	85.3 \pm 0.77	D[10] : 2.20 D[50] : 6.47 D[90] : 23.5 D[4.3] : 11.2 Span : 3.29			96.13	0.58

4.3.2. Effect of the presence of the additive in both, aqueous and organic phases

Additives can be placed either in solvent or anti-solvent. The strength of adsorption of additive molecules on the drug surface depends on the nature of the additive and drug surface (THORAT and DALVI 2012). Additives are being introduced in the LAS crystallization of CRS 74 molecule, firstly, to inhibit particle growth and, subsequently, particle agglomeration. Factors controlling the amount of additive adsorbed on the CRS 74 will probably be related to the solubility of the additive in liquid phase, to the strength of additive-liquid phase interactions and to the strength of additive-drug particle interaction. The later can be complex function of parameters such as functional groups and surface energy as suggested by CHOI et al (2005).

Stabilizing agents such as polymer and surfactant can be combined together to enhance the stabilization through synergistic effect (THORAT and DALVI 2012). In such cases the overall stabilization depends on the pair of the stabilizers used. For instance, synergistic effect have been reported in previous works combining ionic and non-ionic stabilizer (WU et al., 2011) or neutral polymers (HPMC) with anionic surfactant (SDS) (DALVI and DAVE, 2009).

Effect of additives on the CRS 74 particles size were analysed by measuring the drug particles immediately after LAS crystallization. The same experimental sampling already described in previous sections was followed. It was found that the particles at 0 s were discrete with a size of approximate two hundred nanometers with SDS, however two times bigger with Chitosan (Table 4.10). These particles were also examined 150 s after LAS crystallization and found to be 2 times bigger but always in nanometric range of size. At the end of the process, after drying, they were examined and found to be several microns as given in Table 4.10 and graphically represented in Figure 4.8. Surprisingly, the dry particles produced in presence of Chitosan were not bigger than the other ones. Maybe, Chitosan was less effective than SDS in arresting the particle growth, but not less effective to prevent aggregation (high absolute zeta potential given in Table 4.10).

Table 4.11 also shows that the association of additives in both aqueous and organic phases had a positive effect, reducing the contact angle of the drug powder with water to $94.1^{\circ} \pm 4.3$ with P-407/Chitosan and to $74.7^{\circ} \pm 5$ with P-407/SDS, in comparison to the original

drug (136.4 ± 0.8). The powders were characterized by purity higher than 98.8% and residual solvent content ranged from 0.6% to 1.5% (see Table 4.11).

Table 4.10. Initial particle size average (APS) of CRS 74 crystals in suspension in presence of additives in both, aqueous and organic phases.

Experiment	Additive	Time (s)	APS (nm)	Zeta potential (mV)	pH suspension
1	X	t_0	248	*	*
		t_{150}	417	-2.11 ± 0.28	3.28
10	P407 < CMC (0.0003% w/w) + SDS 0.5% w/w	t_0	150	*	*
		t_{150}	368	-17.53 ± 4.77	4.73
11	P407 > CMC (0.02% w/w) + SDS 0.5% w/w	t_0	234	*	*
		t_{150}	440	-3.96 ± 0.17	4.27
12	P407 < CMC (0.0003% w/w) + Chitosan 0.5% w/w	t_0	457	*	*
		t_{150}	990	$+39.40 \pm 3.24$	4.60
13	P407 > CMC (0.02% w/w + Chitosan 0.5% w/w	t_0	596	*	*
		t_{150}	918	$+16.33 \pm 2.73$	4.64

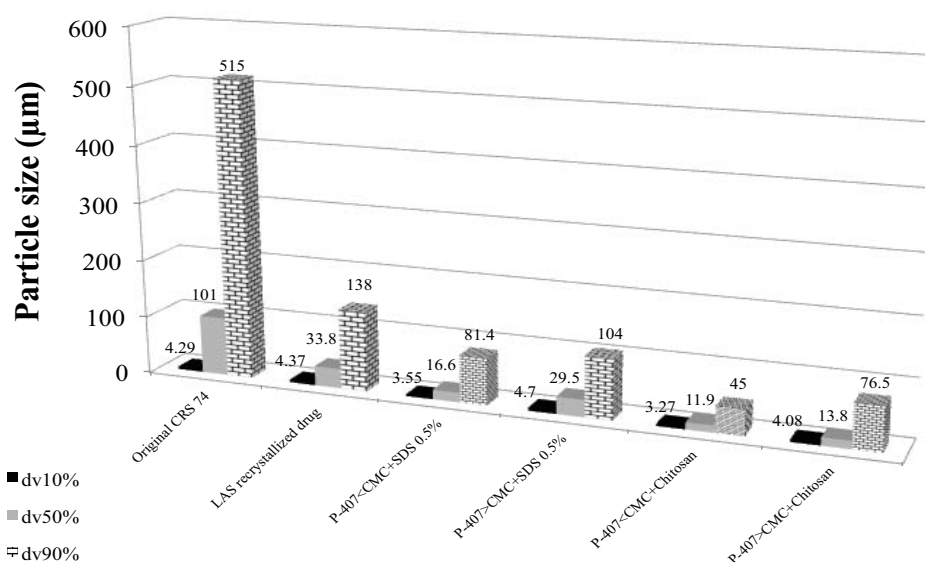
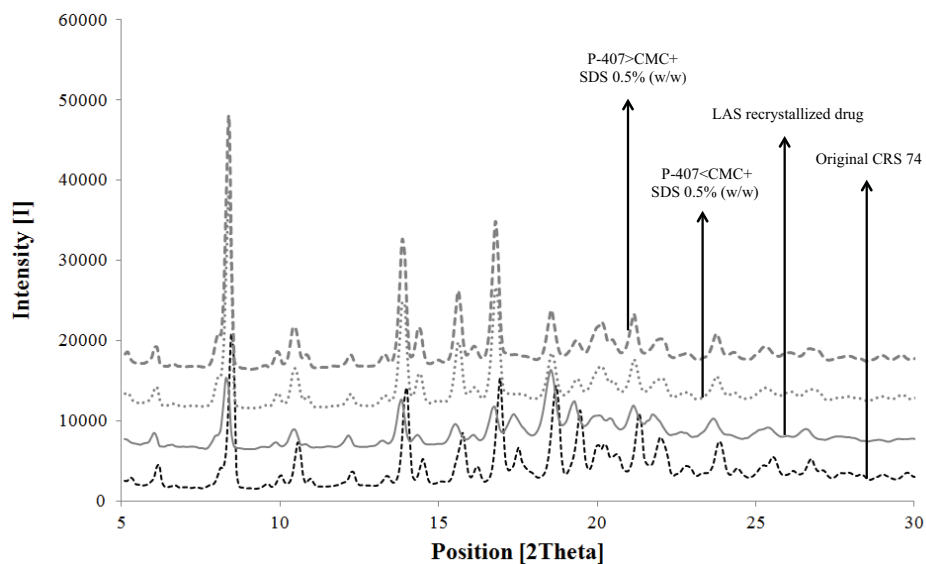
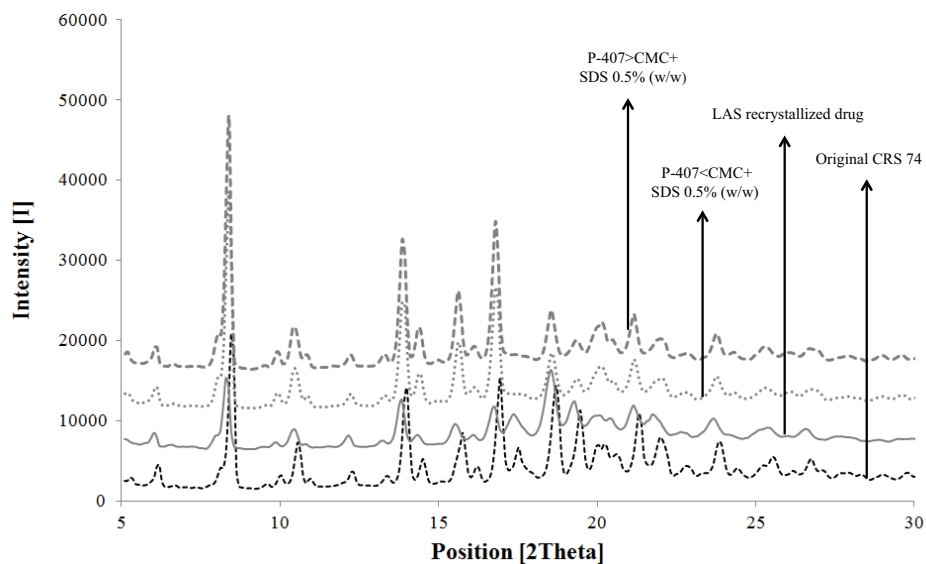


Figure 4.8. Particle size (laser diffraction data) of the drug powders synthesized in presence of additives in both, organic and aqueous phases.

X-ray powder diffraction patterns shown in Figure 4.9 identical to original CRS 74 for crystals generated using P-407/Chitosan and P-407/SDS suggested that these additive are not within the crystal lattice but only adsorbed on the surface.



(a)

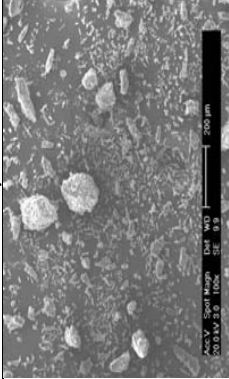
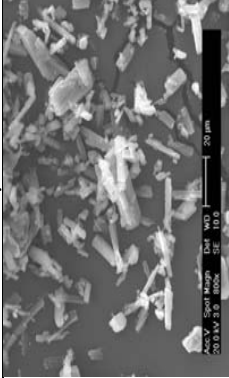
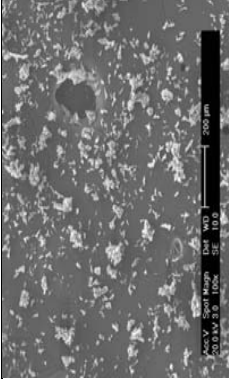
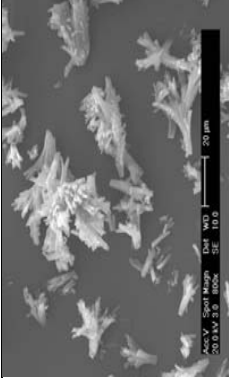
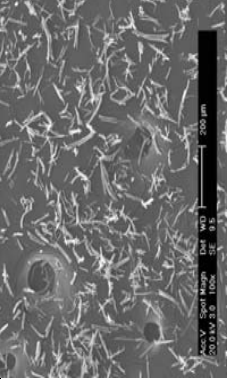
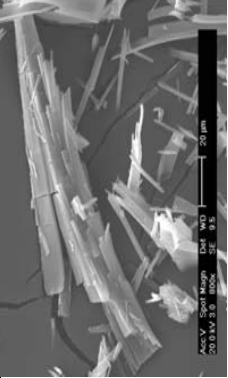
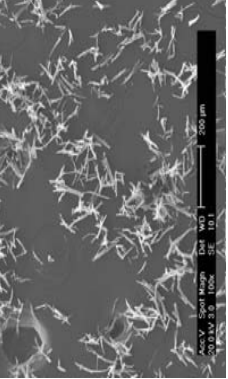
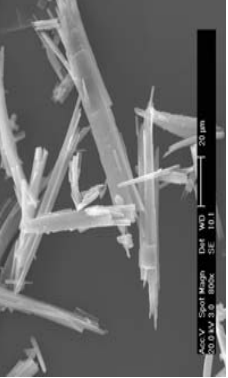


(b)

Figure 4.9. X-Ray diffractograms of drug powders produced with additives in organic phase: a) P-407/SDS; b) P-407/Chitosan.

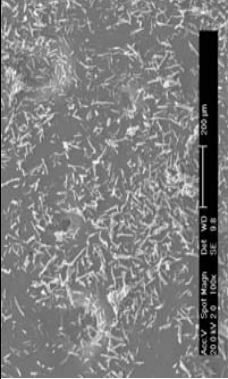
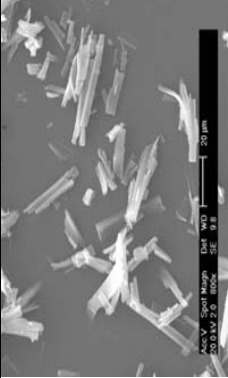
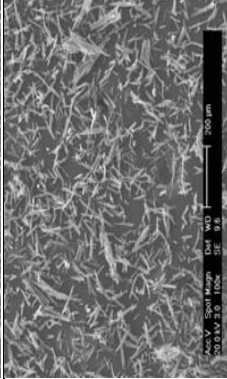
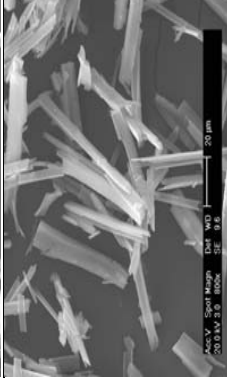
CHAPTER 4

Table 4.11. Identification and characterization of dried powder regarding solid state properties

Exp.	Additive	Contact Angle (°)	Size distribution (µm)	SEM images		Purity (%w/w)	Residual solvent (%)
				200µm	20µm		
Original CRS 74	X	136.4±0.85	D[10] : 4.29 D[50] : 101 D[90] : 515 D[4.3] : 191 Span : 5.06			98.90	0.37
1	X	133.5±1.77	D[10] : 4.37 D[50] : 33.8 D[90] : 138 D[4.3] : 77.7 Span : 3.94			97.00	0.60
10	P-407<CMC (0.0003% w/w)+ SDS 0.5% w/w	107.9±1.20	D[10] : 3.55 D[50] : 16.6 D[90] : 81.4 D[4.3] : 32.8 Span : 4.67			99.87	0.60
11	P-407>CMC (0.02%w/w) + SDS 0.5% w/w	74.7±5.52	D[10] : 4.70 D[50] : 29.5 D[90] : 104 D[4.3] : 43.5 Span : 3.35			99.56	0.94

Effect of Additives in LAS crystallization

Table 4.11. Continued

Exp.	Additive	Contact Angle (°)	Size distribution (µm)	SEMimages 200µm	SEMimages 20µm	Purity (%w/w)	Residual solvent (%)
12	P-407<CMC (0.0003% w/w)+ Chitosan 0.5% w/w	141.8±2.97	D[10] : 3.27 D[50] : 11.9 D[90] : 45.0 D[4.3] : 18.5 Span : 3.51			98.90	1.52
13	P-407>CMC (0.02%w/w) + Chitosan 0.5% w/w	94.1±4.35	D[10] : 4.08 D[50] : 13.8 D[90] : 76.5 D[4.3] : 29.2 Span : 5.23			98.77	0.97

4.3.3. Drug concentration in the organic phase

As we know, an uniform and extremely high supersaturation is required to produce ultra-fine particles by LAS recrystallization. With the aim to improve control on particle size of the recrystallized powder, some additional experiments were made to investigate the effect of supersaturation on the properties of the drug recrystallized in presence of the pairs of stabilizers, P-407/Chitosan and P-407/SDS. Experiments were conducted with reduced initial drug concentration in the organic phase. The corresponding supersaturation values are given in Table 4.12. No remarkable effect of the supersaturation level was observed on the reduction of the drug particle size, as confirmed by Figure 4.10. The ability to achieve high particle concentrations without compromising the particle size significantly is of great interest for scaling up this process. Furthermore, the utilization of relatively concentrated organic solutions to reduce the amount of organic solvent is also beneficial.

Table 4.12 also shows that drug particles recrystallized in presence of Chitosan were always positively charged. Powders presented high purity and low residual solvent content (Table 4.13).

Table 4.12. Initial average particle size (APS) of the CRS 74 crystals in suspension in presence of different stabilizing systems into internal phase and external phase in different supersaturations.

Experiment	Additive	S	Time (s)	APS (nm)	Zeta potential (mV)	pH suspension
1	X	894.04	t ₀	248	*	*
			t ₁₅₀	417	-2.11±0.28	3.28
14	P-407>CMC(0.02%w/w)	374.51	t ₀	199	*	*
			t ₁₅₀	290	-9.70±0.85	4.97
15	P-407>CMC(0.02%w/w)	156.41	t ₀	140	*	*
			t ₁₅₀	301	*	4.96
16	P-407>CMC(0.02%w/w) + SDS 0.5% w/w	104.50	t ₀	186	*	*
			t ₁₅₀	404	-6.39±0.04	5.27
17	P-407>CMC(0.02%w/w) + SDS0.5% w/w	43.25	t ₀	125	*	*
			t ₁₅₀	348	*	5.46
18	P-407>CMC+ Chitosan 0.5% w/w	*	t ₀	489	*	*
			t ₁₅₀	971	+23.87±1.07	4.64
19	P-407>CMC(0.02%w/w) +Chitosan 0.5% w/w	*	t ₀	453	*	*
			t ₁₅₀	1649	+23.03±4.11	4.76

*Data not determined

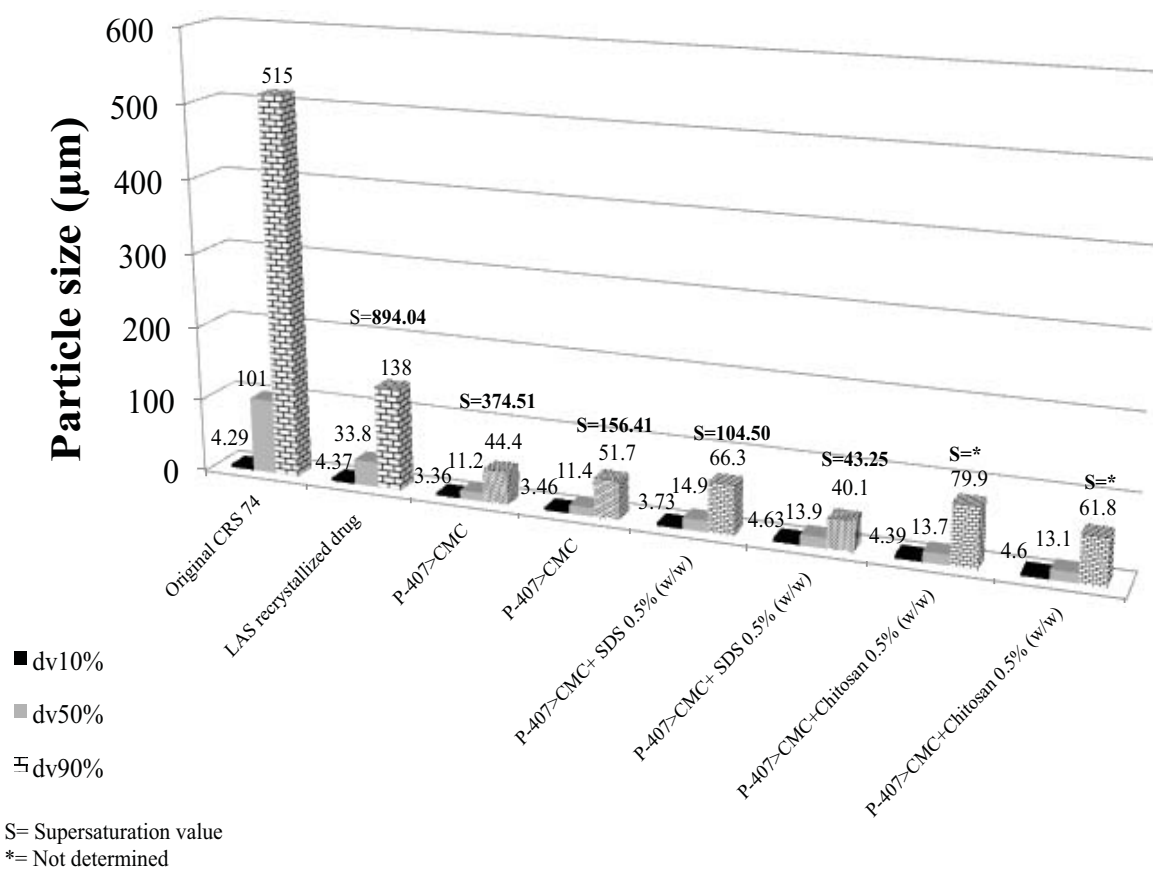
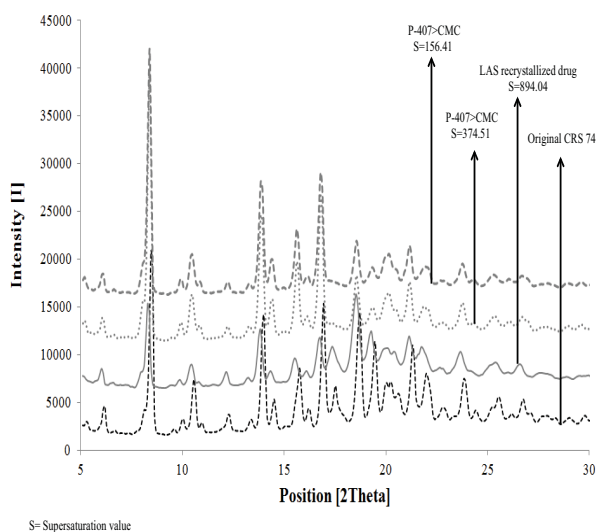
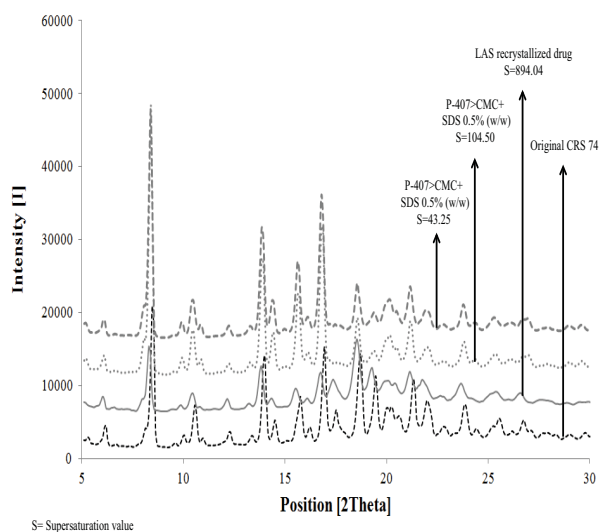


Figure 4.10. Particle size (laser diffraction data) of the drug powders synthesized in presence of additives in organic phase and in both (organic and aqueous) at different supersaturation degrees.

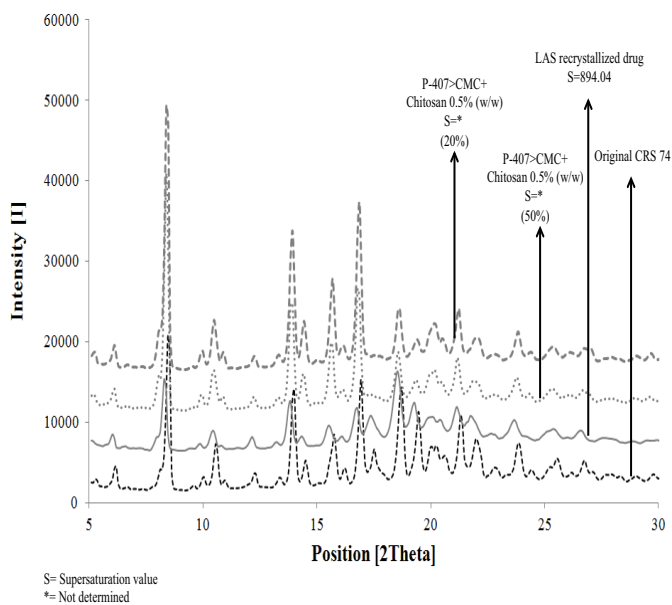
Moreover, no changes on the powder crystallinity were observed as proved by the X-ray diffractograms presented in Figure 4.11.



(a)



(b)

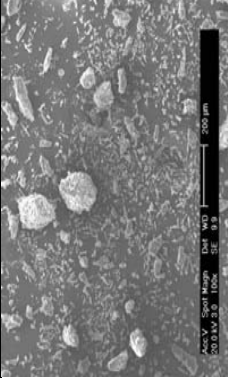
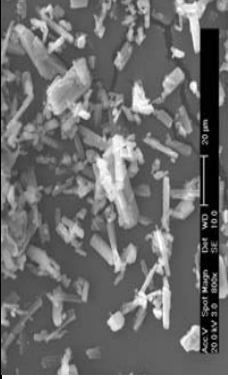
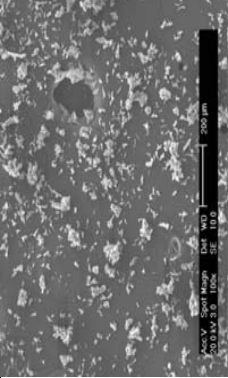
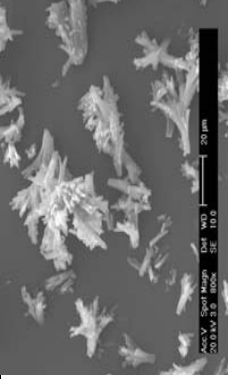
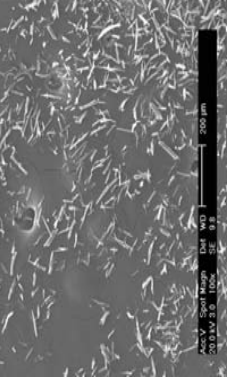
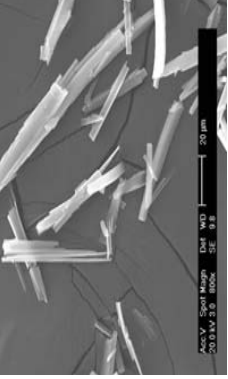
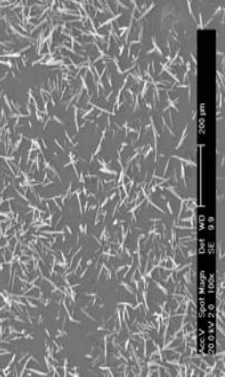
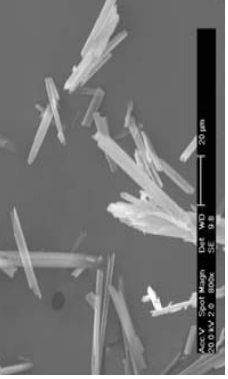


(c)

Figure 4.11. X-Ray diffractograms of the drug powders synthesized in presence of additives in organic phase and in both (organic and aqueous) at different supersaturation degrees: a) P-407; b) P-407/SDS 0.5%; c) P-407/Chitosan.

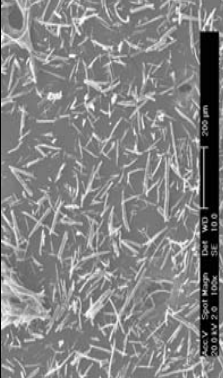
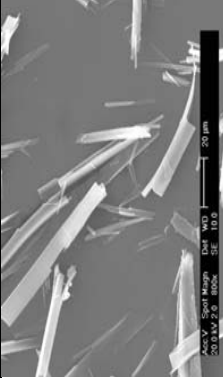
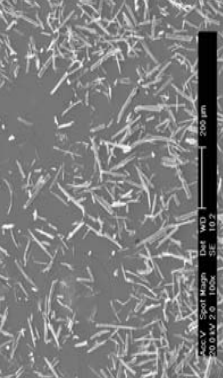
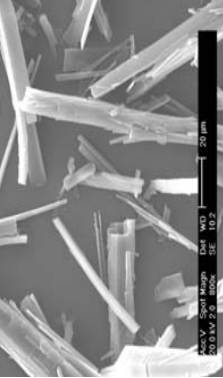
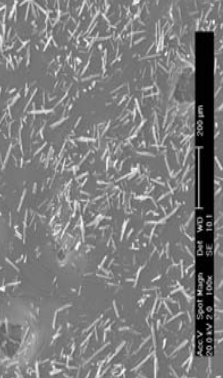
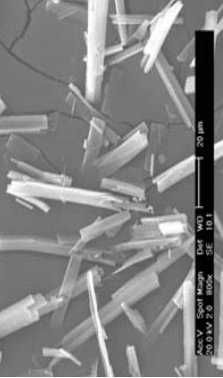
Effect of Additives in LAS crystallization

Table 4.13. Identification and characterization of dried powder regarding solid state properties

Exp.	Additive	S	Size distribution (μm)	SEM images 200 μm	SEM images 20 μm	Purity (%w/w)	Residual solvent (%)
Original CRS 74	X	*	D[10] : 4.29 D[50] : 101 D[90] : 515 D[4.3] : 191 Span : 5.06			98.90	0.37
1	X	894.04	D[10] : 4.37 D[50] : 33.8 D[90] : 138 D[4.3] : 77.7 Span : 3.94			97.00	0.60
14	P407>CMC(0.02%w/w)	374.51	D[10] : 3.36 D[50] : 11.2 D[90] : 44.4 D[4.3] : 19.5 Span : 3.66			102.07	1.00
15	P407>CMC(0.02%w/w)	156.41	D[10] : 3.46 D[50] : 11.4 D[90] : 51.7 D[4.3] : 20.8 Span : 4.23			100.82	*

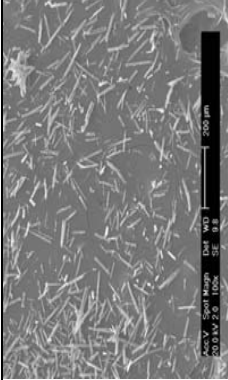
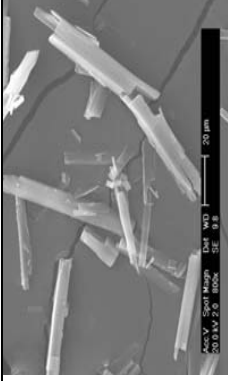
CHAPTER 4

Table 4.13. Continued

Exp.	Additive	S	Size distribution (μm)	SEM images 200 μm	SEM images 20 μm	Purity (%w/w)	Residual solvent (%)
16	P407>CMC(0.02%w/w)+ SDS 0.5% w/w	104.50	D[10] : 3.73 D[50] : 14.9 D[90] : 66.3 D[4.3] : 26.0 Span : 4.20			101.54	0.96
17	P407>CMC(0.02%w/w)+ SDS 0.5% w/w	43.25	D[10] : 4.63 D[50] : 13.9 D[90] : 40.1 D[4.3] : 18.5 Span : 2.55			102.17	*
18	P407>CMC(0.02%w/w)+ Chitosan 0.5% w/w	*	D[10] : 4.39 D[50] : 13.7 D[90] : 79.9 D[4.3] : 30.3 Span : 5.50			100.07	0.78

Effect of Additives in LAS crystallization

Table 4.13. Continued

Exp.	Additive	S	Size distribution (μm)	SEM images 200 μm	SEM images 20 μm	Purity (%w/w)	Residual solvent (%)
19	P407>CMC(0.02%w/w)+ Chitosan 0.5% w/w	*	D[10] : 4.60 D[50] : 13.1 D[90] : 61.8 D[4.3] : 23.9 Span : 4.36			101.89	*

*Data not determined

4.3.4. Reorganized organic phase

In the second part of the additive screening study, P-407 was incorporated into the organic phase (ethanol + drug + P-407). Two concentrations were studied: 0.0003%w/w (<CMC) and 0.02%w/w (> CMC), before the incorporation of the drug.

The results obtained already discussed in the previous section, showed that the higher concentration (> CMC) could prevent crystal growth and agglomeration, and modify the surface properties of the recrystallized powder. Contact angle of the powder with water was reduced from $133.5 \pm 1.8^\circ$ (without additive) to $85.3 \pm 0.8^\circ$ (P-407 0.5%w/w). These results were attributed to the probable attachment of the additive to the hydrophobic drug particle surface lowering the interfacial tension. However, CRS 74 crystals obtained are always micron-sized.

Due to the molecular characteristics of CRS 74, we hypothesized the possibility of a molecular pre-organization of this drug in organic solution favoring uncontrolled growth of crystals after nuclei formation. This hypothesis is investigated in this section.

In fact, a large number of drug molecules are amphiphilic, and self-associate in aqueous solution to form small aggregates. The self-assembly and self-organization are natural and spontaneous processes, occurring mainly through non-covalent interactions such as Van der Waals, hydrogen-bonding, hydrophilic/hydrophobic, electrostatic, donor and acceptor, and metal-ligand coordination networks (WHITESIDES and GRZYBOWSKI, 2002).

Many molecules are amphiphilic, such as phenothiazines, tranquilizers, analgesics, peptides, antibiotics, tricyclic antidepressants, and self-associate in surfactant like-manner in aqueous environment, above a critical concentration value (ATTWOOD and FLORENCE, 1983). It is known that the amphiphilic drug molecules in water form aggregates (MOHD et al., 2010), but it is described in the literature that the amphiphilic aggregates can be formed on nano- or micron-sized in selective solvents, like ethanol (LEE et al., 2008).

Some amphiphilic drugs are well studied in the literature, among them Promethazine hydrochloride (PMT) and Imipramine chloride (IMP), both being used in clinics as antidepressant and antipsychotic drugs. These amphiphilic compounds possess a hydrophobic

nitrogen-containing heterocyclic bound to a short chain carrying a charged amino group (ALAM et al., 2008), as shown in Figure 4.12.

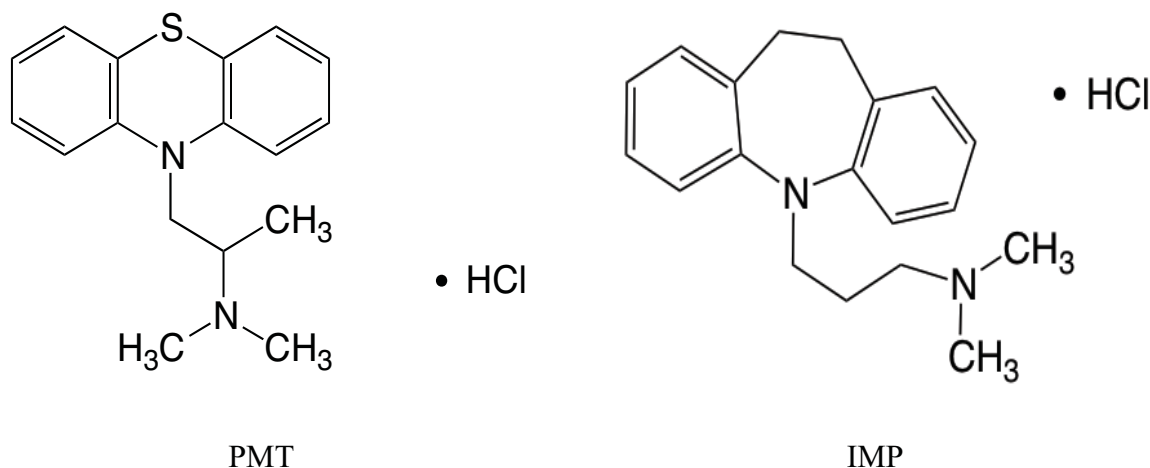


Figure 4.12 Molecular Structure of Promethazine hydrochloride (PMT) and Imprimine hydrochloride (IMP). (ALAM et al., 2008).

Regarding the studied molecule CRS 74 (see Figure 4.13), it has the same chemical function responsible for the drug self-organization in the referred molecules. It possesses a hydrophobic nitrogen-containing heterocyclic bound to a short chain carrying a charged amino group, as discussed before for the PMT and IMP. It means that this molecule could have the same capacity to self-associate in solution above a critical concentration value.

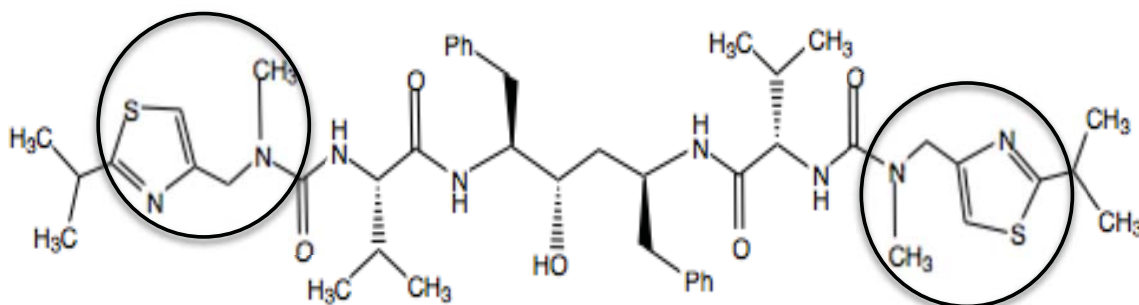


Figure 4.13. Chemical structure of CRS 74.

Some experiments were then carried out in our study to verify the effect of drug concentration in ethanol solution, by dynamic light scattering (PCS) measurements. This methodology has proved to be a useful tool in characterizing colloidal systems (MOHD et al., 2010). The study was realized in order to verify the appearance of micelles depending on the concentration of drug in solution. Figure 4.14 confirms the appearance of drug micelles (1.6 – 1.8 nm) in ethanol at drug concentrations above 0.001 mol/L.

A micellar organization in solution could be the starting point of all LAS crystallization studies conducted up to here, as schematically represented on Figure 4.15. From a pre-aggregated molecular organization, it could be difficult to stop growth after nucleation, which could maybe explain the strong difficulty to stop drug nuclei growth within a nanosize range, even in presence of different additives.

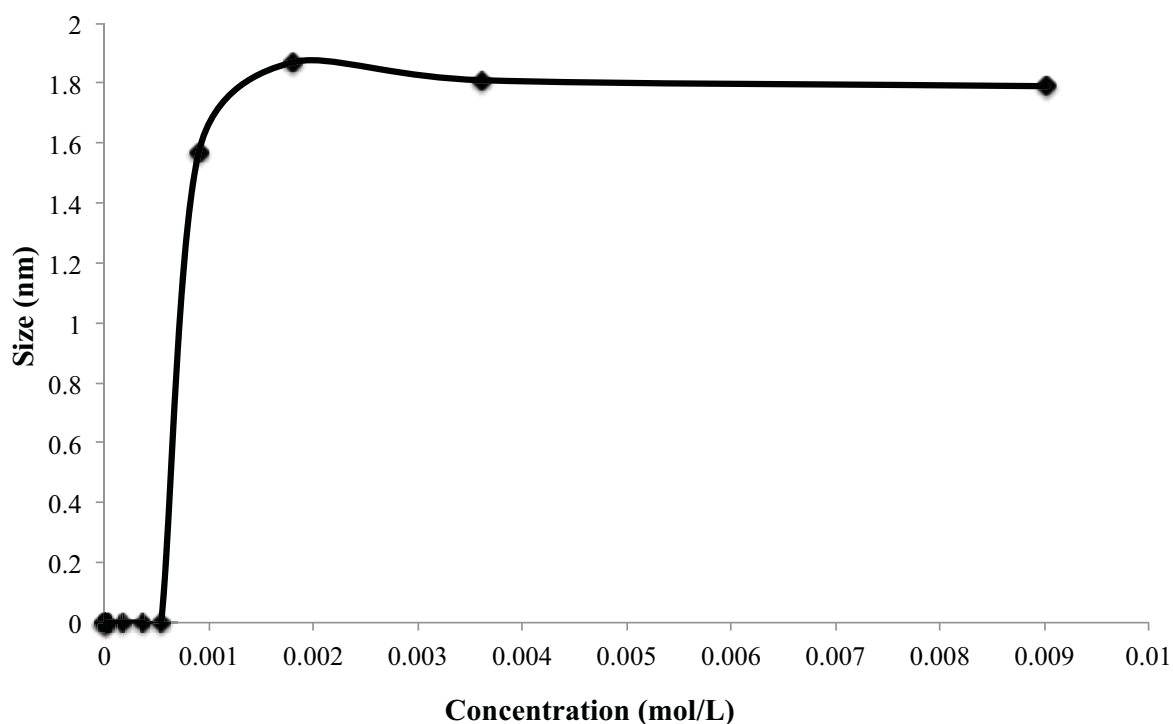


Figure 4.14. Diameter of drug micelles in ethanol as a function of drug concentration (PCS measurements).

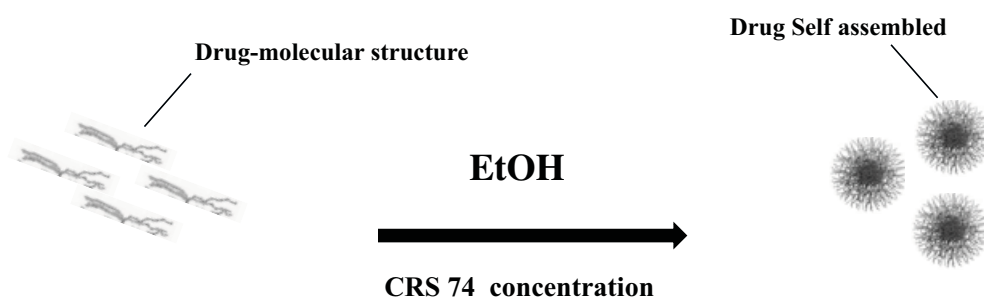


Figure 4.15. Illustration of the effect of increasing concentration of drug in ethanolic media leading to a micellar organization.

Keeping in mind the above hypothesis, complexes molecular aggregates of CRS 74 in organic solution can hinder the crystal size control during LAS crystallization. In order to perturb this molecular organization, some new experiments were carried out. The aim was to introduce the additive P-407 in the organic phase in a dilute system, in order to promote interaction between the additive and the CRS 74 molecule in concentrations below the drug critical micelle organization (0.001 mol/L), as represented on Figure 4.16.

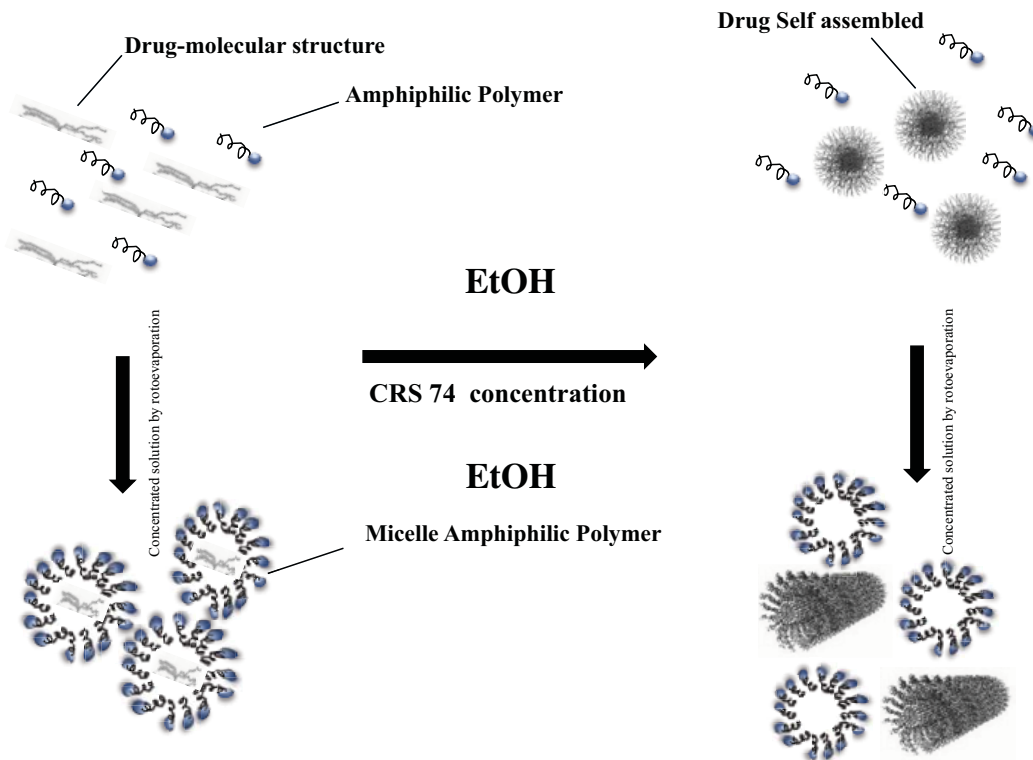


Figure 4.16. Possible schematic representation of drug self-assembled at molecular level in ethanolic solution.

The additive was added to ethanol in a concentration below its CMC (0.0002% w/w). In the following, the drug was added in a concentration below its critical micellar concentration (0.00036 mol/L) to prevent drug self-assembly. The organic phase was then concentrated by rotary evaporation under reduced pressure to a final more concentrated drug solution. Table 4.14 summarizes the results of experiments conducted under the described conditions. A combined effect of Chitosan was also investigated as shown in the same table. Table 4.15 shows SEM images drug and water contents of the powders obtained. Due to low supersaturation, the yield of production was too low and the amount of drug powder obtained was insufficient for further analysis (dry particle size, surface properties, XRD and DSC analysis).

Compared to the previous experiments for which the drug was in contact with the additive in concentrations above its critical micelle concentration, no positive effect in particle size control within the first 150s during LAS crystallization was noted.

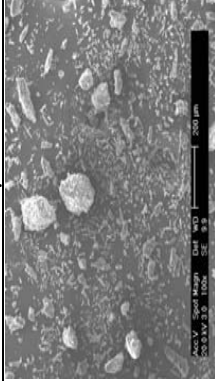
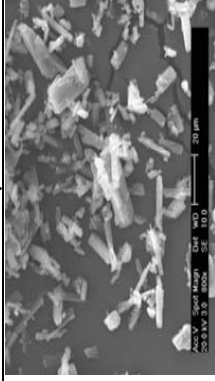
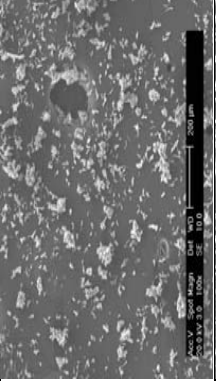
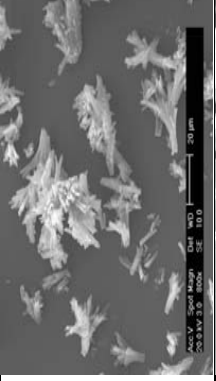
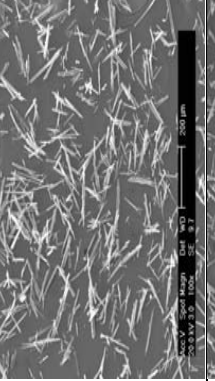
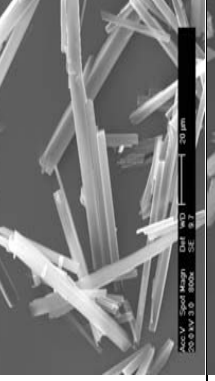
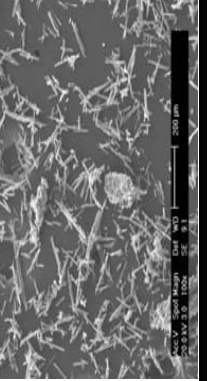
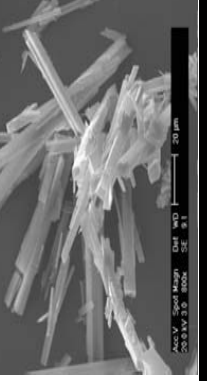
Table 4.14. Initial average particle size (APS) of CRS 74 nanocrystals during LAS crystallization, in presence of P-407 in organic phase, which was concentrated by rotary evaporation.

Experiment	Additive	<i>S</i>	Time (s)	APS (nm)	Zeta potential (mV)	pH suspension
1	X	894.0	t_0	248	*	*
		4	t_{150}	417	-2.11± 0.28	3.28
19	P-407<CMC (0.0003%w/w)	77.59	t_0	203	*	*
		*	t_{150}	319	*	4.87
20	P407<CMC(0.0003% w/w)+Chitosan 0.5% (w/w)	*	t_0	687		*
		*	t_{150}	1237	+19.93±0.25	4.64

*Data not determined; * Supersaturation calculated after ethanol evaporation

Effect of Additives in LAS crystallization

Table 4.15. Identification and characterization of dried powder regarding solid state properties

Exp.	Additive	S	Size distribution (μm)	SEM images 200 μm	SEM images 20 μm	Purity (%w/w)	Residual solvent (%)
Original CRS 74	X	*	D[10] : 4.29 D[50] : 101 D[90] : 515 D[4.3] : 191 Span : 5.06			98.90	0.37
1	X	894.04	D[10] : 4.37 D[50] : 33.8 D[90] : 138 D[4.3] : 77.7 Span : 3.94			97.00	0.60
19	P407<CMC(0.0003%w/w)	77.59	*			100.34	*
20	P407<CMC(0.0003%w/w)+ Chitosan 0.5% w/w	*	*			101.27	*

*Data not determined

4.3.5. Improving process production

Most of LAS recrystallizations realized up to here in order to investigate the influence of several processes or formulation parameters on the properties of the recrystallized drug powder were conducted during a short period of time of approximately 2- 6 min. Experiments in absence of additives, as described in Chapter 3, proved to be quite laborious due to the rapid growth of the produced particles and problems of blockage of the mixer, which precluded the realization of essays over time. This is not interesting for the industrial proceeding.

It seemed that these problems were caused by the affinity of the drug molecule with the material which constitutes the surface of the rapid mixer. Furthermore, the nano-sized drug crystals, freshly formed, have a high-energy surface; this property can increase the high affinity for CRS 74 surface material adsorption reported in Chapter 3.

To solve this blockage problem and to make the LAS crystallization process industrially viable, some studied systems were selected (Table 4.16). The criteria of choice was the surface properties of recrystallized drugs: low contact angle values ($\theta \approx 90^\circ$), that means a decrease in surface hydrophobicity, and probably, a decrease in affinity of the molecule with the material which constitutes the hydrophobic surface of the mixer (stainless steel).

Table 4.16. Stabilizing agents studied to solve the T-mixer blockage problem

Experiment	Additive	θ (°)
9	P-407>CMC	85.3
11	P-407>CMC+SDS 0.5% (w/w)	74.7
13	P-407>CMC+Chitosan 0.5% (w/w)	94.1

As shown in Table 4.16, all the stabilizing systems presented a significant reduction of contact angle value compared to recrystallized drug in absence of additives (136°). However, the better drug surface characteristics were not enough to prevent the affinity of the molecule with the surface material for Experiments 9 and 11 (see Table 4.17). On the contrary, drug particles highly negatively charged by SDS 0.5% showed a strong affinity to T-mixer material walls (blockage of the mixer operation after 2 min). On the other hand, the combined effect of

P-407 placed in the organic phase and Chitosan in the aqueous phase could solve this problem, ensuring a continuous process of production through the T-mixer.

Table 4.17. Initial particle size average (APS) of the nanosuspensions and characteristics of CRS 74 nanocrystals in suspension.

Experiment	Additive	APS (nm)	Zeta potential (mV)	pH suspension	Blockage time (min)
9	P-407>CMC	169.5	-3,94±0.37	4.51	6
11	P-407>CMC+SDS 0.5% (w/w)	225.3	-5,26±0.35	4.78	2
13	P-407>CMC+Chitosan 0.5% (w/w)	706.6	+23,80±2.12	4.65	No blockage

To explain this finding, it was necessary to consider the characteristics of the T-mixer material, i.e. stainless steel. Some materials can be ionized on specific pH; among them, as reported in the literature, stainless steels can present different surface charge properties as a function of pH. The material surface is positively charged over the pH range of 2.5 to 5.0 (TAKEHARA and FUKUZAKI, 2002). Because of this, the surface charge of stainless steel is believed to act as adsorption sites for negatively charged CRS 74, as schematically represented in Figure 4.17.

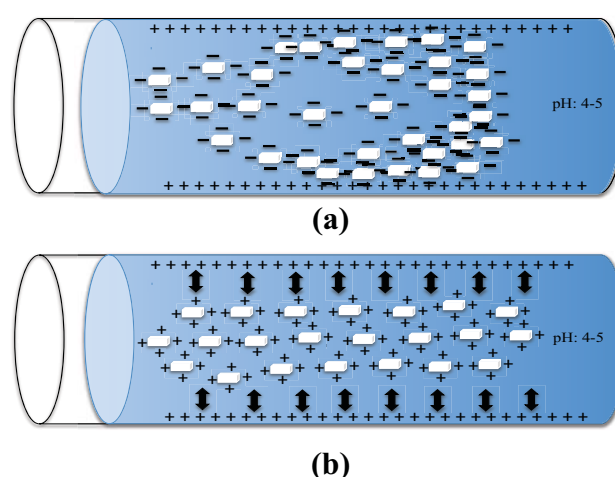


Figure 4.17. The charge interaction between the negatively (a) and positively (b) charged CRS 74 nanocrystals and the negatively surface charged stainless steel (pH in the range 3-5).

In conclusion, the combination of P-407 (organic phase) and Chitosan (aqueous phase) represented a key solution to a continuous production of recrystallized CRS 74 through stainless steel rapid mixers.

4.3.6. Dissolution behaviour of recrystallized powders in presence of additives

In previous sections, it was observed changes on some powders properties, like: wettability, powder agglomeration state and size reduction. These properties will probably have a direct impact on dissolution profile, which will be verified in this section.

In order to evaluate the impact of powders on dissolution kinetics, the powders for this section were selected according the lower agglomeration state and/or low contact angle value. The dissolution of each sample was determined under sink conditions, as discussed in Chapter 2.

Additives can change the drug solubility In the dissolution medium. To ensure sink conditions (maximum drug concentration $\ll C_{eq}$), the solubility of the recrystallized samples in presence of the different additives was firstly measured in 0.1M HCl at 37°C. The same experimental procedure described in Chapter 2, was used. The results are given in Table 4.18 and represented graphically in Figure 4.18. It can be concluded that the probably association of additives to the drug in some cases did not change the drug solubility in the dissolution medium, or very little ($C_{eq} < 0.2 \text{ mg/g}_{\text{solution}}$ in all cases). To sum up, although additives can increase the solubility of poorly soluble compounds, the amounts adsorbed onto the CRS 74 particles crystallized in the presence of additives in our study are probably too small to affect the solubility of the drug in bulk solution.

To assess the differences between original drug and the generated samples, 0.1M HCl was chosen as a discriminatory dissolution medium (The dissolution method was developed and presented in Chapter 2).

Table 4.18. CRS 74 solubility and synthesized powders solubility in HCl 0.1M at 37°C.

Stabilizing system	Solubility (mg/g _{solution}) ±SD
Original CRS 74	0.102±0.008
No additive (recrystallized CRS 74)	0.134±0.005
P407> CMC (0.02%w/w)	0.117±0.006
HPMC 0.5% w/w	0.144±0.008
Tween>CMC 0.5%w/w	0.091±0.003
SDS 0.5%/P-407< CMC (0.0003%w/w)	0.094±0.003
SDS 0.5% /P-407 > CMC (0.02%w/w)	0.110±0.004
Chitosan 0.5%/ P-407> CMC (0.02%w/w)	0.088±0.004
P-407<CMC (0.0003%w/w) <i>Reorganized</i>	0.161±0.009
Chitosan 0.5% / P-407(0.0003%w/w) <i>Reorganized</i>	0.121±0.006

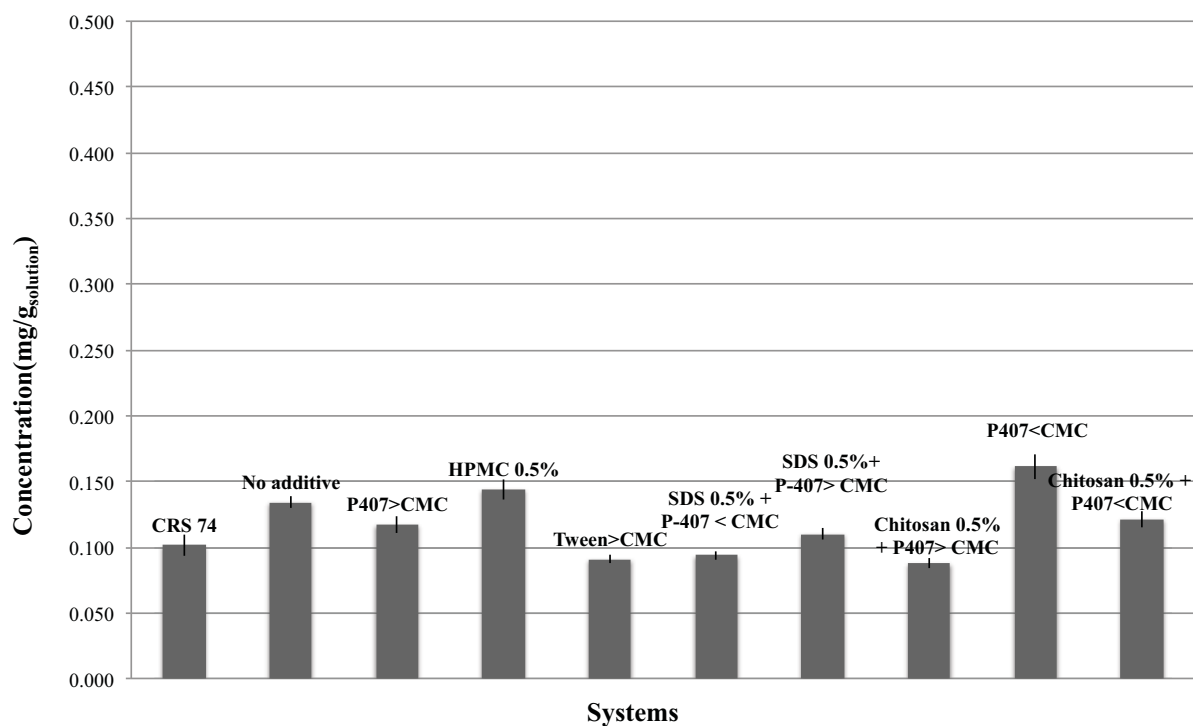


Figure 4.18. Solubility of CRS 74 samples in HCl 0.1M at 37°C (samples recrystallized in presence of different additives; original drug also presented for comparison)

Figure 4.19 shows the dissolution profiles of CRS 74 crystallized in presence of the additives studied in this section. The dissolution profiles of original CRS 74 and the sample crystallized in the absence of additive are also included in this Figure.

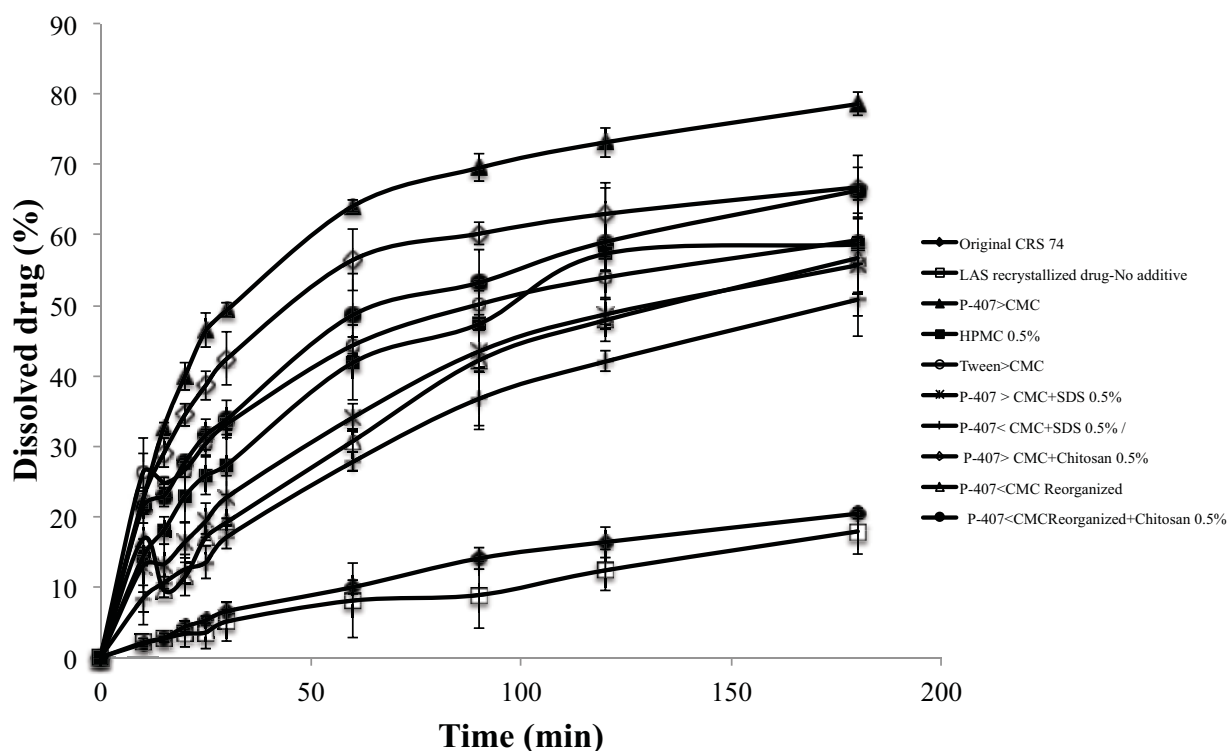


Figure 4.19. Dissolution profiles using 0.1M HCl as discriminatory dissolution medium at 37°C and paddle at 75 rpm. LAS recrystallized drug in presence of additive. Original CRS 74 also included.

The dissolution profiles of recrystallized samples in presence of additives and original CRS 74 were compared by calculating difference factor (f_1) and similarity factor (f_2) for each dissolution profile given in Figure 4.19. Table 4.19 shows the calculated f_1 and f_2 values. f_1 (>0) and f_2 ($50 < f_2 < 85$) values confirmed significant *difference* in dissolution profiles of recrystallized samples in presence of additives compared to the original drug.

The percentage of drug dissolved within the first 20 min. was used to compare dissolution rate of various samples. The values are given in Table 4.20. The data indicates that

there is a marked increase in the dissolution rate of CRS 74 from the recrystallized samples in presence of additive compared to the original drug. The faster dissolution profile led to 80% of drug dissolved in 3 h of against approximate 20% for original drug or even the drug recrystallized without additives.

Table 4.19. Comparison of dissolution profiles through the difference factor (f_1) and the similarity factor (f_2). Original CRS 74 is the reference product for test.

Experiment	Additive	f_1	f_2
Original CRS 74	X	*	*
1	No additive	24.8	98.8
2	HPMC 0.5% w/w	389.92	64.18
6	Tween 20 0.5% w/w	518.62	58.89
9	P-407>CMC	749.52	50.50
10	P-407<CMC+SDS 0.5% w/w	239.86	72.65
11	P-407>CMC+ SDS 0.5% w/w	296.38	69.89
13	P-407>CMC+Chitosan 0.5% w/w	659.33	53.54
19	P-407<CMC <i>Reorganized</i>	130.4	84.49
20	P-407<CMC <i>Reorganized</i> +Chitosan 0.5% w/w	309.13	69.49

Table 4.20. Percentage of drug dissolved within the first 20 min.

Experiment	Additive	Percentage of drug dissolved in 20 min
Original CRS 74	X	4.36 ± 0.75
1	No additive	3.37 ± 1.86
19	P-407<CMC <i>Reorganized</i>	11.45 ± 2.71
10	P-407<CMC+SDS 0.5% w/w	12.53 ± 2.88
11	P P-407>CMC+ SDS 0.5% w/w	16.40 ± 2.01
2	HPMC 0.5% w/w	22.92 ± 3.79
6	Tween 20 0.5% w/w	26.66 ± 1.04
20	P-407<CMC <i>Reorganized</i> +Chitosan 0.5% w/w	27.74 ± 0.64
13	P-407>CMC+Chitosan 0.5% w/w	34.46±1.59
9	P-407>CMC	39.96 ± 1.98

Drug release kinetics

In order to describe the kinetics of the release process of drug from the different samples, two equations were used:

- The first-order equation, which describes the release from systems where dissolution rate is dependent on the concentration of the dissolving species (ISHI, 1996; SERRA, 2007; RATNA et al., 2012):

$$\ln\left(\frac{M_t}{M_0}\right) = kt \quad (4.1)$$

- The Hixson-Crowell cube root law, which describes the release the release from dosage forms which show dissolution rate limitation and which do not dramatically change during the release process. (HIXSON, 1931):

$$1 - \left(1 - \frac{M_t}{M_0}\right)^{1/3} = kt \quad (4.2)$$

The applicability of these two equations was tested for selected dissolution data giving the faster drug release rates. The dissolution data were plotted in accordance with the first-order equation, i.e., the logarithm of the percent remained as a function of time between 10 and 25 min (Figure 4.20) and were also plotted in accordance with the Hixson-Crowell cube root law, i.e., the cube root of the initial concentration minus the cube root of percent remained, as a function of time between 0 and 25 min (Figure 4.21). It is evident from Figures 4.20 and 4.21 that a linear relationship was obtained with r^2 values close to unity as shown in Table 4.21.

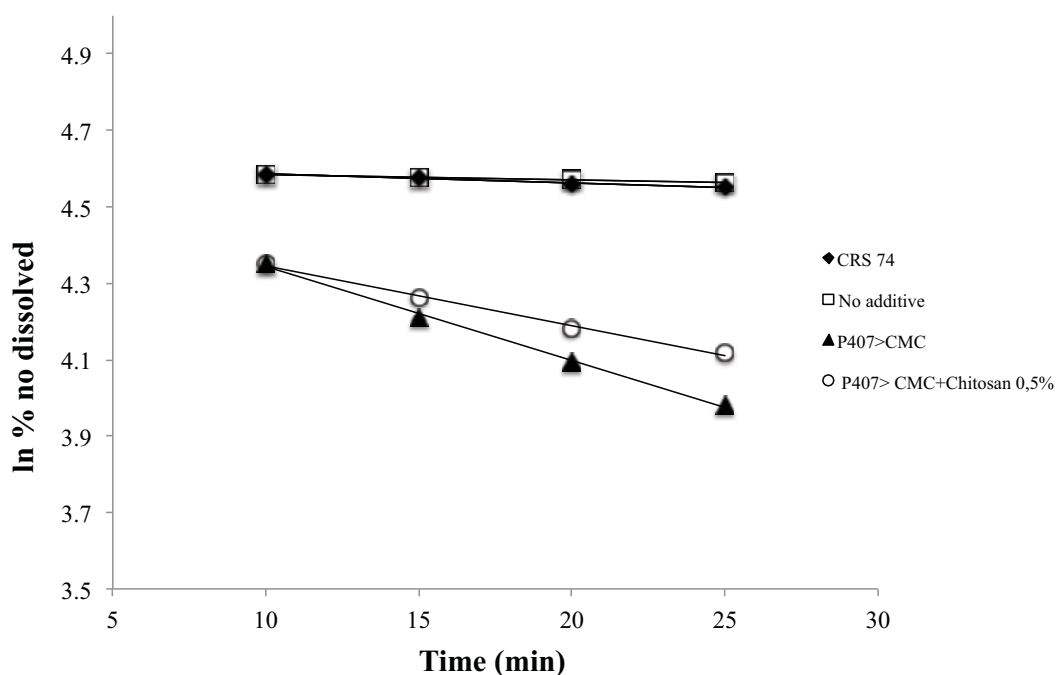


Figure 4.20. A linear plot for the dissolution data of CRS 74 powder samples in accordance with the first-order model equation.

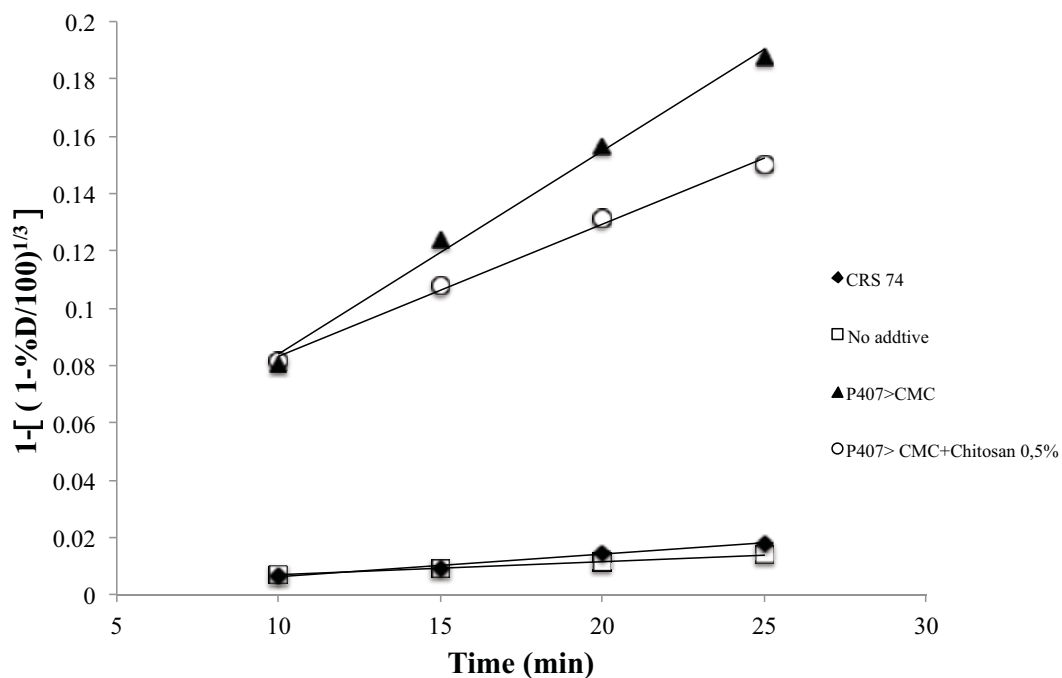


Figure 4.21. A linear plot for the dissolution data of CRS 74 powder samples in accordance with the Hixson-Crowell cube root law.

The first order model describes the release systems for which the dissolution rate is dependent on the concentration of the drug dissolved in the media, whereas the drug surface area remains constant. The Hixson-Crowell model has been used to describe a decrease of the drug particle surface as dissolution occurs. Table 4.21 shows that both mathematical models fitted well the experimental dissolution data probably because during 25 min the decrease of particle surface is very low.

Table 4.21. Release parameters of CRS 74 powder samples recrystallized in presence of additives in comparison to original drug sample.

Exp.	First order			Hixson-Crowell		
	r^2	k (min^{-1})	Linear equation	r^2	k (min^{-1})	Linear equation
CRS 74	0.9846	-0.0024	$y = -0.0024x + 4.6104$	0.9847	0.0008	$y = 0.0008x - 0.0017$
1	0.9973	-0.0014	$y = -0.0014x + 4.598$	0.9974	0.0005	$y = 0.0005x + 0.0024$
9	0.9964	-0.0246	$y = -0.0246x + 4.5899$	0.9939	0.0071	$y = 0.0071x + 0.0131$
13	0.9961	-0.0157	$y = -0.0157x + 4.502$	0.9945	0.0046	$y = 0.0046x + 0.0371$

k = dissolution rate constant

$x = t$ - $e y = \ln$ % No dissolved

** $x = t$ $e y = 1 - [(1 - \% \text{Dissolved}/100)^{1/3}]$

DSC was performed on the recrystallized drug in presence of additive in the organic phase (P-407) and in both organic (P-407) and aqueous phase (Chitosan) in comparison to DSC data for original and recrystallized CRS 74 without additives. The DSC curves of samples are shown in Figure 4.22. From DSC data summarized in Table 4.22, it was concluded that stabilizers did not change the physical state of CRS 74.

Interestingly, CRS 74 recrystallized in presence of P-407 and Chitosan needs less energy for melting when compared to the other samples ($\Delta H_m = 74.8$ J/g), which could be related to a less energy it must overcome to dissolve in according to its faster dissolution rate.

Table 4.22. Melting Temperature ($T_{m(\text{Onset})}$), Heat of Fusion (ΔH_f) for the original and LAS recrystallized drug in presence and absence of additives.

Thermal and dissolution parameters	Original CRS 74	LAS recrystallized CRS 74	LAS recrystallized CRS 74-P-407	LAS recrystallized CRS 74-P-407+Chitosan
$T_{m(\text{Onset})}(\text{°C})$	188.6	187.8	189.0	186.6
$\Delta H_m(\text{J/g})$	86.6	79.2	87.9	74.8
Relative enthalpy(%)	100	91.5	101.5	86.37

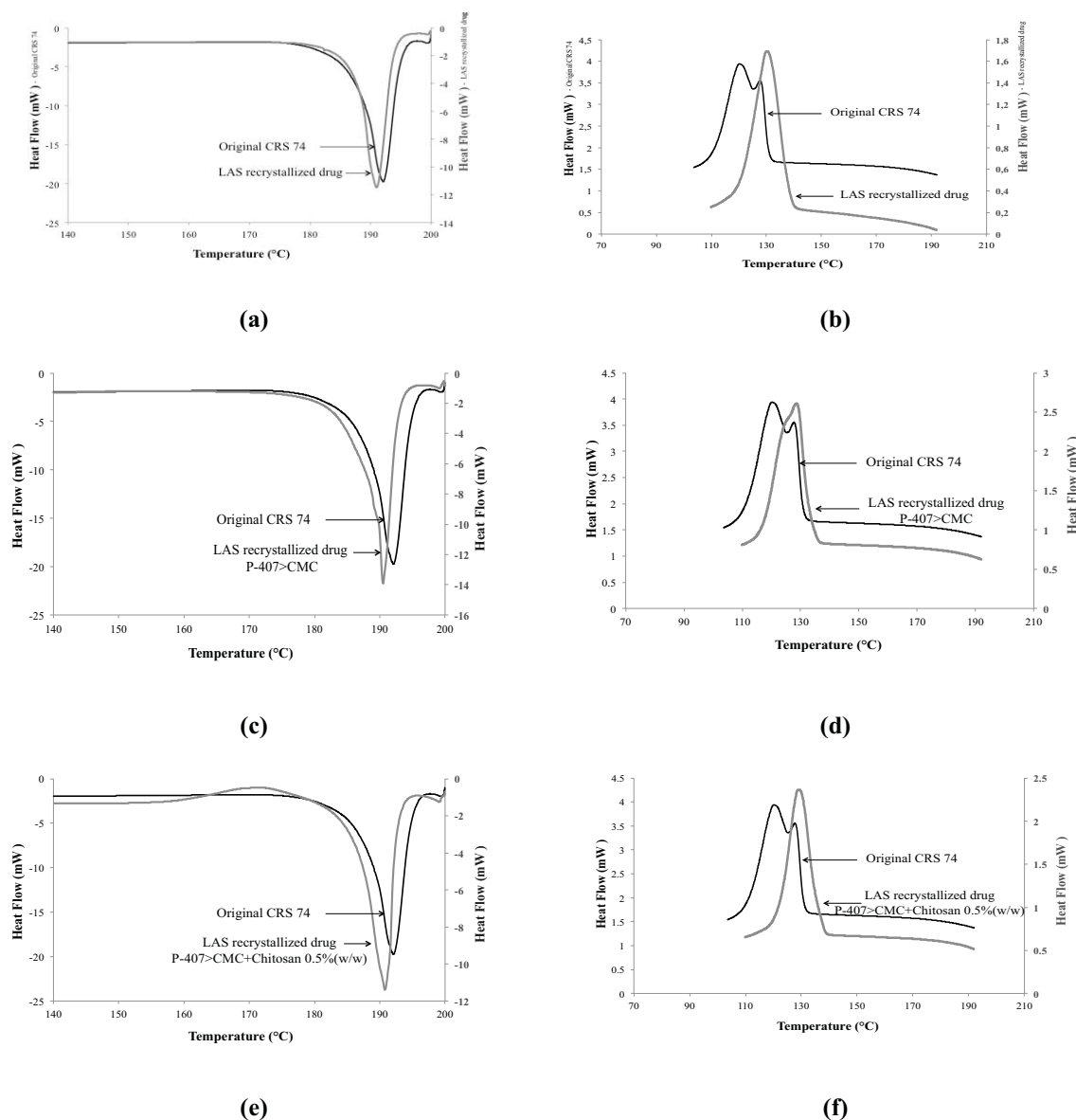


Figure 4.22. **a)** DSC thermograms of original CRS 74 (*first heating*), which consists of a melting endotherm (peak onset temperature $T_{m(\text{Onset})} = 188.64^{\circ}\text{C}$) and LAS recrystallized drug, which consists of a melting endotherm (peak onset temperature $T_{m(\text{Onset})} = 187.79^{\circ}\text{C}$); **b)** DSC thermograms of original CRS 74 (*cooling after first heating*), which consists of a crystallization exotherm (peak onset temperature $T_{c(\text{Onset})} = 132.12^{\circ}\text{C}$) and LAS recrystallized drug, which consists of a crystallization exotherm (peak onset temperature $T_{c(\text{Onset})} = 138.43^{\circ}\text{C}$). **c)** DSC thermograms of original CRS 74 (*first heating*), and LAS recrystallized drug in presence of P-407>CMC, which consists of a melting endotherm (peak onset temperature $T_{m(\text{Onset})} = 189.01^{\circ}\text{C}$); **d)** DSC thermograms of original CRS 74 (*cooling after first heating*), and LAS recrystallized drug in presence of P-407>CMC, which consists of a crystallization exotherm (peak onset temperature $T_{c(\text{Onset})} = 137.61^{\circ}\text{C}$); **e)** DSC thermograms of original CRS 74 (*first heating*) and LAS recrystallized drug in presence of P-407>CMC+Chitosan 0.5% (w/w), which consists of a melting endotherm (peak onset temperature $T_{m(\text{Onset})} = 186.58^{\circ}\text{C}$); **f)** DSC thermograms of original CRS 74 (*cooling after first heating*) and LAS recrystallized drug in presence of P-407>CMC+Chitosan 0.5% (w/w), which consists of a crystallization exotherm (peak onset temperature $T_{c(\text{Onset})} = 136.21^{\circ}\text{C}$).

4.4. CONCLUSION

To improve particle size control during the LAS crystallization process of CRS 74, and they were introduced in the solvent (P-407) or in the anti-solvent (all the other ones) in our CRS 74-ethanol-water system. A maximum concentration was fixed for all additives to give a mass ratio of 1:4 (additive:drug). This corresponds to 0.5%w/w for HPMC, Chitosan, Tween 20 and SDS and 0.02% (w/w) for P-407.

The first results showed that additives enhanced the drug solubility in the ethanol-water mixture, markedly or very little, depending on the additive used. Among them, SDS 0.5% presented the higher capacity to solubilize CRS 74 in the binary solvent mixture, which is attributed to the better solubilization power of anionic surfactants.

Chitosan and SDS 0.5% were proven to be the best additives to ensure an electrostatic repulsion between freshly CRS 74 crystals formed in the LAS process. The higher particles are equally charged, the higher is the electrostatic repulsion between particles. The electrostatic repulsion given by Chitosan (crystals positively charged) played a decisive role in controlling aggregation of freshly formed crystal drug to the mixer walls, also charged positively at pH of the liquid mixture. Contrarily, drug particles highly negatively charged by SDS 0.5% showed a strong affinity to T-mixer material walls (blockage of the mixer operation in a shorter time).

The primary role of stabilizers is to inhibit excessive crystal growth. In a general way, most CRS 74 crystals produced in presence of additives had a smaller particle size compared to original or recrystallized powder without additives. Additives such as HPMC and Tween 20 (concentration below CMC) modestly inhibited agglomeration, while a higher concentration of Tween 20 (above CMC) had a very positive effect on particle size control.

Agglomerates or aggregates were obtained in presence of HPMC. A possible explanation could be an inappropriate diffusion (too slow) of the solvent toward the anti-solvent caused by a high viscosity of the anti-solvent containing 0.5%w/w HPMC. A high viscosity could prevent diffusion between solution and anti-solvent and result in nonuniform supersaturation and agglomeration.

Concerning surface properties, the unique additive placed in the aqueous phase, which was able to reduce consistently the contact angle of this drug with water to approximately 100° , was Tween 20 0.5%.

In the second part of the additive screening study, P-407 was incorporated in the organic phase (ethanol + drug + P-407). The effect of the polymer concentration was investigated by incorporating the additive in ethanol in two different concentrations: 0.0003%w/w (<CMC) and 0.02%w/w (> CMC), before the incorporation of the drug.

These particles were slightly more negative charged ($-5.4/-7.5\text{mV}$) compared to those of drug suspension without additives (-2.1mV).

This result confirmed that the microcrystals, which normally aggregate in order to lower the surface energy, could be stabilized sterically against crystal growth by a layer of protective polymer. The higher concentration of P-407 also modified the surface properties of the recrystallized powder. Contact angle of the powder with water was reduced from $133.5^\circ \pm 1.8$ (without additive) to $85.3^\circ \pm 0.8$ (P-407 0.5%w/w). The remarkable effect on the contact angle can confirm this finding: the additive probably remained attached to the hydrophobic drug particle surface lowering the interfacial tension.

The dry particles produced in presence of Chitosan were not bigger than the other ones. Maybe, Chitosan was less effective than SDS in stopping the particle growth, but more effective to prevent aggregation (higher absolute zeta potential)

The association of additives in both aqueous and organic phases had a positive effect, reducing the contact angle of the drug powder with water to $94.1^\circ \pm 4.3$ with P-407/Chitosan and to $74.7^\circ \pm 5$ with P-407/SDS, in comparison to the original drug ($136.4^\circ \pm 0.8$).

Finally, X-ray powder diffraction patterns confirmed that these additives are not within the crystal lattice, but only adsorbed on the surface.

Dissolution study confirmed the enhancement of the dissolution rate of CRS 74 crystals in presence of additives because of an increase of surface area and of a modification of surface properties of crystal.

CHAPTER 5

General Conclusions and Perspectives

Résumé Chapitre 5- Conclusion

Dans cette étude, la cristallisation par effet anti-solvant a été utilisée pour recristalliser un nouveau médicament antirétroviral. L'objectif était d'améliorer ses propriétés de dissolution. Pour générer un mélange efficace et une sursaturation rapide et uniforme, des mélangeurs spécifiques ont été utilisés (T-mélangeur, mélangeur Roughton). Les meilleures conditions de cristallisation de cette nouvelle molécule ont été définies par une étude de solubilité, un développement de méthodes de dissolution et un screening des paramètres opératoire de la cristallisation et d'additifs.

Il a été démontré la poudre présente une faible solubilité en phase aqueuse et une vitesse de dissolution lente en milieu acide. Ce travail a permis de construire à travers différentes caractérisations une monographie préliminaire de ce solide.

La molécule étudiée est soluble dans l'éthanol (92,6 mg/g de solution) à 30°C. Les résultats de la modélisation des équilibres liquide-solide par un modèle à coefficient d'activité (UNIQUAC) indiquent que ce modèle est un outil approprié pour représenter le comportement de solubilité de ce solide dans des mélanges de solvants (éthanol-eau). Les solubilités expérimentales et calculées présentent un bon accord. La modélisation a permis d'évaluer un ratio éthanol/eau optimum (25/75 % m/m) pour maximiser le rendement théorique en solide.

Le développement du protocole expérimental de recristallisation a montré que les paramètres opératoires (débits d'entrée des solutions, type de pré-mélangeur, concentration) n'ont pas d'influence sur les particules recristallisées. De plus, préparer de fines particules de ce solide est un véritable défi, en raison de la croissance et l'agglomération très rapides des particules produites. Des problèmes de colmatage des canaux du pré-mélangeur ont aussi été constatés.

Il a été montré que la cristallisation de ce solide donne naissance à des particules de tailles nanométriques en sortie de pré-mélangeur. Cependant ces nanoparticules ont une forte tendance à croître et à s'agglomérer. Afin de limiter la croissance et l'agglomération des cristaux, des additifs ont été sélectionnés et introduits dans les solutions initiales. Chaque additif a montré un comportement différent en empêchant la croissance des cristaux. La combinaison de deux additifs (P-407 et chitosane) a été la plus efficace : diminution de la

croissance des cristaux, amélioration de la mouillabilité des particules formées, modification de charge de surface de particules (elle devient positive). Cette modification de charge de surface a empêché le colmatage des canaux au cours de la cristallisation (répulsion électrostatique avec les parois de mélangeur). Dans l'ensemble, les microcristaux synthétisés en présence d'additifs ont montré une vitesse de dissolution nettement plus élevée que les cristaux de la poudre initiale.

L'amélioration de la vitesse de dissolution est principalement due à l'amélioration des propriétés de mouillage grâce à des interactions spécifiques entre la poudre et les additifs. Par conséquent, les microcristaux synthétisés ont de meilleures propriétés physico-chimiques. L'utilisation de cette technique serait donc une alternative pour l'obtention d'une poudre avec de meilleures caractéristiques de dissolution et par conséquent une meilleure biodisponibilité.

Pour continuer ses travaux sur l'amélioration de la biodisponibilité du CRS 74, différentes voies peuvent être suggérées en terme de procédé, de compréhension du mécanisme de stabilisation, et du potentiel du principe actif.

En termes de procédé, il serait intéressant d'étudier l'influence des paramètres opératoires de la cristallisation (débit, concentration en additifs, température ...) pour la formulation comprenant les deux additifs (P-407 et chitosane) afin d'optimiser le processus de production des cristaux. De plus, la cristallisation par effet anti-solvant pourrait être comparée à d'autres technologies « *bottom-up* » prometteuses pour la préparation de nanocristaux de CRS 74, comme par exemple : la préparation de dispersions solides par atomisation ou par extrusion à chaud.

Au cours de cette étude, il était clair que la cristallisation en présence d'additifs peut avoir un effet positif sur la vitesse de dissolution. Il est donc nécessaire d'approfondir la compréhension du mécanisme d'adsorption de l'additif et de déterminer quel est le niveau d'adsorption nécessaire pour obtenir un effet prononcé sur les propriétés de surface des particules. Pour comprendre cette propriété, une détermination quantitative de l'adsorption de l'excipient devra être effectuée. Il sera intéressant d'étudier différentes hypothèses d'attachement à l'échelle moléculaire. L'interaction de l'additif sur la surface cristalline pourrait être étudiée, par exemple, par spectroscopie Raman.

Enfin, la méthodologie de dissolution développée dans cette étude devra être validée afin de pouvoir l'utiliser en tant que technique sensible, fiable et reproductible pour les tests

de bioéquivalence. De plus l'effet biologique du solide recristallisé par rapport au solide d'origine devra être identifié afin d'évaluer les changements de la poudre synthétisée et déterminer le réel effet sur l'amélioration de la biodisponibilité.

This study concerned a novel antiretroviral promising drug candidate, named **CRS 74**.

It could be proven in this study that the original drug powder (as currently produced industrially) exhibits poor aqueous solubility and slow dissolution rate.

The limited low aqueous solubility at 37 °C (< 0.004 mg/g) can be explained by its high crystallinity, its high melting point (188.6°C) and high enthalpy of fusion (86.6 J/g). The low dissolution rate is related to its large particle size (micrometric range, with a broad particle size dispersion) and very poor water wettability ($\Theta = 136.4 \pm 0.8^\circ$).

This molecule is soluble in ethanol (92.6mg/g_{solution}) and presented a maximum in solubility in ethanol-water mixtures as determined in this study using UNIQUAC-based model. To the best of our knowledge, there are no published data of the solubility of such given solute in ethanol-water mixtures to compare with.

There is no monograph of this drug in any pharmacopoeia and, from the characterization study carried out in this thesis, a monograph proposition is suggested:

CRS 74 monograph	
Synonym:	(2S, 3S, 5S)-2, -5 bis- [N-[N-[[N- methyl-N-[(2-isopropyl- 4- tiazolyl) methyl] amino] carbonyl] vanilyl] amino- 1,6-diphenyl- 3- hydroxyhexane
Therapeutic category	HIV protease inhibitor
Formula	C ₄₆ H ₆₆ N ₈ O ₅ S ₂
Description	white powder
Molecular weight (g/mol)	875.2
Melting point (°C)	187-189
Melting enthalpy (J/g)	78-87
Solubility	0.102 mg/g _{solution} in 0.1M HCl pH 1.2, 37°C - <i>Very slightly soluble</i> lower than 0.004 mg/g in water at 37 °C – <i>Insoluble</i> 92.6 mg/g _{solution} in ethanol (solvent) at 30°C - <i>Very soluble</i>

To predict *in vitro* CRS 74 dissolution behavior, a conventional acid medium was chosen. The development of the analytical methodology of quantification and dissolution assays is very important. The inexistence of specific method for CRS 74 in official summaries highlights the importance of above-cited tests for the definition of specific method for such purpose appropriate method to quality control of the drug. The quantification method was developed in this work to quantify the drug in acid media (0.1M HCl) or in water-ethanol solutions. Both developed methods were linear and specific for the drug.

Several original data were experimentally obtained concerning the solubility of CRS 74 in liquid media. They are:

- Acidic aqueous medium (0.1 M HCl) at 37°C;
- Acidic aqueous medium in presence of five different additives at 37°C;
- Hydroalcoholic solutions in different water-ethanol mass proportions at 30°C;
- Pure ethanol at different temperatures (5, 10, 15, 20, 25 and 30°C)
- Water (LAS recrystallized drug) at 37°C.

In hydro-alcoholic solutions, the drug solubility increases as the ethanol ratio in ethanol-water increases, presenting a maximum as determined in this study using UNIQUAC-based model. The calculated data showed good agreement with experimental results and revealed a maximum solubility of CRS 74 of 130.20 mg/g_{solution} for a mass ratio of ethanol/water of 0.83/0.17 (w/w).

The results of the modeling indicate that this model is the appropriate tool for representing the solubility behavior of CRS 74 in ethanol-water solvent mixtures. The measurements and correlation of CRS 74 solubility in binary solvent mixtures provided useful data to estimate the theoretical efficiency of the LAS recrystallization process as a function of ethanol/water mass ratios. An ethanol-water mixture containing 25% (w/w) ethanol was found favorable for the crystallization process and was fixed for the LAS crystallization.

For experimental design to CRS 74 LAS crystallization, two different types of mixers were tested: a T-mixer with two radial entries and a two jets vortex mixer also called Roughton mixer. It was clearly observed, that nano-sized particles were obtained at the outlet of both mixers. However, no remarkable effect of the supersaturation level was observed on the reduction of the drug particle size.

The T-mixer was chosen for further experiments because it generated less agglomerated particles. However to prepare fine particles of CRS 74 without polymer became quite a challenge, due to the rapid growth and agglomeration of the produced particles and problems of blockage of the mixer.

Recrystallized solids were compared to the original drug crystals in terms of particle size, solid state, physical and dissolution properties. The particles of the original powder were found to be larger and exhibited a broad particle size distribution compared to the LAS recrystallized drug. In turn, recrystallized solids seemed more agglomerated than the original ones. In addition, recrystallization did not modify the dissolution profile compared to the original drug. It could be concluded that to improve dissolution kinetics, smaller particles with a more hydrophilic surface need to be produced. So the LAS crystallization was then carried out in presence of different additives.

Stabilizers were screened and introduced in the solvent, or in the anti-solvent, or in both phases. For steric stabilization, we used nonionic surfactant (Polyoxyethylene sorbitan monooleate –Tween 20) polymers (Hydroxypropylmethylcellulose-HPMC) and amphiphilic block copolymers (Poloxamer 407-P-407). For electrostatic repulsion, the anionic surfactant Sodium Dodecyl Sulfate (SDS) was chosen. For a combined effect of steric stabilization and electrostatic repulsion, we tested Chitosan, a copolymer of glucosamine and N-acetyl glucosamine.

The primary role of stabilizers is to inhibit excessive crystal growth. In a general way, most CRS 74 crystals produced in presence of additives had a smaller particle size compared to the original or recrystallized powder without additives.

As a result of introduction of additives in the LAS crystallization study, the crystal size, agglomeration state, dissolution kinetics and drug wettability varied over a wide range depending on the additive involved and its concentration. According to the results, the zeta potential remained almost unchanged when nonionic stabilizers were used. In other hand, charged additives like SDS (negatively charged) and Chitosan (positively charged) adsorbed with the charged parts of the respective molecules onto the drug particle surface.

Over the additives screened, changes on surface properties were observed. A remarkable decrease of contact angle ($\theta < 100^\circ$) was observed for two formulations, one with P-407 (concentration of 0.02 % in organic phase) and another with P-407 combined with

chitosan (P-407 concentration of 0.02 % in organic phase and chitosan concentration equal to 0.5 % in aqueous phase) at the recrystallized powder in the higher concentration of P- 407, P-407 and Chitosan. The enhancement of wetting properties can be attributed to multiple attachments of hydrophobic domains of P-407 on the drug particle surface.

Each additive showed different behavior in preventing crystal growth, but the association of P-407 in the organic phase and chitosan in the aqueous phase was most effective in preventing crystal growth, improving surface wettability, and providing enough electrostatic repulsion due to highly positive charged drug surface.

When placed in the organic phase, P-407 chains are more available to precipitate drug particles upon mixing, since they do not need to diffuse across the interface through the volume of the aqueous phase, which exceeded the organic phase volume. This reduction in time for diffusion of polymer to the drug surface leads to more rapid stabilization against coagulation and condensation. The presence of surfactant at the surface of the clusters may be expected to lower the interfacial tension between the solid surface and solvent mixture and raise the nucleation rate.

Drug microcrystals recrystallized in presence of additives showed significantly improved dissolution velocity in comparison to microcrystals (raw material and without additive). Among the additives tested, P-407 and P-407 + Chitosan gave the best results. They enhanced dramatically the drug dissolution rate from 4% to almost 40% drug dissolved at 20 min. In addition, the presence of chitosan in the crystallization process solved the problem related to the process, the blockage, due to charge repulsion between the positively charged crystals and surface charge of stainless steel.

Overall, the results of this research showed conclusively that the liquid anti-solvent crystallization technique in presence of additives used in this research produced microcrystals that exhibited significantly faster dissolution rates than the original (as-received) CRS 74 crystals. The improved dissolution is attributable to the modification of the particle size of drug crystals and enhancement of wetting properties due to specific interactions between the drug and the additives. Therefore, CRS 74 microcrystals yielded better physicochemical properties and would be one alternative for better CRS 74 dissolution characteristics and thereby bioavailability for commercial purposes.

To continue the work concerning the improvement of the bioavailability of CRS 74,

some strategies are suggested in different fields (process, stabilization mechanism and drug potential).

In term of process, it will be interesting to study the influence of crystallization operating conditions with the association of two additives (P-407, Chitosan) on solid properties in order to optimize and eventually scale up the process. This process could be compared to others promising technologies based on bottom-up preparation of CRS 74 drug nanocrystals, like the preparation of solid dispersions by spray drying and hot melt extrusion. Still in terms of process, there is a need for further understanding excipient adsorption, e.g., what is the level of adsorption needed to provide a pronounced effect on particle properties? In order to understand this point, a quantitative determination of excipient adsorption should be carried out.

During this study it was clear that crystallization in the presence of additives can have a positive effect on dissolution rate. For instance, some hypotheses about the attachment on molecular level of additive on crystal surface were explored. However, a better understanding of these interactions should be carried out. The interaction additive crystal-surface could be explored by Confocal Raman Spectroscopy.

The last research field is related to the drug. The dissolution methodology developed in this study could be validated and used as a sensitive, reliable, and reproducible for bioequivalence testing. Finally, the biological effect of recrystallized solid compared to original solid should to investigate in order to assess the changes of the synthesized powder and its improved bioavailability.

Appendixes

Appendix I

HIV and its life cycle

Human Immunodeficiency Virus (HIV) is a retrovirus (constituted by RNA) belonging to the Lentivirinae subfamily, capable to sponge human immunologic system causing the infectious disease known by the acronym AIDS (Acquired Immuno Deficiency Syndrome).

HIV comprises an outer envelope consisting of a lipid bilayer with spikes of glycoproteins (gp), gp41 and gp120. These glycoproteins are linked in such a way that gp 120 protrudes from the surface of the virus. Inside this envelope is a nucleocapsid (p 17), which surrounds a central core of protein, p24. Within this core, are two copies of single-stranded RNA (the virus genome). Proteins, p7 and p9, are bound to the RNA and are believed to be involved in regulation of gene expression. Multiple molecules of the enzyme, reverse transcriptase (R T), are also found in the core. This enzyme is responsible for converting the viral RNA into proviral DNA (ABBAS, 2000), as shown in the Figure I.1.

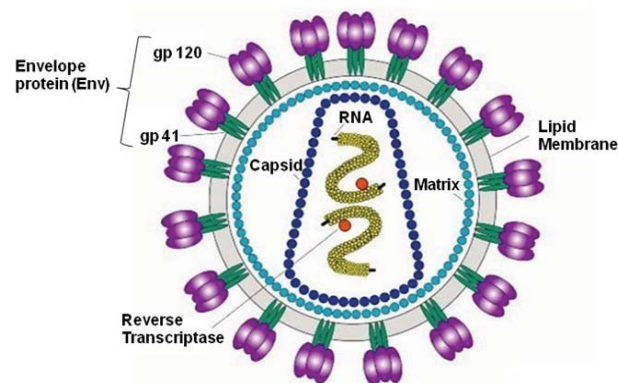


Figure I.1. Schematic drawing of the lentivirus HIV (ENKIRCH, 2011)

HIV may only infects certain types of cells. In general, these are cells which carry CD4 receptors on their surface. Some cells in the immune system have these receptors, in particular, T4-lymphocytes or T-helper cells. Cellular infection occurs when HIV virus binds to a cellular receptor, generally the T CD4+, by means of the gp120 protein; then, virus merges to the cell membrane and the capsid content is released into the cell cytoplasm. The HIV enzyme, reverse transcriptase, catalyses the DNA copy production starting from HIV virus RNA. The double helix DNA copy is then transported to the cellular nucleus where a second HIV enzyme, the integrase, catalyses the incorporation of viral DNA to the host genetic material. Subsequent viral genes expression results in RNA transcription starting from

HIV DNA and in translation of viral proteins. However, newly formed viral proteins are produced in the form of polyproteins precursors that are long unities consisting of viral enzymes and structural proteins added to each other. Polyproteins and viral RNA move to the cell surface where they are incorporated to the new viruses that spring from cell membrane taking part of it with them to form the external layer of the viruses (figure I.2). Newly formed viruses, however, could not be infectious without the action of a third essential HIV enzyme, the protease, that turns viral polyproteins in functional and structural proteins and enzymes. Proteases are enzymes that cleave others proteins at highly specific sites. HIV protease, an aspartyl protease, cleaves viral polyproteins in essential functional proteins during the process of maturation of the "virion" (complete viral particle). This process occurs when each new "virion" springs to outside of the infected cell membrane and it continues after the release of immature virus by the cell. If polyproteins are not cleft, virus formation does not finish and it becomes unable to infect a new cell. Protease inhibitors, as this name implicate, are substances able to inhibit protease enzyme function. They perform their inhibitory effect disabling the enzyme before it cleaves gag/pol polyprotein to form its essential products. It means that, blockage of HIV protease leads to the formation of immature non-infectious- PCT document number 111006 (BOCKELMANN et al., 2005; BOCKELMANN et al., 2010).

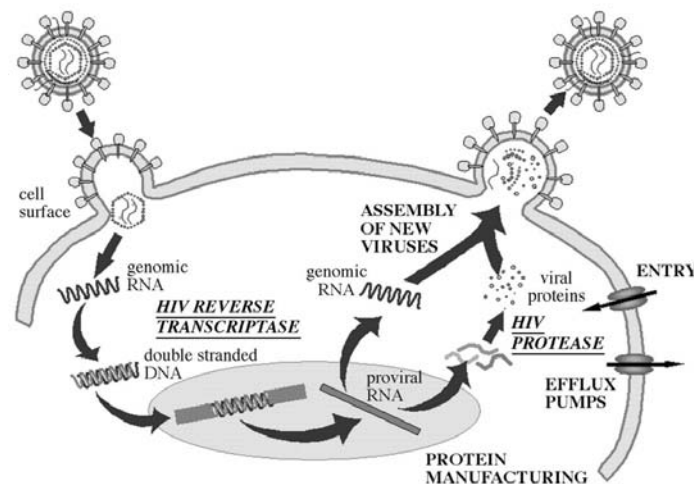


Figure I.2. Life cycle of HIV (HOGGARD and OWEN, 2003).

Appendix II

Calibration pumps

In order to validate the flow of gear pumps (mzr-7255-hs-f S, mzr-7205-hs-f S; HNP Mycosysteme) for the solvent and the anti-solvent system and digital mass flow meter/controller (MIX, Bronhorst), the pumps calibration was realized.

For this purpose, a beaker with the fluid to be pumped was weighed and the software was activated, starting the pump. At the end, after all the fluid has being pumped, the beaker was weighed and the theoretical mass flow of fluid was calculated with the mass used and the time spent in the experiment. Finally, the value of the calculated flow was compared with the flow indicated by the software.

The calibration test was realized for both pumps with water used as the fluid for the anti-solvent's pumps and ethanol to the solvent's pump. According to the table II.1, the value of the calculated flow is in agreement with the flow value indicated by the software.

Table II.1. **Data obtained in the pumps calibration**

Pumped liquid	Mass (g)	Time (min)	Flow rate_{calculated} (g/min)	Flow rate_{software} (g/min)	Error (%)
Ethanol	109.3	15	7.29	7	4.0
Water	749.5	15	49.97	50.17	0.4

In a second time, to ensure that the pumps were pumping fluids in the correct ratio a simple test was performed. Mixtures between ethanol and water in different proportions were made without the aid of the pumps and measured up their refractive indices. Later, the same mixtures were performed using the pumps and they also had their refractive indices measured. Each result is an average of at least 3 replicates.

No changes of refractive indices were observed, for all different ratio ethanol/water using different manners of preparation, as seen in the table II.2. It can be supposed that, the pumps can respond correctly to request flow values and they pumped the fluids in the correct proportions. It means that pumps are working as it should.

Table II.2. Values of the refractive indices measured \pm standard deviation .

Proportion ethanol/water (w:w)	Physical mixture	Mixture with pumps
1:1	1.3582 \pm 0.0001	1.3592 \pm 0.0002
2:1	1.3523 \pm 0.0004	1.3548 \pm 0.0001
3:1	1.3476 \pm 0.0004	1.3478 \pm 0.0002

Appendix III

Particle size distribution

LAS crystallization process conditions

- T-Mixer
- Ratio solvent (ethanol):anti-solvent (water) - 1:3 (25%:75%) ;
- Presence of additive
- Temperature of organic and aqueous phases at 30°C
- Crystals collection: vessel under magnetic stirring

Additive in aqueous phase

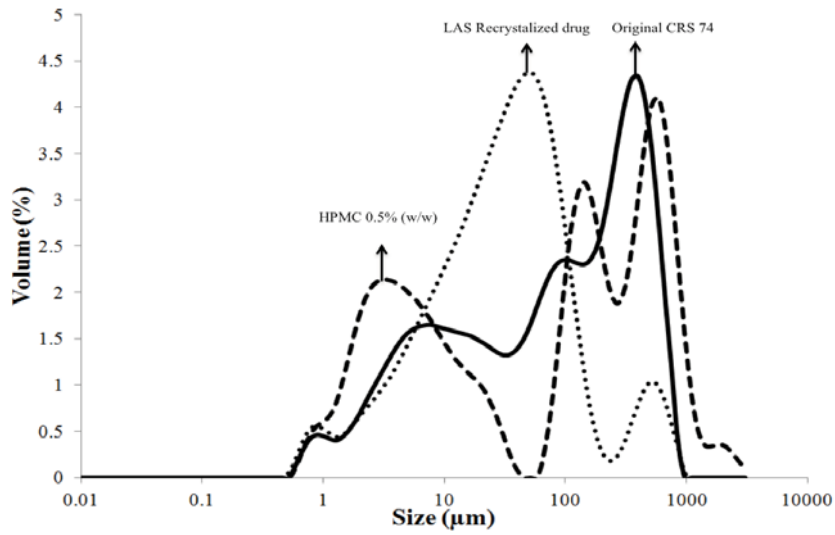


Figure III.1. Particle size distribution pattern for as HPMC 0.5 % (w/w)

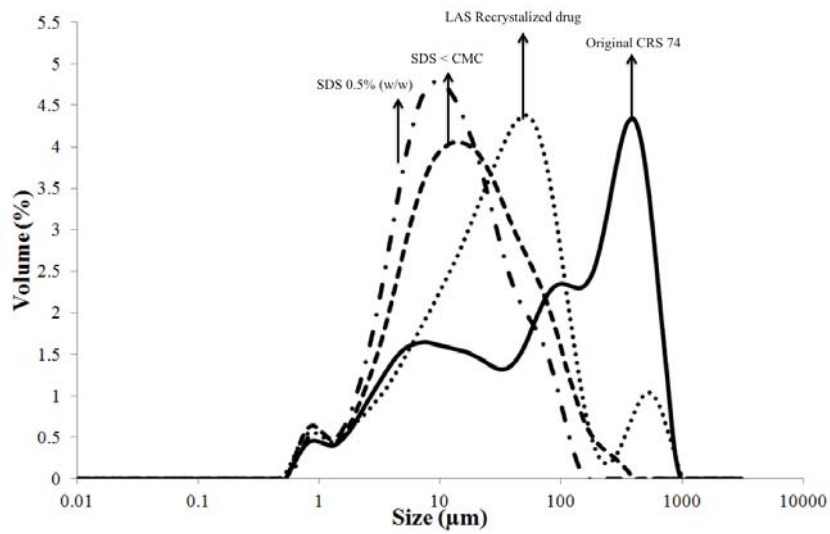


Figure III.2. Particle size distribution pattern for as SDS 0.5 % (w/w) and SDS < CMC.

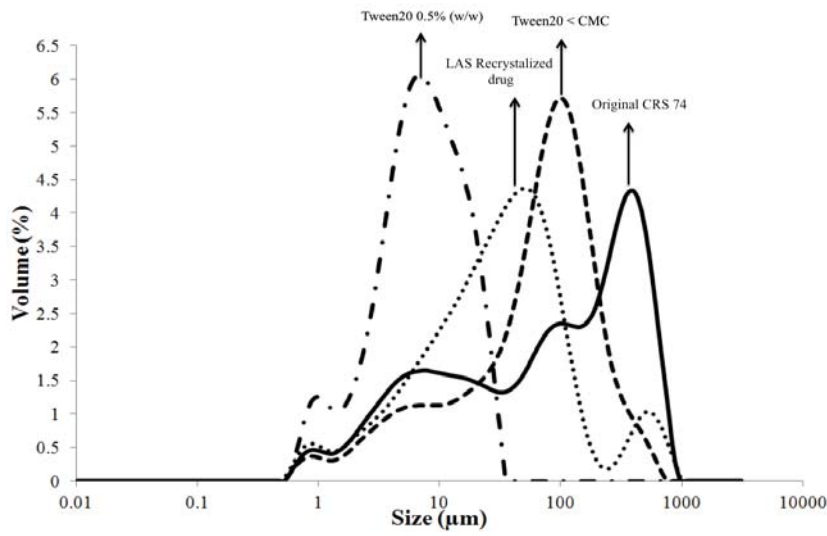


Figure III.3. Particle size distribution pattern for as Tween20 0.5 % (w/w) and Tween20 < CMC.

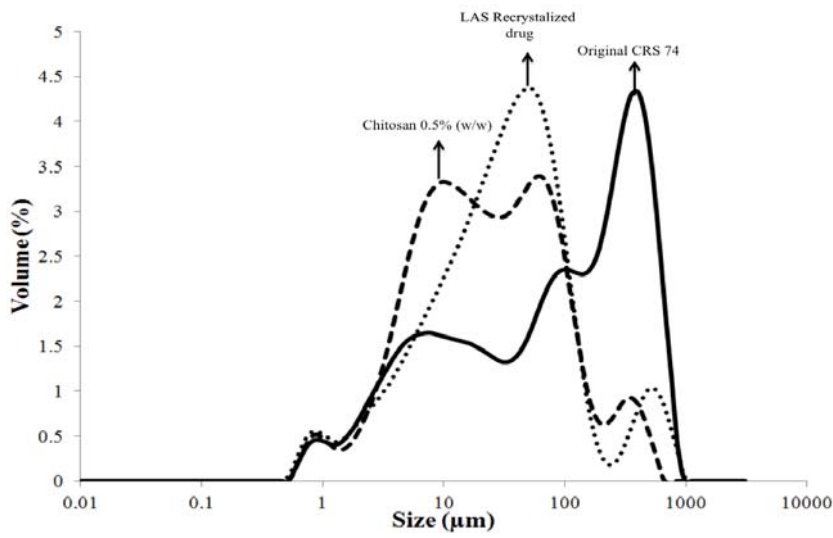


Figure III.4. Particle size distribution pattern for as Chitosan 0.5 % (w/w).

Additive in organic phase

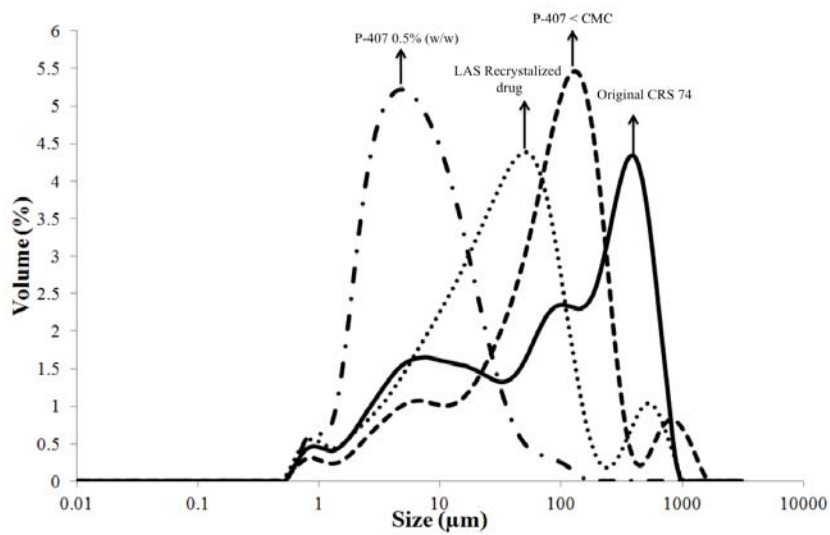


Figure III.5. Particle size distribution pattern for as P-407 0.5 % (w/w) and P-407 < CMC.

Additive in both, organic and aqueous phase

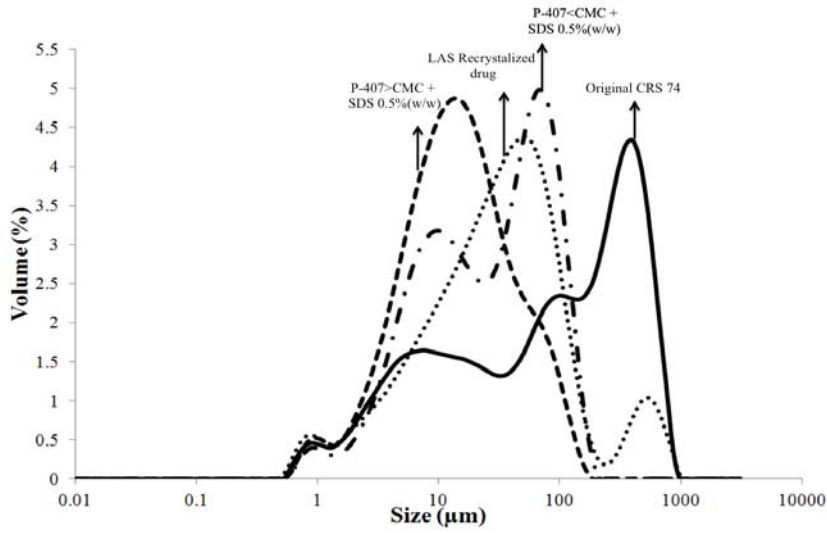


Figure III.6. Particle size distribution pattern for as P-407 < CMC + SDS 0.5 % (w/w) and P-407 > CMC + SDS 0.5 %(w/w).

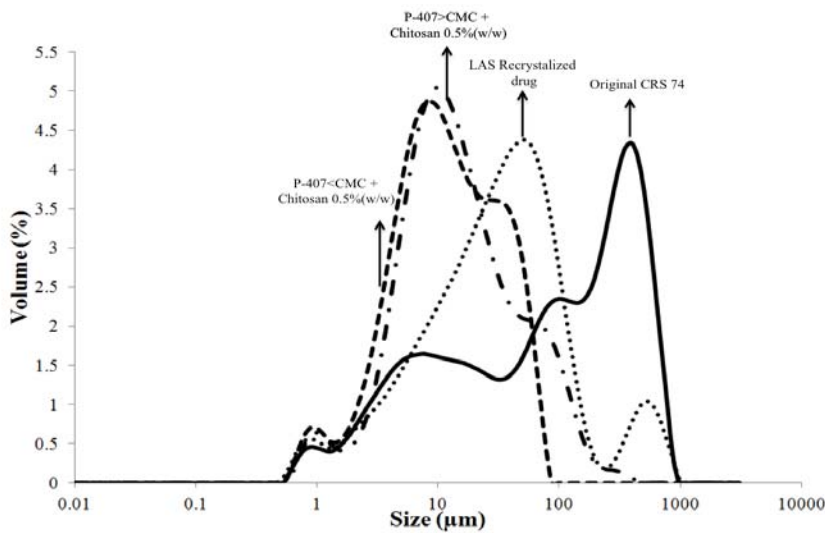


Figure III.7. Particle size distribution pattern for as P-407 < CMC + Chitosan 0.5 % (w/w) and P-407 > CMC + Chitosan 0.5 %(w/w).

Supersaturation degree

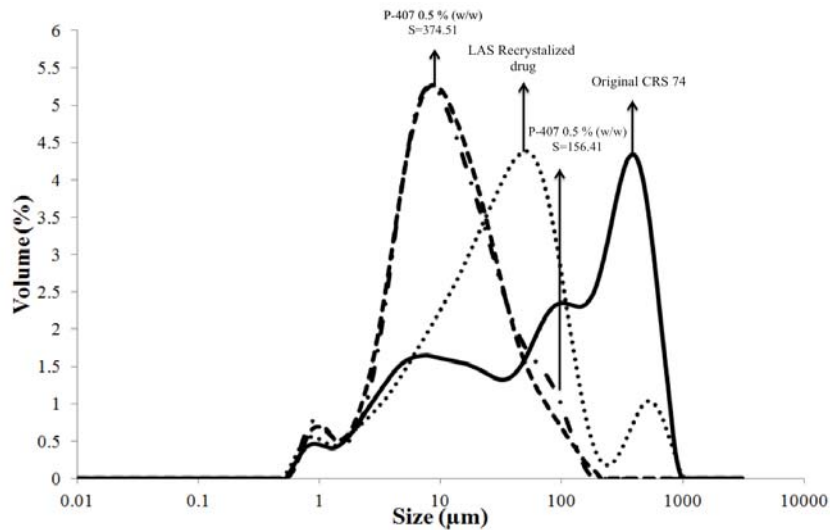


Figure III.8. Particle size distribution pattern for as P-407 0.5 % (w/w) (S =156.41) and P-407 0.5 % (S =374.51)

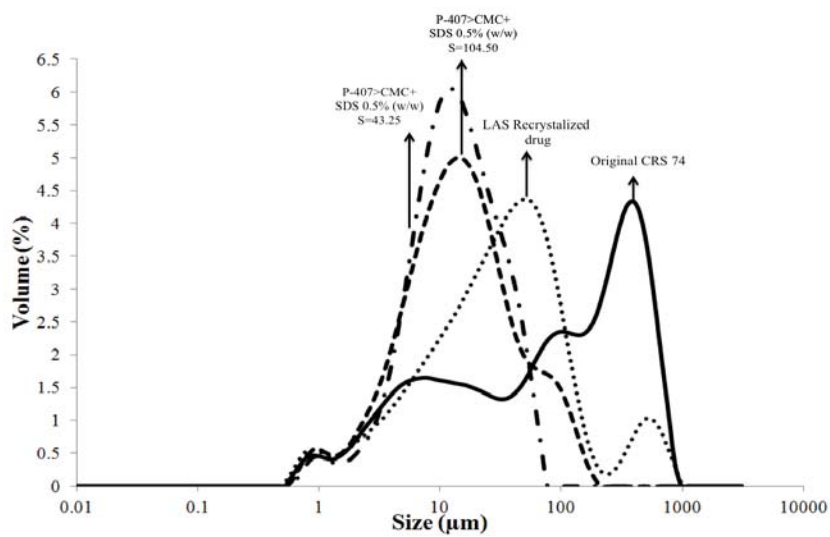


Figure III.9. Particle size distribution pattern for as P-407 > CMC + SDS 0.5 % (w/w) (S = 43.25) and P-407 > CMC + SDS 0.5 % (w/w) (S = 104.5).

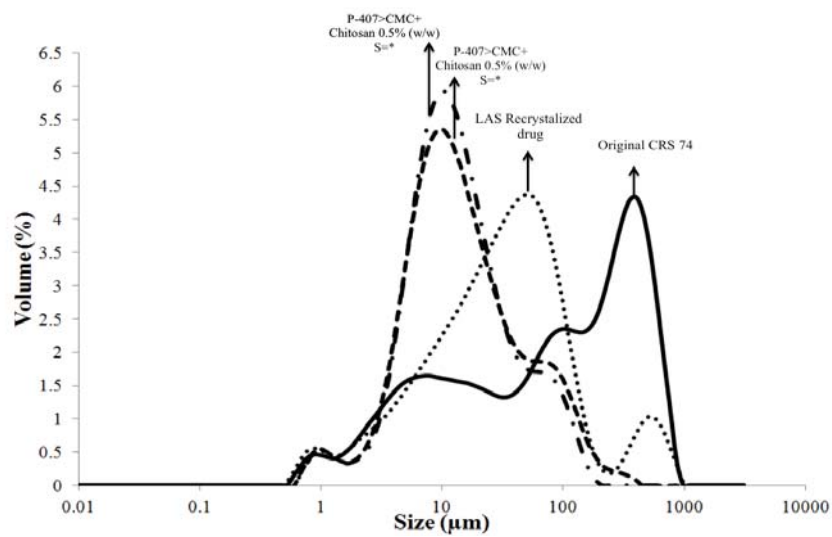


Figure III.10. Particle size distribution pattern for as P-407 > CMC + Chitosan 0.5 % (w/w) (20 %) and P-407 > CMC + Chitosan 0.5 % (w/w) (50 %).

Appendix IV

Contact angle (θ°) as a function of time

LAS crystallization process conditions

- T-Mixer
- Ratio solvent (ethanol):anti-solvent (water) - 1:3 (25%:75%) ;
- Presence of additive
- Temperature of organic and aqueous phases at 30°C
- Crystals collection: vessel under magnetic stirring

Original CRS 074

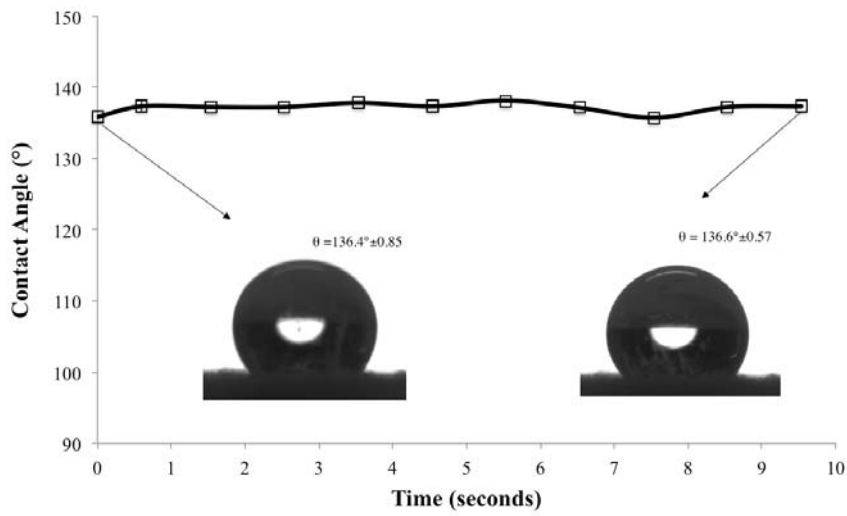


Figure IV.1 Contact angle (°) as a function of time for as CRS 74.

LAS recrystallized drug

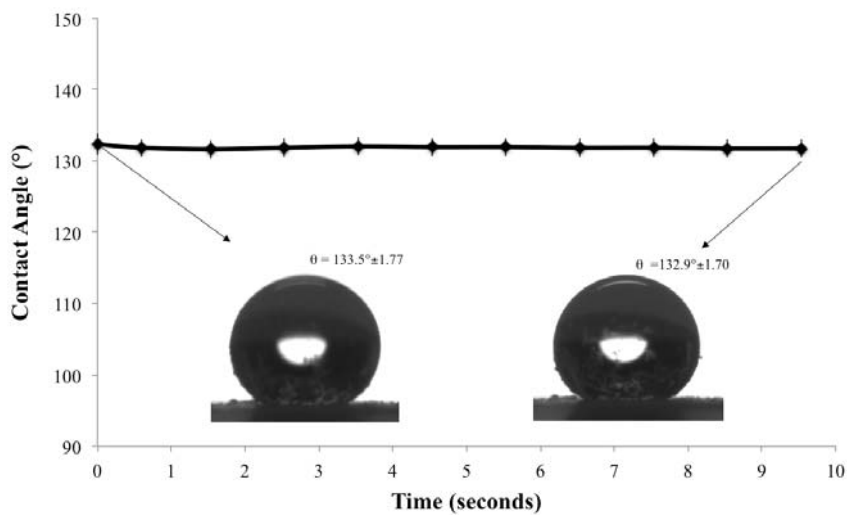


Figure IV.2. Contact angle (°) as a function of time for as LAS recrystallized drug .

Additive in aqueous phase

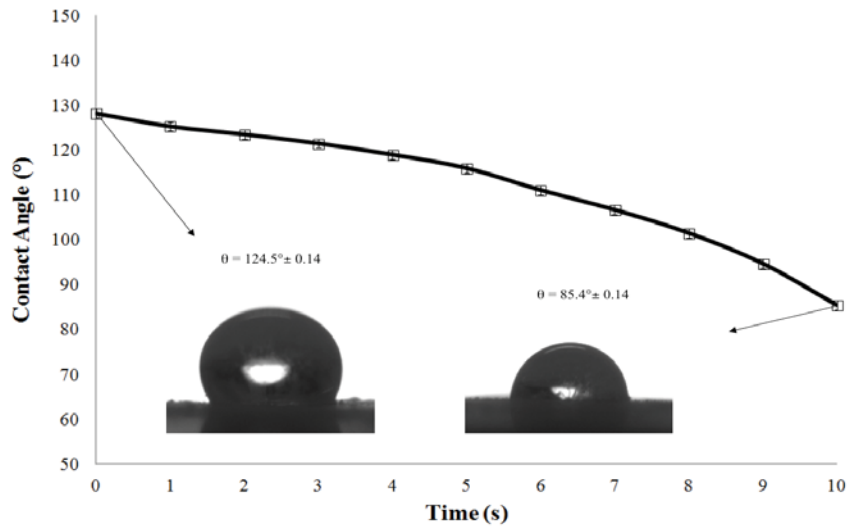


Figure IV.3. Contact angle (°) as a function of time for as HPMC 0.5 % (w/w).

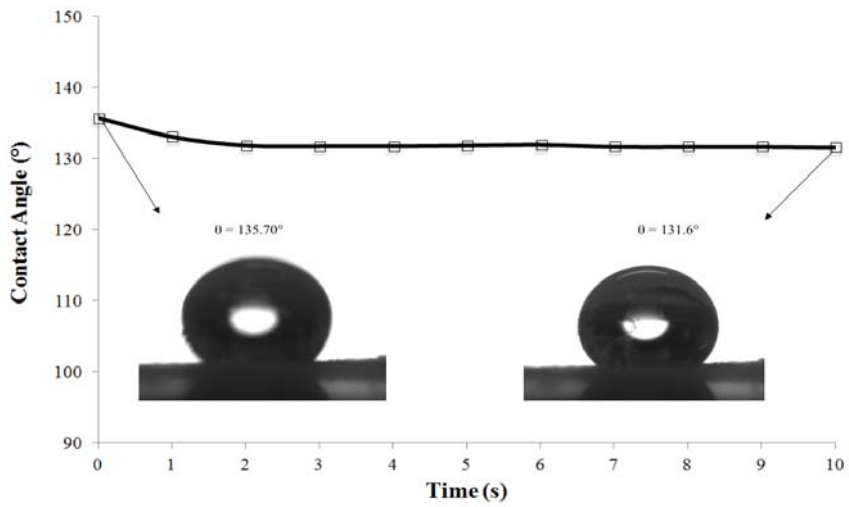


Figure IV.4. Contact angle (°) as a function of time for as SDS < CMC.

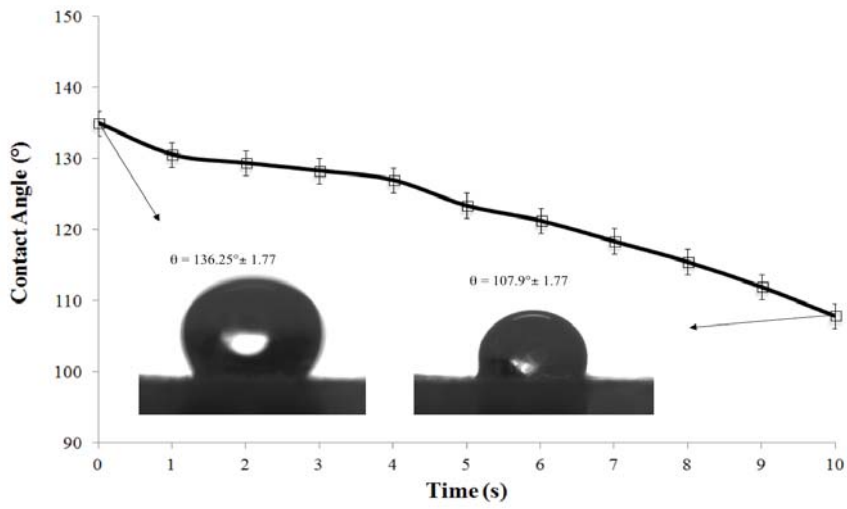


Figure IV.5. Contact angle (°) as a function of time for as SDS 0.5 % (w/w).

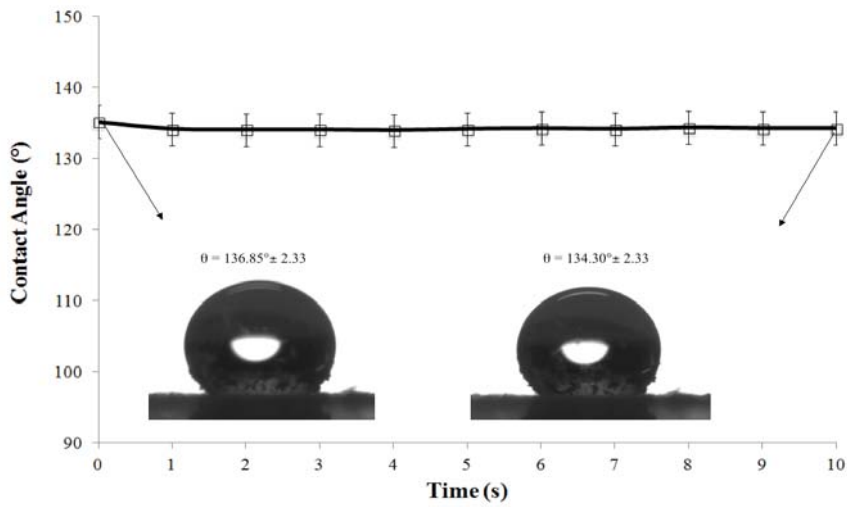


Figure IV.6. Contact angle (°) as a function of time for as Tween 20 < CMC.

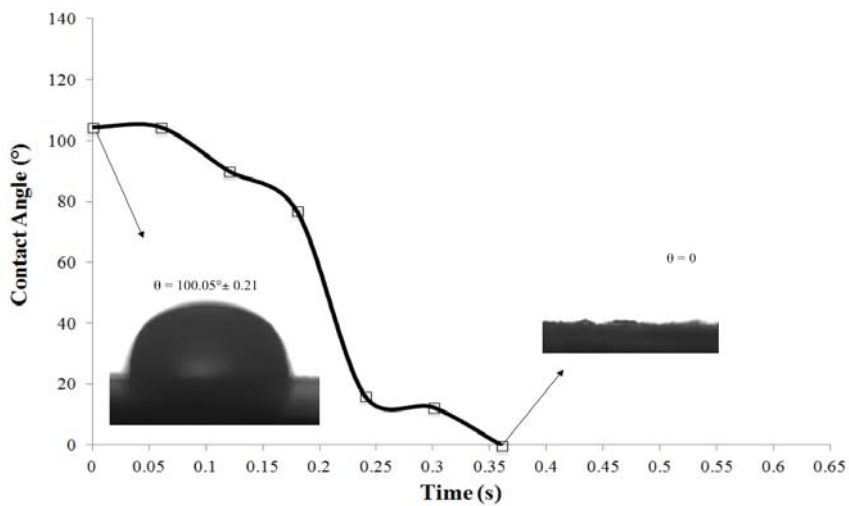


Figure IV.7. Contact angle (°) as a function of time for as Tween 20 0.5 % (w/w).

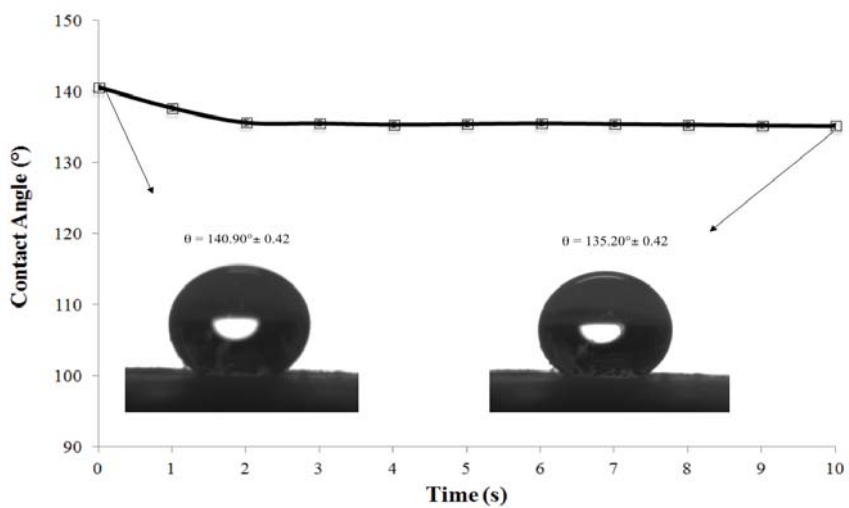


Figure IV.8. Contact angle (°) as a function of time for as Chitosan 0.5 % (w/w).

Additif in the organic phase

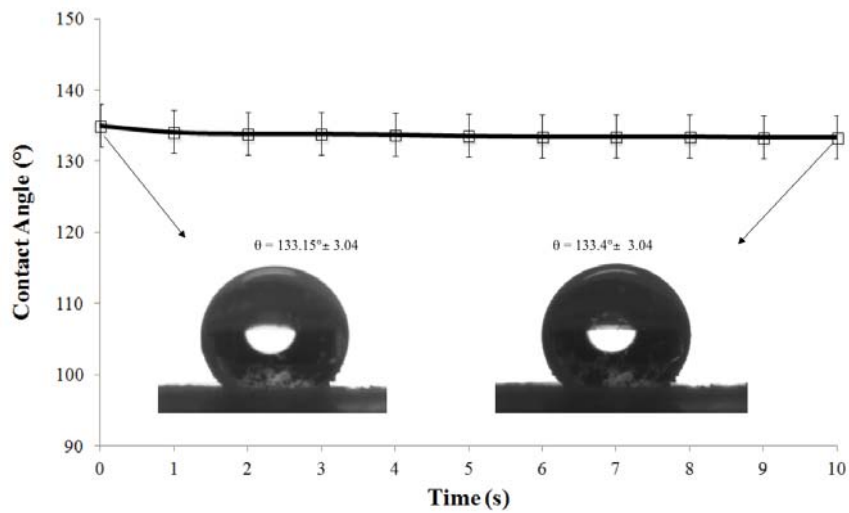


Figure IV.9. Contact angle (°) as a function of time for as P-407 < CMC.

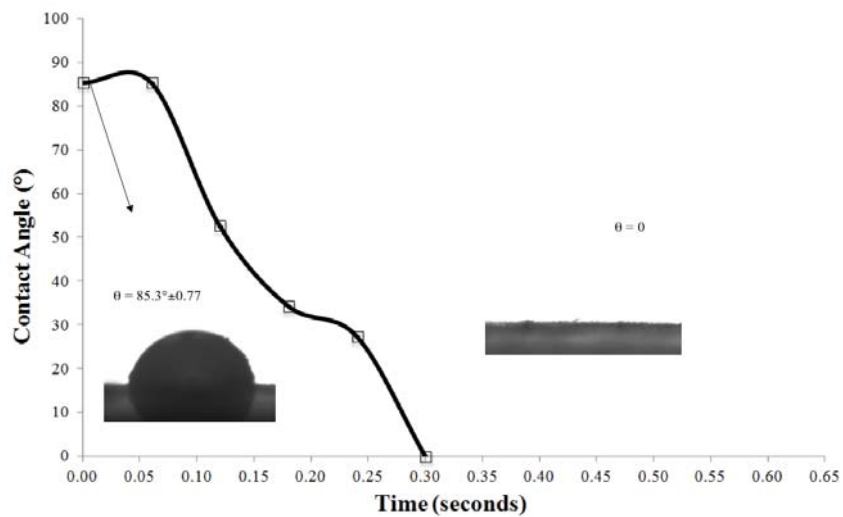


Figure IV.10. Contact angle (°) as a function of time for as P-407 0.5 % (w/w).

Additif in both, organic and aqueous phases

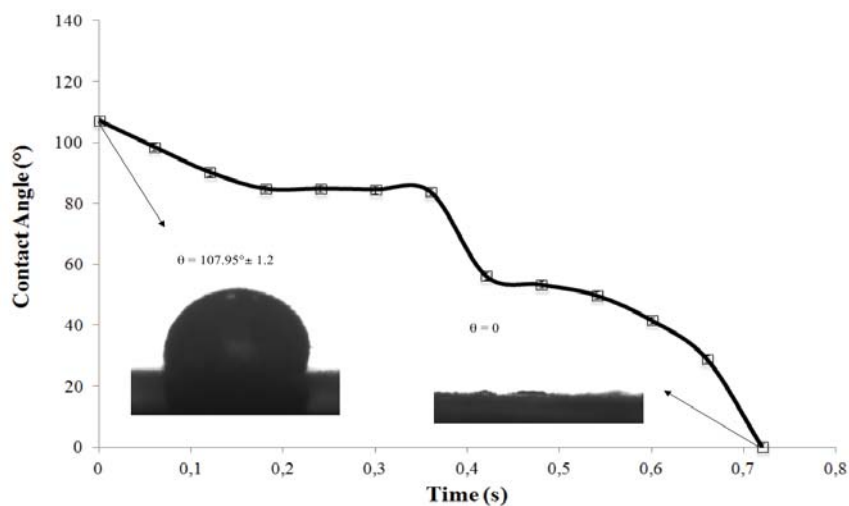


Figure IV.11. Contact angle (°) as a function of time for as P-407 < CMC + SDS 0.5%(w/w).

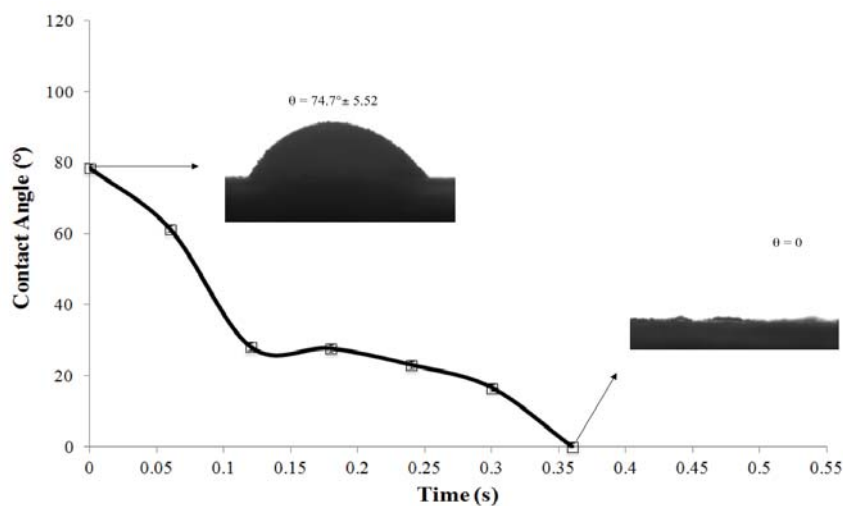


Figure IV.12. Contact angle (°) as a function of time for as P-407 > CMC + SDS 0.5%(w/w).

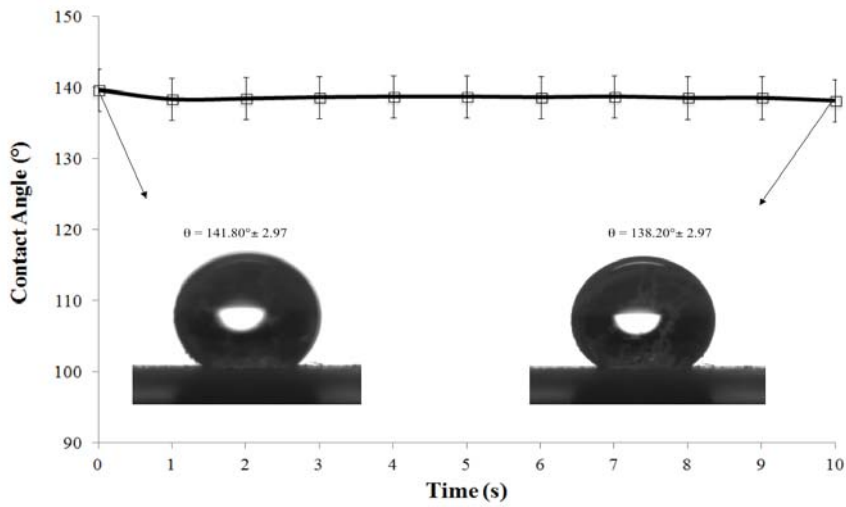


Figure IV.13. Contact angle (°) as a function of time for as P-407 < CMC + Chitosan 0.5 % (w/w).

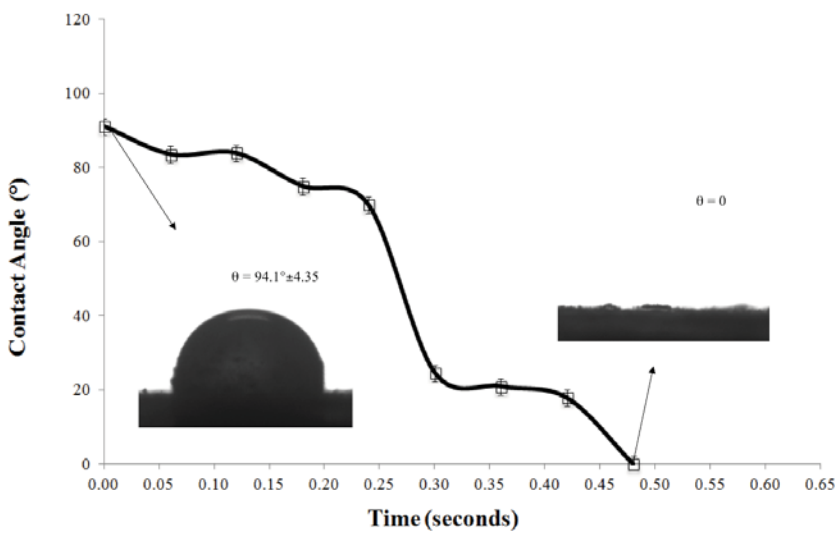
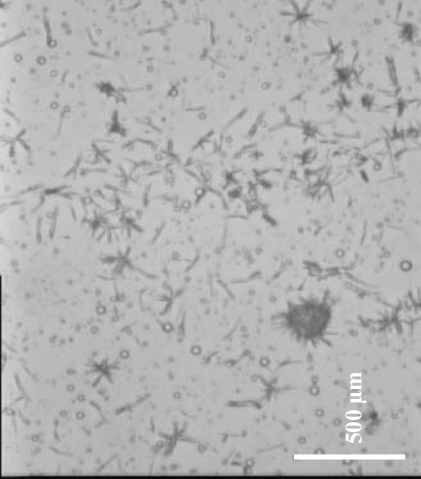
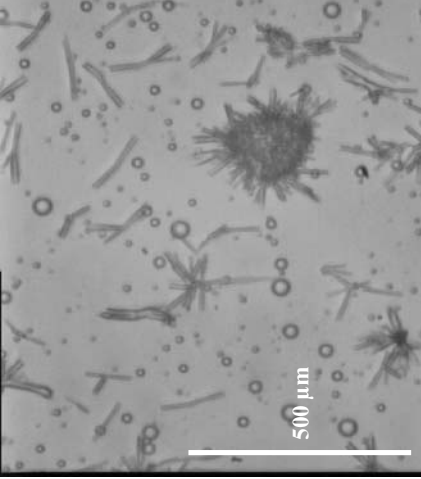
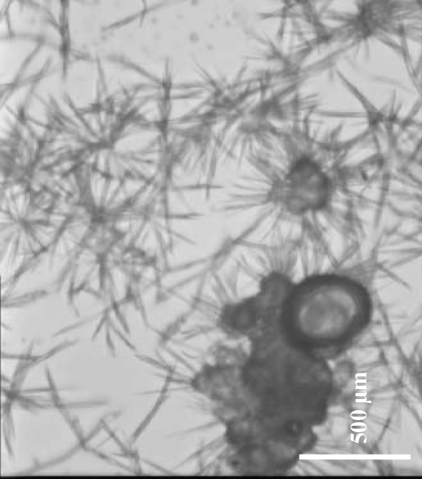
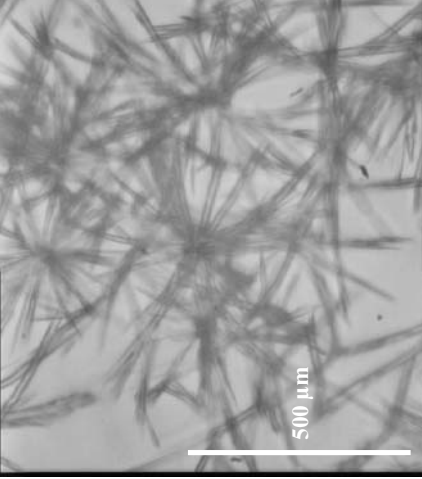


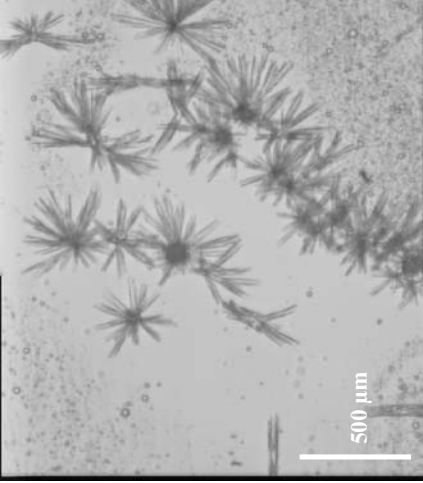
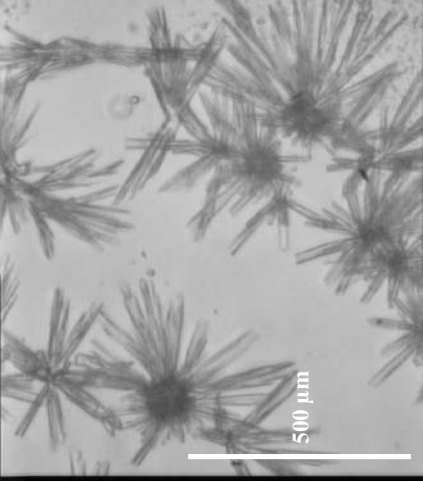
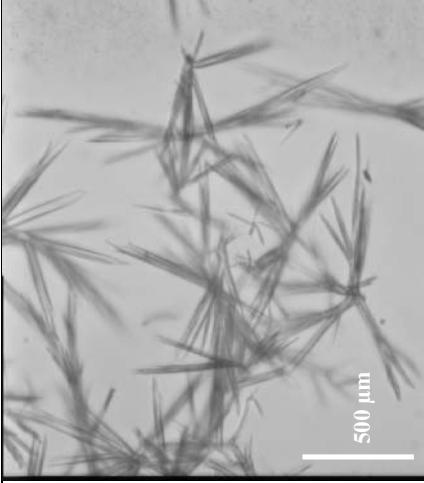
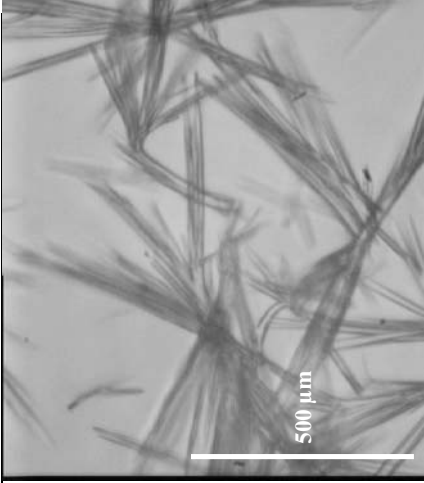
Figure IV.14. Contact angle (°) as a function of time for as P-407 > CMC + Chitosan 0.5 % (w/w).

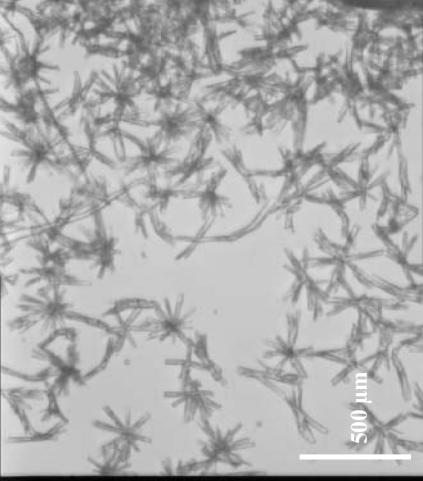
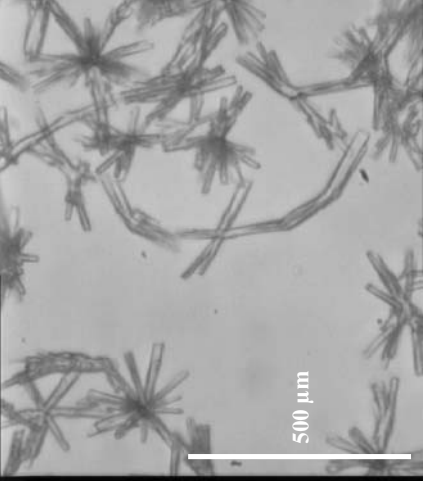
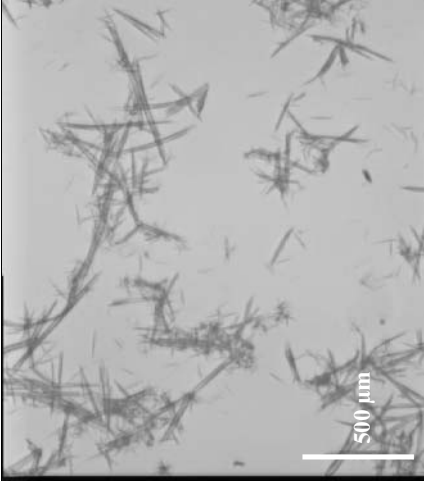
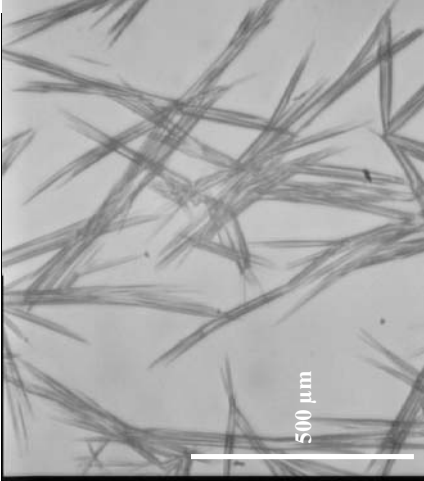
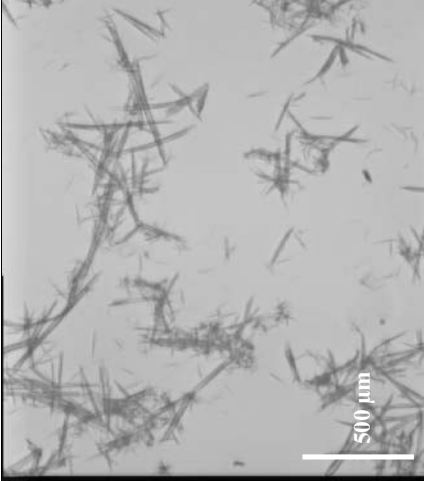
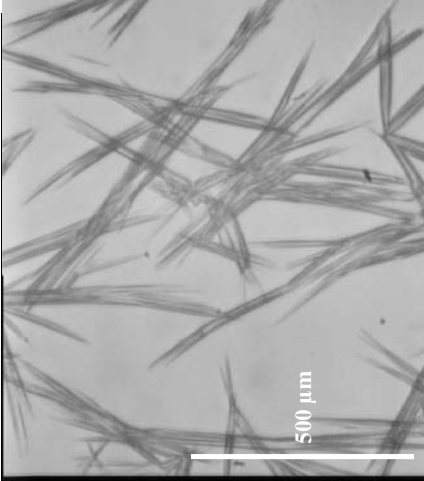
Appendix V

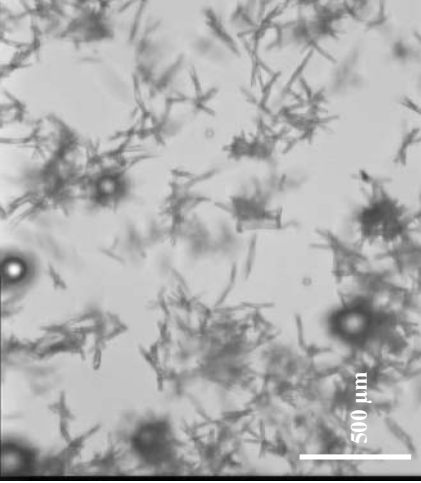
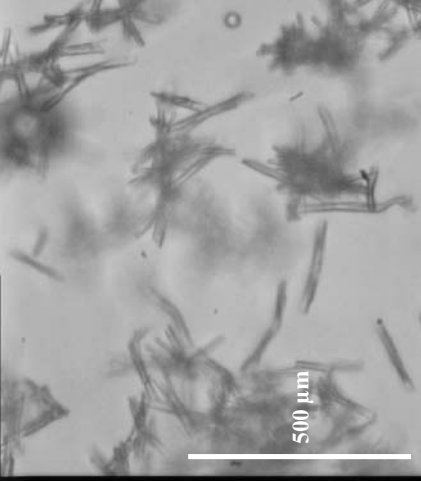
Morphology of crystals in suspension

Additive in aqueous phase

Exp	Additive	Experimental Conditions	Microscopic image 20x	Microscopic image 40x
1	X	Ratio S:AS*1:3 S = 894.04		
2	HPMC 0.5% (w/w)	Ratio S:AS*1:3 S = 445.63		

Exp	Additive	Experimental conditions	Microscopic image	
			20x	40x
3	SDS < CMC (0.008 % (w/w))	Ratio S:AS*1:3 S = 391.85		
4	SDS 0.5% (w/w)	Ratio S:AS*1:3 S = 150.51		

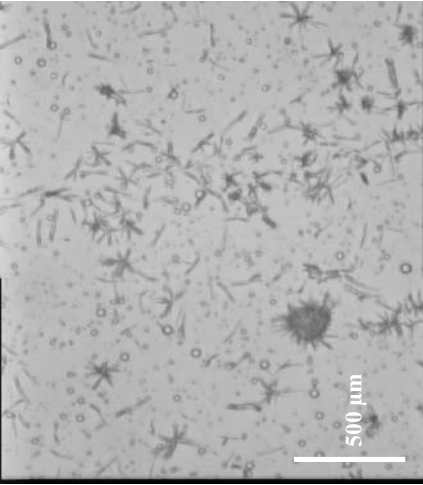
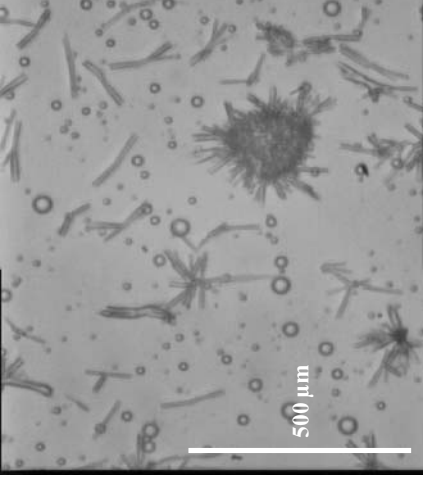
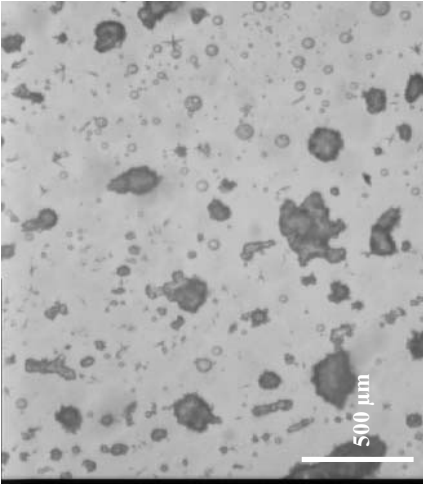
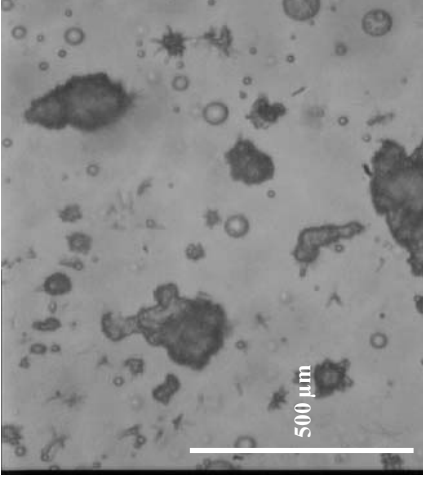
Exp	Additive	Experimental conditions	Microscopic image	
			20x	40x
5	Tween 20<CMC (0.008 % (w/w))	Ratio S:AS*1:3 S = 541.13		
				
6	Tween 20 0.5% (w/w)	Ratio S:AS*1:3 S = 398.72		

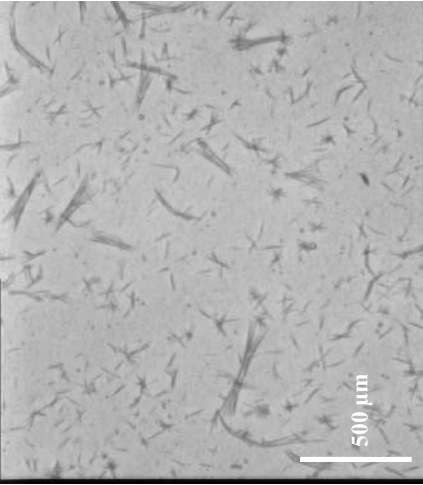
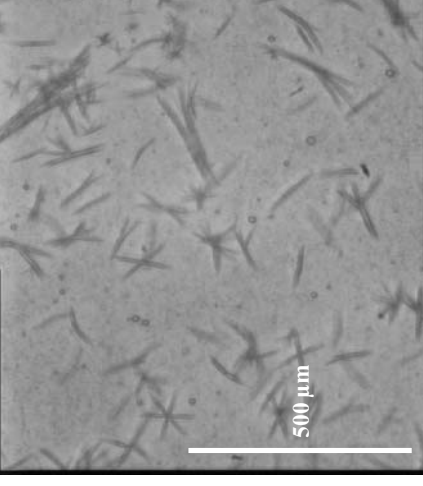
Exp	Additive	Experimental conditions	Microscopic image 20x	Microscopic image 40x
7	Chitosan 0.5% (w/w)	Ratio S:AS*1:3 S = x		

*S: solvent x: data not determined

AS: anti-solvent

Additive in organic phase

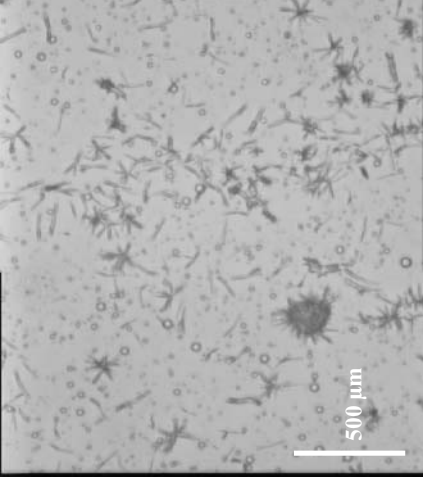
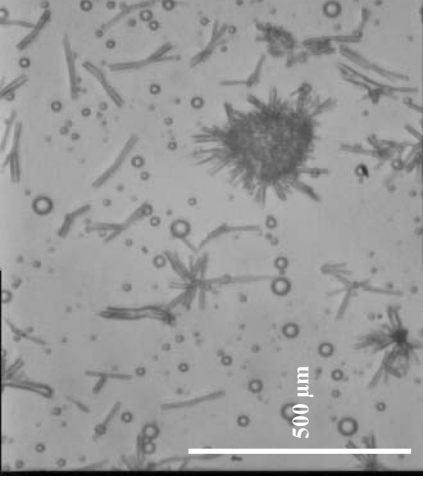
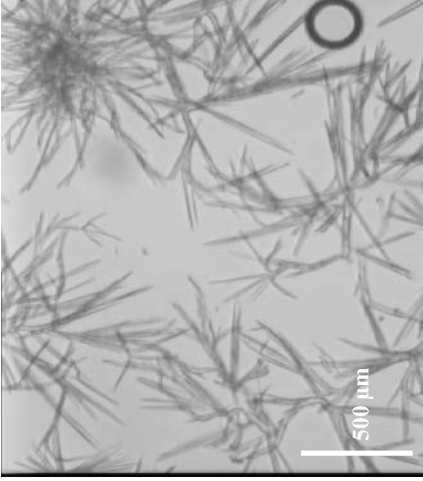
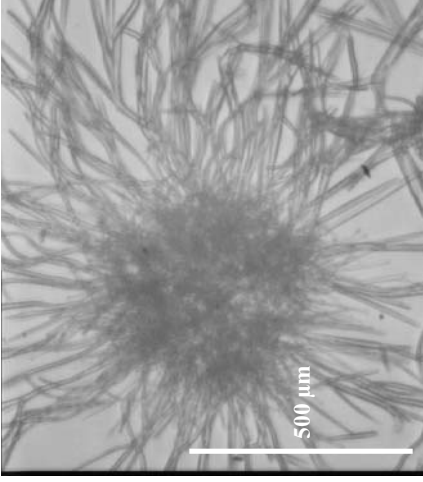
Exp	Additive	Experimental conditions	Microscopic image 20x	Microscopic image 40x
1	X	Ratio S:AS*1:3 S = 894.04		
8	P-407<CMC (0.0003%(w/w))	Ratio S:AS*1:3 S = 901.97		

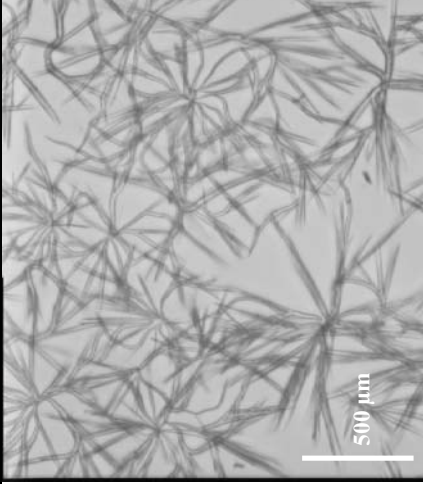
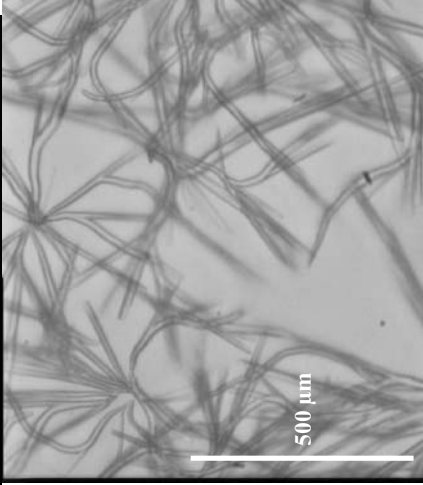
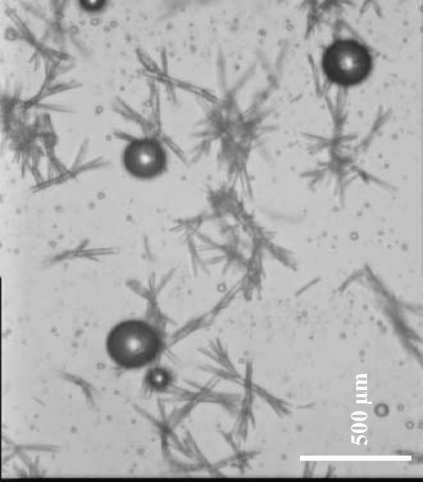
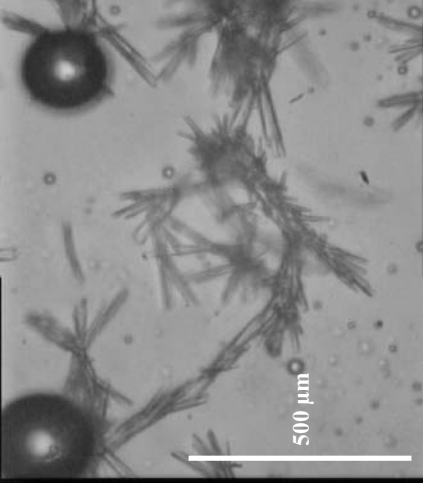
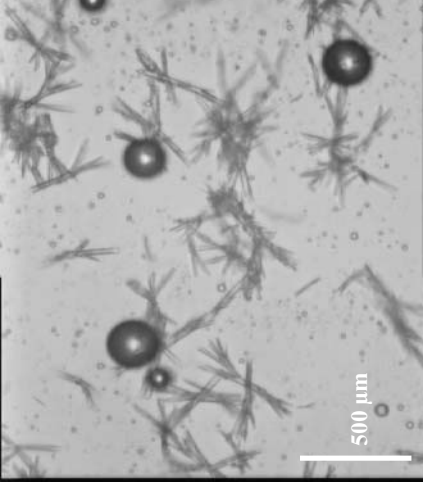
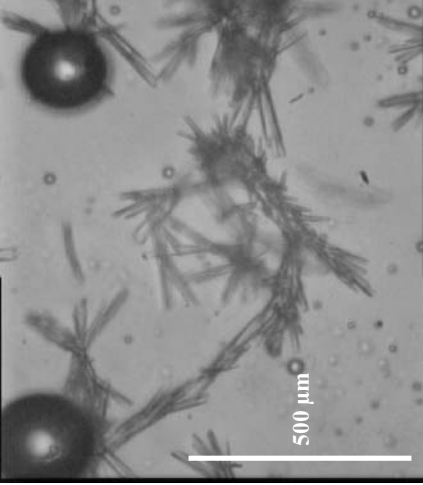
Exp d	Additive	Experimental conditions	Microscopic image 20x	Microscopic image 40x
9	P407>CMC (0.02% (w/w))	Ratio S:AS*1:3 S = 673.40		

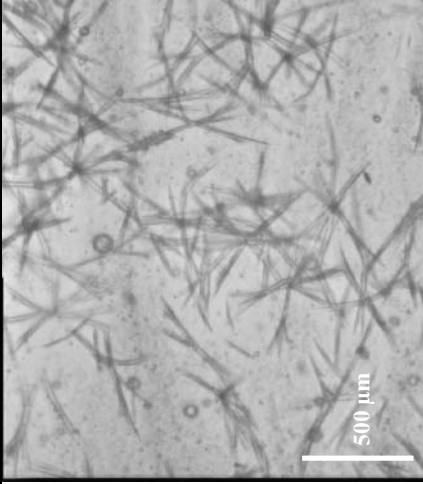
*S: solvent

AS: anti-solvent

Additif in both, organic and aqueous phases

Exp	Additive	Experimental conditions	Microscopic image 20x	Microscopic image 40x
1	X	Ratio S:AS*1:3 S = 894.04		
10	P-407<CMC (0.0003%(w/w)) +SDS 0.5% (w/w)	Ratio S:AS*1:3 S = 217.11		

Exp	Additive	Experimental conditions	Microscopic image	
			20x	40x
11	P-407>CMC (0.02% (w/w))+ SDS 0.5% (w/w)	Ratio S:AS*1:3 S = 194.93		
				
12	P-407<CMC (0.0003%(w/w)) +Chitosan 0.5% (w/w)	Ratio S:AS*1:3 S = x		

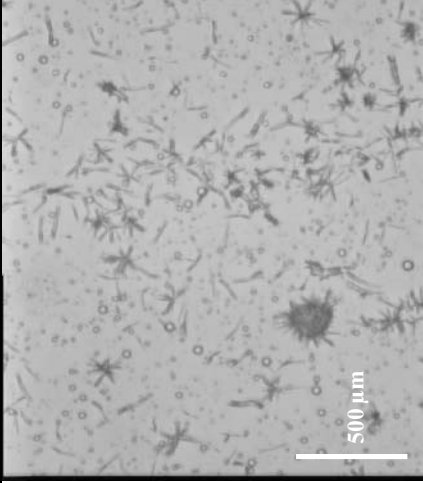
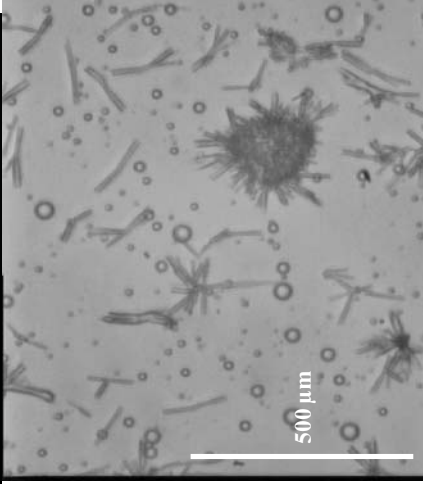
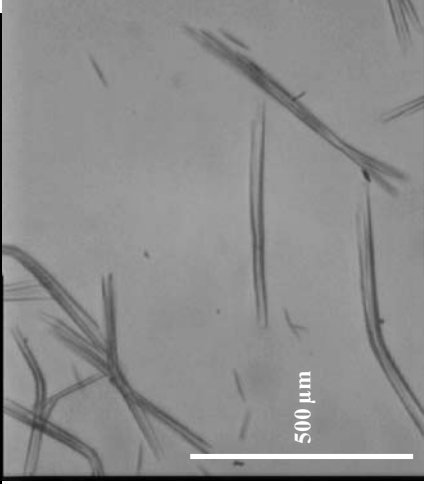
Exp	Additive	Experimental conditions	Microscopic image 20x	Microscopic image 40x
13	P-407>CMC (0.02% (w/w)) +Chitosan 0.5% (w/w)	Ratio S:AS*1:3 S = x		

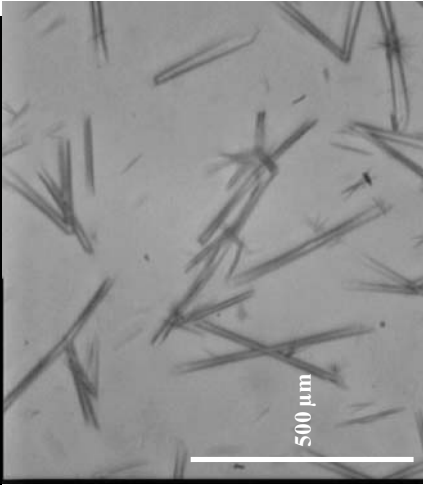
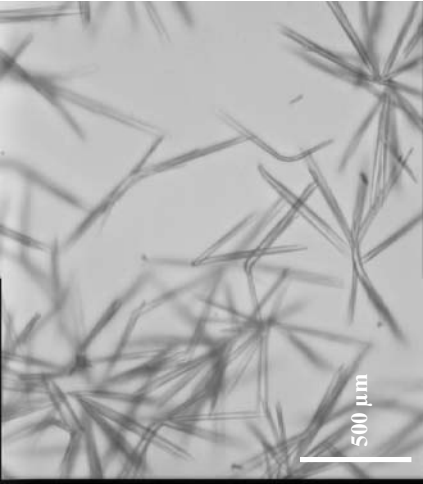
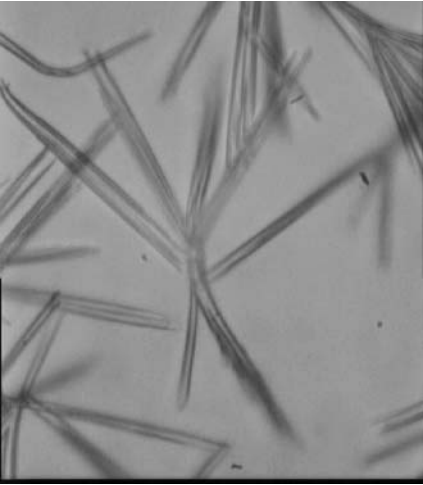
*S: solvent

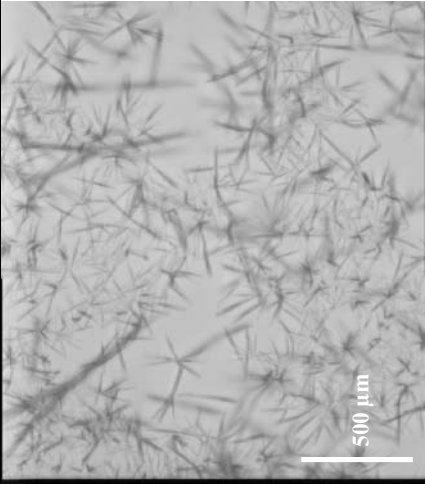
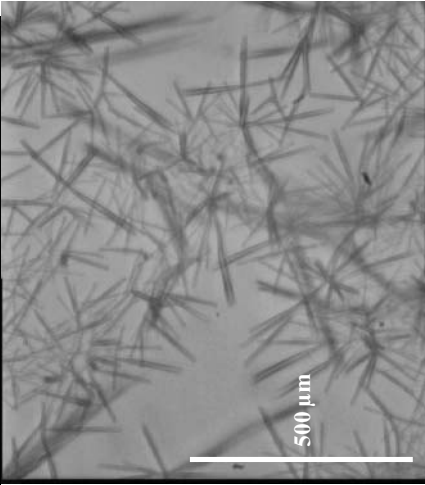
x: data not determined

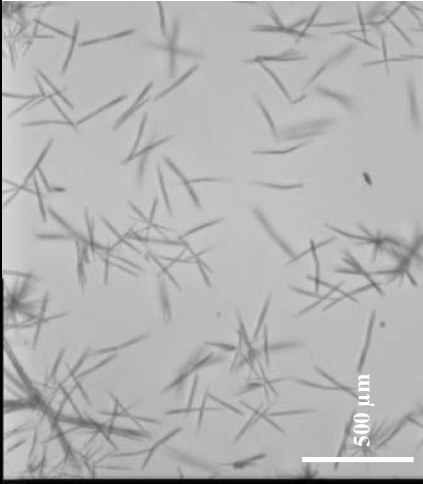
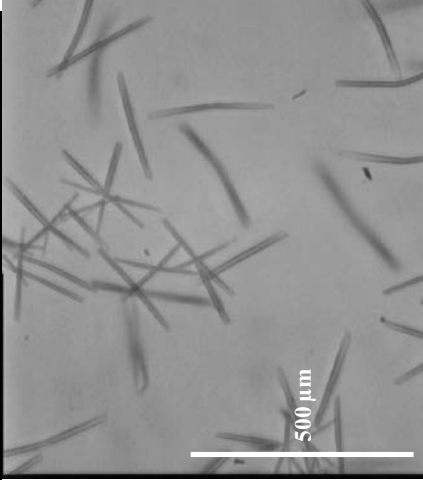
AS: anti-solvent

Supersaturation degree

Exp	Additive	Experimental conditions	Microscopic image 20x	Microscopic image 40x
1	X	Ratio S:AS*1:3 S = 894.04		
14	P-407>CMC (0.02%(w/w))	Ratio S:AS*1:3 S = 374.51		

Exp	Additive	Experimental condition	Microscopic image 20x	Microscopic image 40x
15	P-407>CMC (0.02%(w/w))	Ratio S:AS*1:3 S = 156.41		
16	P-407>CMC (0.02%(w/w)) + SDS 0.5% (w/w)	Ratio S:AS*1:3 S = 104.50		

Exp	Additive	Experimental conditions	Microscopic image 20x	Microscopic image 40x
17	P-407>CMC (0.02%(w/w)) +SDS0.5% (w/w)	Ratio S:AS*1:3 S = 43.25		
18	P-407>CMC (0.02%(w/w)) +Chitosan 0.5% (w/w)	Ratio S:AS*1:3 S = 50 % CI		

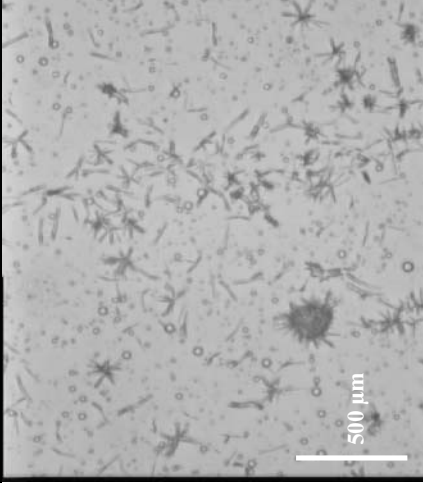
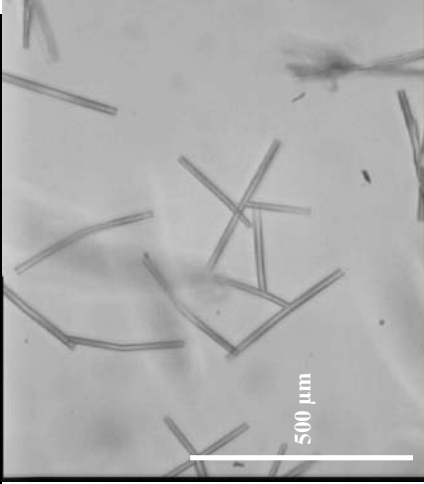
Exp	Additive	Experimental conditions	Microscopic image 20x	Microscopic image 40x
19	P-407>CMC (0.02%(w/w)) +Chitosan 0.5% (w/w)	Ratio S:AS*1:3 S = 20% CI		

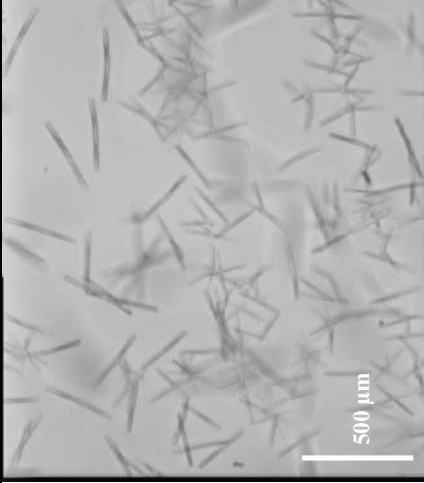
*S: solvent

CI: initial concentration

AS: anti-solvent

Re-structured organic phase containing P-407

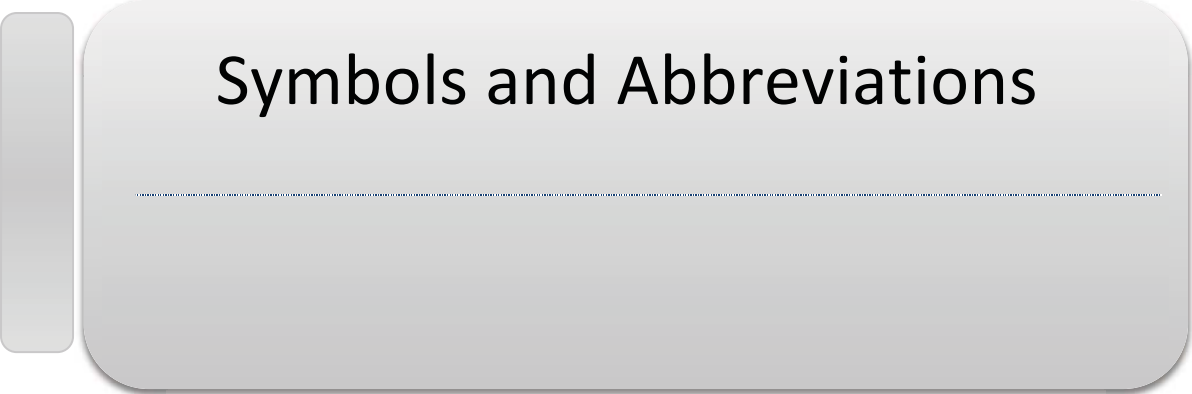
Exp	Additive	Experimental conditions	Microscopic image 20x	Microscopic image 40x
1	X	Ratio S:AS*1:3 S = 894.04		
20	P-407 < CMC (0.0003%(w/w))	Ratio S:AS*1:3 S = 77.59		

Exp	Additive	Experimental conditions	Microscopic image 20x	Microscopic image 40x
21	P-407<CMC (0.0003%(w/w)) +Chitosan 0.5% (w/w)	Ratio S:AS* 1:3 S = x		

*S: solvent

x: data not determined

AS: anti-solvent



Symbols and Abbreviations

List of Abbreviations

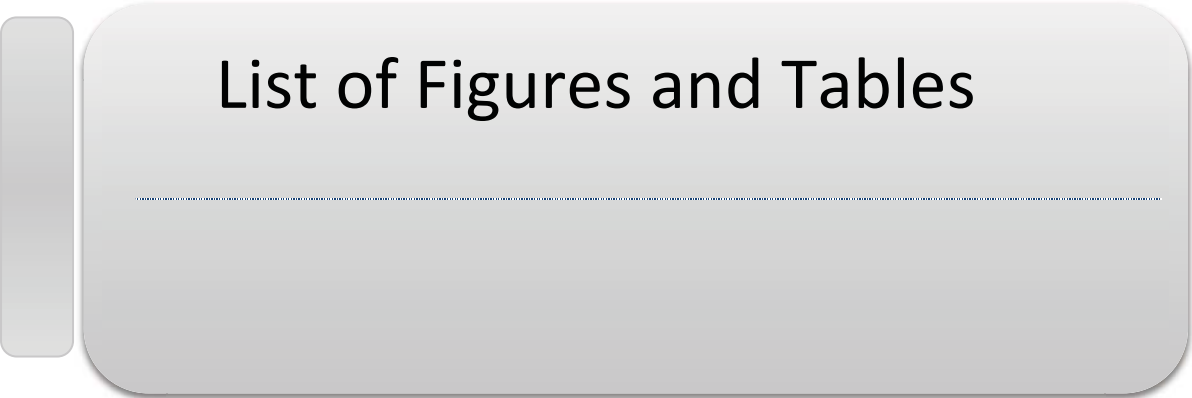
LAS	Liquid Anti-Solvent
API	Active Pharmaceutical Ingredient
GI	Gastrointestinal
BCS	Biopharmaceutical Classification System
FDA	Food and Drug Administration
CD	Cyclodextrin
CMC	Critical Miscellar Concentration
HPH	High Pressure Homogenization
CSTR	Continuous Stirring Tank Reactor
SDS	Sodium dodecyl sulfate
HPC	Hydroxypropyl Cellulose
HPMC	Hydroxypropyl methyl cellulose
PS _{1k-b} -PEO _{3k}	1000 M _w polystyrene-block-3000 M _w polyethylene oxide
PVP	Polyvinylpyrrolidone
MeOH	Methanol
EtOH	Ethanol
ACN	Acetonitrile
PEG	Polyethylene glycol
DMSO	Dimethylsulfoxide
P-407	Poloxamer 407
P-188	Poloxamer 188

TEA	Triethanolamine
Tween	Polyoxyethylene sorbitan monooleate
PVA	Polyvinyl alcohol
NaOH	Sodium Hydroxide
HCl	Hydrochloric acid
PLGA	poly(lactic-co-glycolic acid)
C_{real}	Concentration after dilution
PCS	photon correlation spectroscopy
STD	Standard deviation
J	Nucleation rate
S	Supersaturation ratio
T	Temperature
C	Concentration
C_{eq}	Solubility
S'	supersaturation of solution
Abs	Absorbance
PMT	Promethazine hydrochloride
IMP	Imprimine chloride
APS	Average Particle Size

List of Symbols

γ	Activity coefficient
R_k	Volume parameter
Q_k	Area parameter
$a_{\text{CRS 74 solute}}$	Activity of the solute CRS 74 I liquid phase
$x_{\text{CRS 74 solute}}$	Molar fraction of the solute at saturation
$\gamma_{\text{CRS 74 solute}}$	Activity coefficient of the solute
f_{min}	Minimized function
τ	Residence time
Re	Reynolds number
E_D	Energy dissipation
Q	Volume flow rate
ρ	Density of the mixture
u	Velocity of the flow of the mixture
\dot{Q}	Flow rate of the mixture
D	Diameter of the outlet tube
μ	Viscosity of the mixture
A	Cross sectional area of the outlet tube
f	Friction factor
\bar{C}	Average concentration
V	Velocity of the fluid at the tube
R_t	Percentage of drug dissolved at each time for Reference product

T_t	Percentage of drug dissolved at each time for test products
W_a	Work of adhesion
W_{CL}	Work of cohesion
λ_{LS}	Spreading coefficient
γ	Surface free energy
w	Watt
f_1	Difference factor
f_2	Similarity factor
$T_{m(\text{onset})}$	Peak onset melting temperature (thermal analysis)
$T_{c(\text{onset})}$	Peak onset crystallization temperature (thermal analysis)
$\Delta H_f, \Delta H_m$	Heat of fusion, melting



List of Figures and Tables

List of Figures

Figure 1.1. Anatomy of digestive tract (Modified from MARTINEZ et al., 2002)	27
Figure 1.2. Parameters limiting absorption of drugs taken orally (Adapted from ENGMAN, 2003).....	29
Figure 1.3. Energy diagram of the dissolution of a solid phase (Adapted from BERGESE, 2003).....	31
Figure 1.4. Dissolution of a single particle in a large volume of solvent - Model of Nernst (Adapted from BERGESE, 2003)	32
Figure 1.5. Features of size reduction: 1. Increased dissolution velocity due to increased surface area; 2. Increased saturation solubility due to increased dissolution pressure of strongly curved small nanocrystals (upper); 3. Increased adhesiveness of reduced material due to increased contact area of small versus large particles (Modified from MÜLLER et al., 2011)	37
Figure 1.6. Strategies to increase the amount of dissolved drug at the absorption site (Modified from LAKSHMI et al., 2012).....	38
Figure 1.7. Schematic illustration of the association of free cyclodextrin (CD) and drug to form drug-CD complexes and a truncated cone structure of CD (Modified from : DEL VALLE, 2004)	41
Figure 1.8. Schematic representations of Cds (a) α - CD, (b) β -CD, (c) γ -CD. Containing 6,7 and 8 glucopyranoside units, respectively (MORIN-CRINI and CRINI, 2012).....	41
Figure 1.9. Schematic representation of a hydrophobically assembled polymer micelle. The hydrophobic core loading lipophilic drugs is protected from the environment by the hydrophilic shell (KIM et al., 2010).....	43
Figure 1.10. Possible solid forms of a drug cocrystal (Modified from ALHALAWEH, 2012)	44
Figure 1.11. Amorphous solid dispersion (From GHASTE et al., 2009).	45
Figure 1.12. Schematic representation of ‘bottom up’ and top down’ technology approaches for ultra-fine particles production (micro- or nanometric scale of particle size), (Modified from FLORENCE and KONSTANTIN, 2010).....	46
Figure 1.13. Particle size reduction by milling of drug particles between moving pearls	47

Figure 1.14. Basic homogenization principles: piston-gap (left) and jet-stream arrangement (right) (Adapted from SIVASANKAR and KUMAR, 2010)	48
Figure 1.15. Approach for drug particle formation by LAS crystallization.....	50
Figure 1.16. Schematic representation of the different steps involved in drug particle formation by an LAS crystallization process (Adapted from MENG, 2011)	50
Figure 1.17. The solubility/ supersolubility phase diagram (Modified from DAVEY and GARSIDE, 2000)	52
Figure 1.18. Various kinds of nucleation (Modified from MARSMANN et al., 2001)	54
Figure 1.19. A three-dimensional crystal surface showing three type of growth sites and different steps (I, II and II*) involved in the process of growth to unit cubic (Modified from MERSMANN, 2001)	55
Figure 1.20. Feeding configuration for anti-solvent crystallization (a) single-jet, (c) double-jet with premixing	74
Figure 1.21. Schematics of mixing devices used in chemical and pharmaceutical field (Modified from THORAT and DALVI, 2012)	75
Figure 1.22. Schematic diagram showing the mechanism of growth inhibition and habit modification of crystals by polymers (Modified from RAGHAVAN et al., 2001)	82
Figure 1.23. Types of colloidal stabilization (Modified from WU et al., 2011)	83
Figure 1.24. Schematic illustration of adsorbed polymer layer (From NYLANDE et al., 2006)	84
Figure 1.25. Different conformations of polymers at surfaces: (a) mushrooms conformation of a single adsorbed, where chains are non-interacting on the surface and achieve a size given by the polymer (b) semi-brush where crowding among chains causes extension of the chain from the surface, and (c) brush conformation for high grafting densities, leading to extension of the chains away from the surface (Modified from .J. BUDIJONO et al., 2010)	85
Figure 2.1. Chemical structures of (a) CRS 74 and (b) Ritonavir	95
Figure 2.2. Schematic synthesis of CRS 74 (BOCKELMANN et al., 2005; BOCKELMANN et al., 2010).....	96
Figure 2.3. Schematic diagram of Apparatus II (Paddle Apparatus):D: vessel diameter; h: paddle width, c: distance between the paddle and the vessel bottom, H: liquid height into the vessel	104

Figure 2.4. Schematic representation of a High Performance Liquid Chromatography system	105
Figure 2.5. Experimental setup for solubility measurements	108
Figure 2.6. Particle size distribution for as-received CRS 74 powder sample	109
Figure 2.7. SEM micrographs of the original CRS 74	110
Figure 2.8. X-Ray diffractograms of the as-received CRS 74 sample	111
Figure 2.9. TGA-DSC curve of CRS 74 run in a nitrogen atmosphere and heating rate of 10°C/min	112
Figure 2.10. DSC thermograms of as-received CRS 74 sample (first heating), which consists of a melting endotherm (peak onset temperature) $T_{m(\text{Onset})} = 188.6^{\circ}\text{C}$	113
Figure 2.11. Contact angle ($^{\circ}$) of water as a function of time for original CRS 74.....	114
Figure 2.12. Specific test for CRS 74 in dissolution medium (0.1M HCl); (a) HPLC chromatograms of placebo (dissolution medium); (b) HPLC chromatograms of the component of interest dissolved in the dissolution medium. Flow rate of 1.0 ml/min; mobile phase consisted of acetonitrile:water (50:50).....	117
Figure 2.13. Standard curve used for the determination of CRS 74 in samples produced during dissolution experiments.....	118
Figure 2.14. HPLC chromatograms of the component of interest dissolved in (a) water and (b) phosphate buffer pH 6.8	120
Figure 2.15. Dissolution profile of CRS 74 in 0.1 M HCl at 37°C (n=4; SD =±2)	121
Figure 2.16. Application of Hixson-Crowell mathematical model on CRS 74 release profile	122
Figure 3.1. Schematic of the experimental apparatus used for the LAS crystallization experiments	132
Figure 3.2. Sketch of the mixers used:(a)Roughton mixer, (b) T-mixer.....	133
Figure 3.3. Sketch of particle size analysis for particles in suspension by PCS and laser granulometry	134
Figure 3.4. Experimental (characters) and calculated CRS 74 solubilities (—) in different ethanol-water mixtures at $30 \pm 0.5^{\circ}\text{C}$	142
Figure 3.5. Theoretical yield of CRIS074 in different ethanol/(ethanol-water) mass ratios .	144

Figure 3.6. Particle size distributions by laser granulometry for Roughton mixer at $t_0 = 0$ min and $t_f = 10$ min at total flow rate of 44.51 g/min and ethanol-water ratio of 25-75 % (w/w)	152
Figure 3.7. Particle size distribution by laser granulometry for T-mixer at $t_0 = 0$ min and $t_f = 10$ min at total flow rate of 44.51 g/min and ethanol-water ratio of 25-75 % (w/w)	153
Figure 3.8. Particle size distribution by laser granulometry for T-mixer at total flow rate of 27.09 g/min and ethanol-water ratio of 25-75 % (w/w), at $t_0 = 0$ min and $t_f = 10$ min	156
Figure 3.9. Particle size distribution by laser granulometry for T-mixer at total flow rate of 44.51 g/min and ethanol-water ratio of 25-75 % (w/w), at $t_0 = 0$ min and $t_f = 10$ min	157
Figure 3.10. Particle size distribution by laser granulometry for T-mixer at total flow rate of 69.56 g/min and ethanol-water ratio of 25-75 % (w/w), at $t_0 = 0$ min and $t_f = 10$ min	158
Figure 3.11. Blockage and affixation of CRS 74 crystals on surface of the T-mixer	159
Figure 3.12. Particle size (laser diffraction data) of CRS 74, before and after the LAS recrystallization process	165
Figure 3.13. SEM micrographs of the original (a,b) and LAS recrystallized CRS 74 (c,d)	166
Figure 3.14. X-Ray diffractograms of the original and LAS recrystallized drug powders	167
Figure 3.15. a) DSC thermograms of original CRS 74 (first heating), which consists of a melting endotherm (peak onset temperature $T_{m(\text{Onset})} = 188.64^\circ\text{C}$) and LAS recrystallized drug, which consists of a melting endotherm (peak onset temperature $T_{m(\text{Onset})} = 187.79^\circ\text{C}$); b) DSC thermograms of original CRS 74 (cooling after first heating), which consists of a crystallization exotherm (peak onset temperature $T_{c(\text{Onset})} = 132.12^\circ\text{C}$) and LAS recrystallized drug, which consists of a crystallization exotherm (peak onset temperature $T_{c(\text{Onset})} = 138.43^\circ\text{C}$)	168
Figure 3.16. Dissolution profiles of CRS 74, before and after LAS recrystallization (in 0.1 M HCl at 37°C , $n = 4$)	170
Figure 3.17. Contact angle ($^\circ$) of water as a function of time for: a) original CRS 74; b) LAS recrystallized drug	172
Figure 4.1. Variation in physical properties of surfactant solutions below and above the CMC value (from Laurier et al, 2003)	182
Figure 4.2. Particle size analysis using Zetasizer Nano Zs (particles in suspension) and MasterSizer 3000 (dried powders)	187
Figure 4.3. CRS 74 solubility in ethanol-water mixture (1:3) at 30°C , in presence of different additives	189

Figure 4.4. Particle size of the drug powders synthesized in presence of additives in the aqueous phase (laser diffraction data).....	194
Figure 4.5. X-Ray diffractograms of the drug powders synthesized with additives in the aqueous phase: a) HPMC 0.5% (w/w); b) Tween 20 <CMC and 0.5% (w/w); c) SDS<CMC and 0.5% (w/w); d) Chitosan 0.5% (w/w).....	195
Figure 4.6. Particle size of the drug powders synthesized in presence of P-407 in the organic phase.....	202
Figure 4.7. X-Ray diffractograms of the drug powders synthesized in presence of P-407 in the organic phase.....	202
Figure 4.8. Particle size (laser diffraction data) of the drug powders synthesized in presence of additives in both, organic and aqueous phases.....	206
Figure 4.9. X-Ray diffractograms of drug powders produced with additives in organic phase: a) P-407/SDS; b) P-407/Chitosan.	207
Figure 4.10. Particle size (laser diffraction data) of the drug powders synthesized in presence of additives in organic phase and in both (organic and aqueous) at different supersaturation degrees.....	211
Figure 4.11. X-Ray diffractograms of the drug powders synthesized in presence of additives in organic phase and in both (organic and aqueous) at different supersaturation degrees: a) P-407; b) P-407/SDS 07; c) P-407/Chitosan	212
Figure 4.12 Molecular Structure of Promethazine hydrochloride (PMT) and Imprimine chloride (IMP).....	217
Figure 4.13. Chemical structure of CRS 74	217
Figure 4.14. Diameter of drug micelles in ethanol as a function of drug concentration (PCS measurements).	218
Figure 4.15. Illustration of the effect of increasing concentration of drug in ethanolic media leading to a micellar organisation	219
Figure 4.16. Possible schematic representation of drug self-assembled at molecular level in ethanolic solution	219
Figure 4.17. The charge interaction between the negatively (a) and positively (b) charged CRS 74 nanocrystals and the negatively surface charged stainless steel (pH in the range 3-5)	223
Figure 4.18. Solubility of CRS 74 samples in HCl 0.1M at 37°C (samples recrystallized in presence of different additives; original drug also presented for comparison).....	225

Figure 4.19. Dissolution profiles using 0.1M HCl as discriminatory dissolution medium at 37°C and paddle at 75 rpm. LAS recrystallized drug in presence of additive. Original CRS 74 also included	226
Figure 4.20. A linear plot for the dissolution data of CRS 74 powder samples in accordance with the first-order model equation	229
Figure 4.21. A linear plot for the dissolution data of CRS 74 powder samples in accordance with the Hixson-Crowell cube root law	229
Figure 4.22. a) DSC thermograms of original CRS 74 (first heating), which consists of a melting endotherm (peak onset temperature $T_{m(\text{Onset})} = 188.64^{\circ}\text{C}$) and LAS recrystallized drug, which consists of a melting endotherm (peak onset temperature $T_{m(\text{Onset})} = 187.79^{\circ}\text{C}$); b) DSC thermograms of original CRS 74 (cooling after first heating), which consists of a crystallization exotherm (peak onset temperature $T_{c(\text{Onset})} = 132.12^{\circ}\text{C}$) and LAS recrystallized drug, which consists of a crystallization exotherm (peak onset temperature $T_{c(\text{Onset})} = 138.43^{\circ}\text{C}$). c) DSC thermograms of original CRS 74 (first heating), and LAS recrystallized drug in presence of P-407>CMC, which consists of a melting endotherm (peak onset temperature $T_{m(\text{Onset})} = 189.01^{\circ}\text{C}$); d) DSC thermograms of original CRS 74 (cooling after first heating), and LAS recrystallized drug in presence of P-407>CMC, which consists of a crystallization exotherm (peak onset temperature $T_{c(\text{Onset})} = 137.61^{\circ}\text{C}$); e) DSC thermograms of original CRS 74 (first heating) and LAS recrystallized drug in presence of P-407>CMC+Chitosan 0.5% (w/w), which consists of a melting endotherm (peak onset temperature $T_{m(\text{Onset})} = 186.58^{\circ}\text{C}$); f) DSC thermograms of original CRS 74 (cooling after first heating) and LAS recrystallized drug in presence of P-407>CMC+Chitosan 0.5% (w/w), which consists of a crystallization exotherm (peak onset temperature $T_{c(\text{onset})}=136.21^{\circ}\text{C}$)	232

List of Tables

Table 1.1. Transit time and pH conditions along the GI tract (MARTINEZ et al., 2002)	28
Table 1.2. Biopharmaceutical Classification System according to AMIDON (1995).....	29
Table 1.3. Particle size distribution of pharmaceuticals with respect to dosage form and route of administration (SHEKUNOV et al., 2007)	57
Table 1.4. Classification of common crystal morphologies for pharmaceutical solids accepted by the US Pharmacopoeia	58
Table 1.5. The most important solid-state characteristics, which are affected by crystallization, and the influence of these properties on the stability and downstream processing of pharmaceutical materials. (Modified from SHEKUNOV and YORK, 2000)...	59
Table 1.6. Obtention of drug crystals by LAS precipitation method.	61
Table 1.7. Summary of mixing intensification reports using mixing devices for LAS drug crystallization. (Modified from THORAT and DALVI, 2012)	76
Table 2.1. Physicochemical properties of Ritonavir and its analogous compound CRS 74 ...	97
Table 2.2. Solubility of Ritonavir polymorphs at 5°C in hydroalcoholic solvent systems (CHEMBURKAR et al., 2000)	98
Table 2.3. Different HPLC parameters tested during the HPLC method development.....	107
Table 2.4. Melting Temperature ($T_{m(\text{Onset})}$), Enthalpy of fusion (ΔH_m) for as-received CRS74 sample.....	113
Table 2.5. Work of adhesion (W_A), work of cohesion (W_{CL}) and spreading coefficient (λ_{LS}) for CRS 74.....	115
Table 2.6. Values of k and regression equations for the mathematical models of Hixson-Crowell applied to the CRS 74 dissolution data.	122
Table 3.1. Solubility of CRS 74 in ethanol as function of sample time in temperature range (5-30°C)	137
Table 3.2. Solubility of CRS 74 in 95% (w/w) water - 5% (w/w) ethanol mixture as function of sample time in temperature range (5-30°C).....	138
Table 3.3. Solubility of CRS 74 in Ethanol/water mixtures at 30 °C	139

Table 3.4. Parameter R_k and Q_k	140
Table 3.5. Binary interaction parameters	141
Table 3.6. Experimental and calculated activity coefficients for ethanol/CRS 74 and ethanol/water/CRS 74	143
Table 3.7. Solubility of CRS 74 in pure ethanol at different temperatures.....	143
Table 3.8. Experimental LAS crystallization process conditions	146
Table 3.9. Density (ρ) and viscosity (μ) of ethanol/water mixtures at 30°C (KHATTAB et al., 2012).....	148
Table 3.10. Calculated mixers parameters for: Roughton mixer (a) and T-mixer (b)	148
Tabela 3.11. Evolution of crystallized particle size by PCS in different mixers, Roughton mixer (a) and T-mixer (b) at total flow rate of 44.51 g/min and ratio ethanol:water 1:3.....	150
Table 3.12. Crystals at $t_f=10$ min in suspension observed by optical microscopy	151
Table 3.13. Evolution of crystallized particle growth by PCS in different total flow rate: a) 27.09 g/min; b) 44.51 g/min; c) 69.56 g/min and ethanol-water ratio of 25-75 % (w/w).....	155
Table 3.14. Experimental LAS crystallization process conditions	160
Table 3.15. Particle size distribution by PCS: $S = 894.04$ and $S = 15.4$	161
Table 3.16. Identification and characterization of dried powder regarding solid state properties	163
Table 3.17. Melting Temperature ($T_{m(\text{Onset})}$), Heat of Fusion (Δh_m) for the original and LAS recrystallized drug	169
Table 3.18. Work of adhesion (W_A), cohesion (W_{CL}) and spreading coefficient (λ_{LS}) for CRS 74.....	173
Table 4.1. Different additives used in LAS crystallization of CRS 74	183
Table 4.2. Critical micelle concentration in water of additives used in LAS crystallization at 25°C.	184
Table 4.3. Experimental conditions for LAS crystallization in presence of additive	185
Table 4.4. CRS 74 solubility in ethanol-water mixture (ratio 1:3) at 30°C	189
Table 4.5. Theoretical and Practical Yield (%) of CRS 74 crystals obtained by LAS crystallization process	191

Table 4.6. Initial average particle size (APS) and characteristics of CRS 74 crystals in suspension in presence of different additives in the aqueous phase	192
Table 4.7. Summary of some properties of the dried powder obtained at the end of the LAS crystallization process e.g., particle size, SEM images and contact angle.....	197
Table 4.8. Initial average particle size (APS) and characteristics of CRS 74 crystals in suspension in presence of P-407 in the organic phase	201
Table 4.9. Identification and characterization of dried powder regarding solid state properties	203
Table 4.10. Initial average particle size (APS) of CRS 74 crystals in suspension in presence of additives in both, aqueous and organic phases.	206
Table 4.11. Identification and characterization of dried powder regarding solid state properties	208
Table 4.12. Initial particle size average (APS) of the CRS 74 crystals in suspension in presence of different stabilizing systems into internal phase and external phase in different supersaturations.	210
Table 4.13. Identification and characterization of dried powder regarding solid state properties	213
Table 4.14. Initial average particle diameter (APD) of CRS 74 nanocrystals during LAS crystallization, in presence of P-407 in organic phase, which was concentrated by rotary evaporation	220
Table 4.15. Identification and characterization of dried powder regarding solid state properties	221
Table 4.16. Stabilizing agents studied to solve the T-mixer blockage problem	222
Table 4.17. Initial average particle size (APS) of the nanosuspensions and characteristics of CRS 74 nanocrystals in suspension.....	223
Table 4.18. CRS 74 solubility and synthesized powders solubility in HCl 0.1M at 37°C.....	225
Table 4.19. Comparison of dissolution profiles through the difference factor (f1) and the similarity factor (f2). Original CRS 74 is the reference product for test	227
Table 4.20. Percentage of drug dissolved within the first 20 min.....	227
Table 4.21. Release parameters of CRS 74 powder samples recrystallized in presence of additives in comparison to original drug sample.	230

Table 4.22. Melting Temperature ($T_{m(\text{Onset})}$), Heat of Fusion (ΔH_f) for the original and LAS recrystallized drug in presence and absence of additives..... 231

REFERENCES

ABBAS, A; A. LICHTMAN, AND J. POBER. Cellular and Molecular Immunology. W.B. Saunders: Philadelphia. 2000.

ABDOU M.H. *Dissolution Bioavailability & Bioequivalence*. Easton : Mack Publishing Company. 554p, 1989.

AHFAT N. M., BUCKTON G., BURROWS R., TICEHURST M. D. An exploration of interrelationships between contact angle, inverse phase gas chromatography and triboelectric charging data. *European Journal of Pharmaceutical Sciences*. 9, 271–276, 2000.

AHFAT N.M., BUCKTON G., BURROWSR., TICEHURST M. An exploration of interrelationships between contact angle, inverse phase gas chromatography and triboelectric charging data. *European Journal Pharmaceutical. Sciences*. 9, 271–276, 2000.

ALAM S., GHOSH G. AND DIN K. Light Scattering Studies of Amphiphilic Drugs Promethazine Hydrochloride and Imipramine Hydrochloride in Aqueous Electrolyte Solutions. *The Journal of Physical Chemistry B*. 112, 12962–12967, 2008.

ALHALAWEH A. Pharmaceutical Cocrystals (Formation Mechanisms, Solubility Behaviour and Solid-State Properties). Phd Thesis. *University of technology Luleå*, 2012.

ALI H.S.M., YORK P., ALI A.M.A., BLAGDEN N. Hydrocortisone nanosuspensions for ophthalmic delivery: a comparative study between microfluidic nanoprecipitation and wet milling. *Journal of Controlled Release*. 149, 175–81, 2011.

ALI H.S.M., YORK P., BLAGDEN N. Preparation of hydrocortisone nanosuspension through a bottom-up nanoprecipitation technique using microfluidic reactors. *International Journal of Pharmaceutics*. 375, 107–13, 2009.

ALI R., JAIN G.K., IQBAL Z., TALEGAONKAR S., PANDIT P., SULE S., MALHOTRA G., KHAR R.K., BHATNAGAR A., AHMAD F.J. Development and clinical trial of nanoatropine sulfate dry powder inhaler as a novel organophosphorous poisoning antidote. *Nanomedicine: Nanotechnology, Biology, and Medicine*. 5, 55–63, 2009.

AMIDON G.L., LENNERNÄS H., SHAH V.P., CRISON J.R. A theoretical basis for a biopharmaceutic drug classification: the correlation of in vitro drug product dissolution and in vivo bioavailability. *Pharmaceutical Research*. 12 (3), 413-20, 1995.

ATTWOOD D.; FLORENCE, A. T. *Physical Pharmacy. Surfactants*. Pharmaceutical Press. Chapter 4, pages 58-60, July 2012.

ATTWOOD, D., FLORENCE, A. T.. *Surfactants Systems: Their Chemistry, Pharmacy and Biology*; Chapman and Hall: New York, 1983.

BABA K., PUDAVAR H.E., ROY I., OHULCHANSKY T.Y., CHEN Y., PANDEY R.K., PRASAD P.N. A new method for delivering a hydrophobic drug for photodynamic therapy using pure nanocrystal form of the drug. *Molecular Pharmaceutics*. 4 (2), 289–97, 2007.

BADAWI A.A., EL-NABARAWI M.A., EL-SETOUHY D.A., ALSAMMIT S.A. Formulation and Stability Testing of Itraconazole Crystalline Nanoparticles. *American Association of Pharmaceutical Sciences – Pharmaceutical Science & Technology*. 12, 3, 2011.

BALDYGA J., BOURNE J.R., Simplification of micromixing calculations. I. Derivation and application of new model. *Chemical Engineering Journal*. 42, 83-92, 1989.

BECKMANN W. Nucleation phenomena during the crystallisation and precipitation of Abecarnil. *Journal of Crystal Growth*. 198-199, 1307-14, 1999.

BERGESE P. Pharmaceutical nano-composites generated by microwave induced diffusion (mind). *Phd thesis*. University of Brescia, 2003.

BERTZ R. J. , CHIU Y. L., NAYLOR C., LUFF K, BRUN S C. Lack of effect of gastric acid reducing agents on liponavir/ritonavir Plasma Concentrations in HIV-Infected Patients. *7th Congress on Drug Therapy in HIV Infection*. Glasgow, UK. 14-18 November 2004.

BHAKAY A., MERWADE M., BILGILI E., DAVE R.N. Novel aspects of wet milling for the production of microsuspensions and nanosuspensions of poorly watersoluble drugs. *Drug Development and Industrial Pharmacy*. 37(8), 963–76, 2011.

BHAVNA, AHMAD F.J., MITTAL G., JAIN G.K., MALHOTRA G., KHAR R.K., BHATNAGAR A. Nano-salbutamol dry powder inhalation: A new approach for treating broncho-constrictive conditions. *European Journal of Pharmaceutics and Biopharmaceutic*. 71, 282–91, 2009.

BLAGDEN N., DE MATAS M., GAVAN P.T., YORK P. Crystal engineering of active pharmaceutical ingredients to improve solubility and dissolution rates. *Advanced Drug Delivery Reviews*. 59, 617–30, 2007.

BLANCHARD J., SAWCHUK R.J., BRODIE B.B. *Principles and Perspectives in Drug Bioavailability*, Karger, Basel, 1979.

BOCKELMANN M. A., ROSATTO S. S., FUZETO C. R., VERNUCCI, T. B., BAREL D. C., OLIVEIRA K. M. G., FREITAS, M. P. Ritonavir analogous compound useful as retroviral protease inhibitor, preparation of the ritonavir analogous compound and pharmaceutical composition for the ritonavir analogous compound. *European Patent*, WO 2005/111006. November, 2005.

BOCKELMANN M. A., ROSATTO S. S., FUZETO C. R., VERNUCCI, T. B., BAREL D. C., OLIVEIRA K. M. G., FREITAS, M. P. . Ritonavir analogous compound useful as retroviral protease inhibitor, preparation of the ritonavir analogous compound and pharmaceutical composition for the ritonavir analogous compound. *United States patent* 7763733. July, 2010.

BOYLAN J. C. "Liquids" in *The Theory and Practice of Industrial Pharmacy* (Lachman, L., Lieberman, H. A., Kanig, J. L., Eds.) 460-461, Varghese Publishing House, Bombay, 1987.

BUCH P., MEYER C., LANGGUTH P. Improvement of the wettability and dissolution of fenofibrate compacts by plasma treatment. *International Journal of Pharmaceutics*. 15, 416 (1), 49-54, 2011.

BUCKTON, G. *Interfacial Phenomena in Drug Delivery and Targeting*. Harwood Academic Publishers, Switzerland, 1995.

BUDIJONO S.J., RUSS B., SAAD W., ADAMSON D.H., PRUD'HOMME R.K. Block copolymer surface coverage on nanoparticles. *Colloids and Surfaces A: Physicochemical and Engineering Aspects*. 360, 105–10, 2010.

CAPRETTO L., CHENG W., CARUGO D., KATSAMENIS O.L., HILL M., ZHANG X. Mechanism of co-nanoprecipitation of organic actives and block copolymers in a microfluidic environment. *Nanotechnology*. 23, 375602 (16pp), 2012

CHE E., ZHENG X., SUN C., CHANG D., JIANG T., WANG S. Drug nanocrystals: a state of the art formulation strategy for preparing the poorly water-soluble drugs. *Asian Journal of Pharmaceutical Sciences*. 7 (2), 85-95, 2012.

CHEN J.F., ZHANG J.Y., SHEN Z.G., ZHONG J., YUN J. Preparation and characterization of amorphous cefuroxime axetil drug nanoparticles with novel technology: high-gravity antisolvent precipitation. *Industrial & Engineering Chemistry Research*. 45 8723–7, 2006.

CHI-YUAN WU AND LESLIE Z. BENET .Predicting Drug Disposition via Application of BCS: Transport/Absorption/ Elimination Interplay and Development of a Biopharmaceutics Drug Disposition Classification System. *Pharmaceutical Research*. Vol. 22, No. 1, 2005.

CHIOU H., CHAN H.K., HENG D., PRUD'HOMME R.K., RAPER J.A. A novel production method for inhalable cyclosporine A powders by confined liquid impinging jet precipitation, *Journal of Aerosol Science*. 39, 500–9, 2008.

CHIOU W. L., RIEGELMAN S. Pharmaceutical Applications of Solid Dispersion Systems. *Journal of Pharmaceutical Sciences*. 60, 1281-302, 1971.

CHO E, CHO W, CHA KH, PARK J, KIM MS, KIM JS, PARK HJ, HWANG SJ. Enhanced dissolution of megestrol acetate microcrystals prepared by antisolvent precipitation process using hydrophilic additives. *International Journal of Pharmaceutics*. 396, 91–98, 2010.

CHO, E., CHO W., CHA K.H., PARK J., KIM M.S., KIM J.S., PARK H.J., HWANG S.J. Enhanced dissolution of megestrol acetate microcrystals prepared by antisolvent precipitation process using hydrophilic additives. *International Journal of Pharmaceutics*. 396, 91–98, 2010.

CHOI JY, YOO JY, KWAK HS, UK NAM B, LEE J. Role of Polymeric Stabilizers for Drug Nanocrystal dispersions. *Current Applied Physics*. vol 5: 472-474, 2005.

CHOI S.W., KWON H.Y., KIM W.S., KIM J.H. Thermodynamic parameters on poly(D,L-lactide-co-glycolide) particle size in emulsification–diffusion process. *Colloids and Surfaces A: Physicochemical and Engineering Aspects*. 201, 283–9, 2002.

CHONG-HUI G., KOSTUV C., YOUNG V. JR., GRANT D. J. W. Stabilization of a metastable polymorph of sulfamerazine by structurally related additives. *Journal of Crystal Growth* 235, 471–481, 2002.

CHOW A.H., TONG H.H., CHATTOPADHYAY P., SHEKUNOV B.Y. Particle engineering for pulmonary drug delivery. *Pharmaceutical Research*. 24, 411–37, 2007.

CHOWDARY K.P.R., ANNAMMA D.G.S. Enhancement of Dissolution Rate and Formulation Development of Efavirenz by Solid Dispersion in Poloxamer 407. *Journal of Pharmacy Research*. 5, 6, 2012.

CHRISTIAN LINDENBERG. Optimizing the precipitation of organic compounds. *PhD Thesis*. Swiss Federal Institute of Technology Zurich, 2009.

COSTA P. AND LOBO J.M.S. Modeling and comparison of dissolution profiles. *European Journal of Pharmaceutical Sciences*. 13, 123-133, 2001.

D’ADDIO S.M., KAFKA C., AKBULUT M., BEATTIE P., SAAD W., HERRERA M., KENNEDY M.T., PRUD’HOMME R.K. Novel method for concentrating and drying polymeric nanoparticles: hydrogen bonding coacervate precipitation. *Molecular Pharmaceutics*. 7, 557–64, 2010.

DALVI S.V., DAVE R.N. Analysis of nucleation kinetics of poorly water-soluble drugs in presence of ultrasound and hydroxypropyl methyl cellulose during antisolvent precipitation. *International Journal of Pharmaceutics*. 387, 172–9, 2010.

DALVI S.V., DAVE R.N.. Controlling particle size of a poorly water-soluble drug using ultrasound and stabilizers in antisolvent precipitation. *Industrial & Engineering Chemistry Research*. 48 (16), 7581-7593, 2009.

DANIEL J. PHILLIPS, SAMUEL R. PYGALL, V. BRETT COOPER, AND JAMES C. MANN.. Toward Biorelevant Dissolution: Application of a Biphasic Dissolution Model as a Discriminating Tool for HPMC Matrices Containing a Model BCS Class II. *Drug Dissolution Technologies*, 2012.

DAVEY R. J., GARSIDE J. *From Molecules to Crystallizers*. 26-32. Oxford Chemistry Primer, 86, Oxford University Press, U. K. 2000.

DEL VALLE E.M.M. Cyclodextrins and their uses: a review. *Process Biochemistry*. 39, 9, 31, 2004.

DERJAGUIN B.V., LANDAU L.D. Theory of the Stability of Strongly Charged Lyophobic Sols and the Adhesion of Strongly Charged Particles in Solutions of Electrolytes. *Acta Physicochimica URSS*. 14, 633-62, 1941.

DHUMAL R.S., BIRADAR S.V., YAMAMURA S., PARADKAR A.R., YORK P. Preparation of amorphous cefuroxime axetil nanoparticles by sonoprecipitation for enhancement of bioavailability. *European Journal of Pharmaceutics and Biopharmaceutics*. 70, 109–15, 2008.

DONG Y., NG W.K., HU J., SHEN S., TAN R.B.H. A continuous and highly effective static mixing process for antisolvent precipitation of nanoparticles of poorly water-soluble drugs, *International Journal of Pharmaceutics*. 386, 256–61, 2010.

DONG Y., NG W.K., SHEN S., KIM S., TAN R.B.H. Controlled antisolvent precipitation of spironolactone nanoparticles by impingement mixing. *International Journal of Pharmaceutics*. 410, 175–9, 2011.

DONG Y., NG W.K., SHEN S., KIM S., TAN R.B.H. Preparation and characterization of spiro lactone nanoparticles by antisolvent precipitation. *International Journal of Pharmaceutics*. 375, 84-88, 2009.

DOUROUMIS D., FAHR A. Nano- and micro-particulate formulations of poorly watersoluble drugs by using a novel optimized technique. *European Journal of Pharmaceutics and Biopharmaceutics*. 63, 173–5, 2006.

DOUROUMIS D., FAHR A. Stable carbamazepine colloidal systems using the cosolvent technique. *European Journal of Pharmaceutical Sciences*. 30, 5, 367–74, 2007.

DUMORTIER G., GROSSIORD J. L., AGNELY F., CHAUMEIL J.C. A review of oloxamer 407 pharmaceutical and pharmacological characteristics, *Pharmaceutical Research*. 23, 2709–28, 2006.

EERDENBRUGH B. V., SPEYBROECK M. V., MOLS R., HOUTHOOFD K., MARTENS J. A., FROYEN L., HUMBEECK J. V., AUGUSTIJNS P., MOOTER G. V. D. Itraconazole/TPGS/Aerosil®200 solid dispersions Characterization, physical stability and in vivo performance. *European Journal of Pharmaceutical Sciences* 38, 270–278, 2009.

EL-GENDY N., AILLON K.L., BERKLAND C. Dry powdered aerosols of diatrizoic acid nanoparticle agglomerates as a lung contrast agent. *International Journal of Pharmaceutics*. 391, 305–12, 2010.

EL-GENDY N., BERKLAND C. Combination Chemotherapeutic Dry Powder Aerosols via Controlled Nanoparticle Agglomeration. *Pharmaceutical Research*. 26, 7, 2009.

ENGMAN H. Intestinal barriers to oral drug absorption : Cytchrome P450 3A and ABC Transport Proteins. *PhD Thesis*. Acta Universitatis UAPSLiensis, 2003.

ENKIRCH T. Targeted lentiviral vectors pseudotyped with the Tupaia paramyxovirus glycoproteins. *PhD Thesis*. Combined Faculties for the Natural Sciences and for Mathematics of the Ruperto-Carola University of Heidelberg, Germany, 2011.

ESPITALIER F. , BISCANS B. , LAGUERIE C. Physicochemical Data on Ketoprofen in Solutions. *Journal of Chemical & Engineering Data*. 40, 1222–1224, 1995.

FDA, Food and Drug Administration- Guidance for Industry Dissolution Testing of Immediate Release Solid Oral Dosage Forms, 1997.

FDA, Food and Drug Administration-.*Guidance for Industry. Regulatory Classification of Pharmaceutical Co-Crystals*, 2011.

FLORENCE A.T., ATTWOOD D. *Physicochemical Principles of Pharmacy*. 2nd Ed., London UK: Macmillan Publishers Ltd, pp. 89-90,131-172, 199-208, 1981.

FLORENCE S., KONSTANTIN S. Nanotechnology in concrete – A review. *Construction and Building Materials*. Volume 24, Issue 11, Pages 2060–2071, 2010.

FOX, R. W.; McDONALD, A. T.; PRITCHARD, T. J. *Introduction to Fluid Mechanics*, 6th edition, 35, 2004.

FSC, *Food Safety Commission*. Evaluation Report of Food Additives-Polysorbates (Polysorbates 20, 60, 65 and 80). June, 2007.

GAREKANI H.A., SADEGHI F., BADIEE A., MOSTAFA S.A., RAJABI-SIAHBOOMI. A.R. Crystal Habit Modifications of Ibuprofen and Their Physicomechanical Characteristics. *Drug Development and Industrial Pharmacy*. Sep;27(8):80, 2001.

GARNIER S., PETIT S., COQUEREL G. Influence of supersaturation and structurally related additives on the crystal growth of alpha-lactose monohydrate. *Journal of Crystal Growth* 234, 201-19, 2002.

GARNIER S., PETIT S., COQUEREL G. Influence of supersaturation and structurally related additives on the crystal growth of alpha-lactose monohydrate. *Journal Crystal Growth*. 234, 201-19, 2002.

GASSMANN P., LIST M., Schweitzer A., SUCKER, H. Hydrosols-alternatives for the parenteral application of poorly water-soluble drugs. *European Journal of Pharmaceutics and Biopharmaceutics*. 40, 64–72, 1994.

GHASTE R., CHOUGULE D.D., SHAH R., DHANANJAY G. Solid Dispersions: An Overview. Pharmainfo-<http://www.pharmainfo.net/reviews/solid-dispersions-overview>, 2009.

GHOSH I., BOSE S., VIPPAGUNTA R., HARMON F. Nanosuspension for improving the bioavailability of a poorly soluble drug and screening of stabilizing agents to inhibit crystal growth. *International Journal of Pharmaceutics*, vol. 409, 260–268 , 2011.

GIACONA N., BAUMAN N.J., SIEPLER J.K. Crystallization of three phenytoin preparations in intravenous solutions. *American Journal of Health-System Pharmacy*. 39, 630–4, 1982.

GIBALDI M., FELDMAN S. Establishment of “sink conditions” in dissolutions rate determinations. *Journal of Pharmaceutical Sciences*. 56, 1238, 1967.

GILL P.S., Thermal analysis: developments in instrumentation and applications. *Am. Lab.* , 1984, **16**(1): p. 39. 1984.

GOWTHAMARAJAN K., SINGH S.K. Dissolution Testing for Poorly Soluble Drugs: A Continuing Perspective. *Dissolution Technologies*. pp. 24-32, August 2010.

GRAHAME D.C. The electrical double layer and the theory of electrocapillarity. *Chemical Reviews*. 41, 441–501, 1947.

GRAU M.J., KAYSER O., MULLER R.H. Nanosuspensions of poorly soluble drugs — reproducibility of small scale production. *International Journal of Pharmaceutics*. 196, 155–7, 2000.

GRIFFIN B. Advances in lipid-based formulations: Overcoming the challenges of low bioavailability for poorly water soluble drug compounds. *Am. Pharm. Rev.*, 41-47, March 2012.

GUO Z., ZHANG M., LI H., WANG L., KOUGOULOS E. Effect of ultrasound on antisolvent crystallization process. *Journal of Crystal Growth*. 273, 555–63, 2005.

HALEBLIAN J. K. Characterization of habits and crystalline modification of solids and their pharmaceutical applications. *Journal of Pharmaceutical Sciences*. 64, 1269-87, 1975.

HAN X., GHOROI C., TO D., CHEN Y., DAVÉ R. Simultaneous micronization and surface modification for improvement of flow and dissolution of drug particles. *International Journal Pharmaceutics*. Aug 30;415(1-2):185-95, 2011.

HE X, BARONE MR, MARSAC PJ, SPERRY DC. Development of a rapidly dispersing tablet of a poorly wettable compound – formulation DOE and mechanistic study of effect of formulation excipients on wetting of celecoxib. *International Journal Pharmaceutics*. 353, 176–186, 2008.

HE Y., HUANG Y., CHENG Y. Structure evolution of curcumin nanoprecipitation from a micromixer. *Crystal Growth & Design*. 10, 1021–4, 2010.

HE Y., HUANG Y., WANG W., CHENG Y. Integrating micromixer precipitation and electrospray drying toward continuous production of drug nanoparticles. *Chemical Engineering Journal*. 168, 931–7, 2011.

HERMAN R.A VENG-PEDERSEN P HOFFMAN J KOEHNKE RAND FURST D.E. Pharmacokinetics of low-dose methotrexate in rheumatoid arthritis patients. *Journal of Pharmaceutical Sciences*.78: 165–171, 1989.

HIGUCHI T., CONNORS K.A. Phase-solubility techniques. *Advances in Analytical Chemistry and Instrumentation*. 4, 117-212, 1965.

HIXSON A.W., CROWELL J.H. Dependence of reaction velocity upon surface and agitation. I. Theoretical consideration. *Industrial and Engineering Chemistry*. 23, 923–931, 1931.

HOGGARD, P. G., AND OWEN, A. The mechanisms that control intracellular penetration of the HIV protease inhibitors. *Journal of Antimicrobial Chemotherapy*, 51(3), 493-6. 1.3.2,2003.

HU J., KIONG NG, DONG Y., SHENA S., TAN R.B.H. Continuous and scalable process for water-redispersible nanoformulation of poorly aqueous soluble APIs by antisolvent precipitation and spray-drying. *International Journal of Pharmaceutics* 404, 198–204, 2011.

HU J., NG W.K., DONG Y., SHENA S., TAN R.B.H. Continuous and scalable process for water-redispersible nanoformulation of poorly aqueous soluble APIs by antisolvent precipitation and spray-drying. *International Journal of Pharmaceutics*. 404, 198–204, 2011.

HU T.T., ZHAO H., JIANG L.C., LE Y., CHEN J.F., YUN J. Engineering Pharmaceutical Fine Particles of Budesonide for Dry Powder Inhalation (DPI). *Industrial & Engineering Chemistry Research*. 47 (23), 9623–7, 2008.

ICH- INTERNATIONAL CONFERENCE ON HARMONIZATION-; *Validation of Analytical Procedures: Methodology*, 1996.

IUPAC Compendium of Chemical Terminology 2nd Edition, 1997.

IVESON S.M. , LITSTER J. D. , HAPGOOD K. , ENNIS B.J. Nucleation, growth and breakage phenomena in agitated wet granulation processes: a review. *Powder Technology*. 117, 3–39, 2001.

JINNO J., OH D.M., CRISON J.R., AMIDON G.L. Dissolution of water insoluble drugs: the combined effect of pH and surfactant. *Journal of Pharmaceutical Sciences*. 89, 268-74, 2000.

JOHNSON B.K., PRUD'HOMME R.K. Flash NanoPrecipitation of Organic Actives and Block Copolymers using a Confined Impinging Jets Mixer. *Australian Journal of Chemistry* 56(10), 1021-4, 2003.

JOUYBAN-GHARAMALEKI A. , ROMERO S. , BUSTAMANTE P. , CLARK B.J. Multiple solubility maxima of oxolinic acid in mixed solvents and a new extension of Hildebrand solubility approach. *Chemical & Pharmaceutical Bulletin (Chem Pharm Bull)*.48(2):175-8, 2000.

KAKRAN M., SHEGOKAR R., SAHOO N.G., SHAAL L.A., LI L., MÜLLER R.H. Fabrication of quercetin nanocrystals: Comparison of different methods. *European Journal of Pharmaceutics and Biopharmaceutics*. 80, 113–21, 2012.

KATHERINE BOWMAN AND KAM W LEONG. Chitosan nanoparticles for oral drug and gene delivery. *International Journal of Nanomedicine*; 1(2): 117–128, .2006 .

KEMPF, D. J.; NORBECK, D. W.; SHAM, H. L.; ZHAO, C.; SOWIN, T. J.; RENO, D. S.; HAIGHT, A. R.; COOPER, A. J.; *PCT Int. Appl.* WO 94/14436, 1994.

KHATTAB, I. S.; BARDANKAR, F.; FAKHREE, M. A. A.; JOUYBAN, A. Density, viscosity, and surface tension of water+ethanol mixtures from 293 to 323K. *Korean Journal of Chemical Engineering*, 29, 812-817, 2012.

KIM S., SHI Y., KIM J.Y., PARK K., CHENG J.K. Overcoming the barriers in micellar drug delivery: loading efficiency, in vivo stability, and micelle–cell interaction. *Expert Opinion Drug Delivery*. 7(1), 2010.

KIPP, J.E. The role of solid nanoparticle technology in the parenteral delivery of poorly water-soluble drugs. *International Journal of Pharmaceutics*. 284, 109–122, 2004.

KLINGER C., MÜLLER B.W., STECKEL H. Insulin-micro- and nanoparticles for pulmonary delivery. *International Journal of Pharmaceutics*. 377, 173–179, 2009.

KLUG D.L. in *Handbook of industrial crystallization* (Myerson, A., ed.), pp. 65-87, Butterworth-Heinemann, Boston, 1993.

KRISHNAIAH Y.S.R. Pharmaceutical Technologies for Enhancing Oral Bioavailability of Poorly Soluble Drugs. *Journal of Bioequivalence & Bioavailability*. 2, 2, 28-36, 2010.

KUBOTA N., YOKOTA M., MULLIN J.W. The combined influence of supersaturation and impurity concentration on crystal growth. *Journal of Crystal Growth*. 212, 480-8, 2000.

KUMAR S. D., SUDIPTA R., YUVARAJA K., KHANAM J., NANDA A. Solid Dispersions: An Approach to Enhance the Bioavailability of Poorly Water-Soluble Drugs. *International Journal of Pharmacology and Pharmaceutical Technology*. Pp :2277 – 3436, 2011.

KUMAR V., WANG L., RIEBE M., TUNG H.H., PRUD'HOMME R.K. Formulation and Stability of Itraconazole and Odanacatib Nanoparticles: Governing Physical Parameters. *Molecular Pharmaceutics*. 6 (4), 1118–24, 2009.

LACERA S.P., CERIZE N. N., RE M.I. Preparation and characterization of carnauba wax nanostructured lipid carriers containing benzophenone-3. *International Journal of Cosmetic Science*, 33(4):312-21, 2011.

LAHAV M., LEISEROWITZ L. The effect of solvent on crystal growth and morphology. *Chemical Engineering Science*. 56, 2245-53, 2001.

LAKSHMI M.S., KUMARI P.S., KUMAR T.R. A Novel Approach for Improvement of Solubility and Bioavailability of Poorly Soluble Drugs: Liquisolid Compact Technique. *International Journal of Research in Pharmaceutical and Biomedical Sciences*. 3, 1621-32, 2012.

LAURIER L. SCHRAMM, ELAINE N. STASIUK AND D. GERRARD MARANGONI, Surfactants and their applications. Annual Reports on the Progress of Chemistry Section. Sect. C, 99 , 3–48, 2003.

LAW DEVALINA, KRILL STEVEN L. SCHMITT ERIC A., FORT JAMES J.: YIHONG QIU, WEILI WANG, PORTER WILLIAM R. Physicochemical considerations in the preparation of amorphous ritonavir-poly(ethylene glycol) 8000 solid dispersions. *Journal of Pharmaceutical Sciences*. vol. 90, n°8, pp. 1015-1025, 2001.

LE Y., JI H., CHEN J.F., SHEN Z., YUN J., PU M. Nanosized bicalutamide and its molecular structure in solvents. *International Journal of Pharmaceutics*. 370, 175–80, 2009.

LEE J. M., SAIKIA P. J., LEE K., and CHOE S.. Mechanism of the Formation and Growth of the Cross-Linked Poly(divinylbenzene) Spheres Using Poly(styrene-block-4-vinylpyridine). *Macromolecules*. 41, 2037-2044, 2008.

LEE J.H., HWANG A K.S, JANG S.P, LEE B.H., KIM J.H., CHOI S. U.S, CHOI C.J. Effective viscosities and thermal conductivities of aqueous nanofluids containing low volume concentrations of Al₂O₃ nanoparticles. *International Journal of Heat and Mass Transfer*. 51 2651–2656, 2008.

LEE P.S., HAN J.Y., SONG T.W., SUNG J.H., KWON O.S., SONG S., CHUNG Y.B. Physicochemical characteristics and bioavailability of a novel intestinal metabolite of ginseng saponin (IH901) complexed with beta-cyclodextrin. I *International Journal of Pharmaceutics*. 19;316(1-2):29-36, 2006.

LI X.S., WANG J.X., SHEN Z.G., ZHANG P.Y., CHEN J.F., YUN J. Preparation of uniform prednisolone microcrystals by a controlled microprecipitation method. *International Journal of Pharmaceutics*. 342, 26–32, 2007.

LIDE D R. Editor. *CRC Handbook of chemistry and physics*. 79th ed. New York, N.Y: CRC Press; 1998.

LINDENBERG M., KOPP S., DRESSMAN J. B. Classification of orally administered drugs on the World Health Organization Model list of Essential Medicines according to the biopharmaceutics classification system. *European Journal of Pharmaceutics and Biopharmaceutics*. 58, 265–78, 2004.

LINDENBERG, CHRISTIAN; SCHÖLL, JOCHEN; VICUM, LARS; MAZZOTTI, MARCO; BROZIO, JÖRG. Experimental characterization and multi-scale modeling of mixing in static mixers. *Chemical Engineering Science*, 63, 4135-4149, 2008.

LINDFORS L., FORSSÉN S., WESTERGREN J., OLSSON U. Nucleation and crystal growth in supersaturated solutions of a model drug. *Journal of Colloid and Interface Science* 325, 404–13, 2008.

LIU G., ZHANG D., JIAO Y., ZHENG D., LIU Y., DUAN C., JI L., ZHANG Q., LOU H. Comparison of different methods for preparation of a stable riccardin D formulation via nanotechnology. *International Journal of Pharmaceutics*. 422, 516–22, 2012.

LIU Z., HUANG Y., JIN Y., CHENG Y. Mixing intensification by chaotic advection inside droplets for controlled nanoparticle preparation. *Microfluidics and Nanofluidics*. 9, 773–86, 2010.

LOFTSSON T., JARHO P., MÁSSON M., JÄRVINEN T. Cyclodextrins in drug delivery. *Expert opinion Drug Delivery*. 2, 335-51, 2005.

LOVELYN C., ATTAMA A. Current State of Nanoemulsions in Drug Delivery. *Journal of Biomaterials and Nanobiotechnology*, 2, 626-639, 2011.

MAHAJAN A.J., KIRWAN D.J. Micromixing effects in a two-impinging-jets precipitator, *American Institut of Chemical Engineering Journal*. 42, 1801–14, 1996.

MALMSTEN M. "Microemulsions in Pharmaceuticals," in: P. Kumar and K. L. Mittal (eds.), *Handbook of Microemulsion Science and Technology*, Marcel Dekker Inc., New York., pp. 755-71, 1999.

MANSOURI M., POURETEDAL H.R., VOSOUGHI V. Preparation and Characterization of Ibuprofen Nanoparticles by using Solvent/ Antisolvent Precipitation. *The Open Conference Proceedings Journal*. 2, 88-94, 2011.

MARTINEZ M., AMIDON G., CLARKE L., JONES W.W., MITRA A., RIVIERE J. Applying the biopharmaceutics classification system to veterinary pharmaceutical products. Part II. Physiological considerations. *Advanced Drug Delivery Review*. 4, 54(6), 825-50, 2002.

MATTEUCCI M.E., HOTZE M.A., JOHNSTON K.P., WILLIAMS R.O. Drug nanoparticles by antisolvent precipitation: mixing energy versus surfactant stabilization. *Langmuir*. 10, 22(21), 8951-9, 2006.

MATTEUCCI M.E., PAGUIO J.C., MILLER M.A., WILLIAMS III R.O., JOHNSTON K.P. Flocculated Amorphous Nanoparticles for Highly Supersaturated Solutions. *Pharmaceutical Research*. 25, 11, 2008.

MAULUDIN R. Nanosuspensions of poorly soluble drugs for oral administration. *PhD Thesis*. Faculty of Biology, Chemistry and Pharmacy of the Freie Universität Berlin , 2008.

MEENAN P.A., ANDERSON S.R., KLUG D.L. The influence of impurities and solvents on crystallization. In: Myerson AS, editor. *Handbook of industrial crystallization*. Boston: Butter-Worth-Heinemann. pp. 67–97, 2002.

MENG X. Anti-solvent precipitation and subsequent film formation of hydrophobic drugs for drug delivery. *Phd thesis*. New Jersey Institute of Technology, 2011.

MENG X., CHEN Y., CHOWDHURY S.R., YANG D., MITRA S. Stabilizing dispersions of hydrophobic drug molecules using cellulose ethers during anti-solvent synthesis of microparticulates. *Colloids and Surfaces B: Biointerfaces*. 70, 7–14, 2009.

MERISKO-LIVERSIDGE E.M., LIVERSIDGE G.G. Drug nanoparticles: formulating poorly water-soluble compounds. *Toxicologic Pathology*. 36(1), 43-48, 2008.

MERSMANN A., HEYER C., EBLE A. *Crystallization Technology Handbook*. Chapter 2- Activated Nucleation Second Edition. pp. 43, 2001.

MOHD S. A., GOUTAM G., UD-DIN K. . Amphiphilic drug persuaded collapse of polyvinylpyrrolidone and poly(ethylene glycol) chains: A dynamic light scattering study. *Colloids and surfaces. B, Biointerfaces* . vol. 75, n°2, pp. 590-594, 2010.

MOORE J.W. AND FLANNER H.H. Mathematical Comparison of curves with an emphasis on in vitro dissolution profiles. *Pharmaceutical. Technology*. 20, 64-74, 1996.

MORIN-CRINI N., CRINI G. Environmental applications of water-insoluble β -cyclodextrin–epichlorohydrin polymers. *Progress in Polymer Science*. 2012.

MORIWAKI C., COSTA G.L., FERRACINI C.N., DE MORAES F.F., ZANIN G.M., PINEDA E.A.G., MATIOLI G. Enhancement of solubility of albendazole by complexation with β -cyclodextrin. *Brazilian Journal of Chemical Engineering*. 25, 2, 255-67, 2008.

MÜLLER R. H., JACOBS C., KAYSER O. (2001) Nanosuspensions as particulate drug formulation in therapy rational for development and what we can expect for the future. *Advanced Drug Delivery Reviews* 47, pp.3-19, 2001.

MÜLLER R.H., AKKAR A. Drug nanocrystals of poorly soluble drugs, *Encyclopedia of Nanoscience and Nanotechnology*, ed. H.S. Nalwa, American Scientific Publishers, 627-38, 2004.

MURNANE D., MARIOTT C., MARTIN G.P. Developing an environmentally benign process for the production of microparticles: Amphiphilic crystallization. *European Journal of Pharmaceutics and Biopharmaceutics*. 69, 72–82, 2008.

MYERSON A.S. “Crystallization basics”, in: Myerson AS, editor. *Molecular modeling applications in crystallization*. New York: Cambridge University Press. 55–105, 1999.

MYRDAL P.B., YALKOWSKY S.H. Solubilization of Drugs in Aqueous Media. 2nd ed, *Encyclopedia of Pharmaceutical Technology*. Ed. J. Swarbrick and J.C. Boylan, Vol. 3, New York: Marcel Dekker, Inc. 2458-80, 2002.

Narang A. S., Delmarre D, Gaoc, D., Stable drug encapsulation in micelles and microemulsions, *International Journal of Pharmaceutics* Vol. 345 pp.9–25, 2007

NAPPER D.H. *Polymeric Stabilization of Colloidal Dispersions*, Academic Press, 1983.

NEAU S. H. Chapter 15: Pharmaceutical Salts- Water Insoluble Drug Formulation. Edited by Rong Liu. e-book: ISBN:978-1-4200-0955-2. Pages 417-435, 2008.

NEELAM S., PUNEET G., BHATTACHARYYA A. Enhancement of intestinal absorption of poorly absorbed Ceftriaxone Sodium by using mixed micelles of Polyoxy Ethylene (20) Cetyl Ether & Oleic Acid as peroral absorption enhancers. *Archives of Applied Science Research*, 2 (3): 131-142, 2010.

NGUYEN T. E. AND HAPGOOD N. K. An analysis of the thermodynamic conditions for solid powder particles spreading over liquid surface. *Powder Technology*. Vol. 201, pp. 306-310, 2010.

NYLANDER T., SAMOSHINA Y., LINDMAN B. Formation of polyelectrolyte–surfactant complexes on surfaces. *Advances in Colloid and Interface Science*. Volumes 123–126 , Pages 105–123, 2006.

OSCIER C., BOSLEY N., MILNER Q. Paracetamol - A Review of Three Routes of Administration. *Update in Anaesthesia*. 112-14, 2007.

OTSUBO Y., HORIGOME M.. Effect of associating polymer on the dispersion stability and rheology of suspensions. *Korea-Australia Rheology Journal* 15, No. 1, pp. 27-33, 2003.

PANAGIOTOU T., MESITE S.V., FISHER R.J. Production of norfloxacin nanosuspensions using microfluidics reaction technology through solvent/antisolvent crystallization. *Industrial & Engineering Chemistry Research*. 48, 1761–71, 2009.

PARDEIKE J, STROHMEIER DM, SCHRÖDL N, VOURA C, GRUBER M, KHINAST JG, ZIMMER A. Nanosuspensions as advanced printing ink for accurate dosing of poorly soluble drugs in personalized medicines. *International Journal of Pharmaceutics*. Vol. 420, n 1, 93-100, 2011.

PATEL V. P., GOHEL M. C., PARIKH R. K. In Vitro Dissolution Enhancement of Felodipine. *Indo-Global Journal of Pharmaceutical Sciences*, Vol 1., Issue 2: Page No. 194-205, 2011.

PATEL VR, AGRAWAL YK.. Nanosuspension: An approach to enhance solubility of drugs. *Journal of Advanced Pharmaceutical Technology & Research*. 2(2):81-7, 2011.

PATTEKARI P., ZHENG Z., ZHANG X., LEVCHENKO T., TORCHILIN V., LVOV Y. Top-down and bottom-up approaches in production of aqueous nanocolloids of low solubility drug paclitaxel. *Physical Chemistry Chemical Physics*. 13, 9014–9, 2011.

PELTONEN L, HIRVONEN J. Pharmaceutical nanocrystals by nanomilling: critical process parameters, particle fracturing and stabilization methods. *Journal of Pharmacy & Pharmacology*. 62 (11), 1569-79, 2010.

PEÑA M.A., REÍLLO A, ESCALERA B., BUSTAMANTE P. Solubility parameter of drugs for predicting the solubility profile type within a wide polarity range in solvent mixtures. *International Journal of Pharmaceutics*. 14;321(1-2):155-61, 2006.

PEREPEZKO J. H. Kinetic processes in undercooled melts. *Materials Science and Engineering*. 226, 374-82, 1997.

PODCZECK F., COURSE N., NEWTON J.M., SHORT M.B. Gastrointestinal transit of model mini-tablet controlled release oral dosage forms in fasted human volunteers. *Journal of Pharmacy and Pharmacology*. 59(7), 941-5, 2007.

PORTALONE G., COLAPIETRO M. First example of cocrystals of polymorphic maleic hydrazide. *The Journal of Chemical Crystallography*. 34, 609–12, 2004.

PURI V., DANTULURI A. K., KUMAR M. . KARAR N. . BANSAL A.K. Wettability and surface chemistry of crystalline and amorphous forms of a poorly water soluble drug. *European Journal of Pharmaceutical Sciences*. Volume 40. Issue 2. 12, Pages 84-93, 2010.

QUAN P., SHI K., PIAO H., PIAO H., LIANG N., XIA D., CUI F. A novel surface modified nitrendipine nanocrystals with enhancement of bioavailability and stability. *International Journal of Pharmaceutics*. 430(1-2), 366-71, 2012.

R.J. HUNTER,.Zeta Potential in Colloids Science. *Academic Press*, NY, 1981.

RABINOW B.E. Nanosuspensions in drug delivery. *Nature Reviews Drug Discovery*. 3, 785-96, 2004.

RADZUAN R. B. Study on the development and stability of the nanoparticulates of poorly water soluble drugs. *Master of Science.Faculty of Pharmacy*. UNIVERSITI TEKNOLOGI MARA, 2010.

RAGHAVAN S.L., TRIVIDIC A., DAVIS A.F., HADGRAFT J. Crystallization of hydrocortisone acetate: influence of polymers. *International Journal of Pharmaceutics*. 212, 213–21, 2001.

RAK M., EREMIN N.N., EREMINA T.A., KZUNETSOV V.A., OKHRIMENKO T.M., FURMANOVA N.G., EFREMPOVA E.P. On the mechanism of impurity influence on growth kinetics and surface morphology of KDP crystals-I: defect centres formed by bivalent and trivalent impurity ions incorporated in KDP structure-theoretical Study. *Journal of Crystal Growth*. 273, 3-4, 577-85, 2005.

RANGEL-YAGUI C. O., HSU H.W.L., PESSOA-JR A., TAVARES L.C.. Micellar Solubilization of Ibuprofen – Influence of Surfactant Head Groups on the Extent of Solubilization.. *Brazilian Journal of Pharmaceutical Sciences* vol. 41, n. 2, 295– 309, abr./jun., 2005.

RASENACK N., MÜLLER B.W. Dissolution Rate Enhancement by in Situ Micronization of Poorly Water-Soluble Drugs. *Pharmaceutical Research*, 19, 12, 2002.

RASENACK N., MÜLLER B.W. Micron-size drug particles: common and novel micronization techniques. *Pharm Dev Technol* 9 (1): 1-13, 2004.

RASENACK N., STECKEL H., MULLER B.W. Micronization of anti-inflammatory drugs for pulmonary delivery by a controlled crystallization process. *Journal of Pharmaceutical Sciences*. 92, 35–44, 2003.

REHMAN T.U-R. Controlled Release Gel Formulations and Preclinical Screening of Drug Candidates. *PhD Thesis*. Department of Chemistry Umeå University, Sweden. Doctoral, 2011.

RISTIC R. I. The role of structural defects and interfacial instabilities in the growth behaviour of paracetamol. *International Journal of Modern Physics B*. 16, 329-37, 2002.

RISTIC R.I., FINNIE S., SHEEN D.B. Macro- and micromorphology of monoclinic paracetamol grown from pure aqueous solution. *Journal of Physical Chemistry B*. 105, 9057-66, 2001.

RODRIGUEZ-HORNEDO N., MURPHY D. Significance of controlling crystallization mechanisms and kinetics in pharmaceutical systems. *Journal of Pharmaceutical Sciences*. 88, 651-60, 1999.

RODRÍGUEZ-HORNEDO N., NEHM S.J., JAYASANKAR A. Cocrystals: design, properties and formation mechanisms. *Encyclopedia of Pharmaceutical Technology*, 3rd Ed., Taylor & Francis, London, 615-35, 2007.

RODRÍGUEZ-SPONG B., PRICE C. P., JAYASANKAR A., MATZGER A. J., RODRÍGUEZ-HORNEDO N., General Principles of Polymorphism: A Supramolecular Perspective, *Advanced Drug Delivery Reviews*, Vol. 56, pp. 241-274, 2004.

ROHRS B. R. Dissolution method development for poorly soluble compounds. *Dissolution Technologies*, 2001.

RUCKENSTEIN E., I. SHULGIN. Solubility of drugs in aqueous solutions Part 2: Binary nonideal mixed solvent. *International Journal of Pharmaceutics*. 260, 283–291, 2003.

SAENGER W. Cyclodextrin Inclusion Compounds in Research and Industry. *Angewandte Chemie International Edition in English*. 19, 5, 344–62, 1980.

SAHARAN V.A., CHOUDHURY P.K. Dissolution rate enhancement of piroxicam by ordered mixing. *Pak. Journal of Pharmaceutical Sciences*. 25, 3, 521-33, 2012.

SALAZAR J., HEINZERLING O., MÜLLER R.H. Process optimization of a novel production method for nanosuspensions using design of experiments (DoE). *International Journal of Pharmaceutics*. 420, 395-403, 2011.

SALEM H.F. Sustained-release progesterone nanosuspension following intramuscular injection in ovariectomized rats. *International Journal of Nanomedicine*. 5, 943–54, 2010.

SALEM H.F., ABDELRAHIM M.E., EID K.A., SHARAF M.A. Nanosized rods agglomerates as a new approach for formulation of a dry powder inhaler. *International Journal of Nanomedicine*. 6, 311–20, 2011.

SANTANDER-ORTEGA M.J., JODAR-REYES A.B., CSABA N., BASTOS-GONZALEZ D., ORTEGA-VINUESA J.L. Colloidal stability of Pluronic F68-coated PLGA nanoparticles: A variety of stabilisation mechanisms. *Journal of Colloid and Interface Science*. 302, 522, 2006.

SCHOTT H. Saturation adsorption at interfaces of surfactant solutions. *Journal of Pharmaceutical Sciences*. Volume 69, Issue 7, pages 852–854, 1980.

SCHRADER M. E. Young-Dupre Revisited. *Langmuir*. 11 (9), pp 3585–3589, 1995.

SEEDHER N., BHATIA S. Solubility Enhancement of Cox-2 Inhibitors Using Various Solvent Systems. *American Association for Pharmaceutical Scientists Pharmaceutical Science Technology*. 4 (3), 33, 2003

SHAIK MS I., NIKITA D., BHAMBER D., BHAMBER R. Permeability Enhancement Techniques for Poorly Permeable Drugs: A Review. *Journal of Applied Pharmaceutical Science* 02 (06), 34-39, 2012.

SHEKUNOV B.Y., CHATTOPADHYAY P., TONG H.H., CHOW A.H. Particle size analysis in pharmaceuticals: principles methods and applications. *Pharmaceutical Research*. 24, 203–27, 2007.

SHEKUNOV B.Y., YORK P. Crystallization processes in pharmaceutical technology and drug. Delivery Design. *Journal of Crystal Growth*. 211, 122–36, 2000.

SHEN H., HONG S., PRUD'HOMME R.K., LIU Y. Self-assembling process of flash nanoprecipitation in a multi-inlet vortex mixer to produce drug-loaded polymeric nanoparticles. *Journal of Nanoparticle Research*. 13, 4109–20, 2011.

SHI J. Steric Stabilization : Literature Review. The Ohio State University. Group Inorganic Materials. *Science* 2041 College Road, 281 Watts Hall.Columbus OH 43210-1178. USA, 2002.

SHINODA K. *Solvent Properties of Surfactant Solutions*. M. Dekker, New York. 234-7, 1967.

SIGFRIDSSON K., FORSSÉN S., HOLLÄNDER P.B., SKANTZE U., DE VERDIER J. A formulation comparison, using and different nanosuspensions of a poorly soluble compound. *European Journal of Pharmaceutics and Biopharmaceutics*. 67, 540–7, 2007.

SINGHAL D., CURATOLO W. Drug polymorphism and dosage and dosage form design: a practical perspective. *Advanced Drug Delivery Reviews* 56, 335– 347, 2004.

SIVASANKAR, KUMAR Role of Nanoparticles in Drug Delivery System. *International Journal of Research in Pharmaceutical and Biomedical Sciences*, Vol. 1 (2), 41-66, 2011.

SMITH A. J., KAVURU P., WOJTAS L., ZAWOROTKO M.J. , SHYTLE R.D. Cocrystals of quercetin with improved solubility and oral bioavailability. *Molecular Pharmacology*. 8(5):1867-76, 2011.

SONG R.Q., CÖLFEN H. Additive controlled crystallization. *CrystEngCommunity*. 13, 1249-76, 2011.

SRIDEVI S., CHAUHAN A.S., CHALASANI K.B., JAIN A.K., DIWAN P.V. Enhancement of dissolution and oral bioavailability of gliquidone with hydroxy propyl-beta-cyclodextrin. *Pharmazie*. 58(11), 807-10, 2003.

SRITAPUNYA T., KITIYANAN B., SCAMEHORN J.F., GRADY B.P., CHAVADEJ S. Wetting of polymer surfaces by aqueous surfactant solutions. *Colloids and Surfaces A: Physicochemical. Engineering Aspects*. 409, 30– 41, 2012.

SU X.Y., ALKASSAS R., . PO A.L.W, Statistical modelling of ibuprofen release from spherical lipophilic matrices, *European Journal of Pharmaceutics and Biopharmaceutics*. 40, 73–76, 1994.

SULTANA S., TALEGAONKAR S., ALI R., MITTAL G., BHATNAGAR A., AHMAD F.J. Formulation development and optimization of alpha ketoglutarate nanoparticles for cyanide poisoning. *Powder Technology*. 211, 1–9, 2011.

TALARI R., VARSHOSAZ J., MOSTAFAVI S.A., NOKHODCHI A. Dissolution Enhancement of Gliclazide Using pH Change Approach in Presence of Twelve Stabilizers with Various Physico-Chemical Properties. *Journal of Pharmacy & Pharmaceutical Sciences*. 12(3), 250-65, 2009.

TAN Y., YANG Z., PENG X., XIN F., XU Y., FENG M., ZHAO C., HU H., WU C. A novel bottom-up process to produce nanoparticles containing protein and peptide for suspension in hydrofluoroalkane propellants. *International Journal of Pharmaceutics*. 413, 167– 73, 2011.

TAYLOR L.S., ZOGRAFI G. Spectroscopic characterisation of interactions between PVP and indomethacin in amorphous molecular dispersions. *Pharmaceutical Research*. 14, 1691–8, 1997.

TERAYAMA H., INADA K., NAKAYAMA H., YASUEDA S., ESUMI K. Preparation of stable aqueous suspension of a hydrophobic drug with polymers. *Colloids and Surfaces B: Biointerfaces*. 39, 159–64, 2004.

TEXEIRA-ROSSI C.G.F, DE CASTRO-DANTAS T.N., DANTAS-NETO A.A., MEDEIROS-MACIEL M.A. Microemulsões: uma abordagem básica e perspectivas para aplicabilidade industrial. *Revista Universidade Rural - Série Ciências Exatas e da Terra*. 26, 1-2, 45-66, 2007.

TEYCHENE S., BISCANS B. A Multiscale Approach for the Characterization and Crystallization of Eflucimibe Polymorphs: from Molecules to Particles. *KONA Powder and Particle Journal*. 29, 266-282, 2011.

THAKUR R. K., VIAL C., NIGAM K.D.P., NAUMAN E.B., DJELVEH G. Static Mixers in the Process Industries – A Review. *Institution of Chemical Engineers*, 81, 787-826, 2003.

THELLY T., ISEL H., MOUNTFIELD R. J. The impact of cosolvents and the composition of experimental formulations on the pump rate of the ALZET osmotic pump. *International Journal of Pharmaceutics*. 205, 195-8, 2000.

THOMPSON . Investigating the fundamentals of drug crystal growth using Atomic Force Microscopy. *PhD Thesis*. University of Nottingham for the degree of Doctor of Philosophy, 2003.

THORAT A.A., DALVI S.V. Liquid antisolvent precipitation and stabilization of nanoparticles of poorly water soluble drugs in aqueous suspensions: Recent developments and future perspective. *Chemical Engineering Journal*. 181– 182, 1– 34, 2012.

TIPPETS M., MARTINI S. Effect of oil content and processing conditions on the thermal behaviour and physicochemical stability of oil-in-water emulsions. *International Journal of Food Science and Technology*, 44, 206–215, 2009.

TOKIWA, F. Solubilization Behavior of Sodium Dodecylpolyoxyethylene Sulfates in Relation to their Polyoxyethylene Chain Lengths. *The Journal of Physical Chemistry*.vol 73, 1214–1217, 1968.

VALDER C., MERRIFIELD D. *Pharmaceutical Technology*. Smith Kline Beecham R&D News. 32, 1, 1996.

VARSHOSAZ J., TALARI R., MOSTAFAVI A., NOKHODCHI A. Dissolution enhancement of gliclazide using in situ micronization by solvent change method. *Powder Technology*. 187, 3, 222-30, 2008.

VENKATESH S., LI J., XU Y., RAO V., ANDERSON B. D. Intrinsic solubility estimation and pH-solubility behaviour of cosalane (NSC 658586), an extremely hydrophobic diprotic acid. *Pharmaceutical Research*. 13(10), 1453-9, 1996.

VERMA S., GOKHALE R., BURGESS D.J. A comparative study of top-down and bottom-up approaches for the preparation of micro/nanosuspensions. *International Journal of Pharmaceutics*. 380, 216–22, 2009.

VERWEY E.J.W., OVERBEEK J.T.G. *Theory of the Stability of Lyophobic Colloids*. Elsevier: New York, 1948.

VETTER T., MAZZOTTI M., BROZIO J. Slowing the Growth Rate of Ibuprofen Crystals Using the Polymeric Additive. *Crystal Growth & Design*. 11 (9), 3813–21, 2011.

VIÇOSA A., LETOURNEAU J.-J., ESPITALIER F., RÉ M.I. An innovative antisolvent precipitation process as a promising technique to prepare ultrafine rifampicin particles. *Journal of Crystal Growth*. 342, 1, 1, 80–87, 2012.

VIKRANT V., PANKAJKUMAR S., POONAM K., MANALI S., YOGESH P. Physicochemical characterization of solid dispersion systems of tadalafil with poloxamer 407. *Acta Pharm*. 59, 453–461, 2009.

VIPPAGUNTA, S.R., WANG, Z., HORNING, S., KRILL, S.L. Factors affecting the formation of eutectic solid dispersions and their dissolution behavior. *Journal of Pharmaceutical Sciences*. 96, 294-304, 2007.

WALAS S. M. *Phase equilibria in chemical engineering*, Ed. Butterworth Publishers, Boston, p. 397-400 and 205-207, 1985.

WANG C., HICKEY A.J. Isoxyl Aerosols for Tuberculosis Treatment: Preparation and Characterization of Particles. *American Association of Pharmaceutical Sciences – Pharmaceutical Science & Technology*. 11, 2, 2010.

WANG J.X., ZHANG Q.X., ZHOU Y., SHAO L., CHEN J.F. Microfluidic synthesis of amorphous cefuroxime axetil nanoparticles with size-dependent and enhanced dissolution rate. *Chemical Engineering Journal*. 162, 844–51, 2010.

WANG X., MICHEL A., VAN DEN MOOTER G. Solid state characteristics of ternary solid dispersions composed of PVP VA64, Myrj 52 and itraconazole. *International Journal of Pharmaceutics*. 303, 1-2, 54-61, 2005.

WARD M. D. Organic crystal surfaces: structure, properties and reactivity. *Current Opinion in Colloid and Interface Science*. 2, 51-64, 1997.

WEISSBUCH I., LEISEROWITZ L., LAHAV, M. *Crystallization technology handbook* (Mersmann, A., ed.), pp. 401-457, Marcel Dekker, New York, 1995.

WEISSBUCH I., ZBAIDA D., ADDADI L., LEISEROWITZ L., LAHAV M. Design of polymeric inhibitors for the control of crystal polymorphism - induced enantiomeric resolution of racemic histidine by crystallization. *Journal of the American Chemical Society*. 109, 1869-71, 1987.

WHITESIDES G.M., GRZYBOWSKI B. Self-assembly at all scales. *Science*. 295, 2418, 2002.

WILLIAMS G., SINKO P. Oral absorption of the HIV proteases inhibitors: a current update, *Advanced Drug Delivery Review*. 39, 1999.

WU L, ZHANG J, WATANABE W. Physical and chemical stability of drug nanoparticles. *Advanced Drug Delivery Review*. vol. 63, n 6:,456-69, may 30, 2011.

XIA D., QUAN P., PIAO H., PIAO H., SUN S., YINC Y., CUI F. Preparation of stable nitrendipine nanosuspensions using the precipitation–ultrasonication method for enhancement of dissolution and oral bioavailability. *European Journal of Pharmaceutical Sciences*. 40, 325–34, 2010.

YALKOWSKY S.H. *Solubility and Solubilization in Aqueous Media*. Oxford University Press, New York, 1999.

YALKOWSKY, S.H., ROSEMAN, T.J. Solubilization of drugs by cosolvents, in *Techniques of Solubilization of Drugs*, Edited by Yalkowsky, S.H. Marcel Dekker, Inc., New York. pp. 91-134, 1981.

YEH M.K., CHANG L.C., CHIOU A.H. Improving tenoxicam solubility and bioavailability by cosolvent system. *American Association of Pharmaceutical Scientists Pharmaceutical Science & Technology*. 10(1), 166-71, 2009.

YELLELA SRK. Pharmaceutical technologies for enhancing oral bioavailability of poorly soluble drugs. *Journal of Bioequivalence & Bioavailability*, 2(2):28–36, 2010.

YOSHIZAKI I., SATO T., IGARASHI N., NATSUISAKA M., TANAKA N., KOMATSU H., YODA S. Systematic analysis of supersaturation and lysozyme crystal quality. *Acta Crystallographica*. 57, 1621-9, 2001.

YOUNG S. A. AND BUCKTON G.. Particle growth in aqueous suspensions: the influence of surface energy and polarity. *International Journal of Pharmaceutics*. Volume 60, Issue 3, Pages 235–241, 1990.

YU Y. G., WENTZCOVITCH R.M., VINOGRAD V. L., ANGEL R. J., Thermodynamic properties of MgSiO₃ majorite and phase transitions near 660 km depth in MgSiO₃ and Mg₂SiO₄: A first principles study, *Journal of Geophysical Research*, Vol. 116, pp. 1-19, 2011

ZAWOROTKO M. Crystal engineering of co-crystals and their relevance to pharmaceuticals and solid-state chemistry. *Acta Crystallographica Section A*. A64: C11-C12, 2008.

ZHANG D., TAN T., GAO L., ZHAO W., WANG P. Preparation of azithromycin nanosuspensions by high pressure homogenization and its physicochemical characteristics studies. *Drug Development and Industrial Pharmacy*. 33, 569-75, 2007.

ZHANG H., HOLLIS C.P., ZHANG Q., LI T. Preparation and antitumor study of camptothecin nanocrystals. *International Journal of Pharmaceutics*. 415, 293– 300, 2011.

ZHANG H.X., WANG J.X., SHAO L., CHEN J.F. Microfluidic fabrication of monodispersed pharmaceutical colloidal spheres of atorvastatin calcium with tunable sizes. *Industrial & Engineering Chemistry Research*. 49, 4156–61, 2010.

ZHANG H.X., WANG J.X., ZHANG Z.B., LE Y., SHEN Z.G., CHEN J.F. Micronization of atorvastatin calcium by antisolvent precipitation process. *International Journal of Pharmaceutics*. 374, 106–13, 2009.

ZHANG J.Y., SHEN Z.G., ZHON J., HU T.T., CHENA J.F., MA Z.Q., YUN J. Preparation of amorphous cefuroxime axetil nanoparticles by controlled nanoprecipitation method without surfactants. *International Journal of Pharmaceutics*. 323, 153–160, 2006.

ZHAO H., LE Y., LIU H., HU T., SHEN Z., YUN J., CHEN J.F. Preparation of microsized spherical aggregates of ultrafine ciprofloxacin particles for dry powder inhalation (DPI). *Powder Technology*. 194, 81–86, 2009.

ZHAO H., WANG J., ZHANG H., SHEN Z., YUN J., CHEN J. Facile Preparation of Danazol Nanoparticles by High-Gravity Anti-solvent Precipitation (HGAP) Method. *Product Engineering and Chemical Technology*. 17(2), 318-23, 2009.

ZHAO H., WANG J.X., WANG Q.A., CHEN J.F., YUN J. Controlled liquid antisolvent precipitation of hydrophobic pharmaceutical nanoparticles in a microchannel reactor, *Industrial & Engineering Chemistry Research*. 46, 8229–35, 2007.

ZHAO, CHUN-XIA, HE, LIZHONG, QIAO, SHIZHANG AND MIDDELBERG, ANTON P.J. Nanoparticle synthesis in microreactors. *Chemical Engineering Science*. 66 7: 1463-1479, 2011.

ZHONG J., SHEN Z.G., YANG Y., CHEN J.F. Preparation and characterization of uniform nanosized cephradine by combination of reactive precipitation and liquid anti-solvent precipitation under high gravity environment. *International Journal of Pharmaceutics*. 301, 286–93, 2005.

ZHOU L., ZHOU J.H., DONG C., MA F., WEI S.H. Water-soluble hypocrellin A nanoparticles as a photodynamic therapy delivery system. *Dyes and Pigments*. 82, 1, 90-4, 2009.

ZHU W, ROMANSKI FS, MENG X, MITRA S, TOMASSONE MS. Atomistic simulation study of surfactant and polymer interactions on the surface of a Fenofibrate Crystal. *European Journal of Pharmaceutical Sciences*, Vol. 42 , p-452–461, 2011.

ZHU W.Z., WANG J.X., SHAO L., ZHANG H.X., ZHANG Q.X., CHEN J. F. Liquid antisolvent preparation of amorphous cefuroxime axetil nanoparticles in a tube-in-tube microchannel reactor. *International Journal of Pharmaceutics*. 395, 260–5, 2010.

ZHU Z., ANACKER J.L., JI S., HOYE T.R., MACOSKO C.W., PRUD'HOMME R.K. Formation of block copolymer-protected nanoparticles via reactive impingement mixing, *Langmuir*. 23, 10499–504, 2007.

ZHU Z., MARGULIS-GOSHEN K., MAGDASSI S., TALMON Y., MACOSKO C.W. Polyelectrolyte stabilized drug nanoparticles via flash nanoprecipitation: a model study with carotene. *Journal of Pharmaceutical Sciences*. 99, 4295–306, 2010.

ZILLER K.H., RUPPRECHT H. Control of crystal growth in drug suspensions. *Drug Development and Industrial Pharmacy*. 14, 2341–70, 1988.

ZIMMERMANN A., MILLQVIST-FUREBY A., ELEMA M.R., HANSEN T., MÜLLERTZ A., HOVGAARD L. Adsorption of pharmaceutical excipients onto microcrystals of siramesine hydrochloride: Effects on physicochemical properties. *European Journal of Pharmaceutics and Biopharmaceutics*. 71, 109–16, 2009.